6. SITE 747[1]

Shipboard Scientific Party[2]

HOLE 747A

Date occupied: 6 March 1988

Date departed: 8 March 1988

Time on hole: 1 day, 18 hr, 45 min

Position: 54°48.68′S, 76°47.64′E

Bottom felt (rig floor; m, drill pipe measurement): 1705.5

Distance between rig floor and sea level (m): 10.50

Water depth (drill pipe measurement from sea level, m): 1695.0

Total depth (rig floor; m): 1961.50

Penetration (m): 256.00

Number of cores (including cores with no recovery): 27

Total length of cored section (m): 256.00

Total core recovered (m): 227.34

Core recovery (%): 88

Oldest sediment cored:
Depth (mbsf): 256.00
Nature: nannofossil chalk
Age: Campanian
Measured velocity (km/s): 1.62

HOLE 747B

Date occupied: 8 March 1988

Date departed: 9 March 1988

Time on hole: 13 hr, 25 min

Position: 54°48.68′S, 76°47.64′E

Bottom felt (rig floor; m, drill pipe measurement): 1707.7

Distance between rig floor and sea level (m): 10.50

Water depth (drill pipe measurement from sea level, m): 1697.2

Total depth (rig floor; m): 1758.00

Penetration (m): 50.30

Number of cores (including cores with no recovery): 6

Total length of cored section (m): 50.30

Total core recovered (m): 48.91

Core recovery (%): 97

Oldest sediment cored:
Depth (mbsf): 50.30
Nature: nannofossil ooze
Age: late Miocene
Measured velocity (km)s): 1.51

HOLE 747C

Date occupied: 9 March 1988

Date departed: 12 March 1988

Time on hole: 3 days, 10 hr, 30 min

Position: 54°48.68′S, 76°47.64E

Bottom felt (rig floor; m, drill pipe measurement): 1705.7

Distance between rig floor and sea level (m): 10.50

Water depth (drill pipe measurement from sea level, m): 1695.2

Total depth (rig floor; m): 2056.20

Penetration (m): 350.50

Number of cores (including cores with no recovery): 16

Total length of cored section (m): 144.50

Total core recovered (m): 49.50

Core recovery (%): 34

Oldest sediment cored:
Depth (mbsf): 295.10
Nature: nannofossil chalk
Age: early Santonian
Measured velocity (km/s): 2.29

Basement:
Depth (mbsf): 296.60
Nature: basalt
Measured velocity (km/s): 5.00

Principal results: Site 747 (proposed site SKP-1) lies in the transition zone between the northern and southern parts of the Kerguelen Plateau, approximately 500 km south of the Polar Front (Antarctic Convergence) at 54°48.68′S, 76°47.64′E. A 295.1-m-thick lower Santonian through Pleistocene pelagic sedimentary section and 53.9 m of underlying basalt were cored in three holes with various combinations of the advanced hydraulic piston corer (APC), the extended core barrel corer (XCB), and the rotary core barrel (RCB) in a water depth of 1697.2 m. Although located beneath the present-day Antarctic Water Mass, the sediments contain carbonate throughout except for predominantly Maestrichtian–lower Paleocene volcaniclastic sands, breccias, and cobbles, which denote a major episode of uplift and erosion of the plateau.

The lithologic units that follow are recognized at Site 747.

Unit I (0–32.7 mbsf): Pleistocene to lower Pliocene foraminifer diatom oozes with minor ice-rafted debris and dropstones prevalent only in the upper 20 m, whereas occasional vitric ash layers occur throughout.

Unit II (32.7–181.9 mbsf): upper Miocene to Paleocene nannofossil ooze and chalk divisible into three subunits.

Subunit IIA: upper Miocene to upper Oligocene nannofossil ooze (32.7–151.5 mbsf) with occasional vitric ash layers.

Subunit IIB: upper Oligocene to lower Eocene nannofossil chalk with foraminifers (151.5–170.5 mbsf) and with hardgrounds near the base (169 mbsf).

Subunit IIC: highly bioturbated Danian nannofossil chalk (170.5–181.9 mbsf), with large (centimeter scale) burrows and occasional shallow-water fossils (bivalve fragments, larger benthic foraminifers) and a hardground (173.1 mbsf).

[1] Schlich, R., Wise, S. W., Jr., et al., 1989. *Proc. ODP, Init. Repts.*, 120: College Station, TX (Ocean Drilling Program).

[2] Shipboard Scientific Party is as given in the list of participants preceding the contents.

Unit III (181.9–189.5 mbsf): lower Paleocene–upper Maestrichtian multicolored volcaniclastic, polygenetic sand, breccia, and cobbles with probable intercalated chalk layers.

Unit IV (189.5–295.1 mbsf): upper Maestrichtian to lower Santonian nannofossil chalk and thin nodular chert layers. (Note ~1-m-thick gap between Unit IV and underlying basement rocks. Basement rocks were recovered beginning at 296.5 mbsf.)

Unit V (296.6–350.5 mbsf): basalt flows composed of variably brecciated, veined, and altered aphyric to sparsely phyric basalts.

The sequence documents a succession of tectonic and paleoceanographic events that highlight the geologic evolution of the Kerguelen Plateau. Vesicular basalt flows deposited in a shallow-water to subaerial environment capped the basement structure of the plateau prior to its subsidence and the accumulation of marine sediment, which began at this site by early Santonian times. The oldest sediments recovered are shallow-water glauconitic calcarenites with admixtures of fine volcanic debris eroded from the basement. These are overlain disconformably by deeper-water middle Campanian to Maestrichtian chalks with chert stringers and some *Inoceramus* and pelagic crinoid remains.

The succession is interrupted by a series of Maestrichtian–lower Paleocene debris flows consisting of clay-, sand-, and cobble-size clastics and breccias eroded subaerially from volcanic basement during what appears to have been a major uplift event that affected much of the plateau. Debris flows include angular clasts of previously lithified Campanian chalk and chert that indicate substantial faulting of the seafloor. Uppermost Maestrichtian to lowermost Paleocene sediments are missing, but scattered volcanic debris were shed into the overlying heavily bioturbated Danian chalks. The remaining Paleocene–lower Oligocene section is highly condensed and is cut by three disconformities where most or all of the upper Paleocene, middle to lower upper Eocene, and a small portion of the upper lower Oligocene are missing. Hardgrounds are developed on two of these surfaces.

Sedimentation rates for the remainder of the Neogene are remarkably constant at about 5 m/m.y., and sedimentation for this interval appears to have been continuous until the late Pleistocene. Although the predominance of biosiliceous ooze throughout the Pliocene-Pleistocene denotes the presence of the Antarctic water mass over this site, several species of both planktonic foraminifers and calcareous nannoplankton lived in the surface waters. The top of the section is dated at 0.35 Ma.

The essentially continuous calcareous upper Oligocene to upper Pleistocene record at a site this far south of the present day Polar Front was unexpected, and this section will serve as an important reference section for an integrated high-latitude calcareous and siliceous microfossil biostratigraphy correlated with magnetostratigraphy and lower latitude zonations. A good paleomagnetic polarity record was obtained down to the lower/upper Oligocene contact. Virtually all major events (anomaly correlatives) can be recognized as well as the structure of most of the polarity chrons.

Excellent preservation of planktonic and benthic foraminifers should allow a complementary stable isotope record to be established. Also noteworthy is the pristine preservation of the Danian calcareous microfossils. The Cretaceous planktonic foraminifers and calcareous nannofossil assemblages belong to the cool-water Austral faunal and Falkland Plateau floral provinces, respectively, except for the lowest Campanian core, which shows a more temperate influence. Campanian-Maestrichtian sedimentation rates were a relatively high 20 m/m.y., the result of a high productivity of calcareous and siliceous plankton coupled with a shallow depositional environment.

On the basis of macroscopic observations, the recovered basement rock consists of approximately 15 separate basalt flows. The separate flows appear similar in composition and consist of dominantly aphyric, sparsely plagioclase-pyroxene phyric, and olivine-plagioclase phyric basalts. The flows are vesicular, indicating deposition in a shallow-water to subaerial environment. All volcanics exhibit variable degrees of brecciation, veining, and alteration. The alteration minerals consist of zeolites, clays (celadonite and smectites), and calcite fillings in veins, vesicles, and amygdules. Fresh material was recovered from three flows. Trace-element chemistry is similar to transitional mid-ocean ridge basalt (T-MORB).

The sequence below 90 mbsf was successfully logged despite gale force winds. The resistivity and natural gamma ray logs clearly delimit the major altered and less altered zones in the basement complex (which was cored with only a 38% recovery due to high seas). The logs also detected basalt breccia debris flows in the lower Maestrichtian that were not cored or only partially cored during drilling.

An approach site survey along a single channel seismic line located the site close to the intersection of two multichannel seismic lines. Correlation with existing seismic data is excellent. A reflector at 0.24 s two-way traveltime (TWT) probably corresponds to Unit III, and basement matches a major reflector at 0.35 s TWT. These results agree quite well with the logging data.

BACKGROUND AND OBJECTIVES

The Kerguelen Plateau is divided into two distinct domains (Schlich, 1975; Houtz et al., 1977). To the north, the Kerguelen-Heard Plateau lies between 46°S and 54°S; to the south, the Southern Kerguelen Plateau roughly extends between 57°S and 64°S (see "Introduction" chapter, this volume). Site 747 (54° 48.68′S, 76°47.64′E) is located in the transition zone, between the northern and southern parts of the Kerguelen Plateau, approximately 500 km south of the present-day Antarctic Convergence at a water depth of about 1700 m.

Site 747 (target site SKP-1) is at the intersection of French multichannel seismic (MCS) line MD47-03 (shot point 11400) and Australian MCS line RS02-13 (87.2115, shot point 9000) (Fig. 1), where basement lies within 350–400 m of the seafloor. To the west and to the northwest, the sediment coverage progressively increases and almost reaches 800 m (proposed Site SKP-1A); to the east and to the southeast, the sediment rapidly diminishes to less than 200 m (proposed site SKP-1B). The location of these sites on the seismic sections are given in Figures 2 (MD47-03) and 3 (RS02-13).

Objectives

Site 747 is the northernmost site where basement can easily be reached by drilling on the Kerguelen Plateau. The prime objective of drilling this site was to determine the nature and age of the basement and to compare the results with the data obtained at the two other Southern Kerguelen Plateau basement sites (Leg 119, Site 738, and Leg 120, proposed site SKP-4A).

The origin and crustal structure of the Kerguelen Plateau have always been a matter of controversy. Heezen and Tharp (1966), Laughton et al. (1970), and Schlich et al. (1971) suggested a continental structure. Strontium and lead isotope data obtained first by Watkins et al. (1974) and later by Dosso et al. (1979) for Kerguelen Island igneous rocks show clear affinities with the results derived for other oceanic islands. Schlich (1982) and Coffin et al. (1986) suggested that the Kerguelen Plateau may be an amalgamation of disparate structural elements, including crustal uplifts, oceanic crust, and continental fragments. Recent geological and geophysical studies (*Marion Dufresne* cruises MD26, MD35, MD47, and MD48 and *Rig Seismic* cruise RS02; see also "Introduction" chapter, this volume) favor an oceanic origin for the Kerguelen Plateau. Drilling to basement at Site 747 should provide petrographical and geochemical data that would support one of several models: continental fragment, oceanic island volcanism, or mid-oceanic ridge volcanism.

A second objective at this site was to study the paleoceanographic history of the region. Site 747 belongs to the Kerguelen Plateau Neogene latitudinal and depth transect. The objective of paleoceanographic studies at this site was to trace the movement of the Antarctic Convergence through time using sediment types as well as microfossil assemblages (Kennett, 1978). The location of the site above the present-day regional carbonate-compensation depth (CCD) suggests that carbonate should be present in much of the Neogene section. Piston cores collected by *Marion Dufresne* cruises (MD35 and MD48) reveal the presence of Neogene to Quaternary calcareous and siliceous oozes overlying upper Eocene to Oligocene calcareous nannofossil oozes (Frohlich

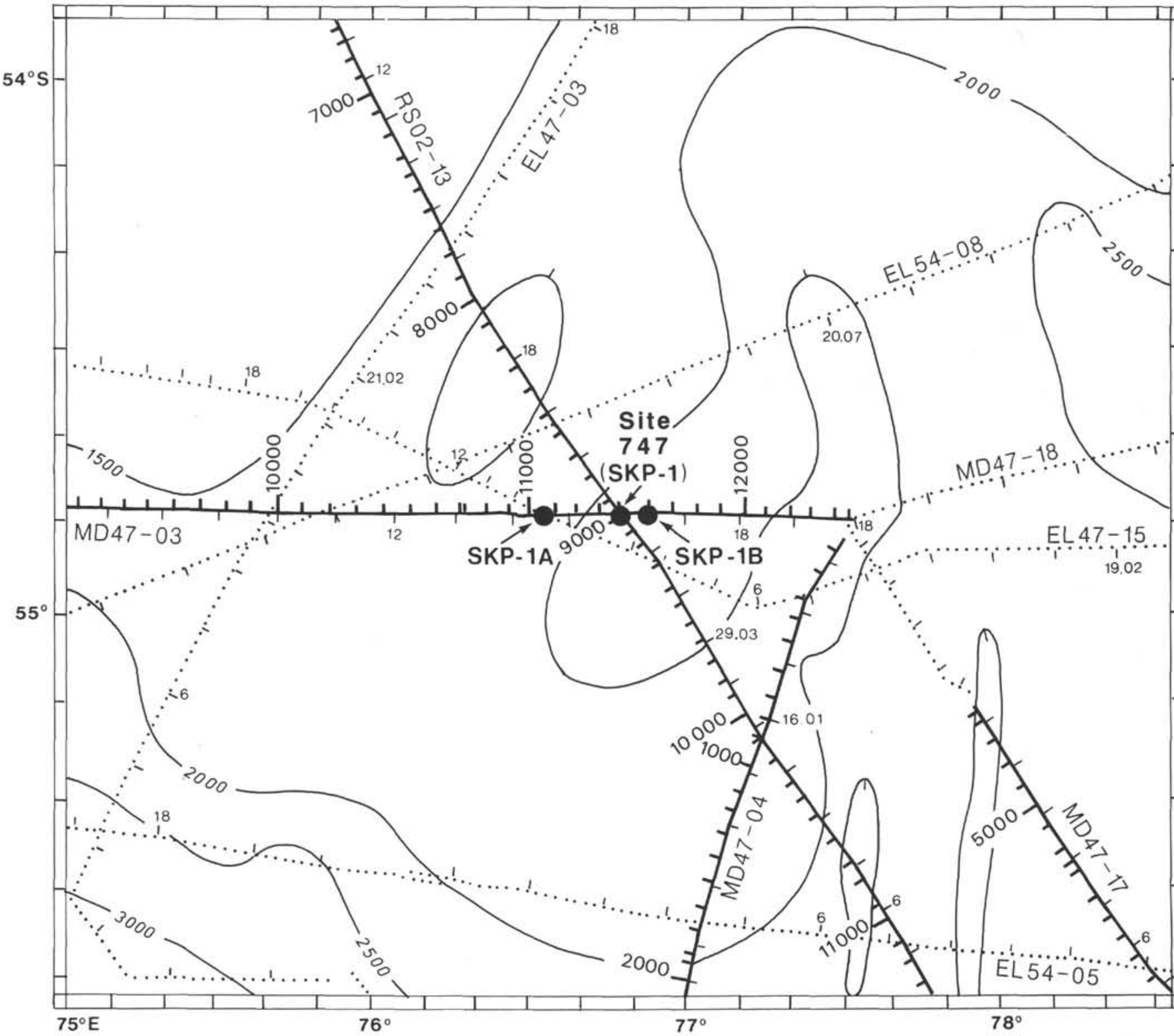

Figure 1. Track lines in the vicinity of Site 747. Bold lines denote *Rig Seismic* (RS02) and *Marion Dufresne* (MD47) multichannel seismic reflection profiles. The bathymetry is from Schlich et al. (1987) and is shown in meters.

et al., 1983; Wicquart and Frohlich, 1986; Leclaire et al., 1987). Sampling the lowermost Paleogene and possibly Cretaceous sediments could provide important information about the tectonic history of the Kerguelen Plateau.

Drilling Strategy

Drilling strategy planned at Site 747 included advanced hydraulic piston coring (APC), followed by the extended core barrel (XCB) until refusal. The rotary core barrel (RCB) was then to be used to achieve penetration into basement (at least 50 m). The first reflector was expected to lie at about 200 m and possibly to correspond with the first appearance of cherts. Basement was predicted to occur between 350 and 400 m.

SITE GEOPHYSICS

JOIDES Resolution departed Fremantle, Australia, on 26 February 1988 in the late evening. Continuous bathymetric and magnetic recording started at 0430 hr (UTC) on 27 February 1988, along a line almost perpendicular to the Southeast Indian Ridge. On 5 March 1988 at 0409 hr (UTC), the ship changed course and headed westward to the Kerguelen Plateau. Bottom depth was not continuously recorded because of sea conditions.

Site 747, the first site to be drilled on Leg 120, lies about 150 nmi southeast of Heard Island. The site was approached from the east following a course of about 263°. The seismic profiling gear was deployed about 24 mi (1020 hr UTC) before reaching the site, the speed was reduced to 6 kt to improve the quality of the records, and the final site approach was made with global positioning system (GPS) satellite navigation. A beacon was dropped on the initial crossing of the proposed site (SKP-1), which is defined by the intersection of *Marion Dufresne* (MD47-03, shot point 11400) and *Rig Seismic* (RS02-13, shot point 9000) multichannel seismic reflection lines (Fig. 1).

Taking into account the precision of the *Marion Dufresne* and *Rig Seismic* transit navigation, it is obvious from direct examination of the seismic analog records that the beacon lies very close to the intersection of the French and Australian seismic lines given at 54°48.8′S and 76°47.4′E. The gear was re-

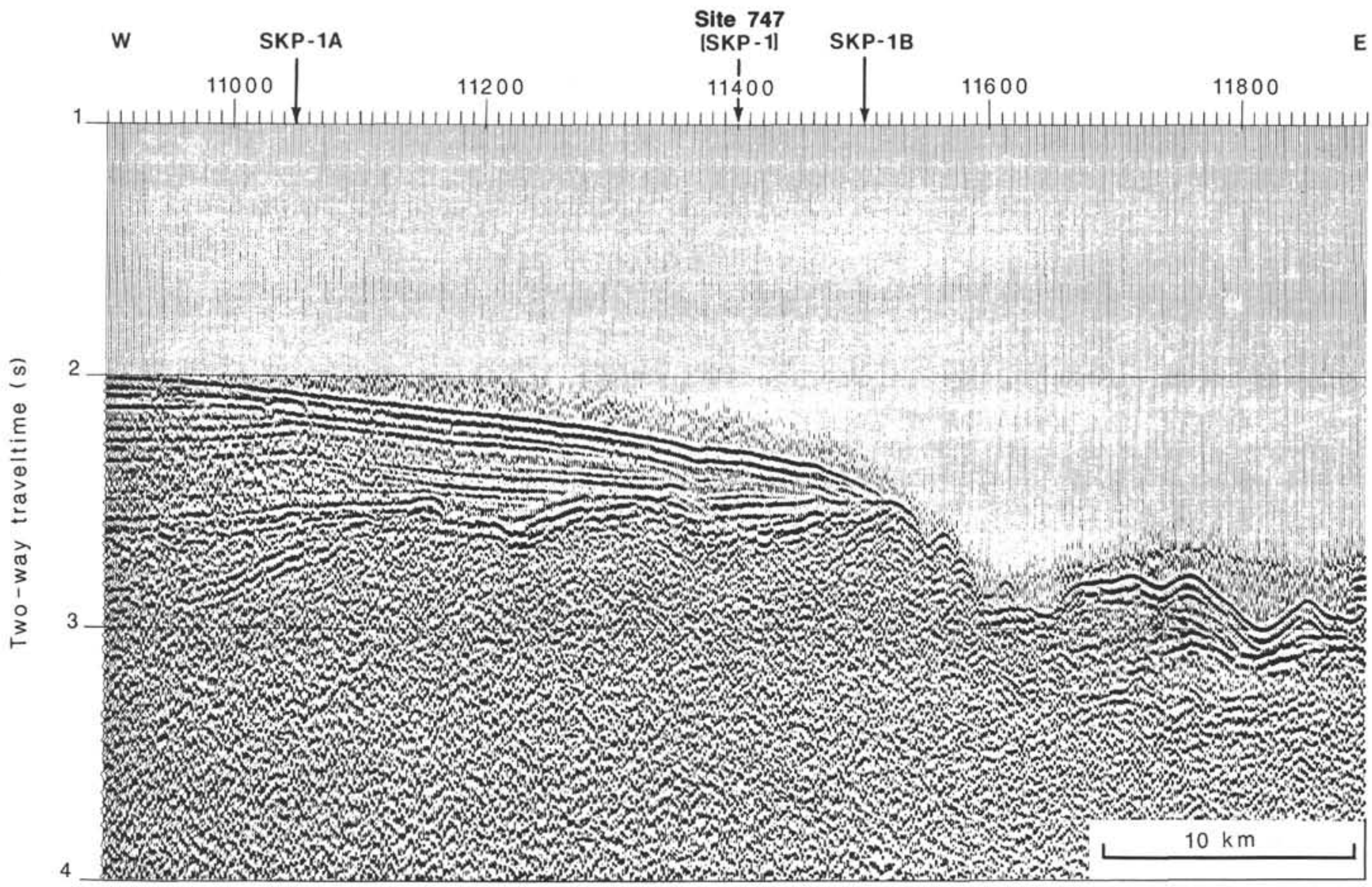

Figure 2. Seismic section MD47-03 (shot points 10900 to 11900) and SKP site locations (SKP-1A, SKP-1, and SKP-1B) along the profile.

trieved as soon as the site was passed, and the ship proceeded back to the beacon to commence drilling. The final coordinates of Site 747 are 54°48.68′S and 76°47.64′E; the water depth (from sea level), as measured from the drill pipe (DPM) and corrected for height of the rig floor above sea level, at the three holes (747A, 747B, and 747C) ranges between 1694.5 m and 1697.2 m (Fig. 4).

The multichannel seismic reflection data that were used to locate the site are displayed on Figures 2 and 3. Both the Australian (air gun) and the French (Flexichoc) multichannel seismic reflection records show a clear basement reflector superimposed by two sedimentary sequences. The latter are separated by a medium-amplitude, rather continuous reflector, which can easily be traced on the Flexichoc record (MD47-03). Using all the available data, an isochron map of the top of the acoustic basement (Fig. 5) and a sediment isopach map (Fig. 6) have been drawn for the area close to the drilling site.

Site 747 is located on a basement high in a northwest-trending direction; it abuts the northern end of the north-trending 77°E Graben structure almost at a right angle. The sediments overlying the basement are relatively thin, especially close to the site. The *JOIDES Resolution* survey line, shot with two 80-in^3 water guns and recorded with a 100-m hydrophone streamer, is shown on Figure 7. The correlation of this single-channel seismic reflection profile with the Australian and French multichannel seismic lines is straightforward. The basement graben structure, so clearly observed along the MD47-03 seismic line and delineated on the acoustic basement isochron and sediment isopach maps (Figs. 5 and 6) appears clearly on the *JOIDES Resolution* record between 1210 and 1350 hrs (UTC).

At Site 747 the basement reflector lies at about 0.35 s TWT (two-way traveltime) below seafloor, whereas the sedimentary reflector can be traced between 0.22 and 0.24 s TWT below seafloor. The correlation with the two multichannel seismic reflection profiles is shown on Figure 8. The survey data collected by *JOIDES Resolution* show these reflectors, but the noise level and the bubble pulses of the source prevent one from scaling them precisely.

Vertical velocity distribution was estimated by taking into account previous sonobuoy experiment results obtained on the Kerguelen Plateau and calculated seismic reflection stack velocities. Assuming velocities of 1.7 and 2.4 km/s respectively for the two sedimentary sequences, basement was expected at a depth of about 340 mbsf. A sonobuoy experiment planned on departure from Site 747 was canceled because of a gale and extremely rough seas.

OPERATIONS

Introduction

Leg 120 is the second of two back-to-back Ocean Drilling Program (ODP) legs concentrated in the southern Indian Ocean in the region of the Kerguelen Plateau and Prydz Bay, Antarctica. Leg 119 drilled the Prydz Bay sites and the northern and southernmost Kerguelen Plateau sites. Leg 120 drilled the central and southern sites on the Kerguelen Plateau.

Fremantle Port Call

Leg 120 officially began at 0715 hr (L), 21 February 1988, in Port Fremantle, Australia. Once the ship was secured at dock-

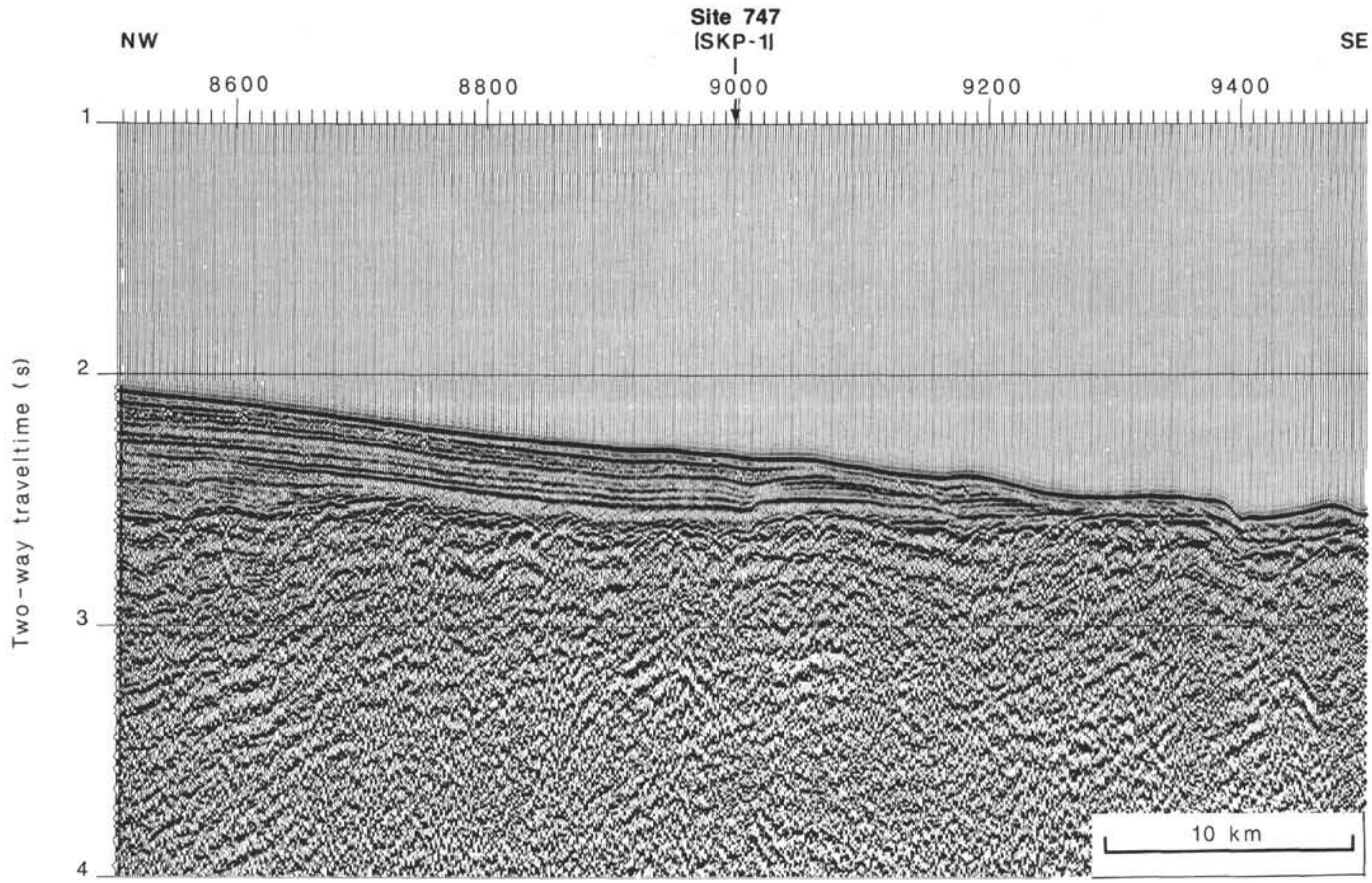

Figure 3. Seismic section RS02-13 (shot points 8500 to 9500) and SKP-1 site location.

side at Victoria Quay, Fremantle, bunkering commenced at 1200 noon. The ODP and SEDCO crew changes were completed.

A total of 1761 metric tons of fuel, 894 short tons of drilling water, and oncoming surface and air freight were loaded. Other port call activities included load testing of the ship's cranes to American Bureau of Shipping specifications; magnaflux inspection of Leg 119's bottom hole assemblies; installation of a new field coil in the P116B propulsion motor; and installation of a new Racal-Decca plotting radar on the bridge.

The MARISAT became inoperative the same day the ship arrived in Fremantle. Necessary parts to effect repairs were not available in southeast Asia, which caused a 16-hr delay in the ship's departure while parts were hand carried from the United States to Fremantle. By 2300 hr (L), 26 February 1988, the MARISAT was repaired, and at 2345 hr (L) the last line was retrieved and the ship was underway.

Fremantle to Site 747 (SKP-1)

The ship sailed at reduced speed while two Institut François du Pétrole (IFP) engineers were calibrating a ship's motion recorder. After the engineers were transferred to a standby boat, the ship was underway at full speed. During the 9-day transit, oncoming freight was stored in the proper places and all coring tools and equipment were checked. By the sixth day into the voyage, heavy seas were encountered, and 40-kt winds from the southwest caused the ship's speed to drop to 7 kt. Wind and sea conditions improved by the time the site survey commenced at 1800 hr (L), 6 March 1988. After a 30-nmi survey, the beacon was deployed on the first pass over SKP-1, thereby initiating Site 747 at 2230 hr.

Site 747

Hole 747A

The APC/XCB bottom hole assemblies (BHA) consisted of an $11^7/_{16}$-in. bit with 4×15 in. angled jets, a long bit sub with float valve, a seal bore core barrel, seven $8^1/_4$-in. drill collars, one $7^1/_4$-in. drill collar, and two stands of $5^1/_2$-in. drill pipe. As the BHA was lowered to the seafloor, the drill string was measured and rabbited.

The mud line was established at 1705.5 m below the rig floor (1695 meters below seafloor [mbsf]) with the first APC core, but a second trip in with the wireline was required because a Type GS pulley tool sheared prematurely and failed to recover the core barrel on the first run. The shear pin problem continued through Core 120-747A-4H. We used a set of $3^1/_2$-in. sinker bars and a $3^1/_2$-in. wireline jar with the Type GS pulley tool for the first time on the APC coring system. The oversized sinker bars and the $3^1/_2$-in. jars were removed from the assembly and some improvement was noted.

A total of 16 APC cores were recovered before the pullout force reached 60,000 lbs. Recovery was 100%. We continued coring with the XCB coring system rigged with a polypak bit seal. Coring was advanced with the XCB coring system using a polypak bit seal. Coring was routine with an average recovery of about 75%. Down to 240 mbsf, chert stringers were found interbedded in soft chalk. The abrasive chert wore the teeth off the XCB cutting shoes while drilling Cores 120-747A-19X to -27X to total depth (TD) at 256 mbsf. Further efforts to penetrate the chert layers would only have resulted in damaged XCB shoes and poor core recovery. Only traces of methane gas were en-

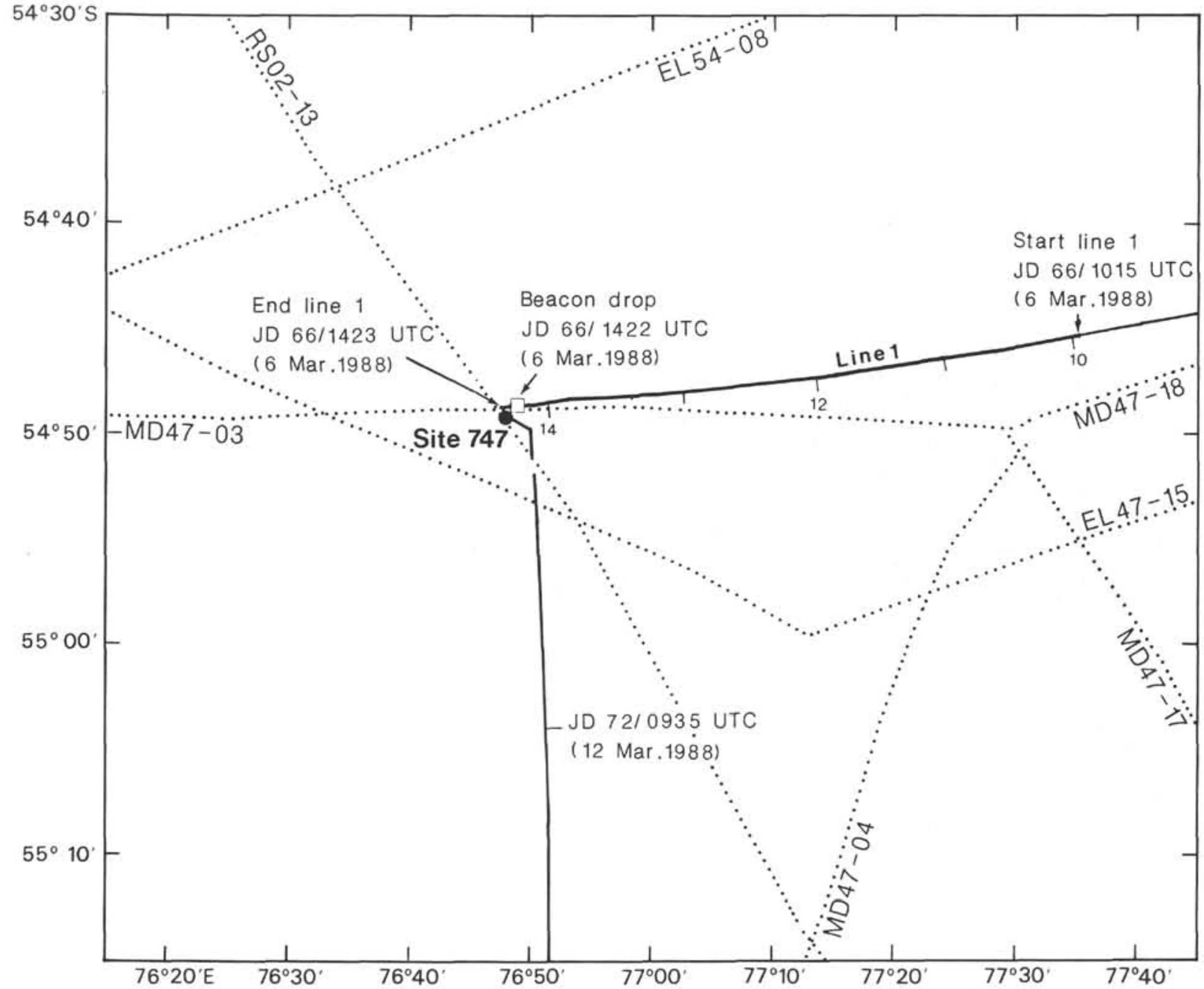

Figure 4. *JOIDES Resolution* site approach and Site 747 location.

countered. The hole was displaced with weighted mud, the drill string was pulled above the mud line at 1730 hr (L), 8 March 1988, and the bit positioned to shoot the mud line for Hole 747B.

Hole 747B

With the bit positioned above the mud line, the APC was deployed six times to 1758 m (50.3 mbsf). The mud line was encountered at 1707.7 m below the rig floor (1697.2 mbsl), 2.2 m shallower than at Hole 747A. This difference may have been caused by the excess heave of the ship, which could have caused the APC to overshoot the mud line at Hole 747A. One heat flow measurement was taken after the last core. With the coring objectives met, the drill string was tripped out at 0645 hr (L), 9 March 1988, and the ship was offset 40 m west of Hole 747B.

Hole 747C

The bottom stand of drill collars were replaced with a rotary coring 9-drill-collar assembly, and a mechanical bit release was added to the BHA.

The drill string was tripped to the mud line, and we were preparing to spud Hole 747C when the positioning alarm sounded. The alarm was set off when one thruster skid dropped off line and the ship moved 3.5% of water depth off location. The problem was quickly identified, and the skid was soon back on line. Since the wind had increased to 40 kt and swells to 14–16 ft, we decided to "wait on weather" (WOW) a few minutes before penetrating the mud line with the stiff BHA.

After WOW for 1 hr, the bit was lowered to the mud line, and the hole was drilled/washed from 1705 to 1864 m. The rotary core barrel (RCB) was deployed, and 5 cores were retrieved. Recovery was poor through this interval in Hole 747A. Efforts were partially successful in that core recovery was not improved, but we did recover some sediments missed previously in Hole 747A. The center bit was again deployed to continue drilling and washing to the next coring interval.

During this period the barometer continued to drop, and the wind gusted up to 45–50 kt, causing a cross swell of 16 ft. With the ship starting to roll from 7° to 10°, coring operations were suspended for 45 min while WOW. With little or no improvement in operating conditions, we decided to resume operations. The hole was drilled and washed to 1957 m. Hole 747C was cored from 1957 to 2000 m with very poor recovery in the chalk with chert stringers. The center bit was deployed to condition the hole and to drill up the chert rubble that had accumulated on bottom. The hole was also flushed with 20 bbl of polymer mud. Core 120-747C-11R was cored from 296.6–303.0 m below seafloor (mbsf) with a very slow rate of penetration (ROP); 3.2 m of olive green basalt was recovered.

When hard basalt was encountered, we realized that the 16–18-ft swell was causing the ship to roll 8° to 14° with 10–12 ft of

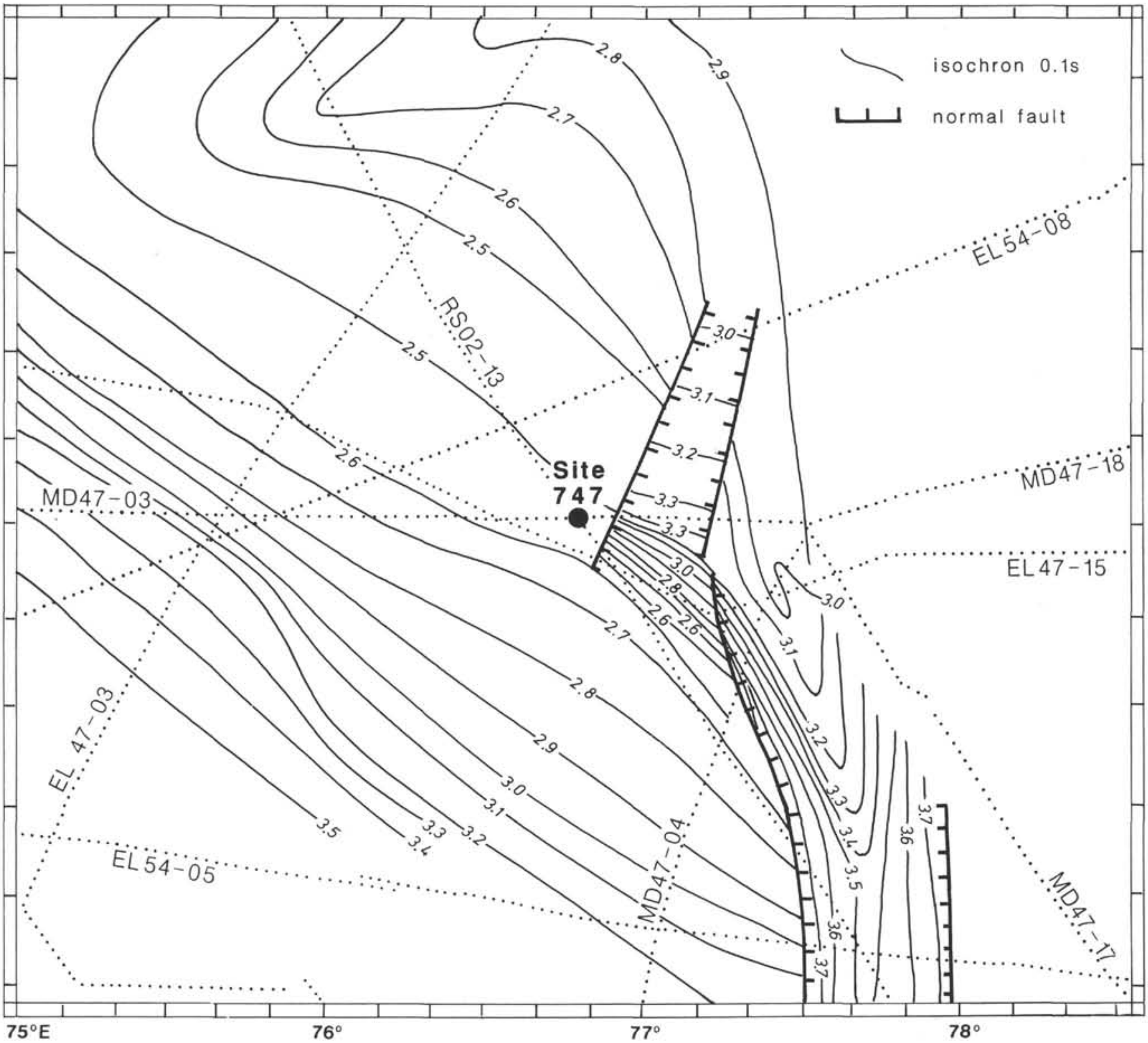

Figure 5. Isochron map of the top of the acoustic basement contoured in seconds (TWT).

vertical heave. The confused swells had a period of 5–6 s, and the drill string heave compensator could not maintain a constant weight on the drill bit; weight on the bit was fluctuating between 0 and 20,000 lb. After coring 54 m into basalt and meeting all of the scientific objectives, the hole was conditioned for logging.

A wiper trip was made up to 100 mbsf and back to bottom. The hole appeared to be in good condition to log. The mechanical bit release (MBR) was successfully released, and the hole was displaced with polymer mud. The trip out to logging depth at 1810 m was unusually slow due to the roll and pitch of the ship.

The logging sheaves were rigged, and after one misrun, one successful suite of logging tools was run. Logging tools consisted of DITE, SDT, MCD, NGT, and TCC (see "Explanatory Notes" chapter, this volume, and "Logging" section, this chapter). The logging tools were rigged down, but the remaining two logging runs were canceled because of the deteriorating weather conditions. An attempt was made to pull the BHA clear of the mud line; after a near accident on the rig floor, however, it was decided to ride out the storm with the drill collars below the mud line.

For the next 4 hr, the wind was in excess of 50 kt and the confused swells were over 20 ft, causing the ship to take rolls more than 20° with 12 ft of vertical heave. After 9-1/2 hr of WOW, sea conditions had improved and normal operations were resumed. Since only traces of methane gas were detected, the hole was left filled with logging mud. The pipe was tripped out, and the ship was underway to Site 748 (SKP-3C) at 1730 hr (L), 12 March 1988.

The coring summary for Site 747 appears in Table 1.

LITHOSTRATIGRAPHY AND SEDIMENTOLOGY

Introduction

Site 747 was drilled in 1695.8 m of water on a broad terrace in the transition zone between the northern and southern parts of the Kerguelen Plateau. The overall lithology of the 295.1-m-

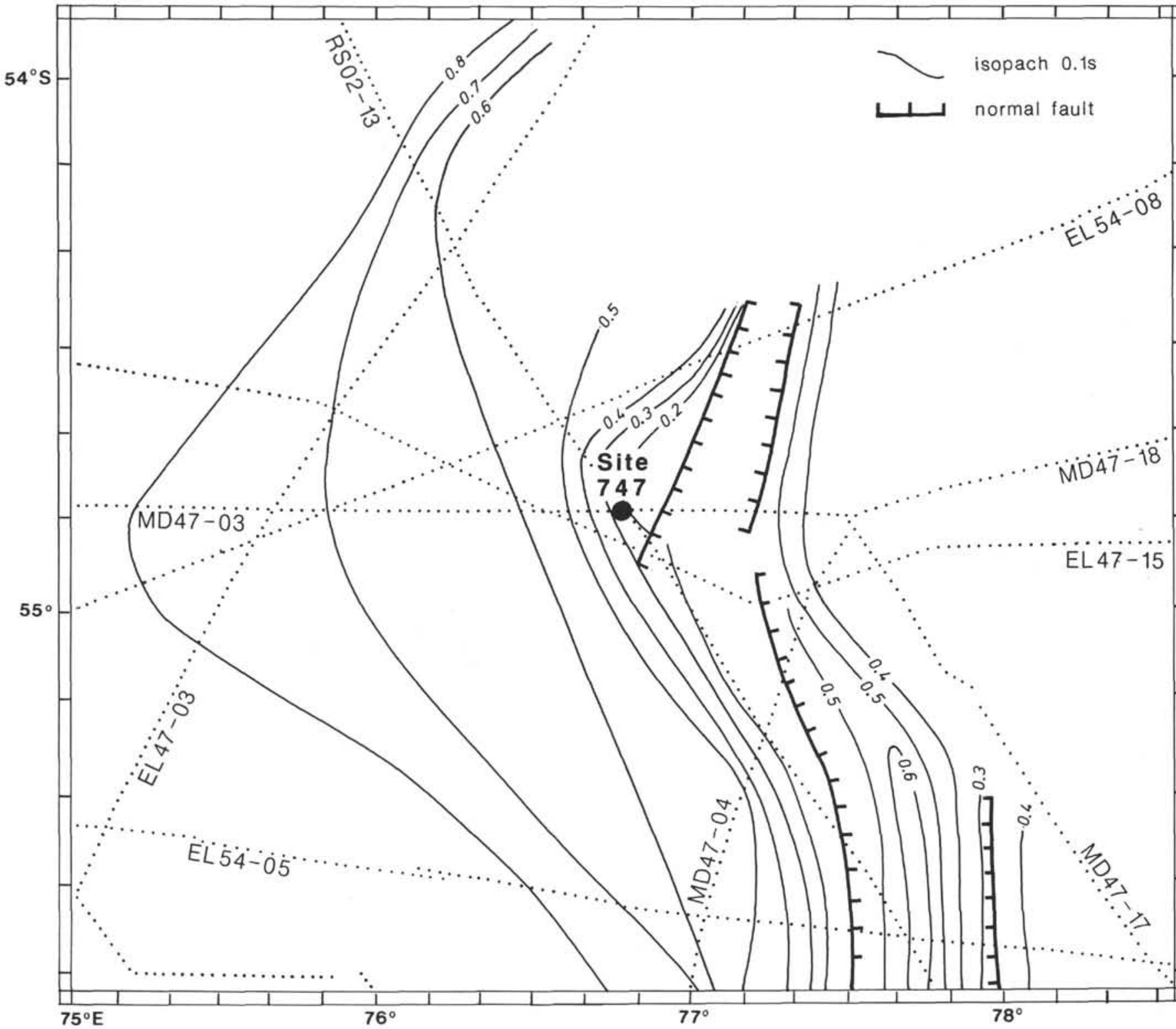

Figure 6. Total sediment isopach map contoured in seconds of reflection time.

thick Upper Cretaceous through Neogene section consists of pelagic carbonate oozes and chalks, with intercalated levels of diatom ooze and vitric ash near the top, minor hardgrounds and volcaniclastic sands to pebbles in the middle, and black chert in the lower section. The three holes drilled at Site 747 were complementary.

In Hole 747A, APC cores to 151.5 mbsf had almost 100 percent recovery and minor to moderate disturbance; XCB cores to 256.0 mbsf had only modest disturbance and good recovery (generally greater than 65%), except in some mixed chalk/volcaniclastic and chert horizons. Hole 747B recored the interval down to 50.3 mbsf with the APC, recovering nearly 100% of an only slightly disturbed section for Neogene paleoceanography. Holes 747A and 747B could be correlated on a centimeter scale by vitric ash layers and magnetic susceptibility. The holes showed good overlap of cored sections, with only about 2-m depth discrepancy. At Hole 747C the Paleogene-Maestrichtian interval was rotary cored from 159.0–206.5 mbsf before continuing the hole from 252.0 mbsf to basement. Problems arise in the correlation between the middle part of the section in Holes 747A and 747C due to differences in apparent amounts of volcaniclastic debris. This is partly a reflection of core recovery, but it is also caused by local variations in thickness of the Upper Cretaceous volcanogenic gravels.

Lithologic Summary

We divided the sedimentary section at Site 747 into four lithologic units (see Table 2). Unit I consists of upper Neogene (Quaternary to upper Miocene) with cream-colored oozes and abundant diatoms. The boundary to the second unit was chosen in a gradational interval where oozes change to more uniform and noticeably whiter hues, with predominantly nannofossils but with pulses of increased foraminiferal abundance. Unit II is divided into three subunits to note distinctive aspects of a >90% carbonate facies consisting of white nannofossil ooze underlain by pale nannofossil chalk with foraminifers, followed by mottled white nannofossil chalk with large burrows.

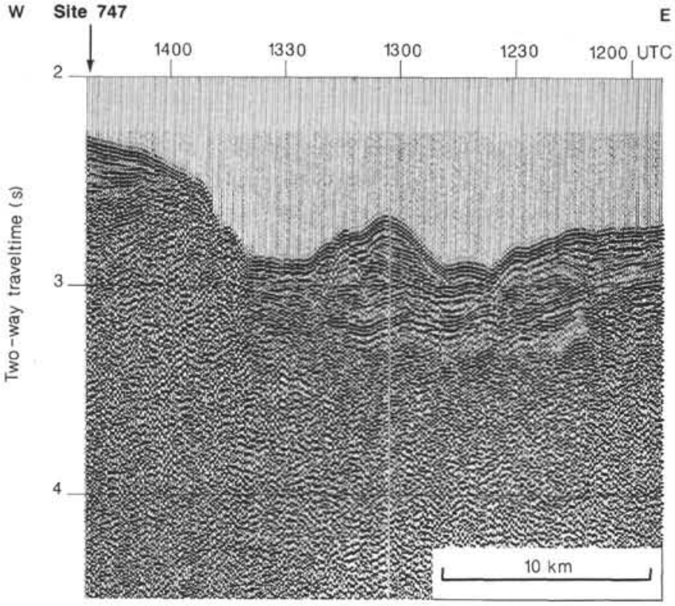

Figure 7. *JOIDES Resolution* single channel reflection profile on approach to Site 747.

Although Unit III is thin, we separated it from the rest of the section to accentuate the significance of the volcaniclastic interval. The boundary was chosen at the top of the first volcaniclastic gravels, although volcanic clasts are sprinkled into chalks over several meters above this contact. Unit IV consists of Upper Cretaceous pure white nannofossil chalks and black cherts that are similar to those in many Deep Sea Drilling Project (DSDP) sections described in the western Pacific. Sediments directly above the basement were poorly recovered and included only a few fragments of a glauconitic bioclastic grainstone and some possibly basaltic gravel. Unit V consists of basaltic basement.

Figure 9 provides a summary lithologic column with core recovery, depths, lithologic units, and age boundaries reflecting the status during shipboard reports.

Lithologic Units

Unit I: Foraminifer Diatom Oozes

Interval: Cores 120-747A-1H to 120-747A-4H-5, 32 cm, and Cores 120-747B-1H to 120-747B-5H-1, 140 cm.
Depth: 0–34.3 mbsf (Hole 747A) and 0–32.7 mbsf (Hole 747B).
Total thickness: 34.3 m (Hole 747A) and 32.7 m (Hole 747B).
Age: Pleistocene to early Pliocene.

Unit I is mainly a foraminifer diatom ooze with varying proportions of planktonic and benthic foraminifers. The mean grain size is over 63 μm, reflecting foraminifer abundances (see Fig. 10 and Table 3). The carbonate content varies from <20% in the topmost diatom-rich intervals in Cores 120-747A-1H and 120-747B-2H, rising to 60% within a few meters sub-bottom, then increasing to over 90% toward the gradational base of Unit I around 40 mbsf (see Fig. 10). Second-order fluctuations of 10% in calcium carbonate probably reflect variations in diatom abundances.

The unit is layered on a meter scale with fuzzy gradational color boundaries in various pale peach-colored tones ranging from pink (5YR 7/3) diatom ooze, to dominantly white (10YR 8/2 and 8/1) and light gray (10YR 7/2 and 7/1) foraminifer diatom ooze. Figure 11 illustrates the sharp contact between diatom and foraminifer nannofossil oozes. Slightly darker tones mark intervals with greater foraminifer abundances. Preservation of both diatoms and foraminifers seems excellent, as was observed by the presence of a few delicate spiny ostracod shells in Core 120-747A-3H-CC.

Coarse fraction samples (>63 μm) from core catchers (e.g., Core 120-747A-3H-CC) showed considerable variety of minor accessory components, including black and red volcanic rock fragments, vesicle fragments, clear pumice ash shards, feldspars, clinopyroxene, amphibole, dark biotite, palagonite, and fresh glass, with ubiquitous diatoms and foraminifers. Benthic foraminifers were present, and two unusual, 5-mm-large *Cyclammina* were noted in Core 120-747A-1H-CC.

Magnetic susceptibility measurements correlating cores from Holes 747A and 747B (Fig. 12) indicate the abundance of volcanogenic components in the oozes and, in particular, highlight the vitric ash layers. These suggest that excellent recovery was achieved and that the two holes have core offsets of about 2 m.

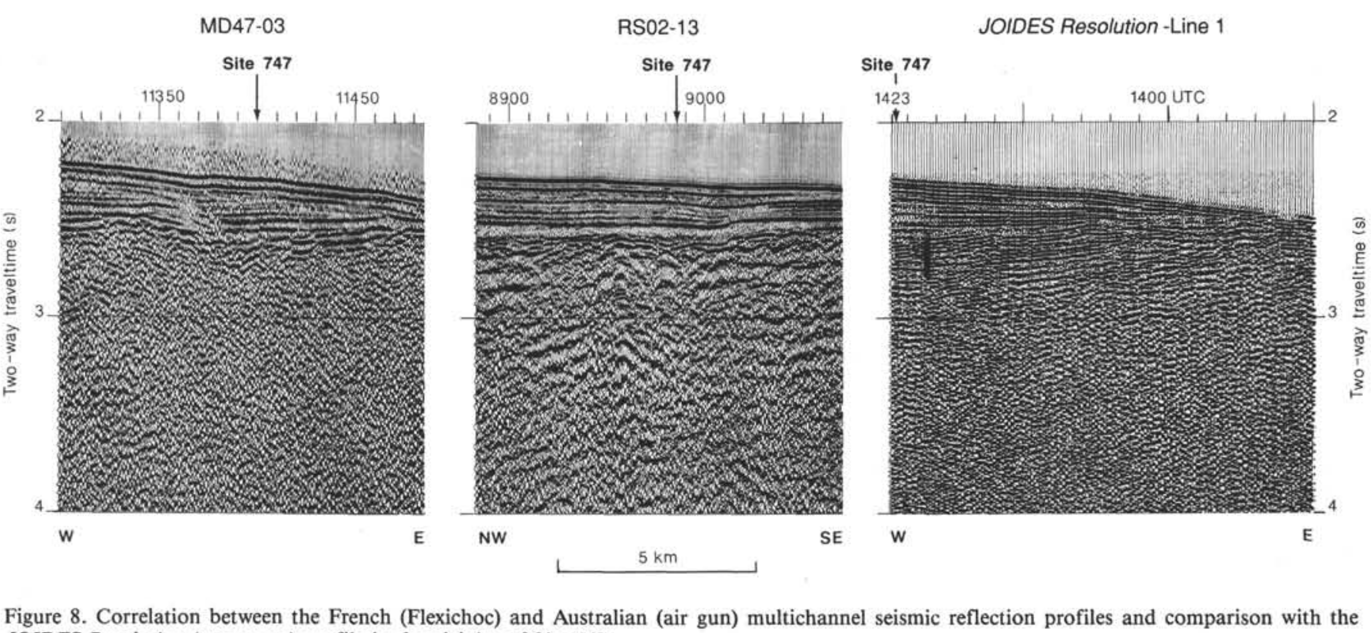

Figure 8. Correlation between the French (Flexichoc) and Australian (air gun) multichannel seismic reflection profiles and comparison with the *JOIDES Resolution* (water gun) profile in the vicinity of Site 747.

Table 1. Coring summary, Site 747.

Core no.	Date (March 1988)	Time (UTC)	Depth (mbsf)	Cored (m)	Recovered (m)	Recovery (%)
120-747A-						
1H	7	1100	0-9.0	9.0	9.00	100.0
2H	7	1200	9.0-18.5	9.5	9.97	105.0
3H	7	1240	18.5-28.0	9.5	8.27	87.0
4H	7	1420	28.0-37.5	9.5	9.95	105.0
5H	7	1520	37.5-47.0	9.5	9.85	103.0
6H	7	1630	47.0-56.5	9.5	9.67	102.0
7H	7	1745	56.5-66.0	9.5	9.92	104.0
8H	7	1850	66.0-75.5	9.5	9.65	101.0
9H	7	1945	75.5-85.0	9.5	10.22	107.6
10H	7	2100	85.0-94.5	9.5	9.61	101.0
11H	7	2320	94.5-104.0	9.5	10.00	105.2
12H	8	0030	104.0-113.5	9.5	10.11	106.4
13H	8	0130	113.5-123.0	9.5	9.73	102.0
14H	8	0330	123.0-132.5	9.5	9.76	103.0
15H	8	0430	132.5-142.0	9.5	9.85	103.0
16H	8	0545	142.0-151.5	9.5	9.93	104.0
17X	8	0830	151.5-161.0	9.5	8.20	86.3
18X	8	0915	161.0-170.5	9.5	4.28	45.0
19X	8	0950	170.5-180.0	9.5	6.22	65.5
20X	8	1030	180.0-189.5	9.5	2.62	27.6
21X	8	1105	189.5-199.0	9.5	6.54	68.8
22X	8	1135	199.0-208.5	9.5	8.81	92.7
23X	8	1220	208.5-218.0	9.5	9.88	104.0
24X	8	1305	218.0-227.5	9.5	7.32	77.0
25X	8	1400	227.5-237.0	9.5	6.55	68.9
26X	8	1450	237.0-246.5	9.5	5.91	62.2
27X	8	1535	246.5-256.0	9.5	5.52	58.1
Coring totals				256.0	227.34	88.8
120-747B-						
1H	8	2000	0-2.8	2.8	2.81	100.0
2H	8	2030	2.8-12.3	9.5	8.60	90.5
3H	8	2110	12.3-21.8	9.5	9.49	99.9
4H	8	2205	21.8-31.3	9.5	8.83	92.9
5H	8	2245	31.3-40.8	9.5	9.75	102.0
6H	9	0100	40.8-50.3	9.5	9.43	99.2
Coring totals				50.3	48.91	97.2
120-747C-						
1R	9	1930	159.0-168.5	9.5	7.70	81.0
2R	9	2010	168.5-178.0	9.5	7.47	78.6
3R	9	2055	178.0-187.5	9.5	4.19	44.1
4R	9	2200	187.5-197.0	9.5	0.31	3.3
5R	9	2250	197.0-206.5	9.5	1.03	10.8
6R	10	0155	252.0-261.5	9.5	1.61	16.9
7R	10	0230	261.5-271.0	9.5	1.95	20.5
8R	10	0310	271.0-280.5	9.5	1.24	13.0
9R	10	0400	280.5-290.0	9.5	1.83	19.2
10R	10	0625	290.0-295.1	5.1	1.81	35.5
11R	10	1300	296.6-303.0	6.4	3.20	50.0
12R	10	1550	303.0-312.5	9.5	4.50	47.3
13R	10	1830	312.5-322.0	9.5	2.86	30.1
14R	10	2050	322.0-331.5	9.5	1.40	14.7
15R	11	0001	331.5-341.0	9.5	3.90	41.0
16R	11	0320	341.0-350.5	9.5	4.50	47.3
Coring totals				144.5	49.50	34.3

Apparently, Hole 747A began slightly below the true mud line as a result of high ship heave (see also "Operations" section, this chapter). Hole 747B appears to represent a slightly thicker section.

Ice-Rafted Debris

Ice-rafted debris (IRD) occurs as coarse sand particles disseminated (<2%) mainly in Cores 120-747A-1H and -2H and in Cores 120-747B-1H and -2H (see Fig. 13). The main intervals noted are listed in Table 4. Dark fine, sand-sized specks in Core 120-747A-1H are attributed to micronodules. The IRD occurrences at core tops (e.g., Cores 120-747B-2H-1, 0-60 cm, and 120-747A-6H-1, 0-1 cm) are possibly displaced stratigraphically by downhole caving.

Ash

Vitric ash (see Fig. 10) was noted in several horizons as both discrete beds and admixtures in the horizons listed in Table 5.

Unit II: White Nannofossil Ooze and Nannofossil Chalk

Intervals: Cores 120-747A-4H-5, 32 cm, to 120-747A-20X-2, 45 cm; Cores 120-747B-5H-1, 140 cm, to 120-747B-6H-CC (TD); and Cores 120-747C-1R to 120-747C-3R-3, 49 cm.
Depth: 34.3-181.9 mbsf (Hole 747A), 32.7-50.3 mbsf (Hole 747B); and 159.0-180.9 mbsf (Hole 747C).
Thickness: 147.6 m (Hole 747A), 17.6 m (Hole 747B), and 21.9 (Hole 747C).
Age: late Miocene to Paleocene.

Subunit IIA: White Nannofossil Ooze

Intervals: Cores 120-747A-4H-5, 32 cm, to 120-747A-16H-CC; and Cores 120-747B-5H-1, 140 cm, and 120-747B-6H-CC (TD).
Depth: 34.3-151.5 mbsf (Hole 747A) and 32.7-50.3 mbsf (Hole 747B).
Thickness: 117.2 m (Hole 747A) and 17.6 m (Hole 747B).
Age: late Miocene-late Oligocene.

Subunit IIA is mainly uniform, firm nannofossil ooze in shades of brilliant white (10 YR 8/1, 2.5Y 8/1, N8) or light gray (10YR 7). Bulk-density measurements (Fig. 10) clearly delineate the Unit I/Subunit IIA boundary (see also "Physical Properties" section, this chapter). Foraminifers persist throughout this unit. Other minor components include radiolarians and traces of tiny glass or volcanic fragments. There are few visible structures. Faintly bioturbated zones and some gray streaks outline evidence of bedding on a meter scale, and faintly mottled darker zones (10YR 8/2) generally have more foraminifers.

Cores 120-747A-6H to -13H are particularly uniform, pure nannofossil ooze with more than 90% carbonate (Fig. 10) and low grain size means between 11-20 μm (Fig. 10). Intervals of creamy hues return in Core 120-747A-13H-5, 85 cm, with traces of volcanic ash and possibly ice-rafted 3-mm subangular quartz grains in Core 120-747A-13H-5, 85 cm. Grain size increases to a mean of 40 μm, which mirrors a greater foraminifer abundance. We observed vitric ash beds with fresh feldspars, unaltered pumiceous shards, and pyroxene in Core 120-747A-7H-3, 63-140 cm, and in several intervals of Section 120-747A-16H-5. The contact with Subunit IIB is gradational.

Subunit IIB: Pale Brown Nannofossil Chalk with Foraminifers

Intervals: Cores 120-747A-17X-1, 0 cm, to 120-747A-19X-1, 2 cm; and Cores 120-747C-1R-1, 0 cm, to 120-747C-2R-4, 133 cm.
Depth: 151.5-170.5 mbsf (Hole 747A) and 159.0-174.3 mbsf (Hole 747C).
Thickness: 19.0 m (Hole 747A) and 15.3 m (Hole 747C).
Age: late Oligocene-early Eocene.

Cores 120-747A-17X and 120-747A-18X are composed of nannofossil chalk with foraminifers and exhibit slightly darker cyclic alternations of cream-colored shades of very pale brown (10YR 7/2), very pale yellow (10YR 7/3), light gray (10YR 7/2), and white (10YR 8/2). Faint burrow mottling is visible and all contacts are gradational. Drilling disturbances are only slight. Core 120-747A-17X marks the transition from firm ooze to soft chalk, partly as a result of the switch over from APC to XCB coring; a few "biscuits" occur, possibly also as a result of the change in coring technique.

Table 2. Summary of dominant lithologic units, Site 747, Southern Kerguelen Plateau.

Unit and subunit	Lithology	Features	Depth (mbsf, hole)	Core intervals	Thickness (m, hole)	Age
I	Foraminifer diatom ooze	Meter-scale gradational variation	0–34.3 (A)	120-747A-1H (top) to 120-747A-4H-5, 32 cm	34.3 (A)	Pleistocene to early Pliocene
			0–32.7 (B)	120-747B-1H to 120-747B-5H-1, 140 cm	32.7 (B)	
IIA	White nannofossil ooze	Foraminifer content variable, white, uniform	34.3–151.5 (A)	120-747A-4H-5, 32 cm, to 120-747A-16H-CC	117.2 (A)	late Miocene to late Oligocene
			32.7–50.3 (B)	120-757B-5H-1, 140 cm, to TD	17.6 (B)	
IIB	Nannofossil chalk with foraminifers	Very pale brown to white	151.5–170.5 (A)	120-747A-17X-1, 0 cm, to 120-747A-19X-1, 2 cm	19.0 (A)	late Oligocene to early Eocene
			159.0–174.3 (C)	120-747C-1R, to 120-747C-2R-4, 133 cm	15.3 (C)	
IIC	White burrowed nannofossil chalk	Large burrows white-grey	170.5–181.9 (A)	120-747A-19X-1, 2 cm, to 120-747A-20X-2, 45 cm	11.4 (A)	early Eocene to Paleocene
			174.3–180.9 (C)	120-747C-2R-4, 133 cm, to 120-747C-3R-3, 49 cm	6.6 (C)	
III	Volcaniclastic sand, breccia, and cobbles	Multicolored polygenic, with clay clasts, weathered igneous rocks	181.9–189.5 (A)	120-747A-20X-2, 45 cm, to 120-747A-21X-1, 2 cm	7.6 (A)	early Paleocene to late Maestrichtian
			180.9–206.5 (B)	120-747C-3R-3, 49 cm, to 120-747C-5R-CC	25.6 (C)	
IV	Nannofossil chalk and chert	White, laminated, with inoceramids	189.5–256.0 (A)	120-747A-21X-1, 2 cm, to TD	66.5 (A)	late Maestrichtian to early Santonian
		glauconite phosphate	206.5–295.1 (C)	120-747C-5R-CC to 120-747C-10R-CC	88.6 (C)	
V	Basalt		296.6–350.5 (C)			

Note: An approximate 1-m-thick gap exists between the base of the sediments and the top of the basement.

Foraminifers are distinctly more abundant, as are traces of black opaque silt (volcaniclastics, micronodules[?], and brown volcanic glass) visible on the split core surfaces. Together these explain an increase in mean grain size to nearly 60 μm. An olive ash layer occurs in Core 120-747A-17X-4, 67–74 cm. Smear slides of the coarse fraction and dark burrow fills confirm the presence of polygenetic mixtures of accessory volcaniclastics, with palagonite blebs, opaques, igneous fragments, and dark, altered glass. Benthic foraminifers are common. Cores 120-747C-1R, -2R, and -3R consist of nannofossil chalks with foraminifers that were not recovered in Hole 747A. The color schemes are similar, with very pale brown to white; bioturbation and large mottles are visible wherever cut surfaces are smooth.

Hardgrounds

A distinctive feature of Subunit IIB is the appearance of abrupt, thin hardgrounds in Core 120-747C-2R-1, 87–93 cm (Fig. 14), Sections 120-747C-2R-3, 142–143 cm, and 120-747C-2R-4, 133 cm. The uppermost 7-cm bed has a very sharp base, with light olive (10YR 6/6) hard calcareous claystone grading up to an irregular, laminated top with 1–1.5 cm of finely laminated black manganese crusts showing thin translucent reddish lamellae. These appear as cryptocrystalline, dispersed reddish blebs in smear slides, identified as collophane (phosphate) by visual inspection and X-ray diffraction (XRD). The olive claystone consists of nannofossils and clay with idiomorphic zeolite clusters, which may be clinoptilolite.

Between the layers there is a gradational zone with micronodules, as well as millimeter-size reddish chips mixed with olive claystone. The manganese nature seems confirmed by pyrolusite XRD patterns, which also indicate concentrations of smectite, illite, and kaolinite. The other two hardgrounds are less distinct, but are marked by a centimeter-thick, slightly more indurated white chalk and outlined by thin manganese stringers. These display penetration of upper sediments from downward burrowing. A round, crunchy, dark gray pebble occurs *in situ* in Core 120-747C-1R-1, 108 cm. It is composed of two idiomorphic, clear minerals, one of high birefringence and high relief and the other of low relief and low birefringence. These are tentatively identified as epidote and albite or zeolite, respectively.

Subunit IIC: White Nannofossil Chalk with Large Burrows

Interval: Cores 120-747A-19X-1, 2 cm, to 120-747A-20X-2, 45 cm, and Cores 120-747C-2R-4, 133 cm, to 120-747C-3R-3, 49 cm.
Depth: 170.5–181.9 mbsf (Hole 747A) and 174.3–180.9 mbsf (Hole 747C).
Thickness: 11.4 m (Hole 747A) and 6.6 m (Hole 747C).
Age: early Eocene to Paleocene.

The contact with Subunit IIC is sharp, defined by a thin white hardground outlined by manganese micronodules. The burrow fillings are filled with cream-colored hues from above, but the host chalk is snow white (N8) to gray (N6). The boundary is seen as a distinct change in bulk density (Fig. 10). This thin subunit of dominantly white (N8, 10YR 8/1), brittle, nannofossil chalk has a distinctive burrow structure ("egg shell") caused by overlapping centimeter-scale oval burrows (*Cylindrichnus*?) (Fig. 15).

The burrows are outlined by light to medium gray liesegangs, with micronodules, and many have white haloes. Other burrow tracks, outlined in dark gray, include several horizons with *Zoophycos* as well as a few zones of *Planolites.* Round burrow centers are commonly granular and filled with reworked foraminifers. In several sections, gray fractures radiate outward from burrow walls. The sediment package is considered coherent and not slumped; flow structures visible in some zones were identified as core disturbance due to plug rotations. Smear slides of chalk show that nannofossils make up 95% of the calcareous component. Carbonate content drops from 90% to 75%, probably reflecting dilution by volcanogenic admixtures (Fig. 10).

Holes 747A and 747C show similar features and can perhaps be correlated by two zones of scattered dark brown millimeter-size, smectitic clay pellets (e.g., Core 120-747C-2R-5, 17 cm and 21 cm, and Core 120-747A-19X-4, 112 cm). A second feature of significance is the presence of more thin hardground zones, typically only 1 cm thick, with brittle yellowish chalk and some

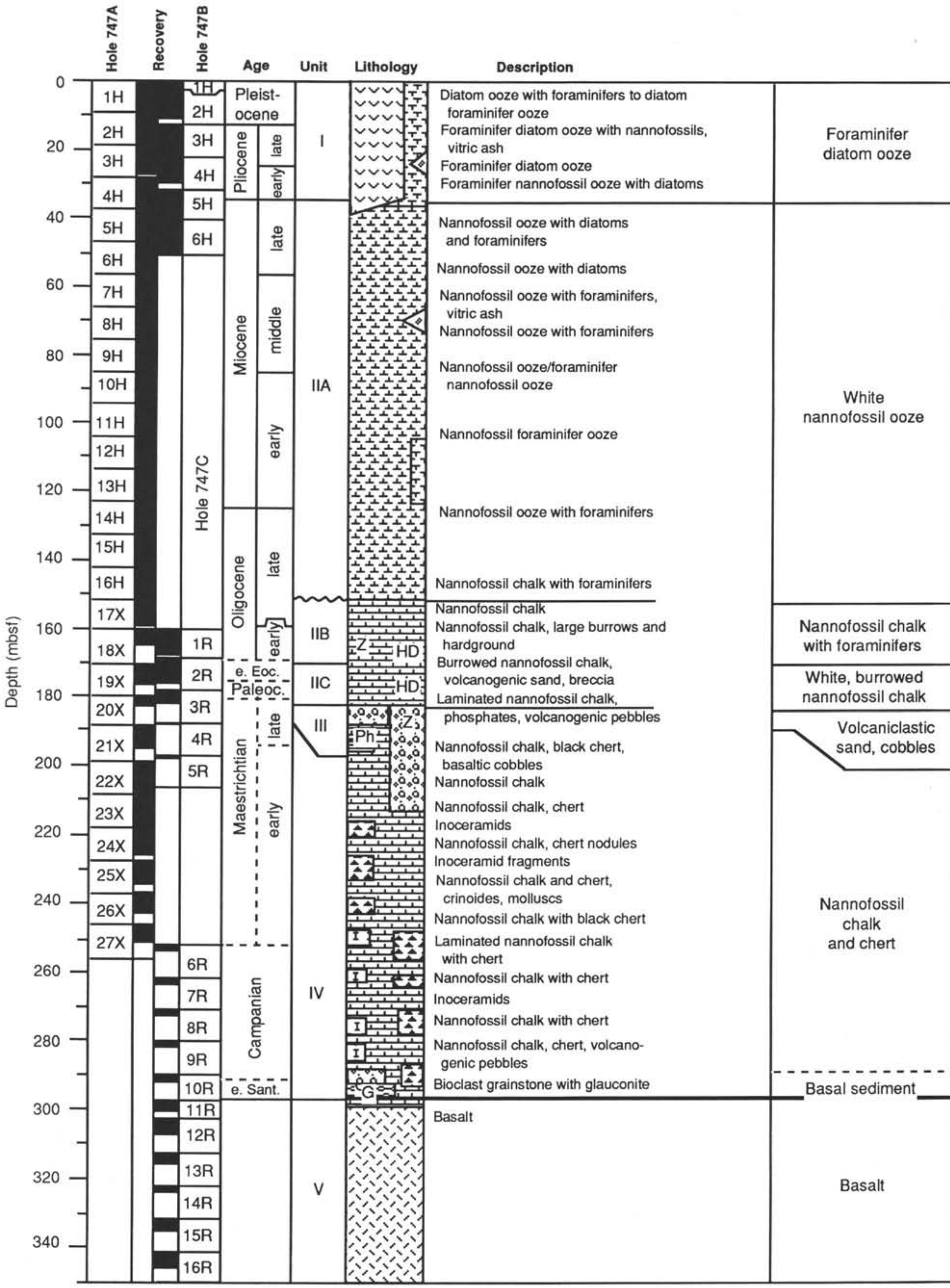

Figure 9. Lithostratigraphy of Site 747, Southern Kerguelen Plateau. Recovered intervals are indicated by shading in the recovery column. HD = hardground, I = inoceramid debris, Z = zeolite, P = phosphate, and G = glauconite. For a key to patterns in the lithology column, see "Explanatory Notes" chapter, this volume.

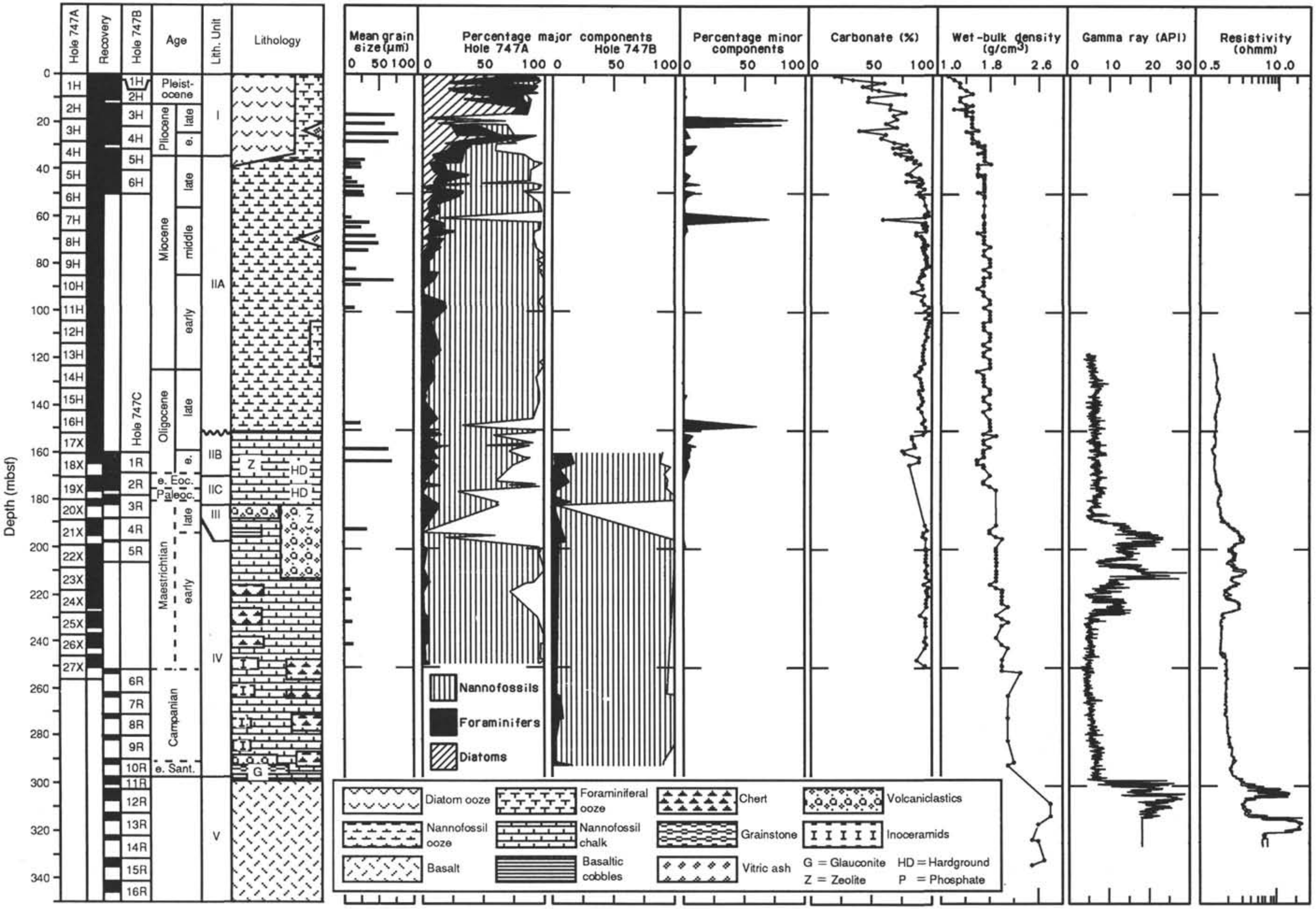

Figure 10. Lithological summary, Site 747. Downhole mean grain size plotted vs. sub-bottom depth, measured with a Labtec 100, laserscan automatic particle-size analyzer; summary plots of downhole smear slide data and ash levels; downhole variation of carbonate and wet-bulk density measurements plotted vs. sub-bottom depth; gamma-ray and resistivity logs showing basal units for Hole 747A.

Table 3. Mean grain size and sand/silt/clay percent, Site 747.

Core, section, interval (cm)	Depth (mbsf)	Mean grain size (μm)	Sand (%)	Silt (%)	Clay (%)
120-747B-3H-3, 50-52	17.30	72.1	53.0	43.0	4.0
120-747A-3H-2, 54-55	20.54	56.6	50.0	48.0	2.0
120-747A-3H-5, 52-54	25.02	76.0	60.0	37.0	4.0
120-747B-4H-5, 53-55	28.33	61.3	47.0	48.0	5.0
120-747A-4H-6, 50-52	36.00	28.6	14.0	72.0	14.0
120-747A-4H-7, 50-52	37.50	22.9	8.0	81.0	11.0
120-747B-5H-6, 50-52	39.30	23.9	9.0	81.0	10.0
120-747B-6H-2, 105-107	43.35	11.0	2.0	64.0	36.0
120-747A-5H-6, 50-52	45.50	18.5	4.0	80.0	16.0
120-747A-5H-7, 50-52	47.00	28.0	15.0	78.0	3.0
120-747A-6H-2, 100-102	49.50	26.4	12.0	79.0	7.0
120-747A-6H-3, 95-97	50.95	28.4	15.0	77.0	8.0
120-747A-7H-3, 50-52	60.00	10.0	0	71.0	29.0
120-747A-7H-4, 120-122	62.20	35.6	22.0	69.0	9.0
120-747A-7H-6, 50-52	64.50	24.9	11.0	81.0	8.0
120-747A-8H-2, 50-52	68.00	45.6	39.0	57.0	4.0
120-747A-8H-4, 50-52	71.00	48.4	41.0	54.0	5.0
120-747A-8H-6, 50-52	74.00	34.6	24.0	69.0	7.0
120-747A-9H-5, 54-56	82.04	17.2	2.0	83.0	15.0
120-747A-9H-8, 50-52	86.50	71.6	57.0	41.0	2.0
120-747A-10H-3, 50-52	88.50	24.3	10.0	78.0	12.0
120-747A-11H-3, 60-62	98.10	15.7	2.0	77.0	21.0
120-747A-13H-5, 50-53	120.00	44.8	35.0	58.0	7.0
120-747A-14H-4, 50-52	128.00	55.4	40.0	54.0	4.0
120-747A-14H-CC	132.50	57.8	44.0	47.0	9.0
120-747A-15H-4, 55-57	137.55	14.1	5.0	63.0	22.0
120-747A-16H-4, 49-51	146.99	23.9	11.0	75.0	14.0
120-747A-17X-5, 52-54	158.02	63.9	55.0	40.0	5.0
120-747A-18X-2, 60-62	163.10	69.0	53.0	43.0	4.0
120-747A-21X-2, 94-96	191.94	33.8	17.0	72.0	11.0
120-747A-23X-7, 10-12	217.60	9.1	2.0	86.0	12.0
120-747A-24X-3, 50-52	221.50	9.9	0	87.0	13.0
120-747A-25X-3, 50-52	231.50	11.3	2.0	80.0	18.0
120-747A-26X-3, 50-52	240.50	13.3	1.0	75.0	24.0

thin concentrations of manganese beneath (e.g., the top of Core 120-747C-2R-4, 133 cm, Core 120-747A-19X-4, 117 cm, and in Sections 120-747A-20X-2 and 120-747C-3R-3).

A third feature of significance is the upward-declining abundance of pebble-to-sand size, angular to rounded volcanogenic clasts (mostly red, green, and black smectitic clay clasts) unsorted and randomly sprinkled into the chalk as individual grains or in small pods. These volcaniclastic components are similar to those in Unit III. They are not layered, except for a few centimeter-thick layers near the base of the unit, but appear to have rained into the oozes. Finally, this chalk subunit has shallow-water macrofossil remnants, including a few bivalve shells in Core 120-747A-19X-2, 119 cm, and a single 1/2-cm-large specimen of a larger benthic foraminifer genus.

The contact with the underlying volcaniclastics is sharp and is marked by a crenulated surface, although volcanogenic clasts persist into the directly overlying chalks.

Unit III: Multicolored Volcaniclastics, Polygenetic Sands, Breccia, and Cobbles

Intervals: Cores 120-747A-20X-2, 45 cm, to 120-747A-21X-1, 2 cm; Cores 120-747C-3R-3, 49 cm, to 120-747C-5R-CC.
Depth: 181.9–189.5 mbsf (Hole 747A) and 180.9–206.5 mbsf (Hole 747C).
Thickness: 7.6 m (Hole 747A) and 25.6 m (Hole 747C).
Age: early Paleocene to late Maestrichtian.

Unit III is a mixture of green, red, black, and white components and was only recovered in the bottom 40 cm of Sections 120-747A-20X-1 and 120-747A-20X-CC. Correlative lithology occurs over a longer interval in Hole 747C, but with poor recovery and more hard cobbles. The upper contacts in both holes are

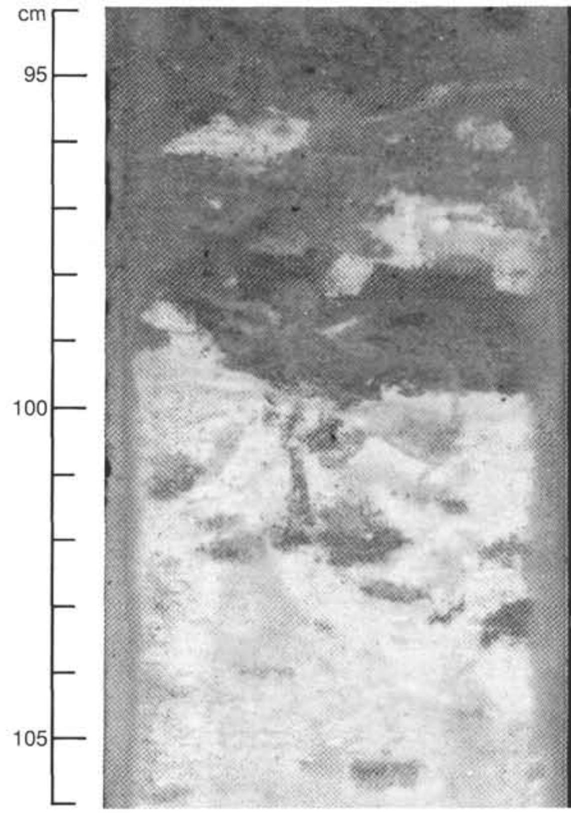

Figure 11. Contact between diatom ooze (darker) and foraminifer ooze (lighter) within Unit I in Core 120-747B-1H-2, 94–106 cm.

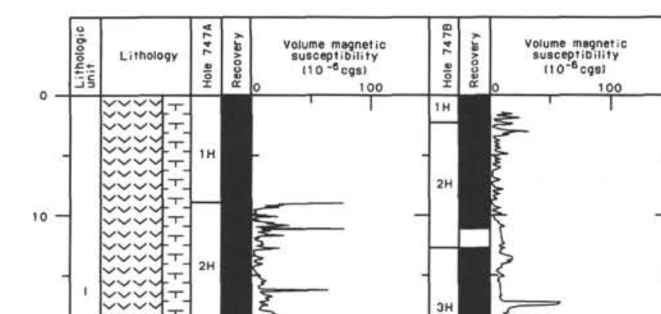

Figure 12. Magnetic susceptibility plot of the uppermost portion of Holes 747A and 747B.

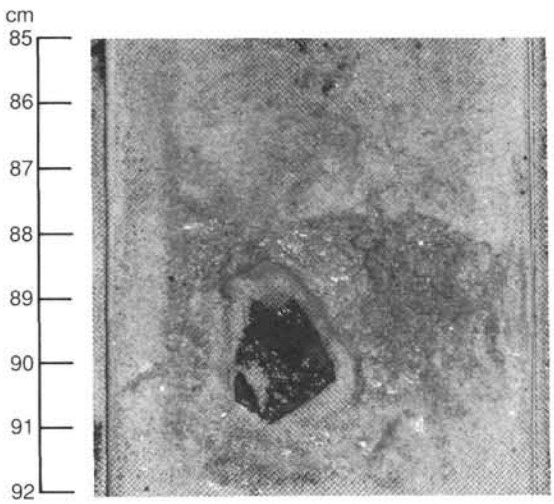

Figure 13. Dropstones in Core 120-747A-1H-6, 85–92 cm.

Table 4. Ice-rafted debris occurrence, Site 747.

Core, section, interval (cm)	Description
120-747A-1H-3, 0–104 cm	Ice-rafted debris throughout
120-747A-1H-6, 0–110 cm	Ice-rafted debris throughout
120-747A-2H-1, 0–150 cm	Ice-rafted debris throughout
120-747A-1H-3, 62 cm	Dropstone, basaltic
120-747A-2H-1, 88 cm	Dropstone, quartz
120-747A-2H-2, 11 cm	Dropstone, quartzite
120-747A-3H-1, 76 cm	Dropstone, weathered amphibole-bearing microgranite
120-747A-3H-4, 130 cm	Dropstone, volcaniclastic
120-747A-6H-1, 0–1 cm	Dropstone, diorite (downhole caving?)
120-747B-2H-1, 0–60 cm	Dropstone (downhole caving?)

Table 5. Volcanic ash occurrence, Site 747.

Core, section, interval (cm)	Description
120-747A-1H-6, 30–42	Trace
120-747A-1H-6	Dark specks throughout
120-747A-3H-1, 25–42 and 120-747A-3H-2, 116–124	Light olive gray (5Y 6/2) vitric ash, sand size, faintly graded, sharp basal contact, clear glass shards, angular, pipe vesicles, and including gas bubbles
120-747B-3H-4, 45–70	Brown ash
120-747B-3H-5, 143 cm, through 120-747B-3H-6, 5 cm	Grayish brown, silt-size vitric ash with shards more altered
120-747B-4H-5, 10–30	Brown vitric ash mixed in foraminifer diatom ooze

practically identical and are well preserved, with slight drill disturbance. They show parallel laminations in some zones and beds of coarser particles, and two or three 5-cm bands of reddish brown silty sand (Fig. 16).

Unit III consists of a stratified sediment of coarse sand to cobble-size gravels, in which most of the clasts are actually smectitic clays or devitrified volcanics. Sorting is poor to moderate and is best seen in some layers of sand-size, well-sorted clay pellets. There is little evidence of graded bedding except in a few centimeter-thick silt interlayers. Some decimeter-thick beds show poorly developed grading over short intervals above parallel stratification, and there are massive beds above. However, the entire unit seems to fine upward.

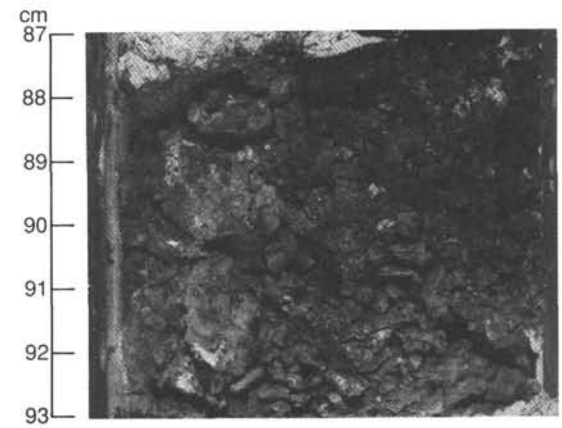

Figure 14. Manganese oxide hardground (corresponding to a hiatus) in Core 120-747C-2R-1, 87–93 cm.

Clasts are of polygenetic origin; there are significant admixtures of sedimentary chert, chert with chalk contacts, chalks and a few hard tan limestone fragments, inoceramid fragments, and crinoids, as well as a diverse suite of igneous components, including hard black, aphyric and aphanitic basalt, and ferruginous, weathered vesicular basalt. The harder chert and unaltered volcanic components are typically very angular. These are compacted in a light green to white clay matrix, partly calcareous, best seen in Core 120-747C-4R-CC (Fig. 17).

Clay clasts are typically rounded, as are weathered red and black basaltic pebbles. Many other components are highly angular breccias. Clay clasts are yellowish green, white, dark red, dark gray, brown, orange, pinkish, ferruginous rust, and black waxy smectites. The groundmass and numerous clasts contain abundant clear, 30-μm zeolite crystals. The polished surface textures of several waxy clay clasts show the original hyaloclastic or variolitic basalt structures, including vesicles and original fracture fillings. These show that the pebbles have a history of devitrification before transport. White chalk fragments contain nannofossils and planktonic and benthic foraminifers. Some breccia intervals may also have a component of calcareous cement, as suggested by calcite peaks on XRD traces.

Multiple Beds

Maestrichtian white nannofossil chalk with thin subhorizontal light gray laminae (7.5YR 8/1) and a few drill-brecciated pieces of black vitreous chert occur sandwiched between cobble layers in Sections 120-747C-5R-1 and 120-747C-5R-CC. Smear slides indicate only nannofossils, typically with a trace amount of foraminifers blackened by pyrite lining in chambers. The chalk may be cavings, but its presence opens the possibility that several polygenetic cobble horizons are present at irregular intervals, which would explain the longer section of Unit III in Hole 747C. Logging confirms the presence of perhaps three separate thick beds of volcaniclastics down to 205 mbsf in Hole 747C.

Sediment and Igneous Contacts

Polygenetic cobbles in Section 120-747C-5R-CC include an unusual biotite olivine basalt, a dark diorite intrusive, and phyric basalt with attached sediment. The weathered character of both the biotite basalt and diorite suggest that they were exhumed from an exposed surface. The phyric basalt (Fig. 18) has a cemented pelagic chalky limestone along one margin with some small rounded pebbles of hard basalt and chert with a chalky patina. These suggest that this cobble was once deposited on the

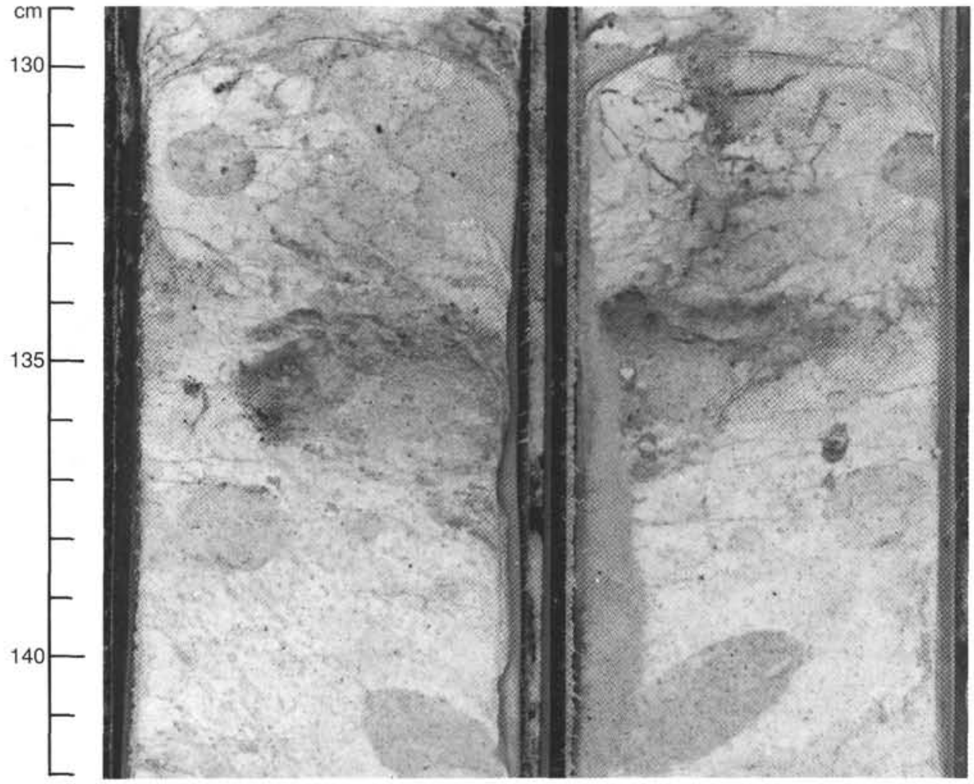

Figure 15. "Egg shell" burrow textures in Core 120-747A-19X-2, 129–142 cm (both working and archive halves are shown).

seafloor and was later exhumed to be included in a second generation cobble conglomerate.

Thin-section examination of Core 120-747C-5R-CC, 1–5 cm, revealed the following: (1) pyroxene plagioclase phyric basalt; (2) sparsely plagioclase pyroxene phyritic basalt; (3) olivine phyric basalt with olivine phenocrysts, plagioclase, titanium dioxides, and clinopyroxene in the groundmass and smectites from devitrification of interstitial glass; (4) sparsely plagioclase pyroxene phyritic basalt; and (5) olivine plagioclase phyric basalt with groundmass plagioclase, olivine, and clinopyroxene as well as smectites from interstitial glasses. These suggest a related suite of medium-grained phyric basalts. Another example of polygenetic depositional history is a large 5-cm clast in Core 120-747C-4R-CC, 8–12 cm, which retains components in the original clay matrix (Fig. 19).

Unit IV: White Nannofossil Chalk and Black Chert

Intervals: Core 120-747A-21X-1, 2 cm, to TD, and Cores 120-747C-5R-CC to 120-747C-10R-CC.
Depth: 189.5–256.0 mbsf (Hole 747A) and 206.5–295.1 mbsf (Hole 747C).
Thickness: 66.5 m (Hole 747A) and 88.6 m (Hole 747C).
Age: late Maestrichtian to early Santonian.

Chalk and Cherts

Unit IV consists mainly of uniform white (10YR 8/1), pure nannofossil chalk with more than 90% carbonate content. The unit is not recrystallized, as shown by the excellent nannofossil preservation, ease of disaggregation,and mean grain size of only 9–13 μm. Foraminifers are rare and are characterized by authigenic pyrite coatings of their inner chamber walls. These are apparent as occasional burrow splotches and streaks of gray. Recovery was hampered by recurring nodules and layers of black (10YR 2/0) vitreous to cloudy cherts, commonly with thin porcellanitic chalk patinas or inclusions (e.g., Fig. 20). Cherts also disturb primary structures. However, in several cores cherts appear in contact with surrounding chalk.

Laminated Chalk and Phosphate

Where the upper parts of Unit IV chalks are undisturbed, they generally show zones with faint greenish laminations that suggest near-suboxic conditions. One section (120-747A-21X-4) displays a unique undisturbed sequence of cyclic units of episodic multicolor laminations overprinting the whitish chalk (Fig. 21). These progress from dark brown through chrome yellow brown (10YR 5/8) and grayish green (5G 5/2) to a bluish turquoise before fading to pale blue green. Rare burrows that cross laminations take on the local color. Yellow brown laminae up to 5 mm seem to have a symmetric structure with thin, brown, brittle phosphate seams along the center.

Cyclic units are about 30 cm thick. Some thin single-grain layers of volcaniclastics (ash?) altered to clay in Core 120-747A-3, 86–93 cm, show reduced, pale blue-green halos in the white chalks, whereas other igneous rock fragments have point-sourced ferruginous yellow halos. All these redox colors fade quickly after splitting. The Maestrichtian chalk intervals with these laminations seem to be devoid of chert. Below this unit, in more cherty sections, the evidence of burrowing is more prevalent.

Bioclastic Grainstone with Glauconite

The lowermost sediments (Cores 120-747A-24X, -25X, and -26X and Cores 120-747C-8R, -9R, and -10R) show scattered inoceramid fragments, rare crinoid stems, rare mollusc fragments, and (in Core 120-747C-10R) additional unidentified bioclasts. Core 120-747C-10R-CC contains a few clasts of a white, calcarenite with cross and parallel laminations highlighted by dark volcaniclastic grains(?), about 10% irregular glauconite pellets, and a few large burrows. The carbonate grains seem to include crinoids and other fine sand-size bioclastic debris. Ad-

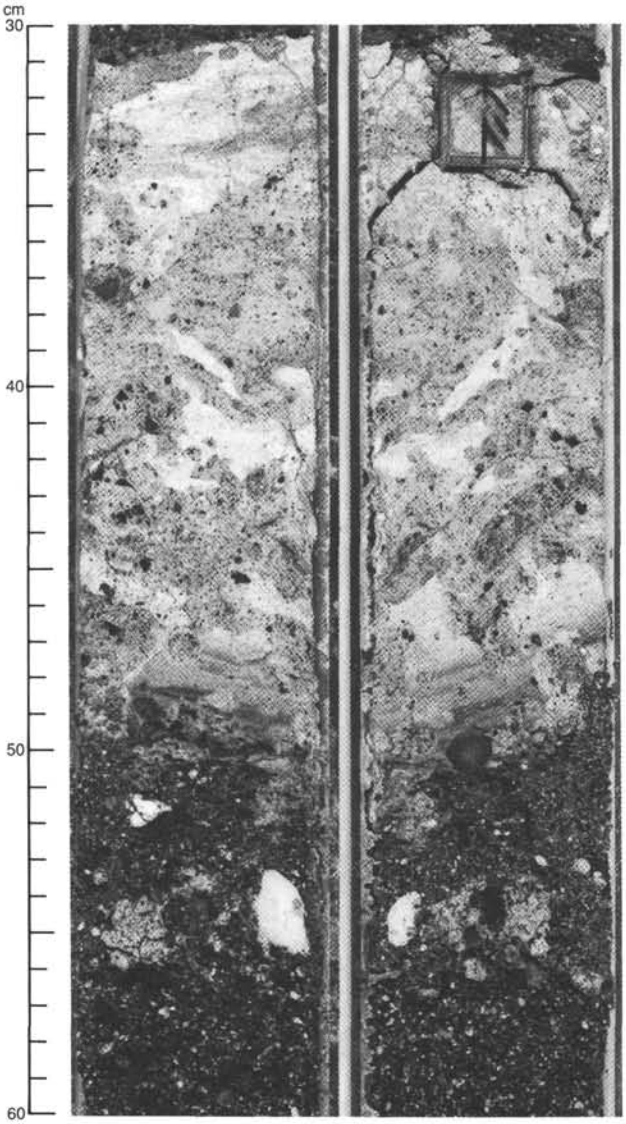

Figure 16. Contact between Unit IIC and III in Core 120-747C-3R-3, 30–60 cm (both archive and working halves are shown).

ditional glauconite was reported in visual core descriptions from Section 120-747C-10R-1.

Basement Contact

Unfortunately, the sediment contact with basalt was not recovered because it was necessary to wash out the drill breccias (mostly chert fragments), which constituted the bulk of the material recovered in Core 120-747C-10R. This left a 1-m unrecovered gap between the sediments and basement (basement is designated as Unit V beginning at 296.6 mbsf). Downhole, drill breccias including chert and basalt chips remained a problem, possibly placing them out of context in the cores. However, logging results suggest that there may be a basaltic gravel layer about 10 m above the basement, intercalated above the softer chalky bioclastic grainstone(?) (Fig. 10).

BIOSTRATIGRAPHY

Introduction

After commencing in a Pliocene-Pleistocene siliceous ooze section approximately 35 m thick, operations at Site 747 recovered carbonates down to basement, contrary to expectations. The only noncarbonate sediments are volcaniclastic sediments of uncertain origin. To a large extent, the section encountered is consistent with geophysical models, and future predictions in the region should be firmer now that a known stratigraphy exists. The biostratigraphic results from the site are summarized in Figure 22.

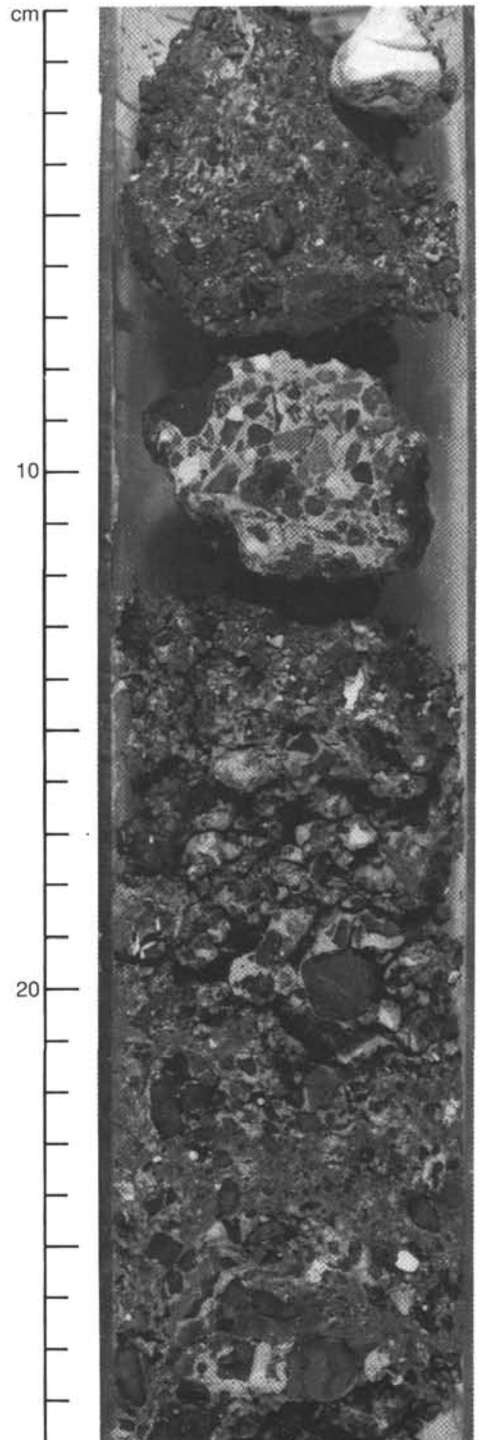

Figure 17. Volcaniclastic conglomerate in Core 120-747C-4R-CC, 1–30 cm.

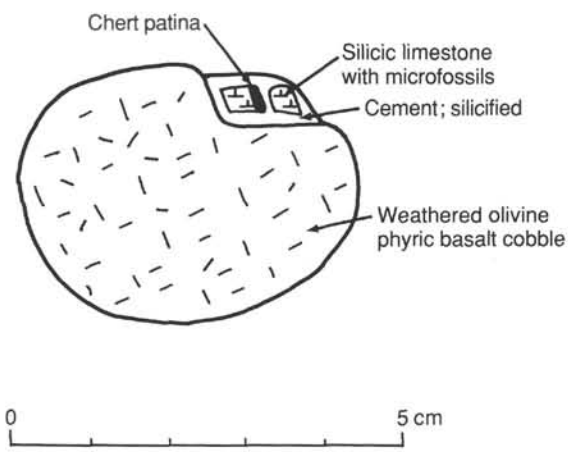

Figure 18. Drawing of basalt clast in cemented contact with chert and chalk in Core 120-747C-5R-CC.

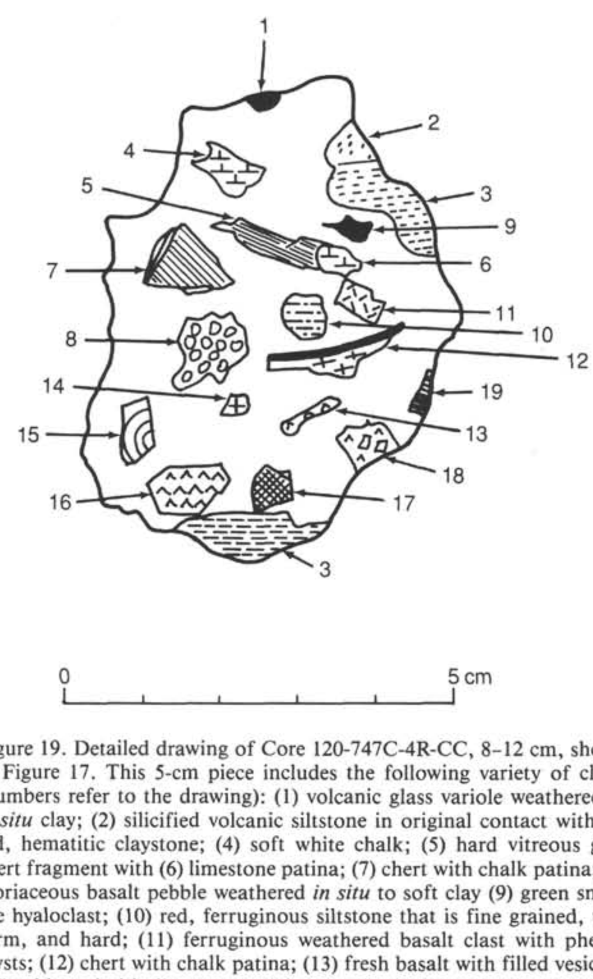

Figure 19. Detailed drawing of Core 120-747C-4R-CC, 8-12 cm, shown in Figure 17. This 5-cm piece includes the following variety of clasts (numbers refer to the drawing): (1) volcanic glass variole weathered to *in-situ* clay; (2) silicified volcanic siltstone in original contact with (3) red, hematitic claystone; (4) soft white chalk; (5) hard vitreous gray chert fragment with (6) limestone patina; (7) chert with chalk patina; (8) scoriaceous basalt pebble weathered *in situ* to soft clay (9) green smectite hyaloclast; (10) red, ferruginous siltstone that is fine grained, uniform, and hard; (11) ferruginous weathered basalt clast with phenocrysts; (12) chert with chalk patina; (13) fresh basalt with filled vesicles; (14) white micritic limestone; (15) green hyaloclast; (16) hard scoriaceous basalt; (17) red-brown vesicular basalt altered to clay; (18) hard phenocryst basalt; and (19) inoceramid fragment. The matrix is pale green to white and consists mainly of clay and traces of carbonate.

The sequence is apparently continuous from the middle Pleistocene into the upper Eocene (175 mbsf) except for a short hiatus at ~22 mbsf (middle Pliocene, <1 Ma) and 35 mbsf (approximately 2 Ma) between the Miocene and Pliocene, and one (approximately 2 Ma) at 169 mbsf within the lower Oligocene.

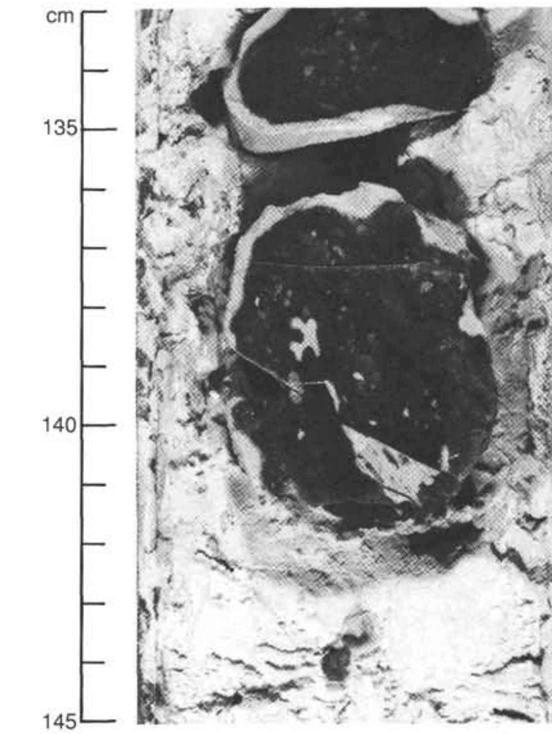

Figure 20. Chert nodules in Section 120-747A-25X-1, 133-145 cm, with chalk patina and burrows.

Throughout the lower Oligocene and younger sediment section, the sediments contain planktonic and benthic foraminifers, calcareous nannofossils, diatoms, radiolarians, and silicoflagellates. This exceptional section will allow integration of mid- and high-latitude zonal schemes over this time interval. This desirable goal has not been achievable before, and the preliminary studies already conducted show the value of this site in high southern latitude stratigraphy. We did not foresee this result for the site when drilling began since we believed that the site would be dominantly siliceous in the Neogene with perhaps only a few carbonate units.

Radiolarians indicate that the Antarctic Convergence has been north of this site throughout most of the Neogene. Thus, the presence of carbonate throughout the Neogene section will allow, for the first time, integrated paleoceanographic studies of Neogene Antarctic surface-water masses using both microfossils and isotopic data. Benthic foraminifers are also found throughout the Neogene; they show several changes in assemblage composition, which will provide parallel information about Neogene Antarctic deep-water history.

Unfortunately, siliceous microfossils were not encountered below the lower Oligocene at this site. Within the Eocene section, there is a major hiatus representing some 14 m.y. between late early and late Eocene. Below a disconformity near the base of the lower Eocene, there is an excellent Danian section in which foraminifers and calcareous nannoplankton are diverse and exceptionally well preserved.

The Cretaceous/Tertiary boundary seems not to be preserved and the uppermost Maestrichtian (latter half at least of the *Abathomphalus mayaroensis* Zone) is missing. During the Maestrichtian, and continuing into the earliest Danian, a series of debris flows was emplaced. A more detailed investigation of the foraminifer and calcareous nannoplankton biostratigraphy of the lower Paleocene with reference to the age of the volcaniclastic debris flow has been made by Aubry and Berggren (this volume). From this level to the base of the Campanian section,

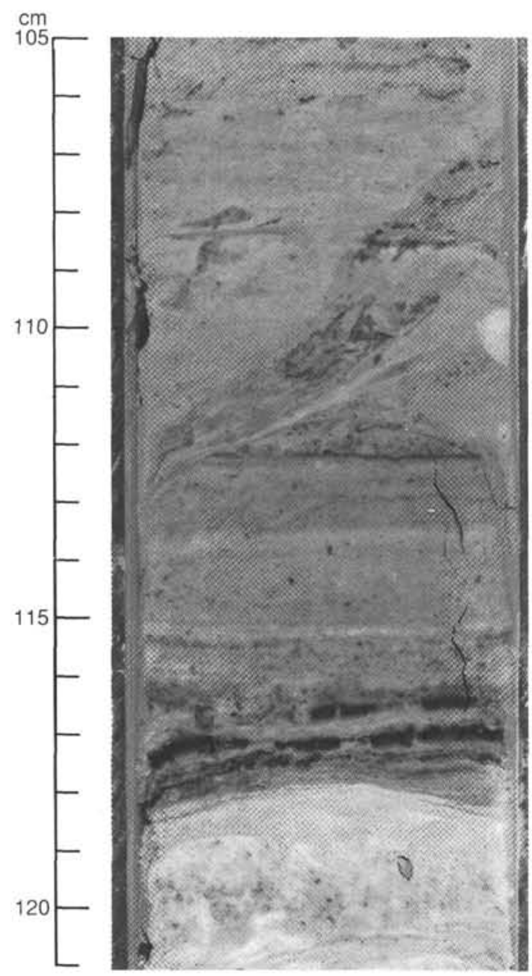

Figure 21. Cyclic laminated chalk with thin millimeter-scale phosphate laminae, Core 120-747A-21X-4, 105-121 cm.

there appears to be a continuous carbonate sequence. Like the Cenozoic, microfossils are generally well preserved and could serve as a standard reference section for the upper Campanian-Maestrichtian of high-latitude southern regions.

Most of the Cretaceous section contains a low-diversity, cool-water foraminifer assemblage of the Austral faunal province except for the lowest part (lower Santonian and middle Campanian), where assemblages are more diverse, and of the Transitional planktonic foraminifer faunal province. The generally austral character also is reflected in the calcareous nannoplankton assemblages.

Diversity of planktonic calcareous microfossils increases generally downhole throughout the Cenozoic, but the trend is reversed when the Cretaceous is penetrated. The trends are consistent with water temperature trends identified elsewhere for the high-latitude Southern Hemisphere. Except for the lower Santonian and lower Campanian parts of the section, which are inner (and perhaps outer) shelf deposits, respectively, the sediments are of a deeper water aspect, dominantly oozes that lack any evidence of CCD-related dissolution events.

The time scale chosen for dating events is that proposed by Berggren et al. (1985a, 1985b, 1985c) for the Cenozoic and that of Kent and Gradstein (1985) for the Mesozoic. They are employed as a guide to the duration of hiatuses and for sediment rate calculations. The section at Site 747 is such that it forms an ideal base for detailed taxonomy of high-latitude southern foraminifer faunas and nannofloras over the last 80-90 m.y. It contains material that will yield valuable isotope and paleoceanographic data over the same time interval.

An additional feature of the results obtained so far is the quality of correlation possible between the microfossil zones and a magnetostratigraphic profile generated on site. This integration is discussed separately below. Some parts of the section are inappropriate for the magnetostratigraphic analysis because they are not indurated enough (near the surface to a depth of 5 mbsf), too indurated to be sampled by the HPC (the XCB was used below 210 mbsf), or the magnetic susceptibility of the sediment is too low to be measured effectively on board ship.

Planktonic Foraminifers

The Paleogene part of the stratigraphic succession at Site 747 can be characterized in terms of a combination of existing schemes: the "P" zonation of Berggren and Miller (1988) for the Danian-Paleocene and a modified form of Jenkins (1971) and Jenkins and Srinivasan (1985) for the late Eocene-Oligocene.

The "M" zonation of Berggren in Berggren et al. (1983), which was developed for use in temperate and mid-latitudes of the South Atlantic, appears to be usable in the lower Miocene (Zones M2 and M3), although the absence of *Globorotalia kugleri* at Site 747 appears to preclude recognition of Zone M1.

Standard temperate to subantarctic middle to late Neogene zonation schemes (Jenkins and Srinivasan, 1985) have been found inappropriate at Site 747. Therefore, a provisional scheme based upon the sequential and biostratigraphically limited occurrences of several characteristic taxa has been developed.

Core-catcher samples have been examined from all Cenozoic sediment cores of Cores 120-747A-1H to -19X and 120-747C-1R to -2R. A few miscellaneous samples have been examined in order to resolve specific problems of biostratigraphy. About 180+ m of Cenozoic sediments were recovered at Site 747 (Cores 120-747A-1H to -20X; 120-747B-1H to -6H [foraminifers from Hole 747B samples are not considered in this report]; and 120-747C-1R to -3R).

With the exception of two hiatuses, the Cenozoic section is apparently complete from the upper Eocene through Pleistocene. In addition to the Miocene/Pliocene hiatus mentioned above, there is another that spans approximately 1-2 m.y. in the early Oligocene. A longer one, spanning about 14 m.y. between the latest early Eocene and the middle part of the late Eocene (see "Calcareous Nannofossils" section, this chapter) has also been identified.

Core-catcher samples from Cores 120-747A-1H to -19X and 120-747C-1H to -2H contain beautifully preserved planktonic foraminifer faunas. Wall textures are faithfully preserved on all Cenozoic material examined, including pristine textures on the Danian faunas in Samples 120-747A-19X-CC and 120-747B-2H-CC. The apparent absence of secondary calcification on planktonic foraminifer tests augurs as well for stable isotope studies.

Low-diversity faunas (usually between 5-8 species) characterize middle to late Neogene assemblages. (Neogene as used here refers to post-Oligocene time, and Pleistocene includes the last 1.6 m.y.; "Holocene" refers to an interglacial episode of the Pleistocene Epoch.) Samples examined from 120-747A-1H-CC to 120-747A-3H-CC are dominated by sinistrally coiled populations of *Neogloboquadrina pachyderma* and *Globigerina bulloides,* typical of late Neogene (Pliocene-Pleistocene) subantarctic assemblages.

Samples 120-747A-1H-CC and 120-747A-2H-CC were provisionally dated as late and early Pliocene, respectively, based on the presence of *Globorotalia puncticulata* as a relatively com-

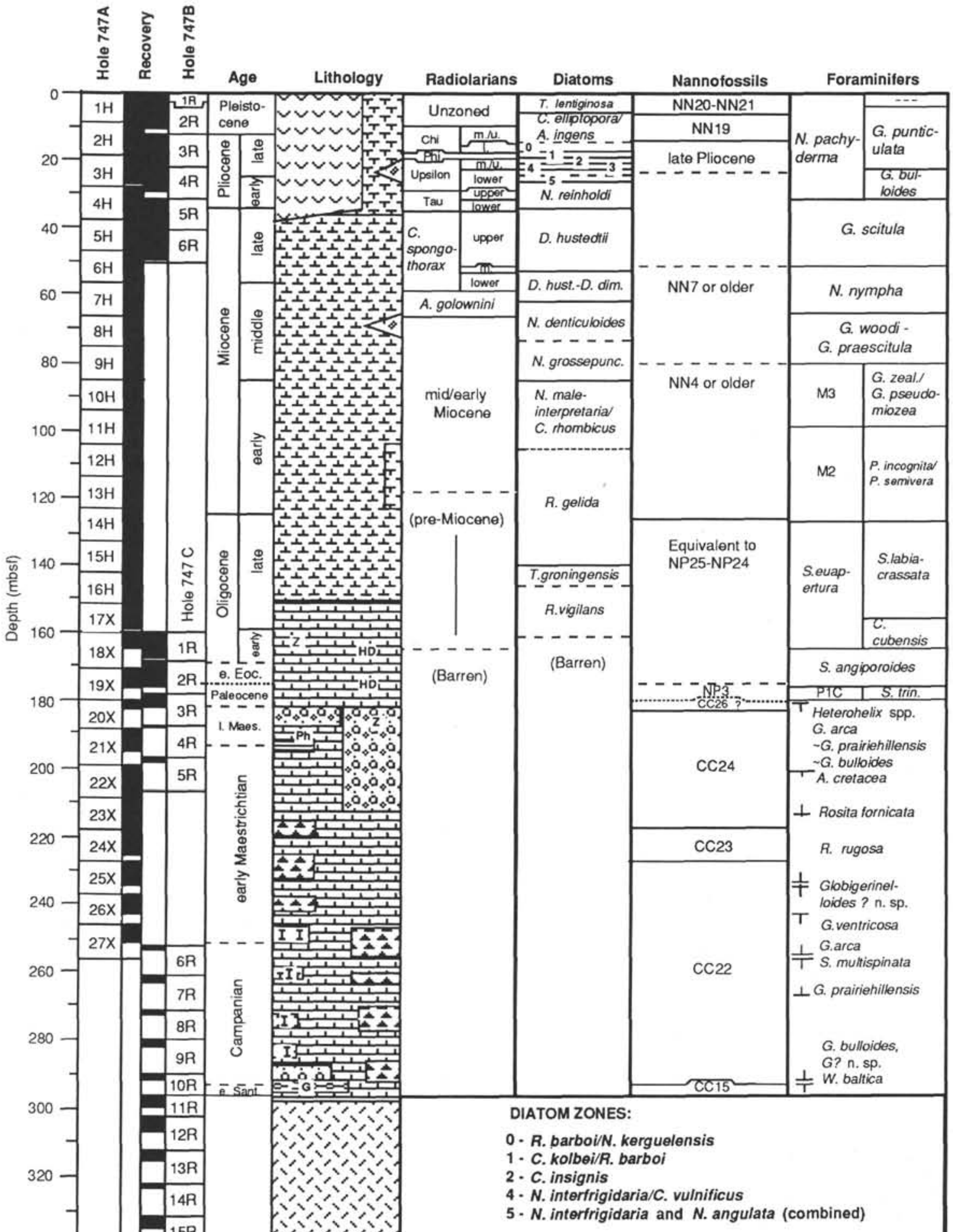

Figure 22. Site 747 biostratigraphic summary.

mon component (2%–3%) of the assemblages. Originally described from modern beach sands at Rimini, on the Adriatic coast of northeastern Italy, it is generally considered to have been reworked from nearby Pliocene outcrops. Valid occurrences of this taxon would appear to indicate an early to late Pliocene (around 4.5–2.5 Ma) range (Stainforth et al., 1975; Kennett and Srinivasan, 1983).

Diatom and radiolarian biostratigraphy, however, yield relatively concordant late Pliocene and Pleistocene ages for these samples. There are no validated records of *G. puncticulata* in plankton tows, sediment traps, or present-day bottom samples, and it would appear that we have prima facie evidence that *G. puncticulata* persisted, at least in the southern, or subantarctic, part of the Indian Ocean in the vicinity of the Northern Kerguelen Plateau, into the late Pleistocene. The absence of *Globorotalia inflata,* its supposed descendant and a form with similar ecologic preferences, is puzzling in this context.

Samples 120-747A-4H-CC and 120-747A-5H-CC contain faunas characterized by small globigerinids (of the *bulloides* stock) and *Globorotalia scitula.* These samples resemble those recovered by Tjalsma (1977) from upper Miocene drift deposits on the Falkland Plateau of DSDP Site 329.

Populations of *Globigerina bulloides, Globigerina woodi* (LAD), and *Neogloboquadrina nympha* characterize Sample 120-747A-6H-CC, which suggests an age of late middle to early late Miocene (late Serravallian to early Tortonian). An examination of samples from Sections 120-747A-7H-1 through 120-747A-7H-7 revealed that the FAD of *N. nympha* occurs in Core 120-747A-7H, 40–44 cm, at a sub-bottom depth between 65 and 66 m at a level closely associated with Anomaly Correlative 5A (see "Paleomagnetics" section, this chapter). Low-diversity faunas (5–6 species) characterize Samples 120-747A-7H-CC and 120-747A-8H-CC and the presence of *Globorotalia miozea* and *G. conoidea* in Sample 120-747A-8H-CC suggests a middle Miocene age.

The presence of the *Globorotalia zealandica–G. pseudomiozea* (LAD) complex in Samples 120-747A-9H-CC and 120-747A-10H-CC (FAD) indicates a late early Miocene age (Burdigalian). These two forms are the nominate taxa of the total range zone, M3, of the southern Atlantic mid-latitude temperate zonation of Berggren et al. (1983). Samples from 120-747A-11H-CC to 120-747A-14H-CC are characterized by catapsydracids (LAD in Sample 120-747A-11H-CC), *Paragloborotalia incognita-semivera,* and well-preserved but indeterminate globigerinids of early Miocene affinities.

Faunas with a more "Oligocene appearance" occur over the interval of Cores 120-747A-14H to -16H. The presence of *Subbotina euapertura* (= *prasaepis*) in Core 120-747A-14H is considered as a proxy indicator for the proximity of the Oligocene/Miocene boundary (see discussion on "Magnetobiostratigraphy," this section, this chapter). Tenuitellids characterize the fine fraction assemblage of Cores 120-747A-14H to -18X, and their study may aid in refining the stratigraphic subdivision of this and younger parts of the sequence. The LAD of *Chiloguembelina cubensis* in Sample 120-747A-17X-CC serves to denote the proximity of the lower/upper Oligocene contact, and the LAD of *Subbotina angiporoides* in Sample 120-747A-18X-CC, together with typical *Subbotina labiacrassata,* indicates the presence of lower Oligocene sediments at Hole 747A.

A rich and diverse cosmopolitan late Danian assemblage (Zone P1C of Berggren and Miller, 1988) occurs in Samples 120-747A-19X-CC and 120-747C-2R-CC. Indeed, this is one of the best preserved and diverse late Danian faunas that W. A. Berggren has observed: *Eoglobigerina edita, E. simplicissima, Planorotalites compressus, Subbotina pseudobulloides, S. triloculinoides, S. danica* (= *moskvini*), *S. trinidadensis, Globoconusa daubjergensis, Igorina spiralis, I. imitata, Chiloguembelina midwayensis, C. morsei,* and others are present.

Cretaceous foraminifers occur in Cores 120-747A-20X to -27X and 120-747C-3R to -10R. No Cretaceous forms are known from Hole 747B. The structure of the Cretaceous foraminifer faunas is surprisingly similar to that recorded by Sliter (1976) for Hole 327A on the northern Falklands Plateau, South Atlantic Ocean. He recorded there a 65-m-thick Santonian–upper Maestrichtian sequence beginning with a Santonian fauna that has some elements in common with those recorded here, followed by a plankton-dominated Campanian-Maestrichtian sequence. The Falklands Plateau section is from a deeper water site (2410 m), and the effects of dissolution are obvious. There are also differences in the balance of the elements of the faunas.

Preservation of foraminifers generally is excellent, but it is very poor in Core 120-747A-20X, with features obscured by overgrowths. Identification generally is still possible, but often it is only tentative. Bone fragments are a minor but conspicuous part of this fauna. In Cores 120-747C-9R and -10R preservation deteriorates noticeably, and it is poor in Core 120-747C-10R. Identification thus is tentative in many cases.

There is no evidence of carbonate dissolution effects in the sequence, suggesting that it has always been above the CCD. Generally, the foraminifers appear to be ideal for oxygen isotope studies, with the exception of the few samples noted above.

The Cretaceous foraminifer faunas at Site 747 are predominantly of planktonic species, generally constituting over 95%. There is a higher benthic component in Cores 120-747C-9R and -10R, consistent with the evolution of the site from subaerial immediately prior to the first sedimentation, through inner and outer shelf conditions to deeper water with time. The only significant glauconite component (Sample 120-747C-10R-CC) also occurs at this time in the shallow-water sediment.

The youngest Cretaceous sequence is from Sample 120-747C-3R-3, 27 cm, some 2 cm below the earliest Cenozoic in the same core. This sample includes *Globotruncanella petaloidea* (Gandolfi), *Abathomphalus intermedius* (Bolli), and *Bolivinoides paleocenicus* (Brotzen), which indicates that the youngest age possible is the earlier part of the *Abathomphalus mayaroensis* Zone and that the latest Maestrichtian is missing. This sample could be as old as the latter half of the *Gansserina gansseri* Zone and thus still late Maestrichtian in age.

The Santonian was identified only in Sample 120-747C-10R-CC. This fauna has a much lower foraminifer content than any others tested and preservation is worse. The early Santonian age is based on the presence of ?*Whiteinella baltica* Douglas and Rankin, *Hedbergella*(?) *amabilis* Loeblich and Tappan, *Globigerinelloides* (*bentonensis* or *aspera*), and *Schackoina multispinata* (Cushman and Wickenden).

The Santonian and Maestrichtian are quite well characterized by index forms, but the cooler water aspect of the Campanian renders it difficult to identify positively (except in Core 120-747C-9R) or to subdivide in the warm-water zonal scheme.

Other than for Cores 120-747C-9R and -10R, the faunas are uniformly dominated by *Heterohelix* (and/or *Gublerina* and *Planoglobulina*), *Hedbergella* (several species), *Rugoglobigerina,* and *Globigerinelloides. Globotruncanella* (possibly a new species) is a significant part of some Maestrichtian assemblages, and there also appears to be a new species of *Globigerinelloides* in the section.

These faunas clearly belong to the austral faunal province of Sliter (1972). Therefore, they are of a cooler water aspect than the coeval transitional/austral assemblages of the western margin of Australia documented by Belford (1959, 1960) that contain a higher globotruncanid component (see Sliter, 1976, for discussion), even though geographically close at the time of deposition.

The lowest Campanian in Core 120-747C-9R and the Santonian in Sample 120-747-10R-CC contain faunas with a much higher proportion of globotruncanids and thus belong to the Transitional faunal province at the time. This represents a warmer interval that may coincide with the one postulated by Herb (1974) for the Santonian in the Indian Ocean. This warmer interval also yields a better array of index planktonic species by which to identify the ages of samples from Cores 120-747C-9R and -10R.

The youngest unequivocally Campanian sample dated using foraminifers is Sample 120-747A-24X-CC. However, there are a few samples above that level that can be categorized on foraminifer evidence as Campanian (or middle Campanian)–lower Maestrichtian. The uppermost Campanian is in Sample 120-747A-27X-CC. This sample is from a level slightly above that of Sample 120-747C-6R-CC, which is also upper Campanian as are Cores 120-747C-7R and -9R.

Campanian index forms are very difficult to find. The lowest occurrence of *Globigerinelloides prairiehillensis* Pessagno is a convenient marker toward the base and the earliest occurrence of *Globotruncana bulloides* is a useful marker for the Santonian/Campanian transition. Campanian is often identified by default when faunas above and below are positively identified as Santonian or Maestrichtian. Elsewhere calcareous nannofossils are very useful. The ranges of *Heterohelix globulosa* (Ehrenberg) and *H. reussi* (Cushman) are much in conflict with those suggested by Caron (1985); this probably reflects a different species concept.

Benthic Foraminifers

Benthic foraminifers were studied at Site 747 from all core catchers. In addition, Samples 120-747B-1H-1, 0–4 cm; 120-747A-1H-1, 25–28 cm; 120-747C-2R-2, 69–71 cm; 120-747C-2R-3, 98–100 cm and 139–141 cm; 120-747A-2R-4, 4–6 cm, 49–51 cm, and 90–92 cm; and 120-747A-2R-5, 117–119 cm, were analyzed. Between 100 and 400 specimens of each sample were picked and mounted from the >125-μm fraction. Benthic foraminifers are generally well preserved and abundant in all core-catcher samples, although they are rare in comparison with the planktonic component. The following benthic foraminifer assemblages were recognized in the Cenozoic sequence of Holes 747A and 747C.

Assemblage 1a: Pleistocene

This assemblage is represented by Samples 120-747B-1H-1, 0–4 cm, and 120-747A-1H-1, 25–28 cm. The fauna is dominated by *Bulimina aculeata* and *Trifarina earlandi. Oridorsalis umbonatus* and *Globocassidulina subglobosa* are frequent constituents. Rare, but characteristic components of this fauna are *Pullenia bulloides, Pyrgo murrhina, Cibicidoides wuellerstorfi, Melonis pompilioides, Epistominella exigua, Fissurina* spp., *Eggerella bradyi, Karreriella* sp., and *Hormosina* sp.

Assemblage 1b: Early Pleistocene–Late Pliocene

The benthic fauna of Sample 120-747A-1H-CC is dominated by *Trifarina earlandi.* Common constituents are *Globocassidulina subglobosa, Cassidulina teretis,* and *Pyrgo murrhina. Epistominella exigua, Karreriella bradyi, Eponides tumidulus, Pullenia quinqueloba, Lagena apiopleura, Bolivina* sp., *Stilostomella* spp., *Ehrenbergina* sp., *Pyrgo* sp., and *Astrononion stelligerum* are minor, but important, components. Comparison with a very similar fauna, living on the eastern continental margin of the Weddell Sea in water depths between 1000 and 1600 m (A. Mackensen, unpubl. data), indicates middle to lower bathyal paleodepth (600–2000 m).

Assemblage 2: Early Pliocene–Late Miocene

This assemblage occurs in Samples 120-747A-2H-CC to 120-747A-4H-CC. Characteristic and common species are *Epistominella exigua, Astrononion pusillum, Oridorsalis umbonatus, Globocassidulina subglobosa, Cibicidoides mundulus, Laticarinina pauperata, Melonis pompilioides,* and *Stilostomella* spp. In addition, *Pullenia bulloides, P. subcarinata, Eggerella bradyi, Eponides* sp., *Gyroidina* spp., *Bolivina* spp., *Lagena* spp., *Uvigerina* spp., and *Lenticulina* spp. are present. The characteristic taxa of Assemblage 1 (*T. earlandi, C. teretis*) are absent from this assemblage. *Pyrgo murrhina* has its first appearance in Sample 120-747A-3H-CC.

One of the characteristic species of Assemblage 2, *Epistominella exigua,* is found in gravity cores from the eastern Weddell Sea continental margin down to at least 1 Ma. There the downcore abundance of *E. exigua* correlates well with the oxygen isotope stratigraphy (Mackensen et al., in press).

Assemblage 3: Middle Miocene–Early Oligocene

Samples 120-747A-5H-CC to 120-747A-18X-CC contain variable benthic foraminifer faunas. They are grouped together because of the common occurrence of *Nuttallides umbonifera* throughout all the core-catcher samples. *Epistominella exigua* becomes very rare in the top of this sequence and has its first appearance in the upper middle Miocene (Sample 120-747A-7H-CC). *Astrononion pusillum, Laticarinina pauperata, Cibicidoides mundulus, Globocassidulina subglobosa,* and several species of *Uvigerina, Gyroidina,* and *Stilostomella* are common in all samples of this assemblage. *Pullenia bulloides, P. subcarinata, Eggerella bradyi, Bolivina* spp., *Lagena* spp., *Fursenkoina* spp., *Pleurostomella* sp., *Fissurina* spp., and *Bulimina* spp. are common accessory components.

The occurrence of some distinct species in core-catcher samples within Assemblage 3 (*Rectuvigerina multicostata* in Samples 120-747A-8H-CC and 120-747A-9H-CC; *Bulimina* cf. *alazanensis* in Samples 120-747A-13H-CC and 120-747A-14H-CC) suggests that a more detailed subdivision of this assemblage is possible by closer sampling and careful identification of taxa (especially a thorough taxonomic analysis of the *Uvigerina* group).

The species composition of Assemblage 3 is very similar to an early Miocene to late Eocene fauna described by Thomas (Shipboard Scientific Party, 1988a, 1988b) from the Maud Rise Holes 689B and 690C of Leg 113. Species found in the sites on the Maud Rise and at Site 747 are all common deep-sea faunal components, suggesting a lower bathyal to abyssal depth during the Miocene and the Oligocene.

The high relative abundance of *N. umbonifera* might indicate a corrosive bottom-water mass with high CO_2 content. Today this species is a dominant component of abyssal assemblages below 4500-m water depth in the Indian Ocean and in lower numbers in the abyssal parts of the Weddell Sea.

Assemblage 4: Early Eocene

A very condensed early Eocene sequence was recovered from Hole 747C. Benthic foraminifer Assemblage 4 was found in Samples 120-747C-2R-4, 4–6 cm, and 120-747C-2R-4, 49–51 cm. This fauna is dominated by *Nuttallides truempyi. Hanzawaia cushmani, Alabamina dissonata, Karreriella* spp., *Anomalina spissiformis, Gyroidina globosa, Aragonia* spp., *Lenticulina* spp., and *Bulimina* spp. are common and frequent species of this assemblage. Characteristic constituents are *Turrilina brevispira, Bulimina semicostata, Bulimina trinitatensis, Buliminella grata, Vulvulina spinosa,* and *Anomalinoides capitatus.* Rare components are *Anomalinoides semicribratus* and *Uvigerina rippensis.*

In contrast to the early Paleocene fauna in this assemblage, *Stensioina beccariiformis* and *Bolivinoides delicatulus* are missing.

Assemblage 5: Earliest Paleocene

This assemblage is found in Sample 120-747A-19X-CC. It is characterized by the high relative abundance of *Stensioina beccariiformis,* the presence of *Nuttallides truempyi, Bolivinoides delicatulus,* and *Bulimina trinitatensis.* Accessory components are *Karreriella chapapotensis, Karreriella* cf. *cubensis, Oridorsalis umbonatus, Gyroidina globosa, Pullenia coryelli, Stilostomella* spp. and *Cibicidoides* sp.

In a detailed study of Paleocene and Eocene faunas of the southern Atlantic Ocean, Tjalsma and Lohmann (1983) found different proportions of *S. beccariiformis* to *N. truempyi* in the early and late Paleocene correlated with different water depths. The benthic foraminifer fauna in Sample 120-747A-19X-CC is strongly dominated by *S. beccariiformis* (31%) with minor importance of *N. truempyi* (18%). This might indicate an abyssal paleodepth (2000–3000 m).

Benthic forms are a component of all Cretaceous samples, but they make up only a small percentage of the fauna except in Samples 120-747C-9R-CC and 120-747C-10R-CC. The fauna is diverse, very dominantly calcareous, and consists largely of "*Anomalinoides*" (sensu Belford, 1960), *Gyroidinoides, Globorotalites, Osangularia,* and *Quadrimorphina* with few nodosariids, uvigerinids, miliolids, or agglutinated forms. *Bolivinoides strigillatus* (Chapman) occurs sporadically throughout (more commonly in the later part of the section) and *Bolivinoides paleocenicus* (Brotzen) in the Maestrichtian. *Neoflabellina praereticulata* Hiltermann and *Stensioina excolata* (Cushman) also occur sporadically throughout. Agglutinated forms occur throughout but are rare and include *Spiroplectammina* and *Gaudryina.*

The fauna is very similar in composition to that described by Belford (1960) from the Santonian-Campanian of Western Australia, as is to be expected from the close geographic proximity and age at the time of deposition of this section. The benthic component is less and the miliolid/nodosariid content is much less on Kerguelen Plateau than in Western Australia.

In Sample 120-747C-10R-CC, benthic foraminifers dominate in a glauconitic calcarenite in which *Inoceramus* prisms are the main arenitic component. The residue of Sample 120-747A-24X-CC is dominated by *Inoceramus* prisms, but otherwise the benthic/planktonic component is as above and below.

Calcareous Nannofossils

A 180-m section through Cenozoic sediments was recovered from Hole 747A. Except for Core 120-747A-19X, only core catchers taken from this section were examined. Hole 747B penetrated 50 m of Pleistocene to upper Miocene sediments (see "Radiolarians" and "Diatoms" sections, this chapter). Only three samples from this hole have been examined to date. Drilling at Hole 747C washed down to 159 mbsf, at which level upper Oligocene sediments were reached. The stratigraphic subdivision of the lower Oligocene to lower Paleocene sediments recovered in Cores 120-747C-2R and -3R has been established in great detail (see below).

Unexpectedly, calcareous nannofossils were abundant and well preserved throughout the sedimentary section except in the upper cores (Pleistocene and upper Pliocene), where they are diluted by siliceous microfossils. Diversity is very reduced in Miocene assemblages, which are strongly dominated by *Reticulofenestra perplexa.* Diversity increases downhole in Oligocene and late Eocene assemblages, and fluctuations in species abundance will be analyzed onshore. Early Eocene and Paleocene assemblages are rich and dominated by species of the genus *Toweius.* The high frequency of species of the genus *Chiasmolithus* and the low frequency of discoasters in Paleogene assemblages indicates general cool temperatures (Bukry, 1973). No information concerning the composition of middle Eocene assemblages is available from this site.

Biozonal subdivision of all sections studied is based on Martini's (1971) zonal scheme in order to allow direct correlation from subantarctic to tropical regions as well as from oceanic to epicontinental areas.

Sample 120-747A-1H-CC yielded an early Pleistocene calcareous nannoflora characterized by the co-occurrence of *Pseudoemiliania lacunosa* and *Gephyrocapsa* spp. Sediments from Sections 120-747A-1H-1 through 120-747A-4H, 140 cm, are of late Pleistocene age (Zones NN20–NN21 undifferentiated).

Assemblages from Sample 120-747A-2H-CC contain scarce specimens of *P. lacunosa.* No placoliths of *Gephyrocapsa* were observed. The absence of representatives of this taxon favors a late Pliocene age for the base of Core 120-747A-2H. *Reticulofenestra* sp. ex gr. *R. pseudoumbilica* is common in sediments from Sample 120-747A-3H-CC, which indicates that the lower/upper Pliocene contact lies within this core. Sample 120-747A-3H-CC belongs to Zone NN15 or older and is at least 3.5 m.y. old. No stratigraphic markers or indicators were observed in Samples 120-747A-4H-CC to 120-747A-6H-CC.

Reticulofenestra floridana in Sample 120-747A-7H-CC characterizes middle Miocene sediments, as confirmed by the common occurrence of *Helicosphaera granulata* in Sample 120-747A-8H-CC. Thus, Sample 120-747A-7H-CC has a stratigraphic position equivalent to Zone NN7 or older and a minimal age of 11.2 Ma.

Helicosphaera ampliaperta in Sample 120-747A-9H-CC indicates a stratigraphic position correlative with the zonal interval NN4–NN2. Neither *Sphenolithus heteromorphus* nor *Sphenolithus belemnos* was observed. *Discoaster druggi* is also absent. The occurrence of *Sphenolithus* sp. cf. *S. conicus* in Samples 120-747A-11H-CC, and 120-747A-12H-CC suggests an early Miocene age.

Sample 120-747A-14H-CC yielded an assemblage that contrasts strongly with those of the overlying core catchers. Common occurrences of *Reticulofenestra bisecta, Zygrhablithus bijugatus,* and *Chiasmolithus altus* indicate that the Oligocene/Miocene contact occurs in Core 120-747A-14H. Samples 120-747A-14H-CC to 120-747A-18X-CC provided similar assemblages. Common occurrences of *Triquetrorhabdulus carinatus* in Sample 120-747A-16H-CC and *Reticulofenestra abisecta* in Samples 120-747A-17X-CC and 120-747A-18X-CC indicate that the interval between Samples 120-747A-14H-CC and 120-747A-18X-CC is late Oligocene in age. The absence of *Sphenolithus ciperoensis* and *Sphenolithus distentus* prevents further stratigraphic subdivision.

Sample 120-747A-19X-CC contained a characteristic early Paleocene assemblage with common *Chiasmolithus danicus* (Zone NP3). Thus, a major unconformity lies in Core 120-747A-19X.

Reworking was noticed at several intervals, in particular in the upper part of the sequence covered by Cores 120-747A-2H to -6H. It is particularly extensive in Sample 120-747A-3H-CC where *Ellipsolithus macellus, Chiasmolithus grandis, Reticulofenestra umbilica,* and *R. floridana,* among others, were recorded. These coccoliths are not indicative of a restricted stratigraphic source interval, although the last three species indicate reworking from middle Eocene strata. The presence of beautifully preserved *E. macellus* suggests erosion from a nearby Paleocene or lower lower Eocene outcrop.

Three samples from Hole 747B (120-747B-1H-2, 70 cm, 100 cm, and 120 cm) were examined. Coccoliths are very scarce at 70 cm and 120 cm and abundant at 100 cm. They are very well preserved and small species of the genus *Gephyrocapsa* are dominant. Scanning electron microscope (SEM) studies are necessary to determine them and verify the possible presence of *Emiliania huxleyi.* Sediments of Sections 120-747B-1H-1 and 120-747B-1H-2 down to 120 cm are of late Pleistocene age and are placed in Zones NN20–NN21 undifferentiated (on the basis of the absence of *P. lacunosa*).

Cretaceous sediments were recovered from Holes 747A and 747C, yielding a composite section spanning the lower Santonian through middle Maestrichtian. Nannofossil preservation is generally good with only thin intervals of degraded preservation in the uppermost Campanian and lower Maestrichtian and in the lower Santonian. Specific biostratigraphic assignments are summarized in Figure 22; general comments on biostratigraphy, preservation, and paleoecology are given below.

The youngest Cretaceous material that may or may not be *in situ* occurs in a thin nannofossil chalk unit (Interval 120-747C-

3R-3, 25–29 cm) immediately overlying a volcanogenic breccia (Unit III interpreted elsewhere as a series of debris flows derived from erosion of volcanic basement). This 4-cm-thick chalk contains nannofossils indicative of middle to late (but not latest) Maestrichtian age, including *Arkhangelskiella cymbiformis* (s.s.), *Cribrosphaerella daniae, Nephrolithus corystus,* and probable *Nephrolithus frequens.* Assuming the presence of *N. frequens* (s.s.), the *Nephrolithus frequens* Zone (CC26) is indicated.

The austral nature of the assemblages is indicated by common *Monomarginatus quaternarius* and *Nephrolithus corystus.* The chalk immediately below the volcanogenic breccia (Sample 120-747A-20X-CC) contains *Reinhardtites levis, Biscutum magnum,* and *Nephrolithus corystus* but not *Nephrolithus frequens,* indicating the *Reinhardtites levis* Zone (CC24) of early to middle Maestrichtian age. Based on these core data, the commencement of deposition of the volcanogenic breccia can be dated as early to middle Maestrichtian. Logging data suggest that other volcanic breccias are present below this cored interval.

Nannofossil determinations for the remainder of the Cretaceous section (Cores 120-747A-21X through -27X and Cores 120-747C-6R through -10R) are based only on core-catcher material.

Early to middle Maestrichtian assemblages of the *Reinhardtites levis* Zone (CC24) occur from Cores 120-747A-21X through -23X based on the occurrence of the nominate species in the absence of *Tranolithus phacelosus.* The addition of rare *Tranolithus phacelosus* in Core 120-747A-24X indicates the earliest Maestrichtian *T. phacelosus* Zone (CC23). The persistent occurrence of *Biscutum magnum* and the sporadic presence of *Biscutum dissimilis* in these assemblages indicate the austral nature of the nannoplankton communities that lived in the overlying surface-water mass. Nannofossil preservation is good throughout the *R. levis* Zone but degrades markedly in the *T. phacelosus* Zone.

Campanian assemblages occur within the interval from Cores 120-747A-25X through 27X (total depth) and Cores 120-747C-6R through -9R (Fig. 22). Preservation is poor at the top of this sequence (Sample 120-747A-25X-CC), but it improves substantially downcore. The poor preservation in Sample 120-747A-25X-CC makes species identification, and therefore precise zonal placement, difficult. Questionable specimens of *Reinhardtites anthophorus* and *Aspidolithus parcus* occur within this sample. If these species identifications are confirmed, this sample can be reliably placed in the middle to late Campanian *Quadrum trifidum* Zone (CC22).

Both species are definitely present in Cores 120-747A-26X through 120-747C-9R. *Quadrum trifidum* is missing throughout most of the sequence, although its appearance in Sample 120-747C-9R-CC allows placement of the entire sequence from Cores 120-747A-26X through 120-747C-9R in the *Quadrum trifidum* Zone. The occurrence of *Q. trifidum* in Sample 120-747C-9R-CC is coincident with a major change in assemblage character. Species richness increases significantly in Sample 120-747C-9R-CC with the introduction of more temperate forms such as *Quadrum gothicum* and *Q. trifidum.* This change from the austral assemblages of the overlying sequence to the more temperate one in Core 120-747C-9R is also evident in the planktonic foraminifers.

Fragments of calcarenite with glauconite in Sample 120-747C-10R-CC contain significantly older nannofossils than the overlying sequence. The presence of rare *Micula concava, Lithastrinus septenarius, Reinhardtites anthophorus,* and *Thiersteinia ecclesiastica* as well as common *Prediscosphaera ponticula* and *Eprolithus floralis* indicate the *Reinhardtites anthophorus* Zone (CC15) of early Santonian age. This assignment is strengthened by the absence of all *Lucianorhabdus* spp., which were common throughout the overlying Cretaceous. Preservation is moderate with significant etching of many forms.

Radiolarians

Radiolarian biostratigraphy is based on an examination of core-catcher samples from all Hole 747A cores, all Hole 747B cores, and Hole 747C core catchers 120-747C-6R-CC through 120-747C-10R-CC. In addition, for Cores 120-747A-1H to -12H, additional samples were examined to locate zonal boundaries to the nearest core section. Radiolarians are common to abundant and generally well preserved in Site 747 sediments of middle Miocene to Holocene age, and rare to few and poorly preserved in sediments of Oligocene to early Miocene age. No radiolarians were seen in older sediments from this site. All existing Antarctic Neogene radiolarian zones and subzones, from the *Actinomma golownini* Zone to the Omega Zone (Fig. 22; "Explanatory Notes" chapter, this volume) were recognized at this site, with the exceptions below.

The boundary between the Pleistocene Omega and Psi Zones was not identified, as *Stylatractus universus* was not seen above Sample 120-747A-2H-2, 45–47 cm, which is within the Chi Zone. *Stylatractus universus* usually is rare in Pliocene-Pleistocene samples from Site 747. The middle-upper subzone boundary was not recognized within the Chi Zone. *Phormostichoartus pitomorphus* was not seen in any of the samples examined.

The middle Upsilon Subzone was not recognized, implying a hiatus between the upper and lower Upsilon Subzones, between Samples 120-747A-3H-3, 45–47 cm, and 120-747A-3H-4, 45–47 cm. The middle Upsilon Subzone, however, is based on the absence of *Prunopyle titan* and may have been confused with the lower Chi Subzone by reworking. The middle *Cycladophora spongothorax* Subzone is only tentatively recognized at Site 747 and can easily be destroyed by reworking. This subzone is thought to be very short (see "Explanatory Notes" chapter, this volume).

No usable radiolarian zones are defined below the base of the *A. golownini* Zone in the Antarctic. Several species of stratigraphic value were encountered in the Miocene interval below the base of this zone, including *Eucyrtidium punctatum, Cycladophora golli* (mostly *C. g. regipileus*), *Lithatractus timmsi,* and *Cyrtocapsella tetrapera.* These species' ranges at Site 747 are similar to the ranges seen for these taxa elsewhere in the Antarctic (Chen, 1975; Lazarus, unpubl. data), and thus suggest the possibility of a new radiolarian zonation for the earlier Miocene. However, additional work will be needed to determine a workable zonation.

A distinctive middle Miocene assemblage, including species such as *Thyrsocyrtis clausa* and a very large pterocanid, was seen between Samples 120-747A-10H-6, 45–47 cm, and 120-747A-8H-6, 45–47 cm. Species in this assemblage, previously reported from middle Miocene sediments by Chen (1975), are absent in other Leg 120 sites, apparently due to hiatuses.

Reworking of older material appears to be minor at Site 747, although significant quantities of reworked older material appear in at least one Pleistocene sample (Pliocene forms such as *Helotholus vema* in Sample 120-747A-1H-4, 45–47 cm). One specimen of the late Eocene species *Lychnocanoma amphitrite* was observed in middle Miocene Sample 120-747A-8H-2, 45–47 cm.

Most radiolarian assemblages appear to be typical of the Antarctic water mass (south of the Antarctic Convergence), although they are often of low diversity (due in part to dissolution in what was generally a low-productivity paleoenvironment). Subantarctic faunal elements such as *Lamprocyclas aegles* appear to be common in uppermost Miocene and lowermost Pliocene samples, and particularly in Sample 120-747A-4H-4, 45–47 cm (lowermost Pliocene). A similar lowermost Pliocene interval with subantarctic faunas was observed in Leg 113 sites from the Weddell Sea (Lazarus, unpubl. data) and may represent a relatively "warm" interval of time.

Diatoms

Diatoms are abundant and well preserved only in the Pleistocene and Pliocene intervals in Holes 747A and 747B. They occur in low abundance and poor to moderate preservation in the lower cores down to Core 120-747A-17H and to the bottom of Hole 747B. The section below Section 120-747A-17H-CC to the bottom of Hole 747A and all of Hole 747C was barren of diatoms.

Most diatoms from Site 747 are characteristic of Southern Ocean assemblages, and standard biostratigraphic zonal schemes for this region were successfully applied. The stratigraphic framework employed here is taken from Ciesielski (1983) for the Pleistocene-Pliocene interval, Weaver and Gombos (1981) for most of the Miocene, and Gombos and Ciesielski (1983) for lower Miocene and Oligocene. Slight modification of these zonal schemes, taking into account new biostratigraphic information from other Leg 120 sites and the discussions presented in the site reports for Legs 113 and 119, was necessary (see "Explanatory Notes," this volume, for diatom datums and zones used during Leg 120).

Continuous core recovery and consistent diatom occurrence enabled the recognition of most zonal datums and all diatom zones for the upper Pleistocene to upper lower Oligocene interval (Fig. 22). The upper five cores of Holes 747A and 747B were divided into biostratigraphic zones through the examination of smear slides prepared by the shipboard sedimentologists during the course of their core descriptions. The remaining lower portions of these holes were divided through study of core-catcher samples that were treated with hydrochloric acid to remove the abundant carbonate component and concentrate the diatoms. Residues were washed in distilled water and centrifuged at 1200 rpm for 3 min to rid the residue of acid.

In Hole 747A the *Thalassiosira lentiginosa* Zone is identified from the surface down to the interval between Samples 120-747A-1H-3, 16–17 cm, and 120-747A-1H-3, 116–117 cm, where the highest occurrence of *Actinocyclus ingens* is noted. This marks the base of the *T. lentiginosa* Zone and the top of the *Coscinodiscus elliptopora–A. ingens* Zone. Within this zone the highest occurrence of *Hemidiscus karstenii* is noted between Intervals 120-747A-1H-2, 84–85 cm, and 120-747A-1H-2, 110–111 cm.

Coscinodiscus vulnificus, whose highest and lowest occurrence define two zonal boundaries in the Pliocene, was not noted and probably is restricted to waters to the south. The highest occurrence of *Rhizosolenia barboi* was also not noted, preventing the identification of the *R. barboi–Nitzschia kerguelensis* Zone. Remaining Pliocene zones are identified in Figure 22 with zonal boundary datums noted between the intervals that follow.

1. Highest *Coscinodiscus kolbei* between Intervals 120-747A-2H-6, 86 cm, and 120-747A-2H-CC defines the top of the *C. kolbei–R. barboi* Zone.
2. Highest *Coscinodiscus insignis* between Intervals 120-747A-2H-CC and 12-747A-3H-1, 21 cm, defines the top of the *C. insignis* Zone.
3. Highest *Nitzschia weaveri* between Intervals 120-747A-3H-1, 27 cm, and 120-747A-3H-2, 49 cm, defines the top of the *N. weaveri* Zone.
4. Highest *Nitzschia interfrigidaria* between Intervals 120-747A-3H-2, 49 cm, and 120-747A-3H-3, 120 cm, defines the top of the *N. interfrigidaria–C. vulnificus* Zone.
5. Lowest *N. interfrigidaria* between Intervals 120-747A-3H-6, 48 cm, and 120-747A-3H-CC defines the top of the *Nitzschia reinholdii* Zone.
6. Lowest *Nitzschia angulata* between Intervals 120-747A-3H-6, 44 cm, and 120-747A-3H-CC defines the top of the *N. reinholdii* Zone.
7. Highest *Denticulopsis hustedtii* between Intervals 120-747A-4H-4, 50 cm, and 120-747A-4H-5, 50 cm, defines the top of the *D. hustedtii* Zone.

The highest occurrence of *Denticulopsis dimorpha* in Sections 120-747A-5H-CC and 120-747A-6H-CC identifies the boundary between the *D. hustedtii* Zone and the underlying *D. hustedtii/D. dimorpha* Zone. The highest occurrence of abundant *D. dimorpha* is within Core 120-747A-6H. This suggests a partition within the middle *D. hustedtii/Denticulopsis lauta* Zone and an age of ~10.2 Ma (R. Gersonde, pers. comm. to J. Barron). We do not apply the *D. hustedtii/D. lauta* Zone of Weaver and Gombos, but propose the *D. hustedtii/D. dimorpha* Zone, the top of which is defined by the highest consistent occurrence of *D. dimorpha,* due to the fact that *D. lauta* was not consistently observed in any Leg 120 holes and was found restricted to the lower middle Miocene.

Other Miocene diatom zones identified in Hole 747A are shown in Figure 22 with the zonal boundary datums recorded at the following intervals:

1. Highest *Nitzschia denticuloides* (zone boundary datum) in the interval between Sample 120-747A-7H-CC and 120-747A-6H-CC, which defines the top of the *D. dimorpha–N. denticuloides* Zone.
2. Lowest *D. dimorpha* (secondary datum) in Sample 120-747A-7H-CC.

The boundary between the *N. denticuloides* and *Nitzschia grossepunctata* Zones is estimated by the highest occurrence of *Denticulopsis maccollumii* in Sample 120-747A-8H-CC, a datum that occurs slightly above the highest *N. grossepunctata* (the top of the *N. grossepunctata* Zone).

1. Lowest *N. grossepunctata* (zone boundary datum) in Sample 120-747A-9H-CC defines the top of the *D. maccollumii* Zone.
2. Highest *Syndiella jouseana* (secondary datum) in Sample 120-747A-9H-CC.

Poor preservation and low numbers of diatoms in Cores 120-747A-10H through -12H prevent reliable zonal definition of the *Nitzschia maleinterpretaria, Thalassiosira fraga,* and *Coscinodiscus rhombicus* Zone and the top of the *Rocella gelida* Zone. The highest occurrence of *Coscinodiscus oligocenicus* in Sample 120-747A-11H-CC and *Rocella gelida* in Sample 120-747A-12H-CC suggests a level within the middle and lower part of the *C. rhombicus* Zone, respectively. The highest *Lisitzinia ornata* occurs in Sample 120-747-13H-CC, indicating a position within the *R. gelida* Zone. *Rossiella symmetrica,* the diatom that marks the top of the *R. gelida* Zone, has its highest appearance in Core 120-747A-16H below the base of the *R. gelida* Zone; further examination may extend the range of this species upward. An acme of *R. gelida* and *Rocella schraderi* is noted in Sample 120-747A-14H-CC.

Reworked lower Oligocene and upper Eocene diatoms occur in Sample 120-747A-17-CC, along with rare benthic diatoms and probably *in-situ* upper lower Oligocene diatoms. Diatoms in Sample 120-747-17H-CC are etched and poorly preserved.

Magnetobiostratigraphy

A major aim of biostratigraphy is to provide a means of subdividing the stratigraphic record of earth history by means of the sequential, nonrepetitive evolutionary changes in fossil faunas and floras. In recent years it has become possible to correlate the biostratigraphic record to the iterative (i.e., repetitive) stratigraphic scale based on changes in the earth's magnetic polarity. This polarity record in rocks and sediments has, in turn, been correlated to the iterative scale based upon seafloor magnetic lineations.

These two scales have assumed a shadowy ordinality of their own by means of numerical calibration using isotopic dates and certain assumptions of linearity in downcore sedimentation rates and/or seafloor-spreading rates. The interpretation and correlation of biostratigraphic data to these scales have allowed the development of integrated magnetobiochronologic scales and their application to regional, if not global, problems of earth history (see Berggren et al., 1985a, 1985b, 1985c, for an example).

In recent years it has been possible to develop an integrated magnetobiochronologic framework for tropical-subtropical Cenozoic calcareous plankton biostratigraphy (Berggren et al., 1985a, 1985b, 1985c). More elusive, however, has been the development of a similar integrated framework (earlier than the late Neogene) for the high southern (and, to a lesser extent, the high northern) latitude Cenozoic. Correlation between these two areas (and biostratigraphies) has often been by indirect, second-order means, with age estimates often tenuous at best and misleading at worst, and with resolution seldom better than several million years.

This rather lengthy introduction serves to emphasize what is considered to be a potential major contribution toward providing a truly integrated global Cenozoic marine biostratigraphy. Leg 120 studies have succeeded in defining a good paleomagnetic polarity record over the upper 160 m of the stratigraphic record of Hole 747A (see "Paleomagnetics" section, this chapter). This interval spans essentially the last 30 m.y. and represents the early/late Oligocene boundary to the late Pleistocene. Virtually all the major events (anomaly correlatives) can be recognized from 1 through 10, and the structure of most of the polarity chrons is recognizable as well despite the low sedimentation rate(s) (<1 cm/1000 yr).

Primary calibration to the standard paleomagnetic polarity scale (General Polarity Time Scale [GPTS]) was achieved by means of the magnetobiochronologic correlations (Table 6). Identification of the other anomaly correlatives and the magnetic polarity chrons was made by integrating biostratigraphic data from siliceous (diatom and radiolarian) fossils (see separate reports earlier in this chapter) and general pattern recognition based on the apparently constant sedimentation rate at this site.

The position of the major chronostratigraphic boundaries of the late Paleogene and Neogene in Hole 747A and of the late Neogene in Hole 747B is listed in Table 7, based on the magnetobiostratigraphic correlation (and associated arguments) presented in the GPTS of Berggren et al. (1985a, 1985b, 1985c).

PALEOMAGNETICS

Site 747, located in the transition zone between the northern and southern parts of the Kerguelen Plateau, provided excellent material for a nearly complete reversal sequence from the present to the middle Oligocene. The archive halves of most cores were measured with the pass-through cryogenic magnetometer to obtain their natural remanent magnetization (NRM). Each section of core was demagnetized at a peak alternating field (AF) of 9 mT. Few sections had magnetizations too strong for the cryogenic magnetometer. We paid attention to all occurring resets (overranging of the flux counter) and repeated measurements on a less sensitive range whenever resets occurred. Initial problems with the belts moving the sample tray were repaired.

Because of the relatively high southern latitude, the inclination could be used as an indicator of magnetic polarity and oriented cores were not required. The absolute values of inclination were about 70° in ideal cases, which is expected for the location in a geocentric axial dipolar magnetic field. In many cases, we observed a shallowing of the inclinations, which is known as the inclination error. The intensity of magnetization of the sediment cores was generally above 0.2 mA/m, the noise level of the cryogenic magnetometer under the ambient conditions.

The background level of the magnetometer drifted with the ship's motion because of the heavy seas and limited sensitivity to the measurement of magnetizations above 0.2 mA/m. One peculiarity we noticed was that the declination did not change in between cores, as one would expect from unoriented cores. In-

Table 6. Primary calibration of Hole 747A samples to the standard paleomagnetic polarity scale (GPTS) based on the magnetobiochronologic correlation.

Planktonic foraminifer and nannofossil datum in Hole 757A	Location in Hole 757A	Age (Ma)	Magnetic anomaly correlation	Depth (mbsf)
1. FAD *N. nympha*	Between 120-747A-7H, 40-44 cm, and 120-747A-7H-CC	10.2	5	64.9-66.0
2. LAD *G. zealandica*	Between 120-747A-8H-CC and 120-747A-9H-CC (75.5-85.0 mbsf)	16.8	5C	85-92
3. FAD *G. zealandica*	Between 120-747A-10H-CC and 120-747A-11H-CC (94.5 and 104.0 mbsf)	17.6	*(5D)	(93-98)
4. LAD *C. dissimilis*	Same as *G. zealandica*	17.6	*(5D)	(93-98)
5. LAD *R. bisecta*	Between 120-747A-13H-CC and 120-747A-14H-CC (123-132.5 mbsf)	23.7	6C	126-129
6. LAD *Chiloguembelina*	Between 120-747A-16H-CC and 120-747A-17H-CC (151.5-161.0 mbsf)	30.0	10	155-159

*Anomaly Correlative 5D is NOT recognized as such in the polarity record in Hole 747A. The FAD of *G. zealandica* and the LAD of *Catapsydrax dissimilis* have been recognized in Hole 516F at the C5c/C5d (= top 5D) boundary (Berggren et al., 1985c). In Hole 747A a short reversed interval occurs below the normal polarity interval identified as Anomaly Correlative 5C. Since Anomaly Correlative 5E is identified below (100-106 mbsf), the relative position and spacing of Anomaly Correlative 5D is correct and the location of the two datum levels (3 and 4) are used to estimate a numerical age for this level. The estimated position/level of Anomaly Correlative 5D is shown in parentheses to indicate that it is NOT actually recorded at Hole 747A.

Table 7. Major chronostratigraphic boundaries based on the magnetobiostratigraphic correlation in Holes 747A and 747B.

Chronostratigraphic boundary	Approximate location in Holes 747A and 747B	Anomaly correlative/ chron
1. Pliocene/Pleistocene	747B: 7 mbsf	Just above 1
2. Miocene/Pliocene	747A: 38 mbsf 747B: 33 mbsf	Between Gilbert "C" and Chron 5 (= 3A)
3. upper/middle Miocene (Tortonian/Messinian)	747A: 52 mbsf	Early part 5
4. middle/lower Miocene (Burdigalian/Langhian)	747A: 87 mbsf	Late 5C
5. Oligocene/Miocene (Aquitanian/Burdigalian)	747A: 127 mbsf	6CN2
6. lower/upper Oligocene (Rupelian/Chattian)	747A: 157 mbsf	mid-10

stead, declination increased continuously from 0° at Core 120-747A-1H to 100° at the bottom of Core 120-747A-16H where APC coring stopped. This relatively constant declination suggests orientation of cores with respect to azimuth during HPC coring.

Furthermore, one would have expected for the case of oriented cores that declination alternates between 0° and 180° together with the reversals determined from the inclination. We attribute the declination around 0° to a small viscous component from the present magnetic field, which was not completely removed by AF demagnetization at 9 mT. Measurements of NRM on a few single sample cubes agreed with the polarity record from the cryogenic magnetometer.

In the Southern Hemisphere, negative inclinations represent normal magnetic polarity whereas positive inclinations indicate reversed. The declination, inclination, and intensity record of NRM from the first 200 m of Hole 747A is shown in Figures 23 and 24. Many sections of the first three cores were quite soupy and therefore unsuitable for paleomagnetic investigation. Starting from Section 120-747A-4H-2, we have a nearly continuous record of inclination down to 165 mbsf.

All core sections were AF demagnetized at 9 mT after the NRM measurement. This magnetic cleaning procedure was applied to remove unwanted soft secondary components of magnetization such as drilling-induced remanent magnetization or viscous remanent magnetization (VRM). The AF demagnetization changed the magnetic record of Figure 23 slightly and revealed more detailed features of the reversal sequence. The results after AF demagnetization are shown by black dots in Figure 24. The results from the shore-based AF-demagnetization experiments agreed in about 90% of the cases with the magnetostratigraphy determined on the ship. As far as the shore-based studies contributed to improve the shipboard magnetic record, these selected results were incorporated in Figures 24 and 25 as black stars.

The interpretation of the inclination record in terms of magnetic reversals is shown to the right of the inclination plot in Figure 24. Normal magnetic chrons and subchrons are shown in black and reversed ones in white. Gaps in the record are indicated by vertical lines and uninterpretable data by diagonal lines. Our interpretation of the reversal sequence has benefited greatly from information provided by the paleontologists on Leg 120. We interpret the first long normal interval in Figure 24A as the Gauss normal polarity chron. Unfortunately, the sedimentation rate was low at Site 747 and our measurements every 15 cm along the core were not able to resolve the shorter subchrons, which could have provided instantaneous "fingerprints" to determine the numeric ages from a standard time scale (Berggren et al., 1985a, 1985b, 1985c).

Chrons C5 and C5c (Anomaly Correlatives 5 and 5c) were identified by correlation with biostratigraphy. Other long normal periods such as 5e and 6 were matched up with the long normal anomalies of the seafloor-spreading record, assuming a constant sedimentation rate for Hole 747A as a first approximation. The three short normal anomaly correlatives (6c) at the beginning of the Miocene are identified in Figure 24C between 126 and 130 mbsf. Even though the quality of the inclination record deteriorated below 150 mbsf where XCB drilling started, we were able to extract polarity information from the cores. The normal Chron C10n (Anomaly Correlative 10 in the middle Oligocene) was identified between 155 and 160 mbsf (Fig. 24). The interpretation of the reversal sequence of Figure 24 was greatly aided by cross-correlation with the appearance of certain microfossil species. For details the reader is referred to the "Biostratigraphy" section ("Magnetobiostratigraphy" subsection), this chapter.

The identification of magnetic polarity chrons in the top 50 mbsf was aided by the inference of an unconformity, which was found from the sedimentation rate determination. There appears to be a hiatus in the sedimentary sequence at about 38 mbsf, above Anomaly Correlative 4A. Evidence for this hiatus just below the normal subchrons of the Gilbert comes from a combination of biostratigraphic and magnetostratigraphic results. The hiatus might coincide with the changes in intensity of magnetization at approximately 38 and 35 mbsf in Figures 24 and 25, respectively.

Hole 747B provided better material for magnetostratigraphy from 0–50 mbsf. The AF demagnetization of the cores of Hole 747B revealed a distinct reversal pattern, as shown in Figure 25. Still, we regard the interpretation of the inclination record in terms of anomaly correlatives (Figs. 24 and 25) as tentative. Further detailed AF demagnetization experiments on the single sample cubes are required for a final interpretation.

We collected 12 basement rock samples from Cores 120-747C-11R, -12R, -14R, and -15R. Inclinations and intensities of NRM were measured with the Molspin magnetometer. Declinations are not known since the cores were unoriented. We progressively AF demagnetized 3 samples up to 50 mT. The AF demagnetization results indicate single stable components of magnetization, and the inclinations of NRM are scattered about a mean value of −47°. Further AF and thermal demagnetization experiments are needed to obtain a reliable estimate for the basement rock inclination and the resulting paleolatitude of Site 747.

In conclusion, we obtained a nearly complete magnetostratigraphy between the Gauss polarity chron and the normal polarity Chron C10n in the middle Oligocene.

SEDIMENTATION RATES

Data

Biostratigraphic and paleomagnetic data were used to construct an age-depth curve for Site 747 (Fig. 26). The biostratigraphic data used are listed in Table 8, and the paleomagnetic data are plotted on the left in Figure 26. The paleomagnetic polarity record from Hole 747B was used instead of the data from Hole 747A for the uppermost 50 m of section, due to the better quality of the paleomagnetic data obtained from Hole 747B.

Methods

Biostratigraphic data were first used to estimate the approximate age of sediments in Site 747. Comparison of the paleomagnetic data from each depth interval to the age-equivalent portion of the paleomagnetic reversal scale (Berggren et al., 1985a, 1985b, 1985c) was then used to identify selected polarity reversal events in the paleomagnetic data (Fig. 26). These levels

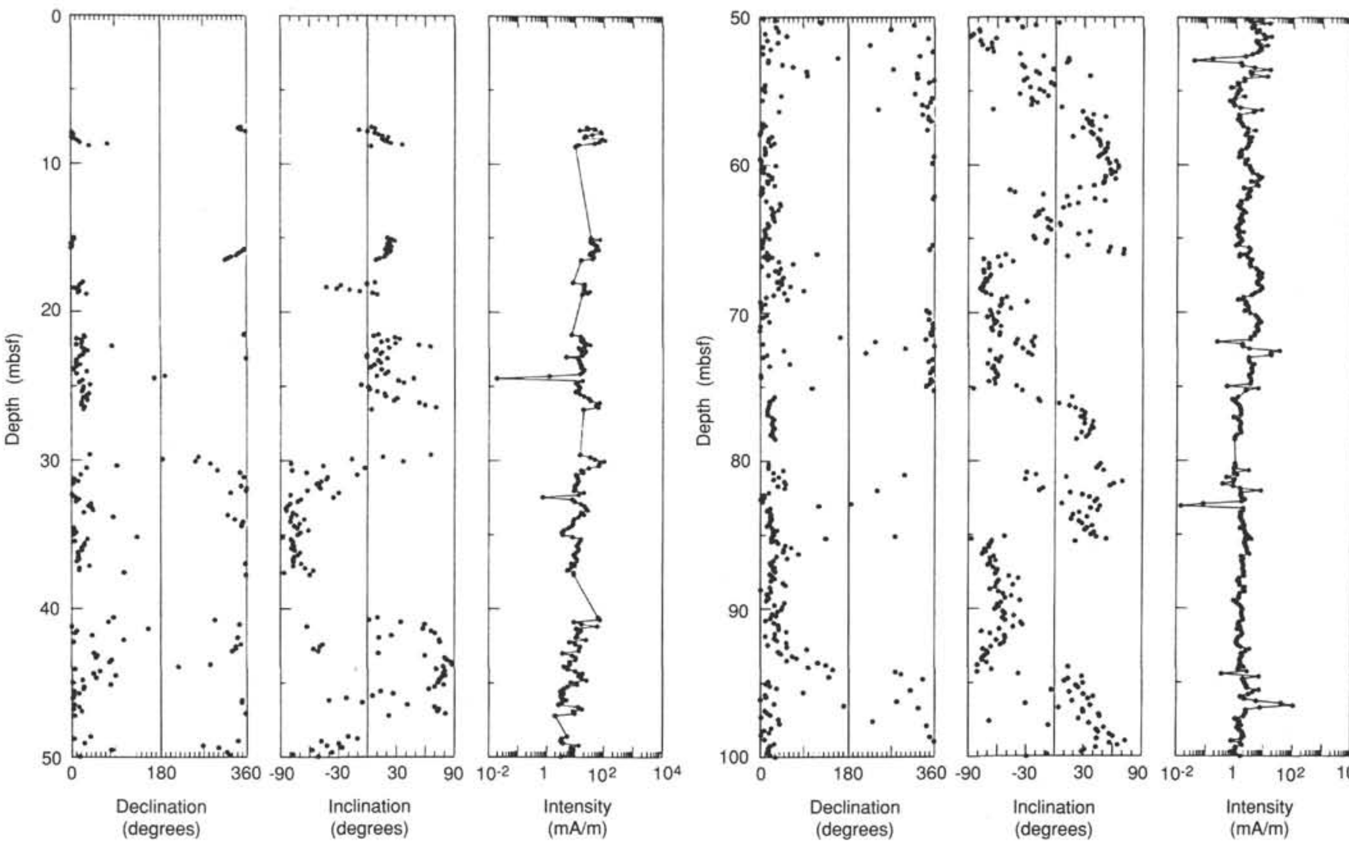

Figure 23. Declination, inclination, and intensity of NRM of archive halves as a function of depth (mbsf) measured with the cryogenic magnetometer for Hole 747A. Negative inclinations represent normal magnetic polarity and positive inclinations represent reversed polarity.

were used in turn to adjust age estimates for the stratigraphic section. The magnetic polarity events thus identified are (1) top of the Gauss (19.5 mbsf; 2.47 Ma); (2) top of "c" event of the Gilbert (31.0 mbsf; 4.4 Ma); (3) base of Chron 11 (52.4 mbsf; 10.4 Ma); (4) top of C5c (85.3 mbsf; 16.2 Ma); and (5) top of C10 (154.5 mbsf; 29.7 Ma).

Line segments forming the age-depth curve for the late Oligocene to Holocene interval were drawn through the paleomagnetic control points and as close as possible to the biostratigraphic control points. The remaining portions of the age-depth curve were drawn using biostratigraphic control points only.

Hiatuses

Several polarity intervals appear to be missing from the magnetostratigraphic data between the base of Chron 11 and the "c" event of the Gilbert. This evidence, together with biostratigraphic evidence for a major change in sedimentation rate between the lower Pliocene and upper Miocene, was used to infer a hiatus of ~2.5 m.y. duration between ~5.0 and 7.2 Ma. Neither biostratigraphic or paleomagnetic data suggest the presence of any other hiatuses in sediments of late Oligocene to Holocene age. Several other hiatuses and/or intervals of very slow sedimentation are apparent in the lower Paleogene and Upper Cretaceous. In fact, most of the upper Maestrichtian through Eocene interval appears to be missing, based on biostratigraphic evidence.

Rates of Sedimentation

Sedimentation rates at Site 747 are low and remarkably constant throughout the late Oligocene to Holocene, with a value of 5 m/m.y. The remainder of the Tertiary section is missing or present in highly condensed intervals only a few meters thick. Rates of sedimentation in the Cretaceous are not strongly constrained by the available biostratigraphic data, but they appear to be at least moderately high (≥ 20 m/m.y.) in the Campanian and Maestrichtian. Insufficient data exists to determine rates of sedimentation in the Santonian sediments at the base of the sequence.

INORGANIC GEOCHEMISTRY

Introduction

At Site 747 three holes were cored in Upper Cretaceous to Holocene sediments in the transition zone between the northern and southern parts of the Kerguelen Plateau. Total sediment thickness drilled was 295.1 m, and core recovery was 89% for the sediments, so continuous sampling for interstitial water (IW) at about 30 m intervals was possible. The sediments recovered provided a sequence of Upper Cretaceous to Pleistocene calcareous oozes and chalk with very minor volcanogenic layers, some chert layers, and underlying basaltic basement rocks. Estimated sedimentation rates are low (<1 cm/1000 yr) during the Cenozoic and somewhat higher (but still <2 cm/1000 yr) during the Cretaceous (see "Lithostratigraphy and Sedimentology" section, this chapter).

A total of 11 samples were obtained from Holes 747A and 747C. From every third core, 5-cm-long, whole-round samples (10-cm-long deeper in the hole) were taken for routine IW analysis. The samples were squeezed at room temperatures (about 20°C) with a 9-cm-wide stainless steel press (Manheim and Sayles, 1974) and a hydrostatic pressure of 14 tons. Determinations of salinity, pH, and alkalinity were carried out immediately, whereas analyses of Cl, Ca, Mg, and Si ions were performed in batches under room temperature conditions after storing the

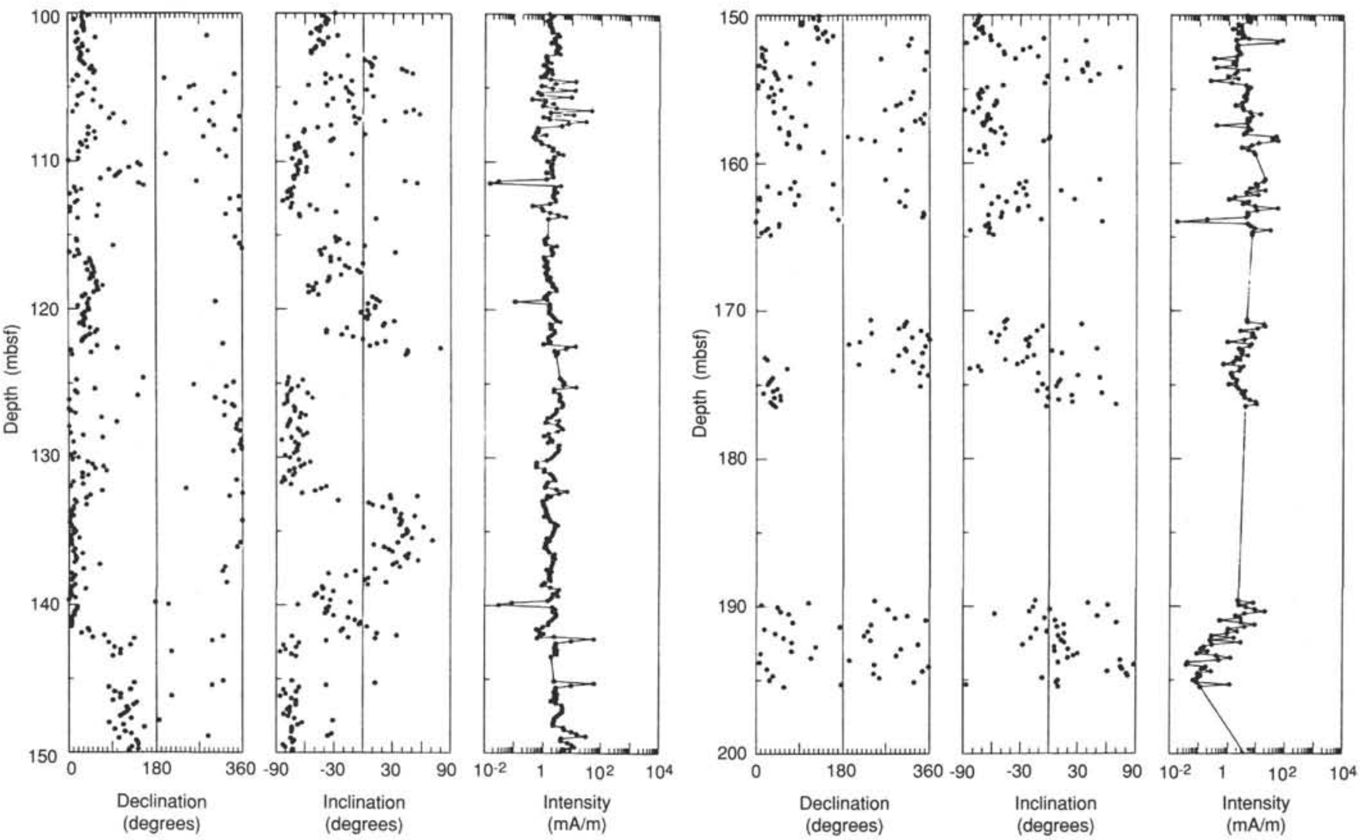

Figure 23 (continued).

samples in a refrigerator. All determinations were carried out within 5 days.

The methods used are outlined in detail in Gieskes and Peretsman (1986) and summarized in the "Explanatory Notes" chapter (this volume). All data presented are reported to the appropriate level of precision for each type of analysis.

Results

All the data obtained by means of shipboard analysis of IW from Site 747 are reported in Table 9 and graphically displayed in Figure 27. Contamination of IW by drill fluids or seawater has influenced only the upper 20–30 m, where the sediment was of an unconsolidated soupy appearance.

Salinity and Chlorinity

Little variation is shown by the salinity values (total dissolved solids), which range from 35.5 to 36.4 g/kg and average 36.1 g/kg. This value is slightly above average seawater (35.2 g/kg); thus, IW salinity is related to high-salinity bottom water and cold high-latitude seawater. The Cl values (555–575 mM), again in the range of seawater or slightly higher, show a slight overall increase with depth. The values of the uppermost sample for salinity (35.5 g/kg) and chlorinity (555 mM) most probably reflect recent to subrecent bottom seawater influence.

Influx of solutions from different sources (low-salinity water, brines) can be excluded. No diagenetic or alteration processes within the calcareous sediments appear to significantly change the salinity or chlorinity of the IW. Diffusion processes in an open system are the only mechanisms affecting salinity and chlorinity of the IW, beside possible contamination with seawater within the upper 30 m.

Alkalinity and pH

An overall decrease in pH from 7.75 near the top of the sediment pile (7.45 mbsf) to 7.43 at the bottom (250.90 mbsf) is observed, with the exception of one scattered low value at 24.45 mbsf. A pronounced pH decrease is evident at depths >194 mbsf, whereas between 50 and 194 mbsf the pH remains constant at about 7.62 + 0.03, indicating stable open system diffusion conditions. Alkalinity values decrease from 3.22 mM at the top to 1.27–1.29 mM at the bottom. The change in alkalinity is discontinuous though still significant up to 164 mbsf downhole.

We noticed a sharp drop to low values (1.27 mM) within the interval between 164 and 194 mbsf (Cores 120-747A-19X to -21X). Within this interval, a volcaniclastic sediment layer is intercalated. Mineral formation and alteration of volcanic glass in this layer may consume some of the alkali bases. Again, this would suggest open system diffusion processes and selective incorporation of alkali bases in mineral-forming processes in the clastic layer.

Another more probable possibility is the precipitation of calcium carbonate (and thus a decrease in HCO_3^-) and/or silicate (and thus a decrease in $H_3SiO_4^-$) below 194 mbsf (Gieskes, 1974). This could be a consequence of increased calcium dissolution and changed lithology and physical properties of the sediments, especially in lower porosities (cementation) and higher thermal conductivity (see "Physical Properties" section, this chapter). The total carbonate contents reflect this change also (see "Organic Geochemistry" section, this chapter).

Magnesium and Calcium

Within the upper 25 mbsf, magnesium and calcium show values only slightly different from seawater. From 53 to 262.90

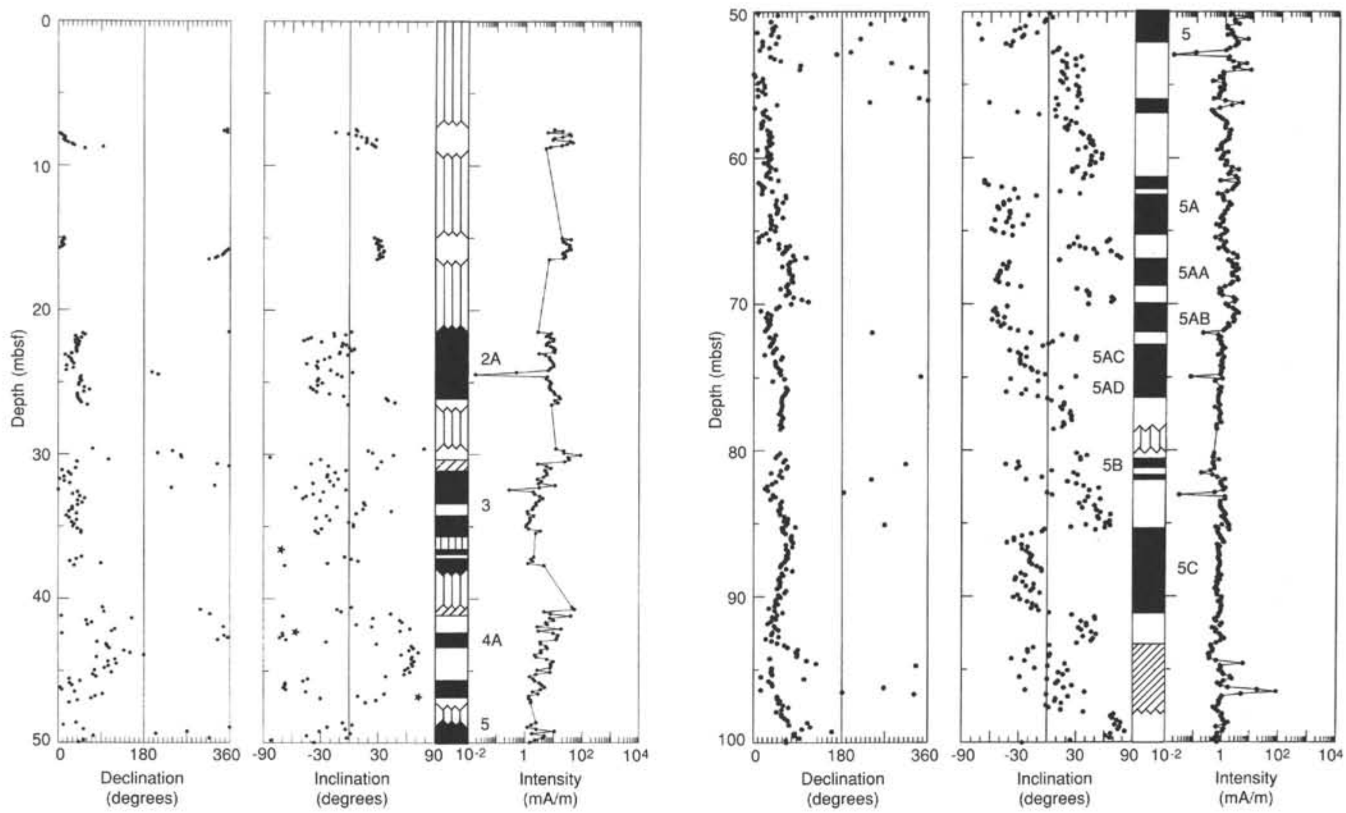

Figure 24. Declination, inclination, and intensity of archive halves of Hole 747A after AF demagnetization at 9 mT shown by black dots. Inclinations of selected single samples that were stepwise AF demagnetized to 40 mT are shown by black stars. A tentative interpretation of the inclination record in terms of polarity reversals (with the possible names and numbers of anomaly correlatives) is shown to the right of the inclination. Normal chrons are shown in black color and reversed ones in white. Data gaps are indicated by vertical lines and uninterpretable data by diagonal lines.

mbsf, Mg and especially Ca display linear changes in their respective concentrations; that is, Mg decreases from 52.5 to 44.2 mM, and Ca increases from 12.79 to 24.25 mM. A significant change in the linear fit is observed at 194 mbsf, where Ca dissolution in IW increases markedly. Preliminary calculations show a dissolution rate for calcium of 0.46 mM/10 m between 24 and 194 mbsf.

No calcareous cement or incrustation of fossils is reported in this interval (see "Lithostratigraphy and Sedimentology" section, this chapter). The Ca dissolution rate drastically increases to 0.8 mM/10 m between 194 and 251 mbsf. Within this interval a change in physical properties (see "Physical Properties" section, this chapter) is noticed.

The only parameters affecting Ca dissolution in IW are depth-controlled diagenesis and lithology and physical properties of the sediment. Down to 194 mbsf, carbonate diagenesis enables enhanced Ca dissolution. From 194 to 251 mbsf, changes in the lithology and physical properties of the sediment (porosity, water content, total carbonate, etc.) are correlated with increased Ca dissolution. Magnesium decreases with increasing depth and mirrors the increasing Ca concentrations. This conservative behavior is not due to the formation of magnesium-bearing minerals (there are none in the calcareous sediments) but, rather, is related to cation exchange with Ca in carbonates. The Mg/Ca ratio decreases by a factor of 2.5 downhole, reflecting an inversely correlated Ca increase and Mg decrease.

Silica

Dissolved silica ranges from 696 to 316 μM and decreases downhole. These values lie considerably above average seawater and reflect active silica dissolution. Sources for silica are siliceous microfossils (see "Biostratigraphy" section, this chapter). A marked drop in dissolved silica is observed between 164 and 194 mbsf. Within this interval a volcaniclastic layer and some chert layers are intercalated, which may serve as a sink for dissolved silica. Below 194 mbsf silica concentrations remain low because of silica precipitation within the chert layers. Silica precipitation, decreases in alkalinity, and presumed calcium-carbonate precipitation are correlated with changed physical properties at depths greater than 194 mbsf.

Summary

Salinity and chlorinity reflect the overall seawater nature of the IW. The decrease in dissolved Mg and increase in dissolved Ca is a result of Ca dissolution and Mg deposition as a function of depth (diagenesis) under nearly constant IW and sediment conditions. Sharp drops in pH and especially alkalinity and dissolved silica at depths >194 mbsf reflect carbonate and silicate precipitation. The increased Ca dissolution (up to 0.8 mM/10 m) seems to enforce this effect.

Three distinct zones can be determined in the IW column: (1) an upper zone (down to about 10 mbsf) with close standard seawater affinities and active silica dissolution; (2) an intermediate zone (down to about 200 mbsf) with conservative, depth-controlled IW behavior; and (3) a lower zone with markedly increased Ca dissolution and drops in pH, alkalinity, and dissolved silica. This zone is located below the volcaniclastic sequence and shows even in its physical properties differences from the upper 200 m of sediment.

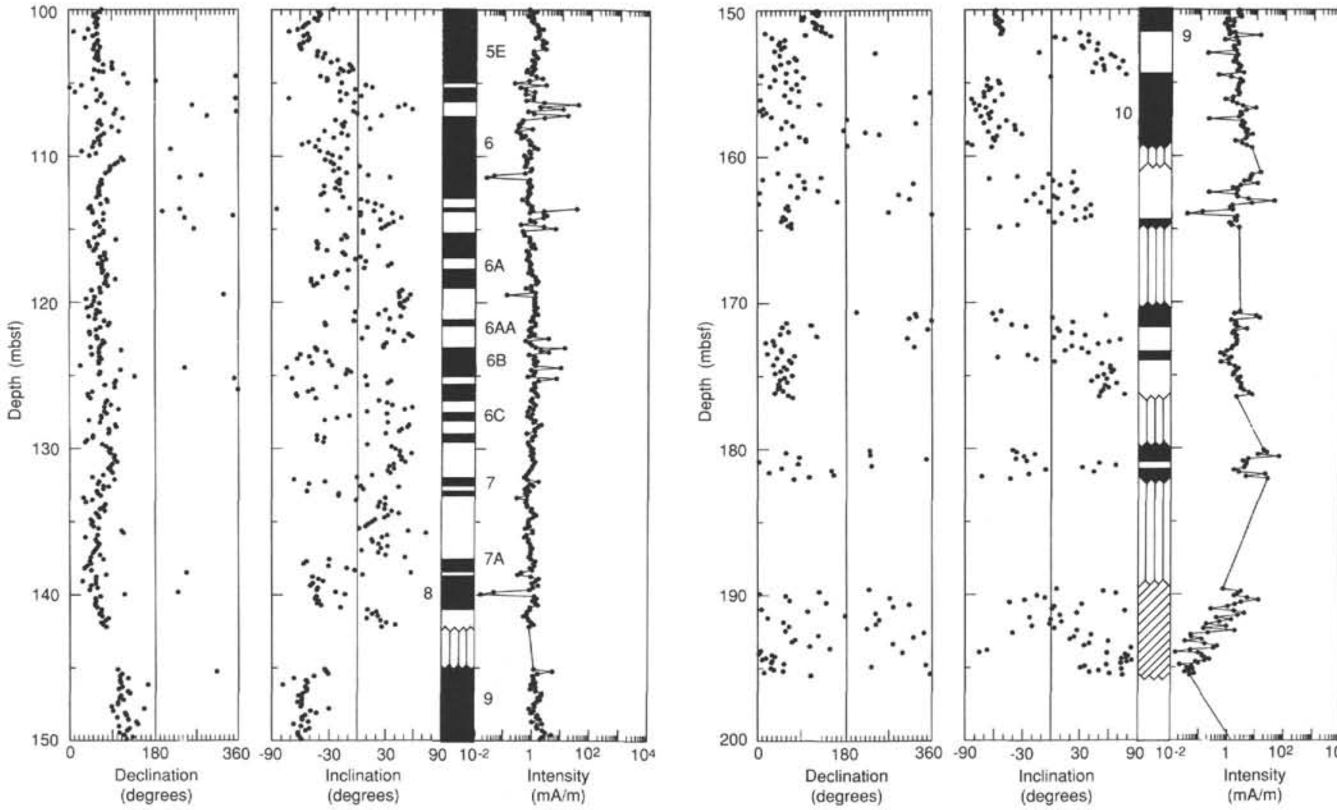

Figure 24 (continued).

The following parameters affect the geochemistry of the IW: (1) diffusion in an open system for the upper 200 m of sediment; (2) diagenesis-controlled calcium dissolution; (3) siliceous fossil- and diagenesis-controlled silica dissolution and precipitation; and (4) changed lithology and physical properties below 200 mbsf.

ORGANIC GEOCHEMISTRY

Inorganic and Organic Carbon

Inorganic carbon analyses were conducted on a total of 180 samples from Holes 747A and 747C. The majority of samples analyzed were physical properties samples taken at 1-per-section intervals. In order to improve the resolution of the carbonate record over the Miocene-Pliocene portion of the record, an additional sample per section was taken specifically for carbonate analyses from Cores 120-747A-3H through -9H. Total organic carbon content (TOC) was determined by the difference in total carbon and inorganic carbon. A smaller number of samples was analyzed for TOC at Site 747 due to the overall highly oxic condition of the sediments. All inorganic and organic carbon results are reported in Table 10 and Figure 28. Analytical methods are outlined in the "Explanatory Notes" chapter (this volume).

Percent calcium carbonate values range from <20% to >98% at Site 747 (Fig. 28). The lowest concentrations were recorded near the top of Hole 747A just 0.5 m below the sediment/water interface. The surface sediments here are composed almost entirely of siliceous microfossils. Below this interval, between 2.5 and 25.02 mbsf, carbonate concentrations display considerable variability, ranging from 34% to 77%. The changes result mainly from the fluctuation in the relative percentages of siliceous and calcareous microfossils.

From 25.02 to 62.0 mbsf, there is a gradual increase in carbonate concentration percentages, reflecting the decrease in the abundance of siliceous microfossils. With the exception of a sharp decrease in carbonate at 181.0 mbsf, the values remain relatively high over the interval from 62.0 to 300.0 mbsf, generally exceeding 90%. The major components of the high carbonate interval are calcareous nannofossils and planktonic foraminifers. The decrease at 181.0 mbsf reflects the presence of a sand- and pebble-rich channel deposit. Other anomalous low values appear to be associated with volcanic-ash- and chert-rich intervals.

In general, the TOC values at Site 747 are relatively low. Although several samples yielded organic carbon contents ranging from 0.2% to 0.5%, the majority of samples analyzed generally contained <0.2% organic carbon, just slightly above the detectable limit on board ship (Fig. 28). Such low organic carbon contents are characteristic of pelagic biogenic sequences with low rates of burial (<1 cm/1000 yr) and average levels of productivity (McIver, 1975; Müller and Suess, 1979).

Hydrocarbon Gases

Gases were extracted from gas pockets in the core barrel by Vacutainer before splitting, and from sediment samples by head-space techniques. Head-space analyses were conducted on a routine basis with sampling of every third core. An outline of analytical procedures is provided in the "Explanatory Notes" chapter (this volume).

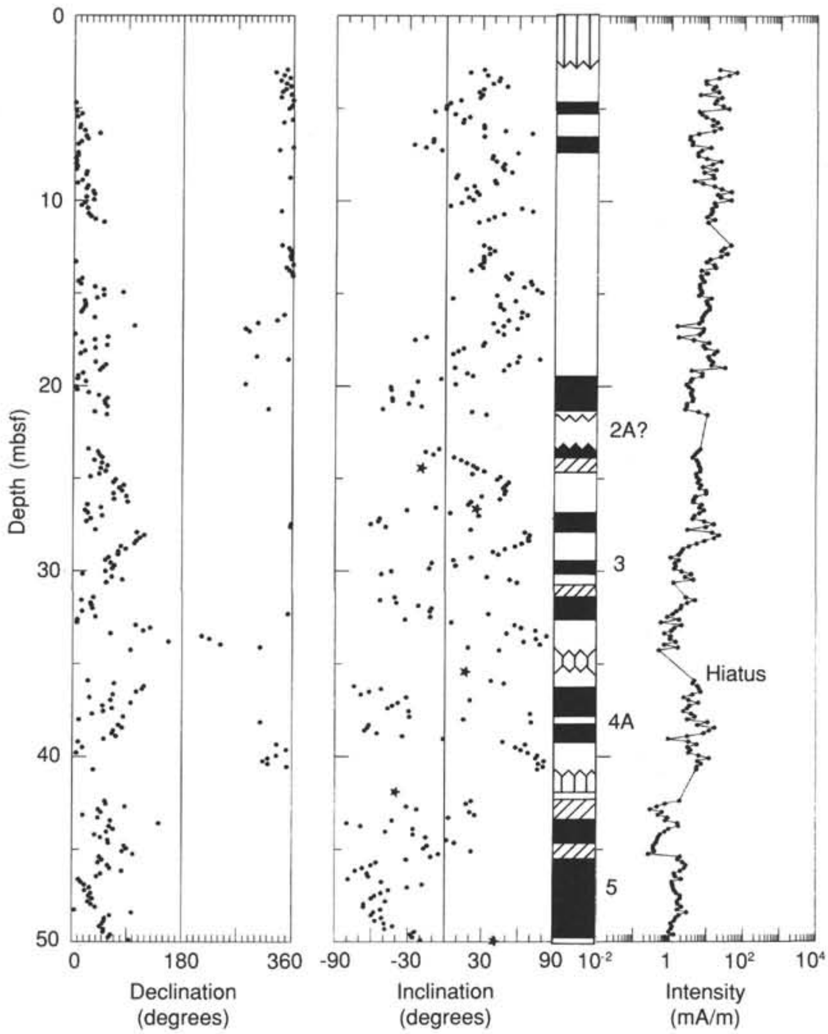

Figure 25. Declination, inclination, and intensity of archive halves of Hole 747B after AF demagnetization at 9 mT. Black stars represent results from AF demagnetization of discrete samples. Interpretation of data as in Figure 24. Hole 747B gave a more complete magnetic record for the first 50 mbsf than Hole 747A.

Hydrocarbon gases were not detected in any of the samples analyzed from Site 747. This finding is consistent with the low TOC contents reported above.

PHYSICAL PROPERTIES

Introduction

The shipboard physical properties program at Site 747 was designed to aid in the interpretation of geological sampling and geophysical results from the Southern Kerguelen Plateau. Three holes (747A, 747B, and 747C) were cored at Site 747. Hole 747A was completed using APC and XCB techniques to 256 mbsf. At Hole 747B, an additional six APC cores were obtained to duplicate the lithologic record for the upper 60 m of Site 747. Coring at Hole 747C with the RCB provided a complementary record of the lower part of the lithologic column. Hole 747C recovered over 50 m of basalt.

Physical properties measurements were made at regular intervals in the sedimentary sequence in order to correlate changes in index properties and compressional wave velocity to the lithologies recovered. Samples of basalt were also measured for compressional wave velocity and bulk density values. The results of these measurements are displayed in graphic and tabular form. In many of the summary figures, the physical properties measurements from the three holes cored have been combined to form semicontinuous profiles for Site 747.

The physical properties measured at Site 747 were (1) index properties–gravimetric determinations of bulk density, grain density, water content, and porosity (Figs. 29 and 30; Table 11); (2) compressional wave velocity (Figs. 31 and 32; Table 12); (3) undrained shear strength (Fig. 33; Tables 13 and 14); (4) thermal conductivity (Fig. 34; Table 15) and downhole temperature (Fig. 35); (5) carbonate content (Fig. 36; see "Organic Geochemistry" section, this chapter); and (6) continuous measurements of GRAPE (Gamma Ray Attenuation Porosity Evaluator) bulk density and *P*-wave velocity (Fig. 37). These measurements were used to evaluate the geotechnical stratigraphy at Site 747.

Geotechnical stratigraphy has been defined by Taylor (1984) as the study of the vertical, successive characteristics of a sediment that can be used to define the distinct geotechnical aspects of a sedimentary unit. The geotechnical properties of a particular lithology are the result of the combined depositional and postdepositional processes that acted on the sediments over geologic time. Variations in physical properties can often be linked to changes in the environment of deposition or tectonic history of a particular region.

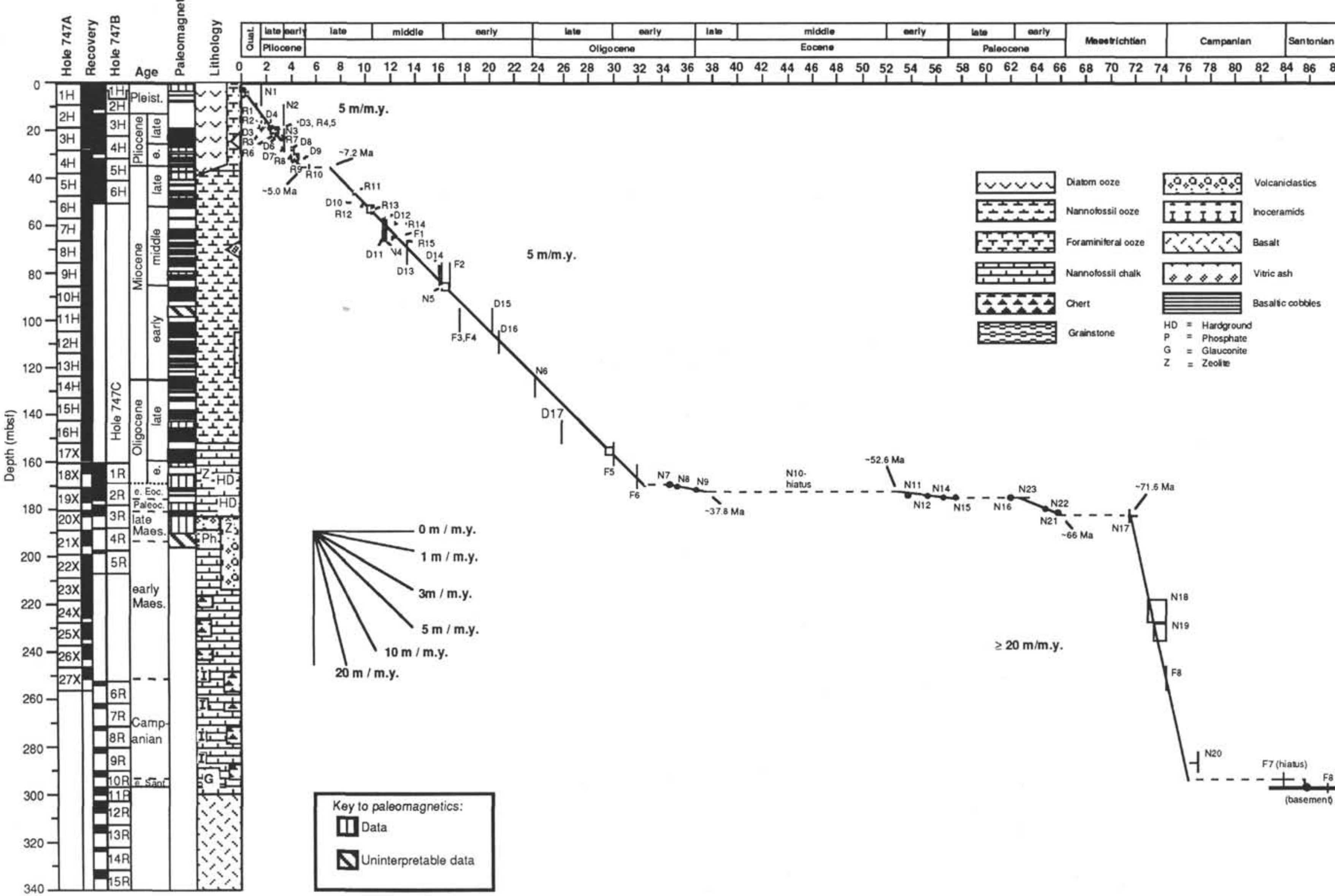

Figure 26. Age vs. depth curve for Site 747 showing sedimentation rates. Ages were determined as described in the text. Paleomagnetic data is from "Paleomagnetics" section, this chapter. Lithology is shown in the right-hand column on the left of the figure; for an explanation of the lithologic column symbols, see "Lithostratigraphy and Sedimentology" section, this chapter, and "Explanatory Notes" chapter, this volume. The time scale (horizontal axis) is from Berggren et al. (1985a, 1985b, 1985c) and Kent and Gradstein (1985). Biostratigraphic datum levels (e.g., "N2," "F6," etc.) are from Table 8, which gives the age, depth, fossil group, and name of each datum. Depth uncertainty in the placement of datum levels is shown by vertical lines, uncertainty in age calibration by horizontal lines, and uncertainties in both depth and age by hollow boxes. Bull's-eye symbols are used for datum levels with depth and/or age uncertainties too small to be visible on plot. Magnetostratigraphic control points (white boxes) are listed and described in the text. Solid line segments of age-depth curve denote continuous sedimentation, dashed lines denote hiatuses. The average rate of sedimentation is shown for major segments of the age-depth curve between hiatuses. For additional details and discussion, see text.

Table 8. Site 747 biostratigraphic data used for sedimentation rate plot.

#	Depth (mbsf)	Age (Ma)	Name
F1	64.9–66.0	12.1	B *N. nympha*
F2	75.5–85.0	16.8	T *G. zealandica*
F3	94.5–104.0	17.6	B *G. zealandica*
F4	94.5–104.0	16.8	T *C. dissimilis*
F5	151.5–161.0	30.0	T *Chiloguembelina*
F6	161.0–170.5	32.0	T *S. angiporoides*
N1	0–9.0	1.68	B *G. oceanica*
N2	9.0–18.5	3.4	B *P. lacunosa*
N3	18.5–28.0	3.5	T *R. pseudoumbilica*
N4	56.5–66.0	11.6	T *R. floridana*
N5	75.5–85.0	16.2	T *H. ampliaperta*
N6	123.0–132.5	23.7	T *R. bisecta*
N7	168.5–169.45	34.6	T *R. umbilica*
N8	170.39–170.67	35.1	T *E. formosa*
N9	171.32–171.48	36.7	T *D. saipenensis*
N10	172.93	37.8–52.6	Unconformity
N11	173.58–173.8	53.7	T *T. orthostylus*
N12	173.97–174.21	55.3	B *D. lodoensis*
N14	174.35–174.55	56.6	B *T. orthostylus*
N15	174.35–174.55	57.6	T *F. tympaniformis*
N16	175.06–175.51	62.0	B *F. tympaniformis*
N17	180.0–184.8	>71.5	T *R. levis*
N18	218.0–227.2	73–74.5	T *T. phacelosus*
N19	227.6–235.2	73.5–74.5	T *A. parcas, R. anthophorus*
N20	282.0–290.4	<77	B *Q. trifidum*
N21	181.14	65.9	B *C. primus*
N22	179.39	64.8	B *C. danicus*
N23	174.60	64.8	T NP3
D1	2.34–2.61	0.195	T *H. karstenii*
D2	3.16–4.17	0.62	T *A. ingens*
D3	17.36–18.50	1.55	T *R. barboi*
D4	18.5–18.71	2.45	T *C. insignis*
D5	18.77–20.49	2.64	T *N. weaveri*
D6	20.49–22.7	2.8	T *N. interfrigidaria*
D7	26.44–28.00	3.3	B *N. interfrigidaria*
D8	26.44–28.00	4.1	B *N. "angulata"*
D9	33.00–34.50	4.5	T *D. hustedtii* (consistent)
D10	~50	8.4–8.8	T *D. dimorpha*
D11	56.5–66.0	11.4	T *N. denticuloides*
D12	56.5–66.0	11.65	B *D. dimorpha*
D13	66.0–75.5	13.4	T *D. maccollumii*
D14	75.5–85.0	16.0	B *N. grossepunctata*
D15	94.5–104.0	20.3	T *C. oligocenicus*
D16	104.0–113.5	20.8	T *R. gelida*
D17	142.0–151.5	25.9	B *R. gelida*
R1	9.0–10.95	1.2	LAD *A. cylindrica*
R2	13.95–16.95	1.6	LAD *C. pliocenica*
R3	16.95–18.5	1.9	LAD *E. calvertense*
R4	18.95–20.45	2.4	LAD *H. vema*
R5	18.95–20.45	2.4	LAD *D. spongiosa*
R6	21.95–23.45	2.6	FAD *C. davisiana*
R7	21.95–23.45	3.2	LAD *P. titan*
R8	28.0–29.95	4.2	FAD *H. vema*
R9	29.95–32.95	4.4	LCO *L. grande*
R10	34.45–35.95	5.4	LAD *C. spongothorax*
R11	45.45–47.0	9.0	FAD *Multishell Collo.* sp.
R12	50.45–51.95	9.7	FAD *E. pseudoinflatum*
R13	51.95–54.95	10.4	LAD *A. golownini*
R14	58.45–59.45	12.3	FAD *C. spongothorax*
R15	66.0–66.45	13.4	FAD *A. golownini*

Changes in gradients for geotechnical parameters are used to divide the sedimentary column into geotechnical units. At Site 747 the variations in index properties, compressional wave velocities, and carbonate content have been used to propose five geotechnical units. This preliminary geotechnical stratigraphy agrees reasonably well with the lithostratigraphy proposed by the shipboard sedimentologists. When compared with core descriptions, the results of downhole logging, and the geophysical profiles for the site, the physical properties data provide a vital link between the geophysical data and the geological record described by the shipboard sedimentologists.

The methods employed in the measurement of the physical properties obtained during Leg 120 are described in the "Explanatory Notes" chapter (this volume). A more detailed discussion of these measurements can be found in Lambe and Whitman (1969) and Boyce (1976, 1977).

Index Properties

The index properties measured at Site 747 were determined gravimetrically using the Penta-pycnometer and a Scientec balance. Values of wet-bulk density, dry-bulk density, grain density, water content, and porosity were determined for each sample. These results are summarized in Table 11 and in Figures 29 and 30. The downhole trends for index properties are closely related to changes in the sediment lithologies. In the upper sequence, bulk density steadily increases and water content decreases. The sediments from 0 to 34 m have been identified as Unit I by the shipboard sedimentologists.

Unit I consists of Pleistocene to lower Pliocene diatom foraminifer ooze. These sediments are predominantly biosiliceous near the top of the interval and are increasingly calcareous downhole. The change from predominantly siliceous to calcareous lithologies is reflected in a decrease in water content from 91.50% at the seafloor to 31.37% at 34.5 mbsf. The effects of coring disturbance in the upper two cores may also influence water content values. The wet-bulk density values increase over the same interval from 1.19 to 1.75 g/cm^3. These changes reflect the influence of decreasing concentrations of the high void ratio, low density, and siliceous tests formed by diatoms, and the increasing concentrations of calcium carbonate observed in the sediment from Unit I.

The variations in calcium carbonate content at Site 747A are displayed in Figure 30. Porosity changes seem to be inversely related to fluctuations in calcium carbonate content in the sedimentary column. The relatively constant carbonate values between 34 and 150 mbsf are reflected in the small gradients observed in the general trends of the bulk density, grain density, water content, and porosity values over the same interval. The scatter in the grain density and bulk density values may result from other lithologic components in the sedimentary sequence.

The character of the noncarbonate matrix in deep-sea calcareous ooze strongly influences the physical properties of these sediments (Lee, 1982). Grain characteristics (size, shape, and sorting), physicochemical factors, and depositional history may also contribute to these changes (Bryant et al., 1981). The individual contributions of several interrelated variables, such as sediment lithology, the depth of burial, and the extent of diagenetic changes, are most likely responsible for the physical state of the sedimentary sequence recovered at Site 747.

The sediment recovered between 34 and 151 mbsf, composing Subunit IIA, consists of 117 m of upper Miocene to upper Oligocene nannofossil ooze and foraminifer nannofossil ooze with a variable foraminifer content. The lower geotechnical boundary of this unit is slightly deeper than the lithologic boundary. This boundary is marked by a slight increase in water content from 32% at 150 mbsf to 44% at 158 mbsf, and a decrease in bulk density from 1.83 to 1.70 g/cm^3 over the same interval (Fig. 29). These changes may reflect a change in grain size as well as lithology at the base of this unit. Below 151 mbsf the sediment changes to a nannofossil chalk with foraminifers, identified as Subunit IIB.

There is an inflection in trend for index properties at 170 mbsf. Bulk density increases from 1.72 to 1.95 g/cm^3, and water content decreases from ~38% to <30% over 3 m of core. This change corresponds to a change in lithology from a pale brown nannofossil chalk containing foraminifers to a white, burrowed nannofossil chalk, identified as Subunit IIC by the shipboard sedimentologists. No sampling for physical properties was con-

Table 9. Interstitial water chemical data, Site 747.

Core, section, interval (cm)	Depth (mbsf)	Vol. (cm^3)	pH	Alk. (mM)	Sal. (g/kg)	Mg^{2+} (mM)	Ca^{2+} (mM)	Cl^- (mM)	SiO_2 (μM)	Mg^{2+}/Ca^{2+}
120-747A-										
1H-5, 145-150	7.45	44	7.75	3.218	35.5	53.60	10.96	555	696	4.89
3H-4, 145-150	24.45	60	7.00	2.796	36.5	53.50	11.75	561	601	4.55
6H-4, 145-150	52.95	35	7.64	2.795	36.2	52.50	12.79	561	565	4.11
9H-6, 145-150	83.04	30	7.59	2.391	36.0	50.60	14.36	564	594	3.52
12H-5, 145-150	111.45	43	7.64	2.646	35.6	49.60	15.81	567	593	3.14
15H-5, 145-150	139.95	43	7.64	2.134	36.2	48.70	17.20	565	555	2.83
18X-2, 145-150	163.95	52	7.61	2.583	36.2	47.80	18.32	568	515	2.61
21X-3, 145-150	193.95	22	7.62	1.373	36.5	46.40	19.56	560	316	2.37
24X-3, 140-150	222.40	30	7.50	1.266	36.2	45.60	21.78	567	427	2.09
27X-3, 140-150	250.90	22	7.43	1.291	36.2	44.30	24.15	564	437	1.83
120-747C-										
7R-1, 140-150	262.90	20	7.54	1.860	36.4	44.20	24.25	575	359	1.82

ducted from 175 to 190 mbsf because of the possible location of the Cretaceous/Tertiary contact within this interval.

Measurements were resumed from 190 mbsf to the base of the hole. The bulk density generally increased and the porosity decreased, at a higher rate than in the overlying unit, to the sediment/basalt boundary at 300 mbsf. A sharp trend discontinuity in grain density, water content, and porosity at 235 mbsf represents values from chert samples. Bulk density values determined in the basaltic cores were variable between 2.45 and 2.75 g/cm^3. Measurements in these cores were limited to only a few samples, and the variation is most likely linked to the number of vesicles and the degree of alteration in the samples.

Compressional Wave Velocity

Compressional wave velocity was measured by both continuous and discrete methods. Continuous measurements of *P*-wave velocity were obtained using the *P*-wave Logger (PWL), which consists of transducers mounted on the GRAPE unit. Discrete measurements of *P*-wave velocity were obtained with the Hamilton Frame Velocimeter. The Hamilton Frame is used to measure discrete samples from the working half of the core. The methods used for obtaining these measurements have been discussed in the "Explanatory Notes" chapter (this volume). Velocities were generally measured parallel to bedding, although some samples were tested at other orientations with the Hamilton Frame to investigate the effects of anisotropy in various lithologies.

The large difference between the velocities measured in the sediments and those obtained from igneous rocks are graphically displayed in Figure 31. The raw data collected from the three holes at Site 747 are also presented in Table 12. The *P*-wave velocity measurements from the sediments range from slightly slower than 1500 m/s, near the top of the hole, to over 2100 m/s near the sediment-basalt contact. The velocities measured in the basalts are highly variable. These velocities range from 3158 to 5858 m/s. Anisotropy is observed in the basalt and may be related to the degree of brecciation and alteration in the flows.

The PWL was used only for APC and XCB cores that filled the core liners; measurements were not made on partially filled core liners. Void spaces within the liner result in inaccurate values of compressional wave traveltimes for the sediment and rock. These voids also attenuate the signal strength of the sonic pulse transmitted by the PWL transducer. Thus, rotary cores are not suitable for measurements using the PWL technique. The values for compressional wave velocity obtained from the Hamilton Frame and the PWL are compared, using the same scale, in Figure 32. In general, the two velocity data sets compare well with each other. Velocity increases with depth in the sedimentary section for both methods.

Velocity increases from the seafloor to 12.5 mbsf. This pattern may be related to the low-density, amorphous silica skeletons of diatoms found throughout this interval. Below 12.5 mbsf the velocity values, measured with the Hamilton Frame, decrease to 25 mbsf before beginning to increase again. A similar velocity inversion was also observed on the Maud Rise in the Weddell Sea (Barker, Kennett, et al., 1988). It was postulated that the density differences between the skeletons formed by siliceous and calcareous organisms caused a drop in velocity values with increasing carbonate content at shallow depths of burial.

Velocity values from 25 mbsf to approximately 150 mbsf increase slightly with depth. The dominant lithology throughout this interval is nannofossil ooze (Subunit IIA) with calcium carbonate values exceeding 90%. The Hamilton Frame measurements indicate a higher velocity section from 152 to 172 mbsf. This interval generally corresponds to Subunit IIB, which is identified by changes in index properties as well as velocities.

Undrained Shear Strength

Undrained shear strength (S_u) measurements were made on relatively undisturbed APC cores and on sediment "biscuits" from XCB cores at Site 747. At Hole 747A these measurements were made using the ODP Motorized Vane device (Table 13), whereas the Wykeham Farrance Vane device was used at Hole 747B (Table 14). The Wykeham Farrance Vane gave much lower values of S_u than the Motorized Vane for comparable lithologies in the upper 50 m of this site (Fig. 33).

A large amount of scatter was seen in the undrained shear strength data obtained using the Motorized Vane. Some of the scatter results from sediment disturbance, which is caused by removal of overburden pressure and by disturbance during coring. Reliable data depends on the selection of "undisturbed" intervals in the cores for undrained shear strength measurements. Another factor that contributed to fluctuations in the undrained shear strength data was the time required to set up the x-y plotter used with the Motorized Vane. After insertion of the vane into the working half of the core, adjustments were necessary to zero the torque potentiometer. This variable time lag may have allowed the pore water to drain out of the sample, thereby increasing intergranular friction during the shearing process for some samples.

In general, undrained shear strength measured with the Motorized Vane was less than 25 kilopascals (kPa) from the seafloor to 118 mbsf. There is a sharp peak in S_u at 86 mbsf that corresponds to a decrease in porosity, grain density, and carbon-

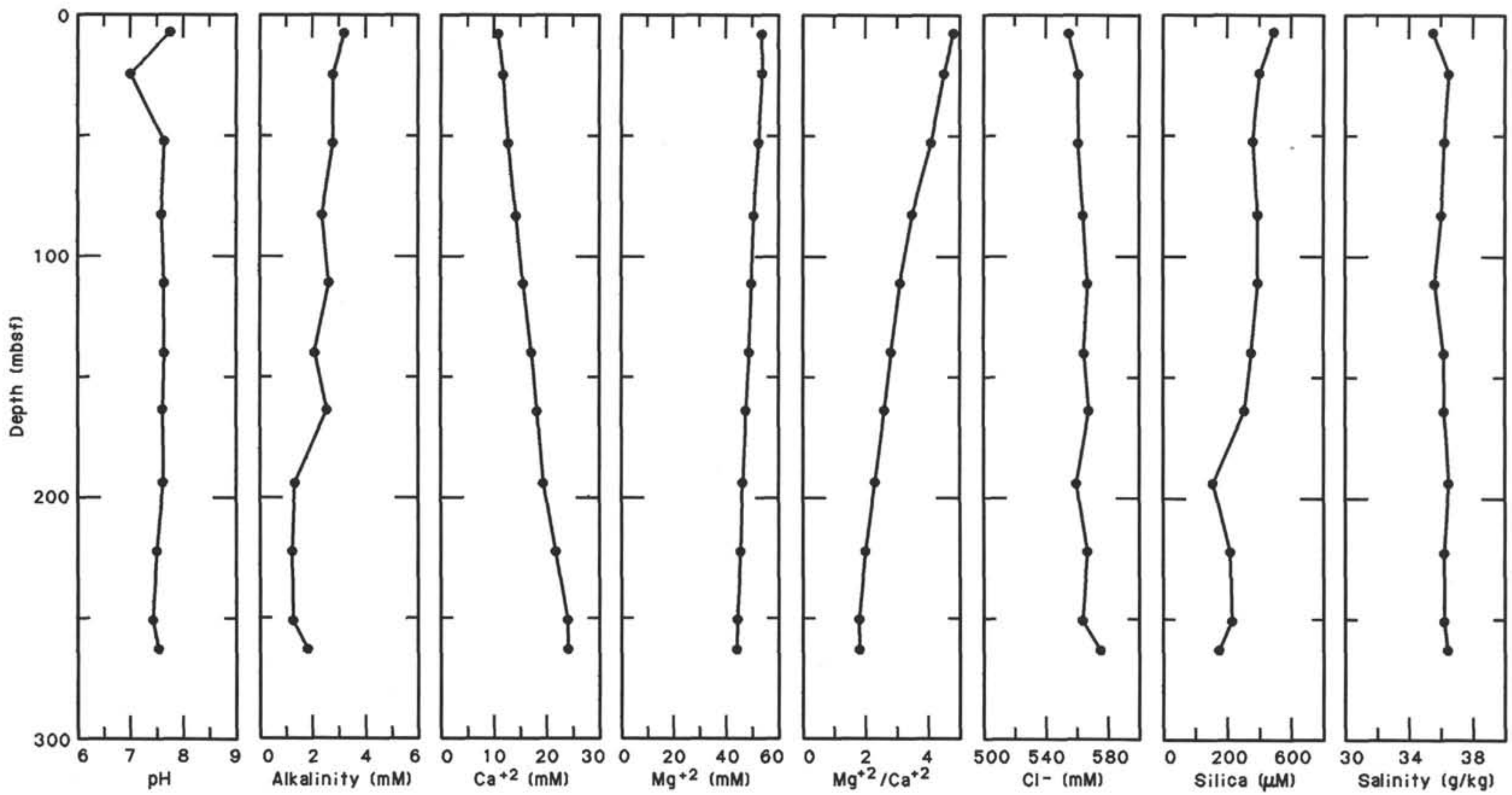

Figure 27. Summary of interstitial water analyses, Site 747, as a function of depth (mbsf).

Table 10. Total carbon, inorganic and organic carbon, and carbonate contents of samples from Holes 747A and 747B.

Core, section, interval (cm)	Depth (mbsf)	Total carbon (%)	Inorganic carbon (%)	Organic carbon (%)	Carbonate (%)
120-747A-1H-1, 50-52	0.50	2.35	2.31	0.04	19.2
120-747A-1H-2, 50-52	2.00		4.08		34.0
120-747A-1H-3, 50-52	3.50		7.13		59.4
120-747A-1H-4, 50-52	5.00		5.11		42.6
120-747A-1H-5, 50-52	6.50		6.65		55.4
120-747A-1H-6, 50-52	8.00		9.25		77.1
120-747A-2H-1, 50-52	9.50	5.38	5.69	0	47.4
120-747A-2H-2, 50-52	11.00		5.60		46.7
120-747A-2H-3, 50-52	12.50		7.84		65.3
120-747A-2H-4, 60-62	14.10		7.79		64.9
120-747A-2H-5, 50-52	15.50		9.28		77.3
120-747A-2H-6, 60-62	17.10		8.13		67.7
120-747A-2H-7, 50-52	18.50		8.49		70.7
120-747A-3H-2, 52-54	20.52	7.47	7.40	0.07	61.6
120-747A-3H-3, 52-54	22.02		8.43		70.2
120-747A-3H-4, 50-52	23.50		4.78		39.8
120-747A-3H-5, 52-54	25.02		7.36		61.3
120-747A-3H-6, 52-54	26.52		6.89		57.4
120-747A-4H-1, 50-52	28.50		8.26		68.8
120-747A-4H-1, 130-131	29.30	9.55	9.43	0.12	78.6
120-747A-4H-2, 120-122	30.70		8.10		67.5
120-747A-4H-2, 130-131	30.80		8.84		73.6
120-747A-4H-3, 50-52	31.50		9.69		80.7
120-747A-4H-3, 130-131	32.30		9.85		82.1
120-747A-4H-4, 50-52	33.00		8.33		69.4
120-747A-4H-4, 130-131	33.80		8.88		74.0
120-747A-4H-5, 52-54	34.52		9.96		83.0
120-747A-4H-5, 130-131	35.30		9.41		78.4
120-747A-4H-6, 50-52	36.00		10.38		86.5
120-747A-4H-6, 130-131	36.80		10.18		84.8
120-747A-4H-7, 50-52	37.50		10.82		90.1
120-747A-5H-3, 118-120	41.68		9.49		79.1
120-747A-5H-3, 130-131	41.80	9.96	9.85	0.11	82.1
120-747A-5H-4, 50-52	42.50		10.04		83.6
120-747A-5H-4, 130-131	43.30		10.73		89.4
120-747A-5H-5, 50-52	44.00		11.01		91.7
120-747A-5H-5, 130-131	44.80		9.46		78.8
120-747A-5H-6, 50-52	45.50		11.06		92.1
120-747A-5H-6, 130-131	46.30		10.86		90.5
120-747A-5H-7, 30-32	46.80		10.55		87.9
120-747A-6H-1, 112-114	48.12	11.35	11.27	0.08	93.9
120-747A-6H-2, 100-102	49.50		10.73		89.4
120-747A-6H-3, 95-97	50.95		10.86		90.5
120-747A-6H-4, 34-36	51.84		11.19		93.2
120-747A-6H-6, 50-52	55.00		11.35		94.6
120-747A-7H-1, 130-131	57.80	11.61	11.61	0	96.7
120-747A-7H-2, 98-100	58.98		11.26		93.8
120-747A-7H-2, 130-131	59.30		11.66		97.1
120-747A-7H-3, 50-52	60.00		11.30		94.1
120-747A-7H-3, 125-126	60.75		7.15		59.6
120-747A-7H-4, 120-122	62.20		11.33		94.4
120-747A-7H-4, 130-131	62.30		11.26		93.8
120-747A-7H-5, 50-52	63.00		11.08		92.3
120-747A-7H-5, 130-131	63.80		11.54		96.1
120-747A-7H-6, 50-52	64.50		11.21		93.4
120-747A-7H-6, 130-131	65.30		11.49		95.7
120-747A-7H-7, 50-52	66.00		11.44		95.3
120-747A-8H-1, 50-52	66.50		10.69		89.1
120-747A-8H-1, 130-131	67.30		10.47		87.2
120-747A-8H-2, 50-52	68.00	10.93	10.93	0	91.1
120-747A-8H-2, 130-131	68.80		11.08		92.3
120-747A-8H-3, 50-52	69.50		11.22		93.5
120-747A-8H-3, 130-131	70.30		11.27		93.9
120-747A-8H-4, 50-52	71.00		11.24		93.6
120-747A-8H-4, 130-131	71.80		11.60		96.6
120-747A-8H-5, 50-52	72.50		11.03		91.9
120-747A-8H-5, 130-131	73.30		11.39		94.9
120-747A-8H-6, 50-52	74.00		11.16		93.0
120-747A-8H-6, 130-131	74.80		11.26		93.8
120-747A-9H-2, 54-56	76.13		11.48		95.6
120-747A-9H-2, 130-131	76.89		11.55		96.2
120-747A-9H-3, 54-56	77.63		11.38		94.8
120-747A-9H-3, 130-131	78.39		11.49		95.7
120-747A-9H-4, 54-56	79.13		11.54		96.1
120-747A-9H-4, 130-131	79.89		11.56		96.3
120-747A-9H-5, 54-56	80.63		11.86		98.8

Table 10 (continued).

Core, section, interval (cm)	Depth (mbsf)	Total carbon (%)	Inorganic carbon (%)	Organic carbon (%)	Carbonate (%)
120-747A-9H-5, 130-131	81.39		11.43		95.2
120-747A-9H-6, 54-56	82.13		11.12		92.6
120-747A-9H-7, 54-56	83.63		11.08		92.3
120-747A-9H-7, 130-131	84.39		11.26		93.8
120-747A-9H-8, 54-56	85.13		10.88		90.6
120-747A-10H-1, 50-52	85.50	10.91	10.81	0.10	90.1
120-747A-10H-2, 50-52	87.00		10.71		89.2
120-747A-10H-3, 50-52	88.50		11.06		92.1
120-747A-10H-4, 50-52	90.00		11.12		92.6
120-747A-10H-5, 50-52	91.50		10.07		93.9
120-747A-10H-6, 50-52	93.00		11.28		94.0
120-747A-11H-1, 50-52	95.00		10.97		91.4
120-747A-11H-2, 50-52	96.50		11.27		93.9
120-747A-11H-3, 60-62	98.10		11.77		98.0
120-747A-11H-4, 60-62	99.60	11.32	11.32	0	94.3
120-747A-11H-5, 60-62	101.10		11.71		97.5
120-747A-11H-6, 60-62	102.60		11.32		94.3
120-747A-11H-7, 20-22	103.70		11.80	9	8.3
120-747A-12H-1, 56-58	104.56	11.69	11.69	0	97.4
120-747A-12H-2, 56-58	106.06		11.61		96.7
120-747A-12H-3, 56-58	107.56		11.48		95.6
120-747A-12H-4, 56-58	109.06		11.45		95.4
120-747A-12H-5, 56-58	110.56		11.60		96.6
120-747A-12H-6, 56-58	112.06		11.35		94.6
120-747A-12H-7, 56-58	113.56	11.34	11.34	0	94.5
120-747A-13H-1, 50-53	114.00	11.28	11.21	0.07	93.4
120-747A-13H-2, 50-53	115.50	11.31	11.26	0.05	93.8
120-747A-13H-3, 50-53	117.00		11.14		92.8
120-747A-13H-4, 50-52	118.50		11.14		92.8
120-747A-13H-5, 50-52	120.00		11.11		92.6
120-747A-13H-6, 50-52	121.50		11.29		94.1
120-747A-13H-7, 50-52	123.00		10.92		91.0
120-747A-14H-1, 50-52	123.50	11.09	11.00	0.09	91.6
120-747A-14H-2, 50-52	125.00		10.77		89.7
120-747A-14H-3, 50-52	126.50		10.40		86.6
120-747A-14H-4, 50-52	128.00	10.89	10.90	0	90.8
120-747A-14H-5, 50-52	129.50		10.96		91.3
120-747A-14H-6, 50-52	131.00		11.04		92.0
120-747A-14H-7, 55-57	133.05		10.77		89.7
120-747A-15H-2, 55-57	134.55	10.95	10.86	0.09	90.5
120-747A-15H-3, 55-57	136.05		11.08		92.3
120-747A-15H-4, 55-57	137.55		11.18		93.1
120-747A-15H-5, 55-57	139.05		10.99		91.6
120-747A-15H-6, 55-57	140.55		10.71		89.2
120-747A-15H-7, 55-57	142.05		11.07		92.2
120-747A-16H-3, 49-51	145.49		11.37		94.7
120-747A-16H-4, 49-51	146.99		11.14		95.5
120-747A-16H-5, 49-51	148.49		11.42		95.1
120-747A-16H-6, 49-51	149.99		11.46		95.5
120-747A-16H-7, 49-51	151.49		11.21		93.4
120-747A-17X-1, 76-78	152.26	10.29	10.06	0.23	83.8
120-747A-17X-2, 39-41	153.39		10.11		84.2
120-747A-17X-3, 114-116	155.64		10.31		85.9
120-747A-17X-4, 100-102	157.00		10.41		86.7
120-747A-17X-5, 82-84	158.32		9.14		76.1
120-747A-17X-6, 37-39	159.37		9.35		77.9
120-747A-18X-1, 36-38	161.36	10.81	10.81	0	90.1
120-747A-18X-2, 60-62	163.10		10.80		90.0
120-747A-18X-3, 48-50	164.48		9.82		81.8
120-747C-2R-5, 53-54	175.03	11.11	11.06	0.05	92.1
120-747C-2R-5, 122-123	175.72	10.82	10.80	0.02	90.0
120-747C-3R-1, 70-71	178.70	11.17	11.17	0	93.1
120-747C-3R-3, 3-4	180.50	8.14	8.02	0.12	66.8
120-747C-3R-3, 131-132	181.78	2.97	2.88	0.09	24.0
120-747A-21X-1, 39-41	189.89	11.72	11.37	0.35	94.7
120-747A-21X-2, 94-96	191.94		11.58		96.5
120-747A-21X-3, 69-71	193.19		11.27		93.9
120-747A-21X-4, 69-71	194.69		11.11		92.6
120-747A-21X-5, 8-10	195.58		11.44		95.3
120-747A-22X-1, 50-52	199.50	11.52	11.40	0.12	95.0
120-747A-22X-2, 50-52	201.00		11.34		94.5
120-747A-22X-3, 50-52	202.50		11.33		94.4
120-747A-22X-4, 50-52	204.00		11.35		94.6
120-747A-22X-5, 50-52	205.50		11.31		94.2
120-747A-22X-6, 50-52	107.00		11.47		95.6
120-747A-23X-1, 50-52	209.00	11.79	11.31	0.48	94.2

Table 10 (continued).

Core, section, interval (cm)	Depth (mbsf)	Total carbon (%)	Inorganic carbon (%)	Organic carbon (%)	Carbonate (%)
120-747A-23X-2, 40-42	210.40		11.48		95.6
120-747A-23X-3, 50-52	212.00		11.39		94.9
120-747A-23X-4, 50-52	213.50		11.72		97.6
120-747A-23X-5, 50-52	215.00		11.16		93.0
120-747A-23X-6, 50-52	216.50		11.58		96.5
120-747A-23X-7, 10-12	217.60		11.42		95.1
120-747A-24X-1, 50-52	218.50	11.50	11.47	0.03	95.6
120-747A-24X-2, 50-52	220.00		11.60		96.6
120-747A-24X-3, 50-52	221.50		11.43		95.2
120-747A-24X-4, 50-52	223.00		11.37		94.7
120-747A-24X-5, 50-52	224.50		11.43		95.2
120-747A-25X-1, 50-52	228.00	11.03	10.80	0.23	90.0
120-747A-25X-2, 50-52	229.50		11.35		94.6
120-747A-25X-3, 50-52	231.00		11.37		94.7
120-747A-25X-4, 50-52	232.50		11.36		94.6
120-747A-26X-1, 50-52	237.50	11.46	11.35	0.11	94.6
120-747A-26X-2, 50-52	239.00		11.20		93.3
120-747A-26X-3, 50-52	240.50		11.45		95.4
120-747A-26X-4, 60-62	242.10		11.22		93.5
120-747A-27X-1, 46-48	246.96	10.82	10.46	0.36	87.1
120-747A-27X-2, 136-138	249.36		11.29		94.1
120-747A-27X-3, 22-24	249.72		11.21		93.4
120-747A-27X-4, 53-55	251.53		11.48		95.6
120-747C-6R-1, 47-49	252.47	11.28	11.28	0	94.0
120-747C-7R-1, 79-81	262.29	11.33	11.29	0.04	94.1
120-747C-8R-1, 53-55	271.53	11.40	11.40	0	95.0
120-747C-9R-1, 84-87	281.34	11.27	11.25	0.02	93.7
120-747C-10R-1, 0-2	290.00	7.81	7.75	0.06	64.6
120-747C-10R-1, 31-33	290.31	11.07	11.07	0	92.2

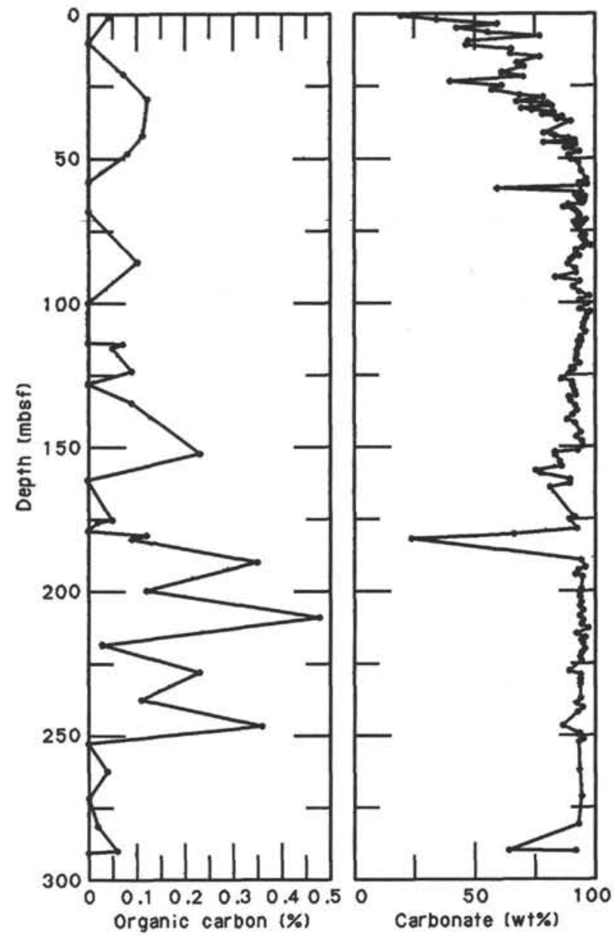

Figure 28. Total organic carbon and carbonate contents plotted vs. depth (mbsf) at Site 747.

ate content (Figs. 29 and 30). An increase in compressional wave velocity is also noted at this depth. A zone of generally higher undrained shear strength from 118 to 130 mbsf can be correlated with decreased carbonate content and increased *P*-wave velocity. The increased undrained shear strength below 147 mbsf is indicative of a lithologic change from nannofossil ooze to nannofossil chalk. Increased undrained shear strength also reflects the change from APC to XCB coring at 150 mbsf. Measurements were discontinued at 159 mbsf at which point it became impossible to insert the vane into the XCB "biscuits" without fracturing them.

Thermal Conductivity, Downhole Temperature, and Heat Flow

Samples from Site 747 were measured for thermal conductivity using two techniques. For sediment, a needle probe was inserted and heated; and measurements were made over a 6-min period (Von Herzen and Maxwell, 1959). For igneous rock, a heated needle probe was sandwiched between a slab of low conducting material and the sample, and measurements were taken for 6 min (Vacquier, 1985; Robinson, Von Herzen, et al., 1988). Only runs that displayed a temperature drift rate less than 0.04°C/min were retained for analysis (Table 15). Downhole temperature was measured with the Uyeda temperature probe (T-probe) and standard operating procedures (see "Explanatory Notes" chapter, this volume).

Thermal conductivity values range from 0.86 W/m·K near the seafloor to 1.95 W/m·K at 230 mbsf. The scatter in the thermal conductivity data is small. Changes in the conductivity gradients occur over discrete intervals, which generally correspond to lithologic boundaries. Thermal conductivity increased sharply from 0.86 W/m·K, near the mud line, to 1.47 W/m·K at 35 mbsf (boundary between Unit I and Subunit IIA). This increase is the result of a decrease in water content and an increase in bulk density with increasing carbonate content.

Thermal conductivity is relatively uniform from 35 mbsf to 151 mbsf, where values increase at the lithologic boundary between nannofossil ooze (Subunit IIA) and nannofossil chalk (Subunit IIB). Below this boundary the conductivity increases to 1.66 W/m·K at 175 mbsf. Thermal conductivity continues to increase downhole until it decreases in the basaltic flows below 297 mbsf.

Strong relationships exist between thermal conductivity, physical properties, and lithology. Changes in index properties, such as in bulk density, porosity, and water content, cause changes in thermal conductivity downhole. Variations in calcium carbonate content seem directly related to thermal conductivity values at Site 747 (Fig. 36).

The Uyeda T-probe was deployed three times, twice in Hole 747A (94.5 and 123.0 mbsf) and once in Hole 747B (53.0 mbsf) (Fig. 35). The downhole temperatures determined from the T-probe are (1) mud line (mean) = 1.8°C; (2) 53.0 mbsf = 4.7°C; and (3) 123.0 mbsf = 6.7°C. The temperature record at 94.5 mbsf is assumed to be unreliable due to the few equilibration measurements made after the insertion of the T-probe into the sediment. A Schlumberger tool provided a temperature of 22°C at 337.0 mbsf. This value is also considered unreliable because the method does not sample *in-situ* sediment temperature.

Variation in probe equilibration duration and the motion of the wireline during the measurements cast some uncertainty on the downhole temperature profile (Fig. 34); however, a calculated average geothermal gradient of 48°C/km is a reasonable value. Post-cruise fitting of recorded temperature curves to decay curves should improve the reliability of this value. An average thermal conductivity for the 0–123.0 mbsf interval was

Table 11. Index properties data from Site 747.

Core, section, interval (cm)	Depth (mbsf)	Water content (%)	Porosity (%)	Wet-bulk density (g/cm^3)	Dry-bulk density (g/cm^3)	Grain density (g/cm^3)
120-747A-1H-1, 50	0.50	91.50	97.14	1.19	0.10	2.97
120-747A-1H-2, 50	2.00	92.39	97.65	1.23	0.09	3.21
120-747A-1H-3, 50	3.50	60.50	78.90	1.35	0.53	2.45
120-747A-1H-4, 50	5.00	63.16	80.81	1.32	0.49	2.46
120-747A-1H-5, 50	6.50	56.90	77.86	1.40	0.60	2.68
120-747A-1H-6, 50	8.00	48.63	71.63	1.54	0.79	2.69
120-747A-2H-1, 50	9.50	62.10	79.35	1.34	0.51	2.35
120-747A-2H-2, 50	11.00	59.34	77.67	1.36	0.55	2.40
120-747A-2H-3, 50	12.50	56.54	76.93	1.44	0.62	2.58
120-747B-3H-1, 50	12.80	50.09	71.28	1.51	0.75	2.50
120-747A-2H-4, 50	14.00	56.80	76.44	1.42	0.61	2.48
120-747B-3H-2, 50	14.30	42.05	63.84	1.26	0.73	2.46
120-747A-2H-5, 50	15.50	48.59	71.47	1.55	0.80	2.68
120-747B-3H-3, 50	15.80	52.04	70.23	1.42	0.68	2.19
120-747A-2H-6, 50	17.00	51.42	74.71	1.49	0.72	2.82
120-747B-3H-4, 101	17.81	48.27	70.56	1.53	0.79	2.59
120-747A-2H-7, 50	18.50	48.87	71.24	1.52	0.78	2.62
120-747B-3H-5, 50	18.80	44.84	67.63	1.57	0.87	2.60
120-747B-3H-6, 50	20.30	46.98	69.60	1.58	0.84	2.61
120-747A-3H-2, 52	20.52	51.91	75.54	1.52	0.73	2.89
120-747A-3H-3, 52	22.02	45.59	68.70	1.58	0.86	2.65
120-747A-3H-4, 50	23.50	46.06	69.42	1.67	0.90	2.69
120-747B-4H-2, 53	23.83	52.85	73.89	1.45	0.68	2.54
120-747A-3H-5, 52	25.02	51.93	73.17	1.53	0.73	2.55
120-747A-3H-6, 50	26.50	48.69	70.65	1.55	0.80	2.56
120-747B-4H-4, 53	26.83	49.52	71.18	1.52	0.77	2.54
120-747B-4H-5, 53	28.33	43.61	67.43	1.61	0.91	2.71
120-747A-4H-1, 50	28.50	49.27	72.93	1.57	0.79	2.80
120-747B-4H-6, 53	29.83	39.29	63.89	1.73	1.05	2.77
120-747A-4H-2, 50	30.00	44.64	68.70	1.62	0.90	2.75
120-747A-4H-3, 50	31.50	42.37	69.48	1.74	1.00	3.14
120-747B-5H-1, 50	31.80	39.34	63.80	1.70	1.03	2.75
120-747A-4H-4, 50	33.00	41.53	65.27	1.67	0.97	2.68
120-747B-5H-2, 50	33.30	35.99	59.90	1.73	1.10	2.69
120-747A-4H-5, 50	34.50	31.37	53.10	1.75	1.20	2.51
120-747A-4H-6, 50	36.00	37.29	62.16	1.77	1.11	2.80
120-747A-4H-7, 50	37.50	34.95	59.58	1.82	1.18	2.78
120-747B-5H-5, 50	37.80	43.92	68.42	1.65	0.92	2.80
120-747B-5H-6, 50	39.30	37.03	59.39	1.68	1.06	2.52
120-747A-5H-3, 118	41.68	44.78	69.39	1.66	0.92	2.83
120-747B-6H-1, 132	42.12	38.27	63.00	1.72	1.06	2.78
120-747A-5H-4, 50	42.50	40.72	63.61	1.67	0.99	2.57
120-747B-6H-2, 105	43.35	37.74	62.30	1.73	1.08	2.76
120-747A-5H-5, 50	44.00	37.89	62.69	1.73	1.08	2.79
120-747A-5H-6, 50	45.50	37.28	61.03	1.74	1.09	2.67
120-747B-6H-4, 61	45.91	37.10	60.87	1.74	1.10	2.67
120-747A-5H-7, 50	47.00	34.43	57.98	1.79	1.17	2.66
120-747B-6H-5, 89	47.69	36.11	60.04	1.74	1.11	2.69
120-747A-6H-1, 112	48.12	38.86	63.93	1.71	1.05	2.82
120-747B-6H-6, 95	49.25	36.11	60.36	1.73	1.10	2.73
120-747A-6H-2, 100	49.50	39.43	63.06	1.67	1.01	2.65
120-747A-6H-3, 95	50.95	37.05	60.92	1.70	1.07	2.68
120-747A-6H-4, 34	51.84	36.95	61.28	1.74	1.10	2.73
120-747A-6H-6, 50	55.00	35.29	59.82	1.75	1.13	2.77
120-747A-7H-2, 98	58.98	37.12	62.27	1.74	1.10	2.83
120-747A-7H-3, 50	60.00	36.13	59.13	1.70	1.09	2.59
120-747A-7H-4, 120	62.20	38.11	61.61	1.72	1.06	2.64
120-747A-7H-5, 50	63.00	38.63	63.63	1.73	1.06	2.81
120-747A-7H-6, 50	64.50	37.28	61.98	1.74	1.09	2.78
120-747A-7H-7, 50	66.00	34.59	59.32	1.79	1.17	2.79
120-747A-8H-1, 50	66.50	37.79	61.57	1.69	1.05	2.67
120-747A-8H-2, 50	68.00	37.10	59.95	1.73	1.09	2.57
120-747A-8H-3, 50	69.50	37.98	63.01	1.74	1.08	2.82
120-747A-8H-4, 50	71.00	35.54	58.81	1.74	1.12	2.62
120-747A-8H-5, 50	72.50	33.79	60.11	1.85	1.22	2.99
120-747A-8H-6, 50	74.00	31.74	54.32	1.79	1.22	2.59
120-747A-9H-2, 54	76.13	34.98	59.28	1.79	1.16	2.74
120-747A-9H-3, 54	77.63	34.62	58.68	1.81	1.18	2.72
120-747A-9H-4, 54	79.13	34.45	58.32	1.81	1.19	2.70
120-747A-9H-5, 54	80.63	33.85	59.65	1.82	1.20	2.93
120-747A-9H-6, 54	82.13	34.28	57.64	1.75	1.15	2.64
120-747A-9H-7, 54	83.63	32.93	58.38	1.86	1.25	2.90
120-747A-9H-8, 54	85.13	33.50	59.45	1.83	1.22	2.95
120-747A-10H-2, 54	87.04	38.06	62.18	1.76	1.09	2.71
120-747A-10H-3, 54	88.54	35.55	59.94	1.76	1.14	2.75
120-747A-10H-4, 54	90.04	37.47	60.43	1.69	1.05	2.58
120-747A-10H-5, 54	91.54	35.50	58.82	1.73	1.11	2.63
120-747A-10H-6, 54	93.04	35.56	60.13	1.76	1.14	2.77
120-747A-11H-1, 50	95.00	35.48	61.53	1.84	1.18	2.95
120-747A-11H-2, 50	96.50	34.44	58.12	1.81	1.19	2.68
120-747A-11H-3, 60	98.10	33.62	58.12	1.79	1.19	2.78
120-747A-11H-4, 60	99.60	36.15	60.77	1.82	1.16	2.77
120-747A-11H-5, 60	101.10	32.98	55.81	1.81	1.22	2.60
120-747A-11H-6, 60	102.60	35.85	62.45	1.83	1.18	3.02
120-747A-11H-7, 20	103.70	33.14	57.57	1.80	1.20	2.77
120-747A-12H-1, 57	104.57	38.19	63.20	1.73	1.07	2.82
120-747A-12H-2, 56	106.06	38.08	63.08	1.74	1.08	2.81

Table 11 (continued).

Core, section, interval (cm)	Depth (mbsf)	Water content (%)	Porosity (%)	Wet-bulk density (g/cm^3)	Dry-bulk density (g/cm^3)	Grain density (g/cm^3)
120-747A-12H-3, 56	107.56	37.19	61.47	1.72	1.08	2.73
120-747A-12H-3, 56	107.56	37.19	61.47	1.72	1.08	2.73
120-747A-12H-4, 56	109.06	35.03	60.38	1.81	1.18	2.87
120-747A-12H-5, 56	110.56	31.73	55.62	1.88	1.29	2.73
120-747A-12H-6, 56	112.06	34.02	58.06	1.82	1.20	2.72
120-747A-12H-7, 56	113.56	34.68	58.85	1.78	1.16	2.73
120-747A-13H-1, 50	114.00	36.34	60.58	1.75	1.11	2.73
120-747A-13H-2, 50	115.50	35.23	60.48	1.81	1.17	2.85
120-747A-13H-3, 50	117.00	36.71	61.28	1.75	1.11	2.76
120-747A-13H-4, 50	118.50	35.76	59.62	1.78	1.14	2.69
120-747A-13H-5, 50	120.00	32.98	58.22	1.86	1.25	2.87
120-747A-13H-6, 50	121.50	33.74	58.35	1.80	1.19	2.79
120-747A-13H-7, 50	123.00	32.44	57.41	1.84	1.25	2.85
120-747A-14H-1, 50	123.50	33.32	58.08	1.81	1.21	2.81
120-747A-14H-2, 50	125.00	39.52	62.22	1.66	1.00	2.55
120-747A-14H-3, 50	126.50	36.62	62.25	1.77	1.12	2.89
120-747A-14H-4, 50	128.00	39.53	65.18	1.78	1.08	2.90
120-747A-14H-5, 50	129.50	36.89	62.62	1.76	1.11	2.90
120-747A-14H-6, 50	131.00	36.17	60.21	1.73	1.10	2.70
120-747A-14H-7, 50	132.50	32.09	56.85	1.81	1.23	2.83
120-747A-15H-1, 56	133.06	31.84	56.58	1.84	1.25	2.83
120-747A-15H-2, 56	134.56	33.49	58.15	1.82	1.21	2.80
120-747A-15H-3, 56	136.06	34.60	60.06	1.77	1.16	2.88
120-747A-15H-4, 56	137.56	35.64	58.95	1.74	1.12	2.63
120-747A-15H-5, 56	139.06	34.72	60.13	1.80	1.17	2.87
120-747A-15H-6, 56	140.56	35.24	60.96	1.82	1.18	2.91
120-747A-15H-7, 56	142.06	33.07	56.29	1.79	1.20	2.64
120-747A-16H-3, 49	145.49	34.08	60.03	1.83	1.21	2.94
120-747A-16H-4, 49	146.99	34.42	59.35	1.83	1.20	2.82
120-747A-16H-5, 49	148.49	30.35	55.70	1.89	1.32	2.93
120-747A-16H-6, 49	149.99	32.92	57.61	1.83	1.23	2.81
120-747A-16H-7, 49	151.49	34.66	57.13	1.76	1.15	2.54
120-747A-17X-1, 76	152.26	36.61	65.10	1.90	1.20	3.27
120-747A-17X-2, 106	154.06	35.30	60.83	1.76	1.14	2.89
120-747A-17X-3, 114	155.64	37.73	61.05	1.73	1.08	2.62
120-747A-17X-4, 100	157.00	36.35	62.41	1.86	1.18	2.95
120-747A-17X-5, 82	158.32	44.04	68.49	1.70	0.95	2.79
120-747C-1R-1, 36	159.36	40.11	64.51	1.75	1.05	2.75
120-747A-17X-6, 37	159.37	40.01	67.09	1.72	1.03	3.10
120-747C-1R-2, 52	161.02	38.15	61.14	1.72	1.06	2.58
120-747A-18X-1, 36	161.36	38.60	63.55	1.73	1.06	2.81
120-747C-1R-3, 57	162.57	41.67	66.14	1.69	0.99	2.77
120-747A-18X-2, 60	163.10	41.22	64.98	1.66	0.97	2.68
120-747C-1R-4, 51	164.01	42.20	64.57	1.69	0.98	2.52
120-747A-18X-3, 48	164.48	41.49	67.35	1.72	1.01	2.95
120-747C-1R-5, 57	165.57	36.39	60.25	1.72	1.09	2.68
120-747C-2R-1, 34	168.84	34.63	58.71	1.80	1.17	2.72
120-747C-2R-2, 141	171.41	37.76	60.36	1.75	1.09	2.54
120-747C-2R-3, 73	172.23	35.75	57.62	1.72	1.10	2.47
120-747C-2R-4, 54	173.54	32.77	56.15	1.84	1.23	2.66
120-747C-2R-5, 52	175.02	30.07	54.72	1.95	1.36	2.85
120-747A-21X-1, 39	189.89	28.76	52.67	1.95	1.39	2.80
120-747A-21X-2, 94	191.94	27.88	49.89	1.89	1.36	2.61
120-747A-21X-3, 69	193.19	31.99	57.11	1.84	1.25	2.87
120-747A-21X-4, 69	194.69	2.87	5.49	1.95	1.90	1.99
120-747A-21X-5, 8	95.58	24.41	48.06	2.05	1.55	2.91
120-747A-22X-1, 50	199.50	27.05	50.70	1.92	1.40	2.81
120-747A-22X-2, 50	201.00	26.96	49.36	1.94	1.41	2.68
120-747A-22X-3, 50	202.50	27.48	49.89	1.91	1.39	2.66
120-747A-22X-4, 50	204.00	26.28	48.79	1.93	1.42	2.71
120-747A-22X-5, 50	205.50	28.93	51.96	1.93	1.37	2.69
120-747A-22X-6, 50	207.00	24.59	47.15	1.99	1.50	2.78
120-747A-23X-1, 50	209.00	24.55	45.09	1.94	1.47	2.56
120-747A-23X-2, 40	210.40	27.13	50.20	1.92	1.40	2.75
120-747A-23X-3, 50	212.00	27.29	50.54	1.98	1.44	2.76
120-747A-23X-4, 50	213.50	27.56	51.41	1.94	1.40	2.82
120-747A-23X-5, 50	215.00	27.11	50.58	1.86	1.35	2.79
120-747A-23X-6, 50	216.50	25.27	47.50	1.98	1.48	2.71
120-747A-23X-7, 10	217.60	20.96	41.53	2.09	1.65	2.72
120-747A-24X-1, 50	218.50	26.22	49.15	2.00	1.47	2.76
120-747A-24X-2, 50	220.00	24.48	46.16	2.01	1.51	2.68
120-747A-24X-3, 50	221.50	24.67	46.89	2.03	1.53	2.74
120-747A-24X-4, 50	223.00	24.24	47.07	2.04	1.55	2.82
120-747A-24X-5, 50	224.50	21.12	41.39	2.10	1.66	2.68
120-747A-25X-1, 50	228.00	27.96	51.12	1.95	1.40	2.73
120-747A-25X-2, 50	229.50	22.14	43.51	2.07	1.61	2.75
120-747A-25X-4, 50	232.50	22.94	44.01	2.04	1.57	2.68
120-747A-26X-1, 50	237.50	52.63	65.57	1.97	0.93	1.71
120-747A-26X-3, 50	240.50	35.52	54.94	2.08	1.34	2.24
120-747A-26X-4, 50	242.00	23.75	45.77	2.14	1.63	2.75
120-747A-27X-1, 46	246.96	23.81	46.00	2.03	1.55	2.77
120-747A-27X-2, 136	249.36	23.82	45.69	2.08	1.58	2.73
120-747A-27X-3, 22	249.72	24.47	47.90	2.04	1.54	2.88
120-747A-27X-4, 53	251.53	25.23	47.45	2.02	1.51	2.71
120-747C-6R-1, 47	252.47	20.58	41.84	2.33	1.85	2.82
120-747C-7R-1, 79	262.29	21.63	41.78	2.11	1.66	2.64
120-747C-8R-1, 53	271.53	21.35	42.22	2.19	1.72	2.73

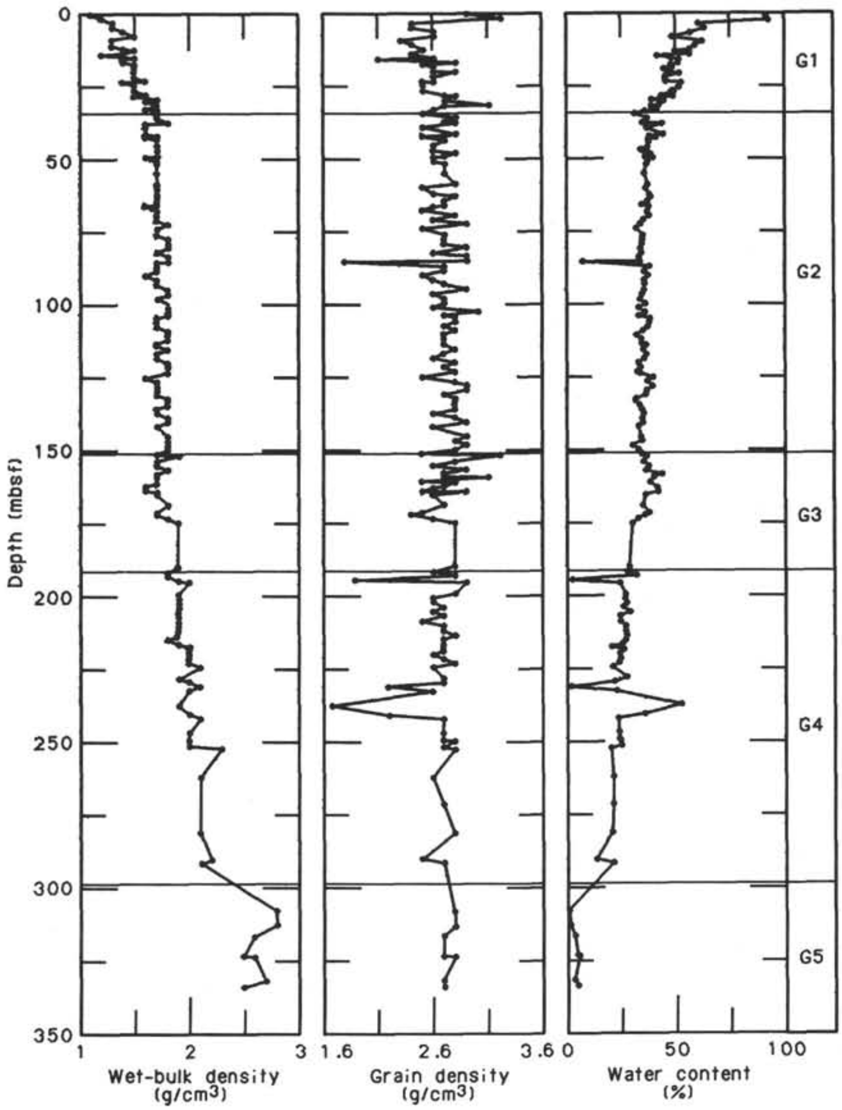

Figure 29. Downhole changes in index properties (wet-bulk density, grain density, and water content) at Site 747 illustrating the geotechnical units described in the text.

computed by taking the mean of weighted, equally spaced (0.5 m) values calculated from the discrete thermal conductivity data over the entire interval.

The average geothermal gradient and an average thermal conductivity of 1.28 W/m·K were used to calculate a mean value for heat flow equal to 61 mW/m^2 at Site 747.

GRAPE and *P*-Wave Logger

The GRAPE and the PWL provided a semicontinuous record of wet-bulk density and compressional wave velocity, respectively. These two instruments provide closely spaced measurements, parallel to bedding, through the plastic core liner of the whole-round APC or XCB core sections. The data from these two measurements at Hole 747A show general trends of increasing GRAPE bulk density and *P*-wave velocity with depth (Fig. 37). These data exhibit trends that are similar to those seen in the discrete (gravimetric bulk density and compressional wave velocity) measurements discussed in previous sections of this report.

Concluding Discussion

The trends in index properties, together with changes in compressional wave velocity, provide a tentative geotechnical stratigraphy for Site 747. Changes in two or more properties can be used to propose five geotechnical zones (Fig. 29), as follows.

1. Unit G1 (0–34 mbsf): Wet-bulk density increases from 1.19 to 1.75 g/cm^3 (0.016 g/cm^3/m), water content decreases from 91.5% to 31.37% (1.743 %/m), and porosity decreases from 97.14% to 53.10% (1.277 %/m).
2. Unit G2 (34–151.5 mbsf): Wet-bulk density gradually increases from a minimum value of 1.65 g/cm^3 at 37.8 mbsf to a maximum of 1.89 g/cm^3 at 148.5 mbsf (0.002 g/cm^3/m). Water content and porosity exhibit similar decreasing gradients of 0.136%/m and 0.144%/m, respectively.
3. Unit G3 (151.5–190.0 mbsf): Water content (max = 44.0%) and porosity (max = 68.5) increased, whereas bulk density (min = 1.66 g/cm^3 at 163 mbsf) decreased over the same interval. Missing data are included in this unit (175–190 mbsf).

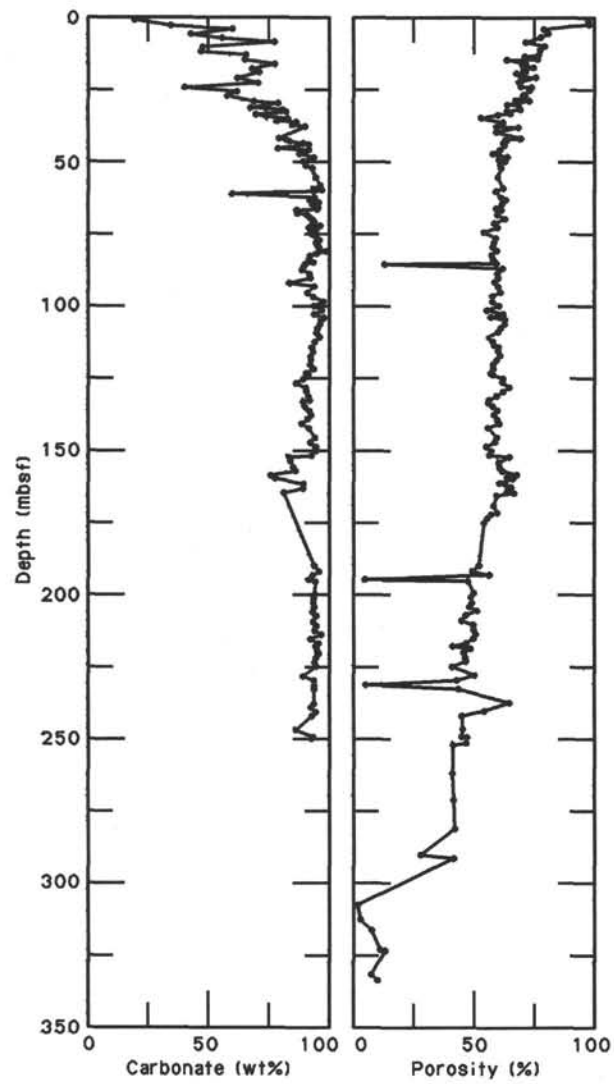

Figure 30. Downhole changes in carbonate content and porosity at Site 747.

4. Unit G4 (190.0–296.5 mbsf): The overall trend in this unit is for decreased water content and porosity, and increased bulk density values to near the basalt contact. Gradients for these properties are 0.09 %/m, 0.113 %/m, and 0.004 g/cm^3/m, respectively.
5. Unit G5 (below 296.6 mbsf): Basalt.

The upper section of Unit G4 may constitute a separate geotechnical unit, but not enough measurements were obtained to separate this interval from the rest of Unit G4. The geotechnical units identified compare well with the lithologic units described by the shipboard sedimentologists (see "Lithostratigraphy and Sedimentology" section, this chapter). The results of downhole logging (see "Logging" section, this chapter) and seismic stratigraphy (see "Seismic Stratigraphy" section, this chapter) should be integrated with the physical properties data to develop a more comprehensive synthesis of results from Site 747.

IGNEOUS PETROLOGY

Introduction

Basaltic basement was encountered below lower Santonian sediments at 296.6 mbsf and cored to a depth of 350.5 mbsf with 38% recovery (Cores 120-747C-11R to -16R). The sediment/basement contact was not recovered. The basalts have been divided into numerous units (see the core descriptions at the end of this chapter) based on macroscopic structures and the relative degree of alteration. They do form a mineralogically and geochemically coherent group, however, and for the purpose of this report, they are described as a single unit.

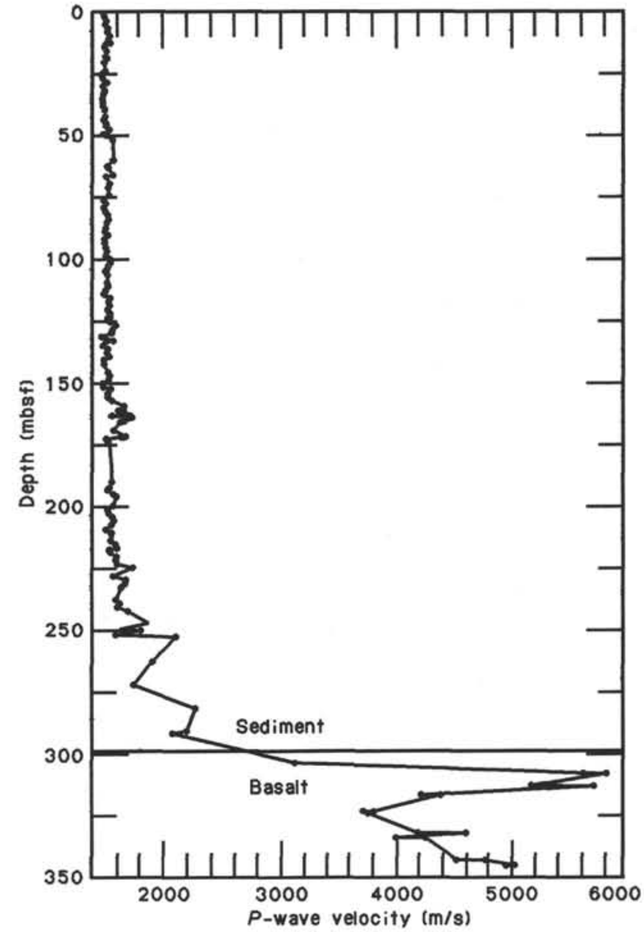

Figure 31. Compressional wave velocity for Site 747 measured with the Hamilton Frame Velocimeter. Increased velocities below 290 mbsf indicate basement.

Macroscopic Core Descriptions

The 53.9 m of basement penetrated consists of alternating, slightly to highly altered massive and brecciated basalts. They range from aphyric to sparsely phyric basalts. Phenocrysts range from 0.5 mm to 2 mm in size and occur in a slightly to highly vesicular, microcrystalline to fine-grained groundmass.

Zones of basaltic breccia occur throughout the basement and, along with chilled margins, delimit flow boundaries. In one example (Core 120-747C-15R-3, 84–96 cm), a red-colored, microcrystalline flow top grades downward into a fine-grained, gray-colored, and more vesicular basalt (Core 120-747C-15R-3, 96–150 cm). In the same core (Fig. 38), a chilled vesicular flow top is overlain by a green-gray basaltic breccia. In a fashion similar to flow tops, the base of some flows are also finer grained (e.g., Core 120-747C-12R-1, 60–67 cm).

Vesicles vary in size and distribution and have been infilled by secondary minerals to produce amygdules (Fig. 39). The amygdules tend to become larger (up to 2 cm), more irregular in shape, but less common, toward the center of flows. The apparent lack of glassy rinds, hyaloclastites, and pillow structures,

Table 12. Compressional wave velocity measured using the Hamilton Frame.

Core, section interval (cm)	Depth (mbsf)	DIR	Velocity (m/s)
120-747A-1H-1, 50	0.50	C	1507.5
120-747A-1H-2, 50	2.00	C	1518.7
120-747A-1H-3, 50	3.50	C	1534.8
120-747A-1H-4, 50	5.00	C	1521.7
120-747A-1H-5, 50	6.50	C	1543.1
120-747A-1H-6, 50	8.00	C	1542.3
120-747A-2H-1, 50	9.50	C	1560.3
120-747A-2H-2, 50	11.00	C	1553.5
120-747A-2H-3, 50	12.50	C	1569.0
120-747B-3H-1, 50	12.80	C	1528.3
120-747B-3H-2, 50	14.30	C	1515.2
120-747B-3H-3, 50	15.80	C	1537.9
120-747B-3H-4, 101	17.81	C	1530.6
120-747B-3H-5, 50	18.80	C	1538.7
120-747B-3H-6, 50	20.30	C	1516.1
120-747B-4H-2, 53	23.83	C	1528.7
120-747B-4H-3, 53	25.33	C	1487.0
120-747B-4H-4, 53	26.83	C	1504.3
120-747B-4H-5, 53	28.33	C	1542.1
120-747B-4H-6, 53	29.83	C	1504.1
120-747B-5H-1, 50	31.80	C	1528.4
120-747B-5H-2, 50	33.30	C	1515.5
120-747B-5H-3, 50	34.80	C	1507.0
120-747B-5H-4, 50	36.30	C	1509.4
120-747B-5H-5, 50	37.80	C	1510.3
120-747B-5H-6, 50	39.30	C	1526.1
120-747B-6H-1, 132	42.12	C	1527.8
120-747B-6H-2, 105	43.35	C	1516.8
120-747B-6H-3, 102	44.82	C	1534.5
120-747B-6H-4, 61	45.91	C	1535.3
120-747B-6H-5, 89	47.69	C	1565.4
120-747B-6H-6, 95	49.25	C	1513.8
120-747A-6H-2, 100	49.50	C	1533.9
120-747A-6H-4, 34	51.84	C	1589.0
120-747A-7H-3, 50	60.00	C	1600.9
120-747A-7H-4, 120	62.20	C	1542.9
120-747A-7H-5, 50	63.00	C	1556.4
120-747A-7H-7, 50	66.00	C	1597.7
120-747A-8H-1, 50	66.50	C	1531.4
120-747A-8H-3, 50	69.50	C	1569.4
120-747A-8H-4, 50	71.00	C	1558.2
120-747A-8H-6, 50	74.00	C	1565.9
120-747A-9H-2, 54	76.13	C	1515.2
120-747A-9H-3, 54	77.63	C	1533.6
120-747A-9H-4, 54	79.13	C	1518.0
120-747A-9H-5, 54	80.63	C	1531.4
120-747A-9H-6, 54	82.13	C	1553.7
120-747A-9H-7, 54	83.63	C	1560.3
120-747A-9H-8, 54	85.13	C	1542.2
120-747A-10H-1, 54	85.54	C	1541.9
120-747A-10H-2, 54	87.04	C	1534.6
120-747A-10H-3, 54	88.54	C	1529.0
120-747A-10H-4, 54	90.04	C	1551.8
120-747A-10H-5, 54	91.54	C	1526.4
120-747A-10H-6, 54	93.04	C	1528.6
120-747A-11H-1, 50	95.00	C	1535.0
120-747A-11H-2, 50	96.50	C	1540.7
120-747A-11H-3, 60	98.10	C	1537.7
120-747A-11H-4, 60	99.60	C	1565.7
120-747A-11H-5, 60	101.10	C	1577.0
120-747A-11H-6, 60	102.60	C	1552.2
120-747A-11H-7, 20	103.70	C	1542.1
120-747A-12H-1, 57	104.57	C	1532.0
120-747A-12H-2, 56	106.06	C	1550.1
120-747A-12H-4, 56	109.06	C	1548.7
120-747A-12H-5, 56	110.56	C	1559.9
120-747A-12H-6, 56	112.06	C	1539.7
120-747A-12H-7, 56	113.56	C	1520.2
120-747A-13H-1, 50	114.00	C	1531.0
120-747A-13H-2, 50	115.50	C	1570.9
120-747A-13H-3, 50	117.00	C	1560.3
120-747A-13H-4, 50	118.50	C	1567.1
120-747A-13H-5, 50	120.00	C	1552.9
120-747A-13H-6, 50	121.50	C	1573.2
120-747A-13H-7, 50	123.00	C	1572.3
120-747A-14H-1, 50	123.50	C	1557.7
120-747A-14H-2, 50	125.00	C	1574.3

Table 12 (continued).

Core, section interval (cm)	Depth (mbsf)	DIR	Velocity (m/s)
120-747A-14H-3, 50	126.50	C	1619.2
120-747A-14H-4, 50	128.00	C	1596.5
120-747A-14H-5, 50	129.50	C	1588.4
120-747A-14H-6, 50	131.00	C	1500.5
120-747A-14H-7, 50	132.50	C	1594.3
120-747A-15H-1, 55	133.05	C	1540.3
120-747A-15H-2, 55	134.55	C	1513.7
120-747A-15H-3, 55	136.05	C	1552.3
120-747A-15H-4, 55	137.55	C	1544.2
120-747A-15H-5, 55	139.05	C	1569.1
120-747A-15H-6, 55	140.55	C	1520.0
120-747A-15H-7, 55	142.05	C	1522.5
120-747A-16H-3, 49	145.49	C	1557.2
120-747A-16H-4, 49	146.99	C	1568.1
120-747A-16H-5, 49	148.49	C	1565.5
120-747A-16H-6, 49	149.99	C	1516.0
120-747A-16H-7, 49	151.49	C	1515.7
120-747A-17X-1, 76	152.26	C	1585.8
120-747A-17X-2, 105	154.05	C	1553.6
120-747A-17X-3, 114	155.64	C	1557.8
120-747A-17X-4, 100	157.00	C	1591.5
120-747C-1R-1, 36	159.36	C	1694.5
120-747C-1R-1, 36	159.36	A	1694.9
120-747C-1R-2, 52	161.02	A	1646.3
120-747C-1R-2, 52	161.02	B	1693.7
120-747C-1R-2, 52	161.02	C	1677.2
120-747C-1R-3, 57	162.57	A	1688.8
120-747C-1R-3, 57	162.57	B	1763.5
120-747C-1R-3, 57	162.57	C	1695.9
120-747A-18X-2, 60	163.10	C	1596.9
120-747C-1R-4, 51	164.01	A	1756.8
120-747C-1R-4, 51	164.01	B	1736.2
120-747C-1R-4, 51	164.01	C	1748.1
120-747C-1R-5, 57	165.57	A	1694.3
120-747C-1R-5, 57	165.57	C	1662.7
120-747C-2R-1, 34	168.84	C	1601.1
120-747C-2R-2, 141	171.41	A	1667.6
120-747C-2R-2, 141	171.41	B	1687.4
120-747C-2R-2, 141	171.41	C	1704.8
120-747C-2R-3, 73	172.23	C	1541.5
120-747C-2R-4, 54	173.54	C	1559.7
120-747C-2R-5, 52	175.02	C	1575.7
120-747A-21X-1, 39	189.89	C	1591.0
120-747A-21X-2, 94	191.94	C	1569.3
120-747A-21X-3, 69	193.19	C	1555.0
120-747A-21X-4, 69	194.69	C	1604.1
120-747A-21X-5, 8	195.58	C	1631.5
120-747A-22X-1, 50	199.50	C	1605.0
120-747A-22X-2, 50	201.00	C	1556.9
120-747A-22X-3, 50	202.50	C	1566.2
120-747A-22X-4, 50	204.00	C	1597.7
120-747A-22X-5, 50	205.50	C	1608.0
120-747A-22X-6, 50	207.00	C	1586.4
120-747A-23X-1, 50	209.00	C	1541.8
120-747A-23X-2, 40	210.40	C	1584.8
120-747A-23X-3, 50	212.00	C	1594.4
120-747A-23X-4, 50	213.50	C	1579.4
120-747A-23X-5, 50	215.00	C	1620.2
120-747A-23X-6, 50	216.50	C	1630.1
120-747A-23X-7, 10	217.60	C	1569.2
120-747A-24X-1, 50	218.50	C	1574.4
120-747A-24X-2, 50	220.00	C	1626.9
120-747A-24X-3, 50	221.50	C	1622.7
120-747A-24X-4, 50	223.00	C	1632.6
120-747A-24X-5, 50	224.50	C	1767.5
120-747A-25X-1, 50	228.00	C	1602.6
120-747A-25X-2, 50	229.50	C	1712.0
120-747A-25X-3, 50	231.00	C	1706.2
120-747A-25X-4, 50	232.50	C	1674.2
120-747A-26X-1, 50	237.50	C	1624.7
120-747A-26X-2, 50	239.00	C	1661.8
120-747A-26X-3, 50	240.50	C	1640.7
120-747A-26X-4, 60	242.10	C	1730.4
120-747A-27X-1, 46	246.96	C	1907.8
120-747A-27X-2, 136	249.36	C	1663.2
120-747A-27X-3, 22	249.72	C	1836.0
120-747A-27X-4, 53	251.53	C	1628.4

Table 12 (continued).

Core, section interval (cm)	Depth (mbsf)	DIR	Velocity (m/s)
120-747C-6R-1, 47	252.47	A	2128.9
120-747C-7R-1, 79	262.29	C	1936.7
120-747C-8R-1, 53	271.53	C	1775.2
120-747C-9R-1, 84	281.34	A	2300.2
120-747C-10R-1, 31	290.31	A	2221.0
120-747C-10R-CC, 0	291.65	C	2103.6
120-747C-12R-1, 56	303.56	A	3157.8
120-747C-12R-4, 45	307.95	C	5663.6
120-747C-12R-4, 45	307.95	A	5858.6
120-747C-13R-1, 45	312.95	C	5217.6
120-747C-13R-1, 45	312.95	A	5750.4
120-747C-13R-3, 104	316.54	C	4255.7
120-747C-13R-3, 104	316.54	A	4424.3
120-747C-14R-1, 113	323.13	C	3843.0
120-747C-14R-1, 113	323.13	A	3753.5
120-747C-14R-2, 28	323.68	C	3790.4
120-747C-15R-1, 35	331.85	C	4226.3
120-747C-15R-1, 35	331.85	A	4631.1
120-747C-15R-2, 91	333.91	C	4038.2
120-747C-15R-2, 91	333.91	A	4287.4
120-747C-16R-2, 85	342.80	C	4562.5
120-747C-16R-2, 85	342.80	A	4810.2
120-747C-16R-4, 26	345.00	C	5069.8
120-747C-16R-4, 26	345.00	A	5004.6

Note: DIR = direction of propagation; A = perpendicular to bedding; B = parallel to bedding in core; and C = perpendicular to split face of core.

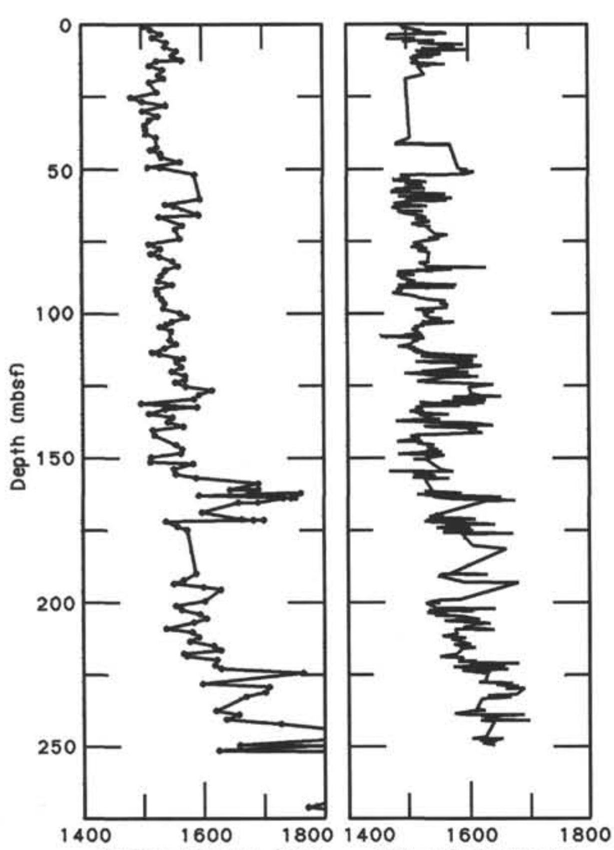

Figure 32. Comparison of discrete and continuous compressional wave velocity measurements in Hole 747A.

Table 13. Undrained shear strength (S_u) measured using ODP Motorized Vane.

Core, section, interval (cm)	Depth (mbsf)	S_u (kPa)
120-747A-1H-1, 100	1.00	6.3
120-747A-1H-2, 100	2.50	11.8
120-747A-1H-3, 100	4.00	11.1
120-747A-1H-4, 100	5.50	19.2
120-747A-1H-5, 100	7.00	7.0
120-747A-1H-6, 95	8.45	9.1
120-747A-2H-1, 100	10.00	9.8
120-747A-2H-2, 100	11.50	6.9
120-747A-2H-3, 100	13.00	13.1
120-747A-2H-4, 103	14.53	3.8
120-747A-2H-5, 95	15.95	5.0
120-747A-2H-6, 100	17.50	11.2
120-747A-2H-7, 55	18.55	10.9
120-747A-3H-1, 103	19.53	15.3
120-747A-3H-2, 73	20.73	8.5
120-747A-3H-3, 102	22.52	18.1
120-747A-3H-4, 75	23.75	17.4
120-747A-3H-5, 106	25.56	22.7
120-747A-3H-6, 42	26.42	18.6
120-747A-4H-1, 91	28.91	5.7
120-747A-4H-2, 121	30.71	6.4
120-747A-4H-3, 115	32.15	4.5
120-747A-4H-4, 116	33.66	11.6
120-747A-4H-5, 44	34.44	12.1
120-747A-4H-6, 84	36.34	20.1
120-747A-5H-3, 117	41.67	20.7
120-747A-5H-4, 37	42.37	22.2
120-747A-5H-4, 133	43.33	11.9
120-747A-5H-5, 95	44.45	16.8
120-747A-5H-6, 78	45.78	16.4
120-747A-6H-1, 112	48.12	3.5
120-747A-6H-2, 100	49.50	5.0
120-747A-6H-3, 94	50.94	5.4
120-747A-6H-4, 34	51.84	11.2
120-747A-7H-2, 100	59.00	2.8
120-747A-7H-3, 79	60.29	4.1
120-747A-7H-4, 128	62.28	8.3
120-747A-7H-4, 134	62.34	11.1
120-747A-7H-5, 82	63.32	4.0
120-747A-7H-6, 97	64.97	12.4
120-747A-8H-1, 114	67.14	15.6
120-747A-8H-1, 108	67.08	14.3
120-747A-8H-2, 74	68.24	11.9
120-747A-8H-3, 74	69.74	21.9
120-747A-8H-4, 79	71.29	17.4
120-747A-8H-5, 131	73.31	17.3
120-747A-8H-6, 124	74.74	16.1
120-747A-9H-2, 100	76.59	4.1
120-747A-9H-3, 100	78.09	3.1
120-747A-9H-4, 100	79.59	7.7
120-747A-9H-5, 100	81.09	4.6
120-747A-9H-6, 65	82.24	8.3
120-747A-9H-7, 100	84.09	17.7
120-747A-9H-8, 65	85.24	37.8
120-747A-10H-1, 100	86.00	9.9
120-747A-10H-2, 100	87.50	5.8
120-747A-10H-3, 100	89.00	5.1
120-747A-10H-4, 100	90.50	5.1
120-747A-10H-5, 100	92.00	13.9
120-747A-10H-6, 100	93.50	12.1
120-747A-11H-1, 100	95.50	13.0
120-747A-11H-2, 100	97.00	22.5
120-747A-11H-3, 100	98.50	21.6
120-747A-11H-4, 100	100.00	19.6
120-747A-11H-5, 100	101.50	16.9
120-747A-11H-6, 120	103.20	3.0
120-747A-11H-7, 65	104.15	6.1
120-747A-12H-1, 99	104.99	5.7
120-747A-12H-2, 99	106.49	5.8
120-747A-12H-3, 99	107.99	7.4
120-747A-12H-4, 99	109.49	10.6
120-747A-12H-5, 99	110.99	19.6
120-747A-12H-6, 99	112.49	10.4
120-747A-12H-7, 71	113.71	5.0
120-747A-13H-1, 100	114.50	20.1

Table 13 (continued).

Core, section, interval (cm)	Depth (mbsf)	S_u (kPa)
120-747A-13H-2, 105	116.05	15.4
120-747A-13H-3, 100	117.50	31.9
120-747A-13H-4, 100	119.00	24.8
120-747A-13H-5, 100	120.50	37.6
120-747A-13H-6, 100	122.00	22.5
120-747A-13H-7, 39	122.89	10.5
120-747A-14H-1, 100	124.00	33.7
120-747A-14H-2, 100	125.50	25.1
120-747A-14H-3, 100	127.00	46.1
120-747A-14H-4, 100	128.50	29.6
120-747A-14H-5, 100	130.00	33.1
120-747A-14H-6, 100	131.50	20.1
120-747A-14H-7, 39	132.39	8.3
120-747A-15H-1, 47	132.97	11.8
120-747A-15H-1, 106	133.56	11.8
120-747A-15H-2, 108	135.08	10.6
120-747A-15H-3, 82	136.32	11.8
120-747A-15H-4, 111	138.11	14.9
120-747A-15H-5, 50	139.00	29.7
120-747A-15H-6, 135	141.35	18.9
120-747A-15H-7, 24	141.74	20.1
120-747A-16H-3, 57	145.57	23.6
120-747A-16H-3, 123	146.23	21.3
120-747A-16H-4, 87	147.37	41.4
120-747A-16H-5, 12	148.12	42.6
120-747A-16H-6, 73	150.23	37.8
120-747A-16H-7, 21	151.21	29.6
120-747A-17X-1, 71	152.21	43.7
120-747A-17X-2, 101	154.01	47.3
120-747A-17X-2, 106	154.06	63.8
120-747A-17X-3, 61	155.11	34.3
120-747A-17X-3, 115	155.65	28.4
120-747A-17X-4, 101	157.01	63.8
120-747A-17X-5, 81	158.31	44.9
120-747A-17X-6, 24	159.24	78.0

Table 14. Undrained shear strength (S_u) measured using Wykeham Farrance Vane.

Core, section, interval (cm)	Depth (mbsf)	S_u (kPa)
120-747B-2H-2, 100	5.30	6.4
120-747B-2H-3, 109	6.89	8.9
120-747B-2H-4, 86	8.16	12.2
120-747B-2H-5, 106	9.86	6.4
120-747B-2H-6, 64	10.94	3.7
120-747B-3H-1, 112	13.42	2.5
120-747B-3H-2, 103	14.83	3.7
120-747B-3H-3, 57	15.87	4.1
120-747B-3H-5, 40	18.70	5.0
120-747B-3H-5, 99	19.29	3.9
120-747B-3H-6, 33	20.13	5.9
120-747B-3H-6, 123	21.03	6.8
120-747B-3H-7, 13	21.43	7.1
120-747B-4H-2, 65	23.95	5.8
120-747B-4H-3, 125	26.05	6.9
120-747B-4H-4, 98	27.28	7.2
120-747B-4H-5, 101	28.81	12.8
120-747B-4H-5, 122	29.02	14.3
120-747B-4H-6, 94	30.24	16.2
120-747B-5H-1, 65	31.95	9.1
120-747B-5H-5, 62	37.92	12.0
120-747B-5H-5, 125	38.55	11.3
120-747B-5H-6, 53	39.33	8.6
120-747B-5H-6, 107	39.87	10.1
120-747B-6H-1, 128	42.08	9.9
120-747B-6H-2, 109	43.39	5.8
120-747B-6H-3, 105	44.85	9.1
120-747B-6H-4, 64	45.94	10.6
120-747B-6H-5, 87	47.67	9.9
120-747B-6H-6, 93	49.23	5.3

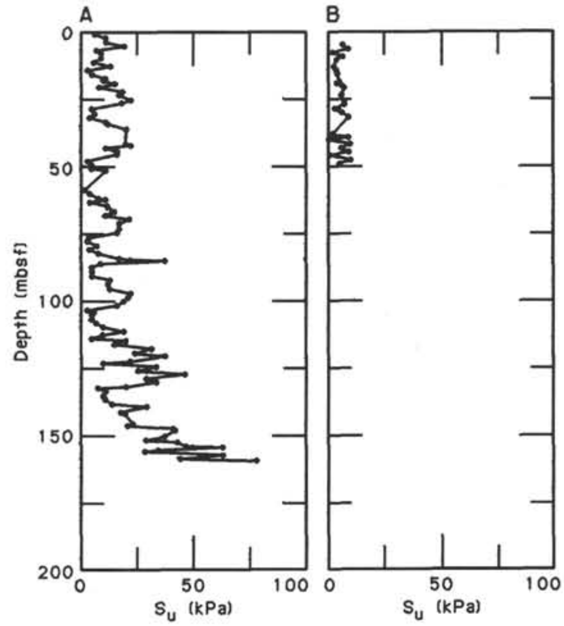

Figure 33. **A.** Undrained shear strength in Hole 747A measured with the ODP Motorized Vane device. **B.** Undrained shear strength in Hole 747B measured with the Wykeham Farrance Motorized Vane device.

and the presence of oxidized flow tops suggest subaerial eruption. In one flow (Core 120-747C-15R-2, 15–80 cm), the oxidized and reddened zone extends well into the interior, suggesting a significant hiatus between this flow and the following eruption. In some cases, amygdules may show flow orientation and are flattened in a plane with a maximum dip of about 15° (Fig. 40), suggesting that the basalt flowed over a near-horizontal topography.

The brecciated basalts consist of dark angular fragments (1–7 cm) of highly altered, microcrystalline vesicular basalt cemented with brownish red to yellow clays (e.g., Core 120-747C-13R-2, 35–55 cm). In the upper flows of the basement, this matrix also contains calcite (Fig. 41). White calcite veins occur in variable amounts throughout the basalts but are most common in the top 10 m of basement. The veins range in width from <1 mm to 3 cm, and they crosscut amygdules (Fig. 42). The crosscutting relationships between amygdules and veins suggest that at least two successive hydrothermal events have affected the basalts. Relatively fresh basalt occurs above the highly calcite-veined and brecciated basalts at the top of the first core (Core 120-747C-11R-1, 0–40 cm). This suggests that the eruption of these basalts may have occurred after hydrothermal alteration of the underlying brecciated basalt.

The maximum observed thickness of massive basalt, without apparent breccias or chilled margins, is 5.4 m (Cores 120-747C-12R-1, 122 cm, to 120-747C-13R-1, 102 cm). The maximum observed thickness of the breccia is 75 cm (Core 120-747C-11R-1, 50–125 cm). The breccias constitute a small proportion of the recovered basement and generally occur as loose rubble. The thickness of the flows and the apparent amount of breccias is in contradiction with the wireline logs.

On the shallow resistivity and gamma ray records (see "Logging" section, this chapter), two zones of high resistivity are separated by zones of lower resistivity. The zones of high resistivity are composed of a series of peaks occurring at approximately 1-m intervals that are interpreted as individual lava flows separated by thin breccias. We interpret the 5-m-thick zones of low resistivity as composed mainly of highly permeable basaltic

Table 15. Thermal conductivity values for Site 747.

Core, section, interval (cm)	Depth (mbsf)	Thermal conductivity (W/m/K)
120-747B-1H-2, 65	2.15	0.8600
120-747B-2H-2, 30	4.60	1.0090
120-747A-2H-3, 95	12.95	0.9110
120-747B-3H-4, 85	17.65	1.1960
120-747B-3H-6, 70	20.50	1.0250
120-747A-3H-4, 55	23.55	1.1470
120-747B-4H-2, 30	23.60	1.0840
120-747B-4H-4, 60	26.90	1.1120
120-747B-4H-6, 90	30.20	1.1200
120-747A-4H-3, 70	31.70	1.2210
120-747A-4H-4, 70	33.20	1.2170
120-747A-4H-5, 70	34.70	1.4670
120-747A-4H-6, 70	36.20	1.3330
120-747B-5H-4, 94	36.74	1.4010
120-747B-5H-5, 79	38.09	1.2050
120-747B-5H-6, 86	39.66	1.4180
120-747A-5H-3, 70	41.20	1.3040
120-747A-5H-4, 70	42.70	1.2460
120-747A-5H-5, 70	44.20	1.3780
120-747A-5H-6, 70	45.70	1.3020
120-747B-6H-4, 85	46.15	1.3350
120-747B-6H-5, 86	47.66	1.3150
120-747B-6H-6, 86	49.16	1.3270
120-747A-6H-3, 70	50.70	1.3000
120-747A-6H-4, 70	52.20	1.3280
120-747A-6H-5, 70	53.70	1.3350
120-747A-7H-3, 100	60.50	1.3130
120-747A-7H-4, 60	61.60	1.4800
120-747A-7H-5, 100	63.50	1.3610
120-747A-7H-6, 71	64.71	1.3380
120-747A-8H-3, 60	69.60	1.3190
120-747A-8H-4, 60	71.10	1.5390
120-747A-8H-5, 60	72.60	1.5580
120-747A-8H-6, 86	74.36	1.4290
120-747A-9H-3, 70	77.79	1.4360
120-747A-9H-4, 89	79.48	1.4750
120-747A-9H-5, 51	80.60	1.5130
120-747A-9H-6, 52	82.11	1.4260
120-747A-10H-1, 100	86.00	1.2830
120-747A-10H-3, 70	88.70	1.4060
120-747A-10H-4, 40	89.90	1.3110
120-747A-10H-6, 70	93.20	1.3080
120-747A-11H-1, 60	95.10	1.3540
120-747A-11H-3, 80	98.30	1.4180
120-747A-11H-5, 50	101.00	1.4480
120-747A-11H-7, 40	103.90	1.3390
120-747A-12H-1, 80	104.80	1.4080
120-747A-12H-3, 65	107.65	1.4590
120-747A-12H-5, 60	110.60	1.4680
120-747A-12H-7, 60	113.60	1.4090
120-747A-13H-1, 40	113.90	1.4650
120-747A-13H-3, 70	117.20	1.3850
120-747A-13H-5, 70	120.20	1.2460
120-747A-13H-6, 70	121.70	1.3550
120-747A-14H-1, 30	123.30	1.4270
120-747A-14H-3, 40	126.40	1.3330
120-747A-14H-4, 50	128.00	1.1850
120-747A-14H-6, 60	131.10	1.2770
120-747A-16H-1, 30	142.30	1.4150
120-747A-16H-3, 50	145.50	1.4640
120-747A-16H-4, 70	147.20	1.4800
120-747A-16H-6, 95	150.45	1.3660
120-747A-17X-3, 70	155.20	1.2930
120-747A-17X-4, 60	156.60	1.3900
120-747A-17X-5, 40	157.90	1.3130
120-747A-17X-6, 15	159.15	1.2130
120-747A-18X-2, 76	163.26	1.4160
120-747A-19X-2, 67	172.67	1.6220
120-747A-19X-3, 66	174.16	1.6360
120-747A-19X-4, 67	175.67	1.6590
120-747A-24X-2, 75	220.25	1.6640
120-747A-24X-3, 75	221.75	1.7910
120-747A-24X-4, 75	223.25	1.6680
120-747A-25X-2, 80	229.80	1.9490
120-747A-25X-3, 60	231.10	1.9380
120-747A-26X-1, 50	237.50	1.7790
120-747A-26X-3, 60	240.60	1.8840
120-747A-26X-4, 70	242.20	1.7820
120-747A-27X-2, 50	248.50	1.7590
120-747A-27X-3, 60	250.10	1.8470
120-747A-27X-4, 30	251.30	1.8340
120-747C-12R-1, 21	303.21	1.4870
120-747C-12R-2, 100	305.50	1.6230

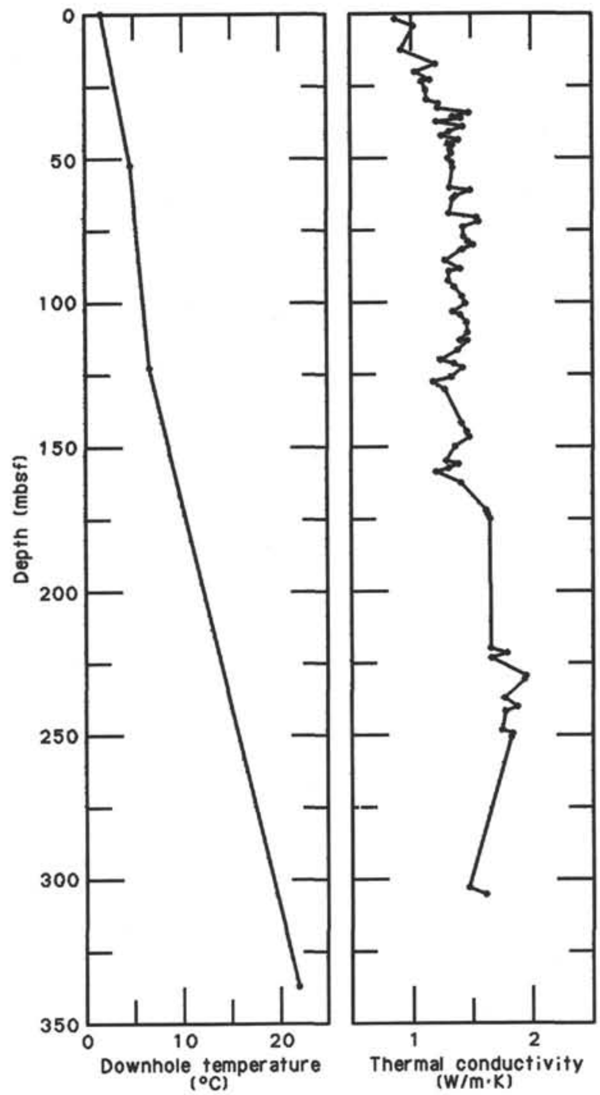

Figure 34. Thermal conductivity and downhole temperature measured at Site 747.

breccias. These zones of low resistivity apparently correspond to Cores 120-747C-12R and -14R, which contain mainly massive basalt, but with recovery of 47% and 12%, respectively. If the interpretation of the wireline logs is correct, this would suggest that at least 12 lava flows with an average thickness of about 1 m were penetrated and that a large proportion of the breccias were not recovered.

Petrography

The basalts of Site 747 are aphyric to sparsely phyric. Phenocrysts consist of olivine and plagioclase with rare clinopyroxene. Subhedral to euhedral olivine phenocrysts (0.5–3 mm) have been replaced by pseudomorphs of brown smectite and iddingsite. Plagioclase phenocrysts (An_{67-84}) occur as fresh euhedral laths (0.5–5 mm) and as pseudomorphs replaced by zeolites and smectites. Some crystals contain brown smectites, which may represent devitrified melt inclusions (Fig. 43). The plagioclase is sometimes zoned compositionally and may also exhibit resorption textures. Fresh clinopyroxene phenocrysts are subhedral to anhedral and range in size from 0.5–2 mm. Some of the larger clinopyroxene phenocrysts exhibit resorption textures and thin

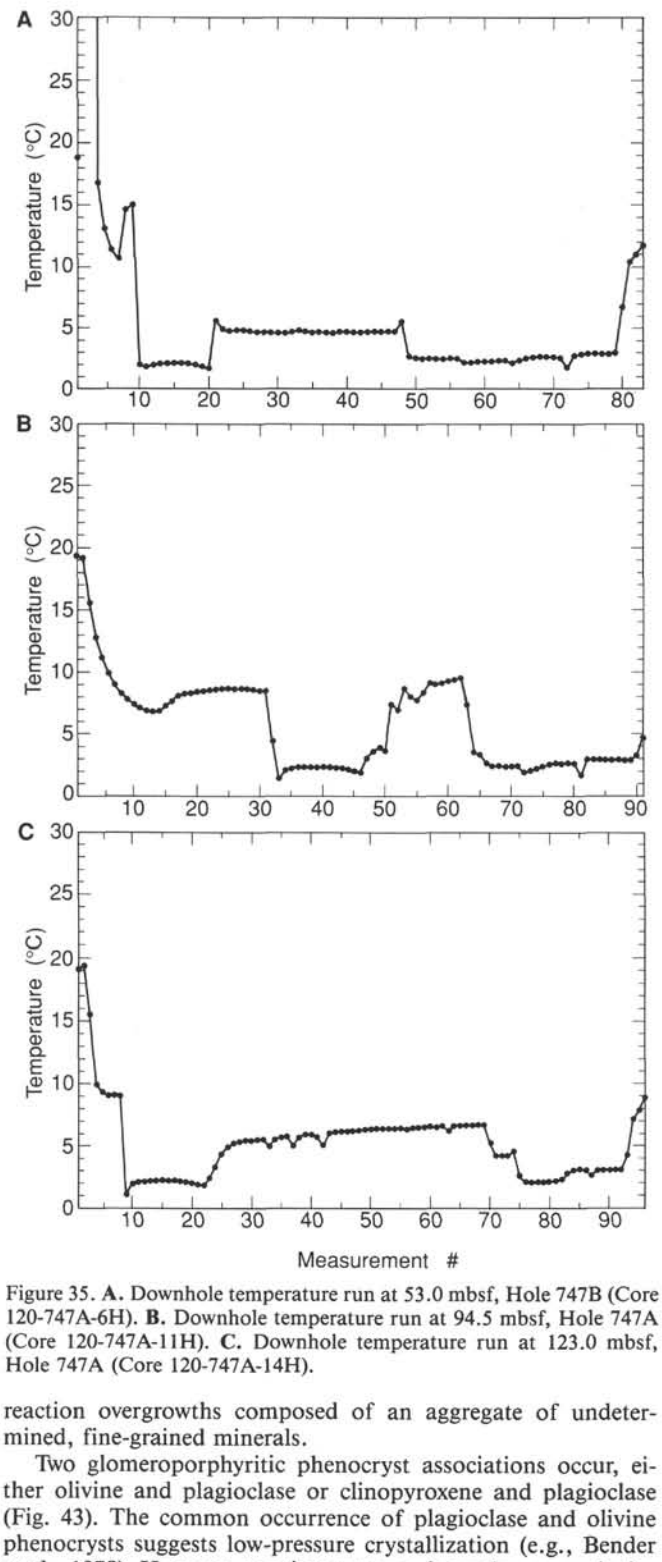

Figure 35. **A.** Downhole temperature run at 53.0 mbsf, Hole 747B (Core 120-747A-6H). **B.** Downhole temperature run at 94.5 mbsf, Hole 747A (Core 120-747A-11H). **C.** Downhole temperature run at 123.0 mbsf, Hole 747A (Core 120-747A-14H).

reaction overgrowths composed of an aggregate of undetermined, fine-grained minerals.

Two glomeroporphyritic phenocryst associations occur, either olivine and plagioclase or clinopyroxene and plagioclase (Fig. 43). The common occurrence of plagioclase and olivine phenocrysts suggests low-pressure crystallization (e.g., Bender et al., 1978). However, reaction textures shown by some plagioclase and clinopyroxene glomerocrysts may also suggest two-stage, polybaric crystallization; that is, high-pressure crystallization followed by low-pressure reaction and/or magma mixing (Kuo and Kirkpatrick, 1982; Barton et al., 1982).

The groundmass varies from microcrystalline to fine grained with intergranular to subophitic textures. The mineralogy consists of a network of plagioclase laths (An_{40}) with Fe-Ti oxides,

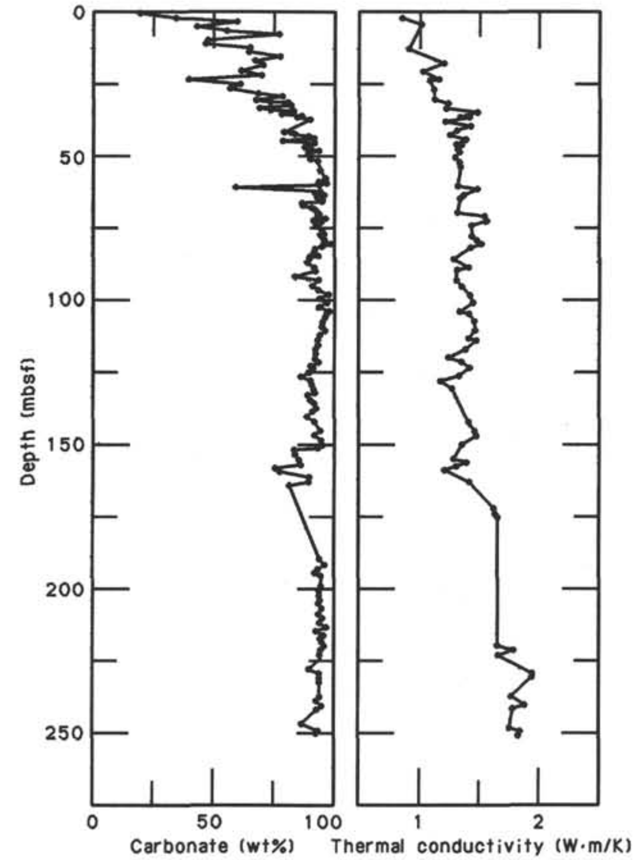

Figure 36. Profiles of carbonate content and thermal conductivity at Site 747.

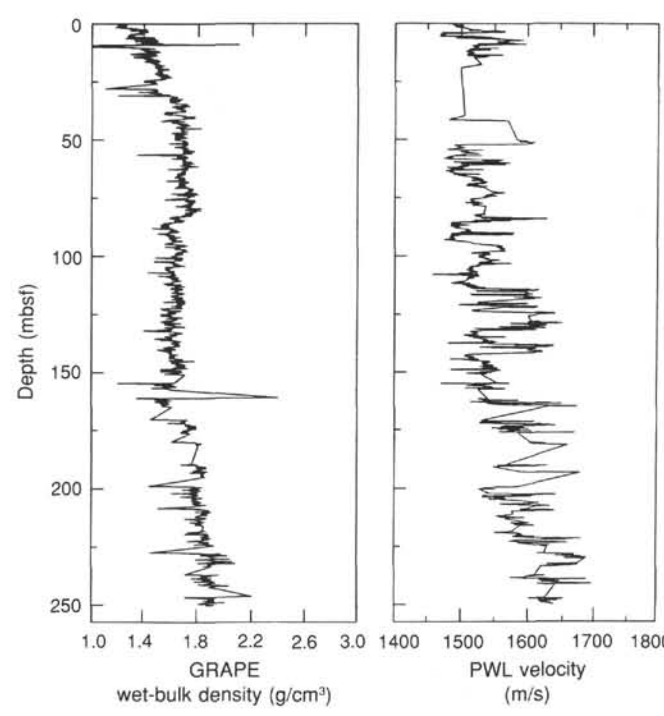

Figure 37. Downhole profiles of GRAPE wet-bulk density and *P*-wave logger compressional wave velocity measured with the *P*-wave logger (PWL) at Hole 747A.

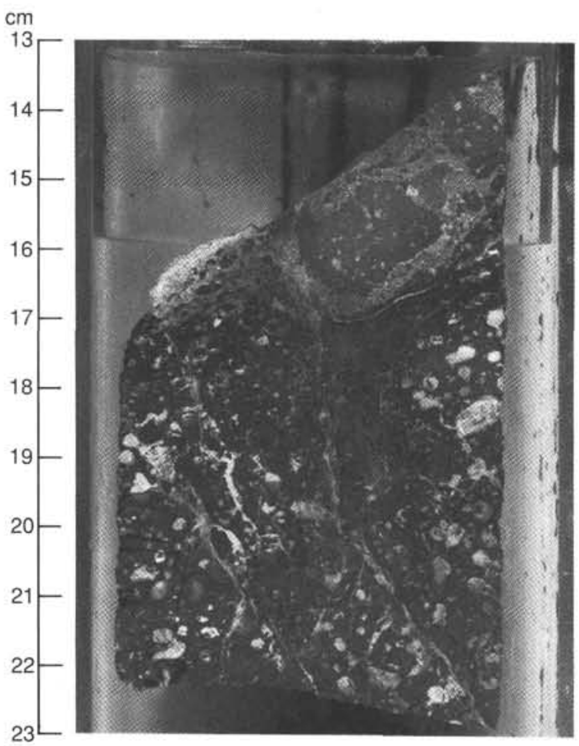

Figure 38. Contact between basal flow breccia and chilled, vesicular flow top (Core 120-747C-15R-2, 13–23 cm).

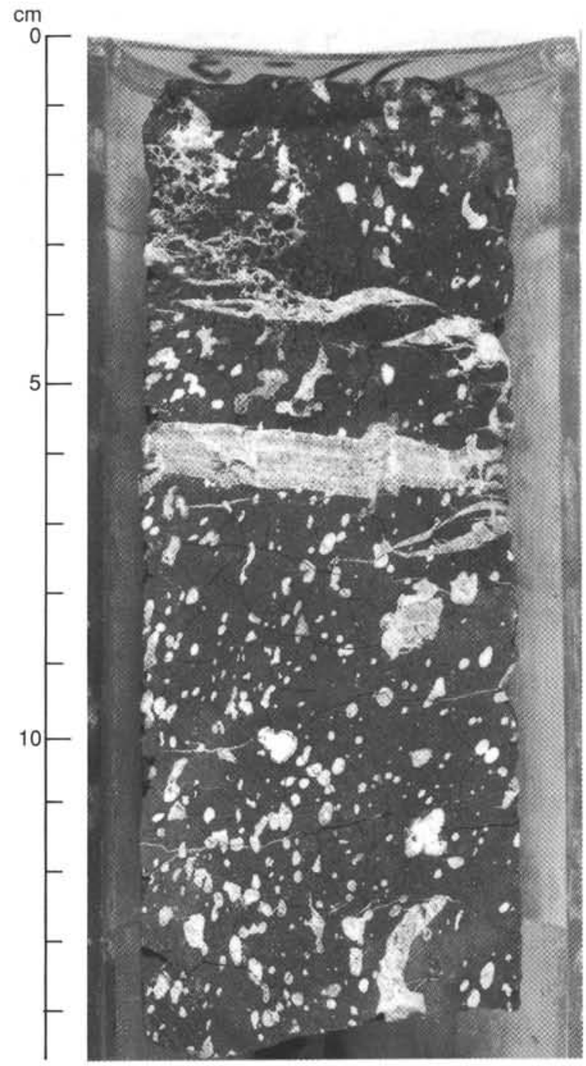

Figure 39. Aphyric basalt with stretched vesicles filled with zeolites, clay, and minor calcite (Core 120-747C-11R-3, 0–15 cm).

sometimes accompanied by clinopyroxenes. Clinopyroxenes are either interstitial or subophitic. Some amygdules are rimmed by a dark halo up to a few millimeters in width that consists of microcrystalline ilmenite in a devitrified glass that has been altered to smectite and iron hydroxide.

Alteration

The more massive basalts are generally fresher than the brecciated basalts, which are extensively altered. The secondary minerals are clays, zeolites, prehnite, goethite, calcite, and quartz. They were identified by a combination of optical microscopy and XRD.

Brown- and green-colored clay minerals are observed in thin section. The XRD patterns indicate that they consist of smectite and celadonite, respectively. However, since the powders analyzed were not pure, further XRD work is needed to determine the exact nature of the clay minerals. The zeolites form prismatic crystals in the amygdules (Fig. 44) and radiating, fibrous crystals in the groundmass and altered plagioclase phenocrysts. Three different zeolites have been identified: heulandite-clinoptilolite, chabazite, and stilbite. They occur in a nonsystematic fashion throughout the basement section and may all coexist at the same horizon.

A radial aggregate of prismatic, twinned crystals of prehnite occurs with zeolite and calcite in a vein at the top of the basement section (Fig. 45). Calcite occurs as large crystals infilling vesicles and fractures and, rarely, in the groundmass. Immediately adjacent to most of the veins is a brown-reddish halo that consists mainly of goethite. The yellow color of some of the alteration also suggests the presence of other iron oxides and hydroxides. Quartz occurs as a minor secondary mineral in some vesicles. Neither chlorite nor the zeolite phillipsite were observed.

Vesicles and fractures commonly show a pronounced zonation of secondary minerals. Where this zonation is most complete, the following crystallization sequence can be inferred (Fig. 45): brown smectite adjacent to the vesicle or fracture wall is successively overgrown by green smectite, zeolites, prehnite(?), and, last of all, calcite or quartz.

The nature of the alteration products in the basalts from Hole 747C have a different character from that commonly observed in mid-oceanic ridge basalts (MORB) (Honnorez, 1981). The main differences are the variety of zeolite minerals and the absence of phillipsite, which is commonly observed in altered MORB. The absence of sulfide minerals and the presence of goethite and green smectites indicate some of the alteration occurred in an oxidizing environment. The sequence of crystallization of the secondary minerals is controlled essentially by varying Eh-pH conditions and the alkalinity of the hydrothermal fluids. The crystallization of smectites is normally favored by higher Eh and lower pH relative to the zeolites and calcite. This is supported by the presence of iron hydroxide halos around the vesicles and the fractures.

The observed secondary mineralogy of Hole 747C basalts bears some resemblance to that observed in regions of high heat flow in the extensive subaerial tholeiitic flood basalts of Iceland (Kristmannsdòttir and Tòmasson, 1978; Pàlmason et al., 1979). The zeolite assemblages correspond to the intermediate temperature (between 50°C and 100°C) zone of the zeolite facies.

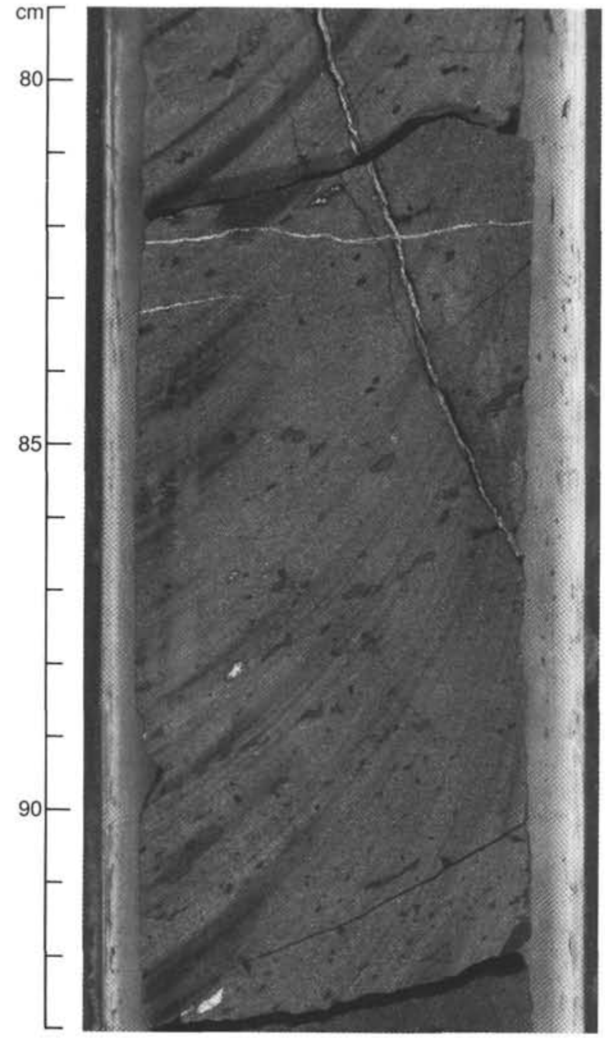

Figure 40. Shallow-dipping amygdules (Core 120-747C-13R-1, 79-93 cm).

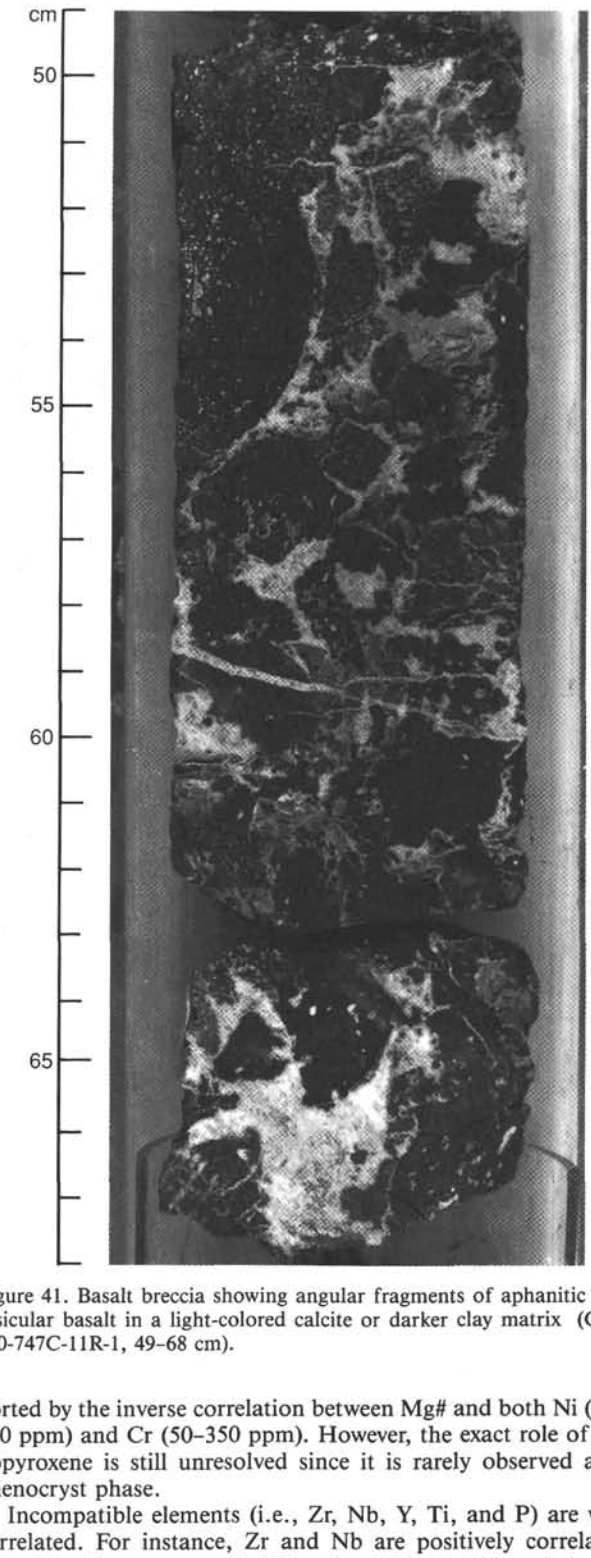

Figure 41. Basalt breccia showing angular fragments of aphanitic and vesicular basalt in a light-colored calcite or darker clay matrix (Core 120-747C-11R-1, 49-68 cm).

Geochemistry

Whole-rock major and trace element analyses are listed in Tables 16 and 17. With the exception of two silica-undersaturated rocks (nepheline normative), the cored basement consists of olivine-hypersthene normative basalts. Loss on ignition (LOI) ranges from 0.61 to 16.7 wt% (with highest values in the brecciated basalts; e.g., Sample 120-747C-11R-3, 32-33 cm) and reflects the variable degrees of alteration exhibited by the basement volcanics.

The elements Na, K, Ba, and Rb, which are prone to alteration (Humphris and Thompson, 1978), do not show systematic variations with fractionation indexes (e.g., Mg# = Mg/Mg + Fe^{2+}). This shows that these elements were mobile and redistributed during alteration processes. Only elements (e.g., Ni, Cr, Ti, P, Y, Nb, and Zr) that show a systematic variation with differentiation indexes (i.e., Mg# and Zr) are assumed to be immobile during alteration. They can be used to describe the magmatic origin and evolution of these volcanic rocks.

In a plot of the CaO/Al_2O_3 ratio against Mg# (Fig. 46), most samples plot on a trend that indicates plagioclase and olivine fractionation. This is consistent with the observed phenocryst assemblage. Two samples with the lowest Mg# have the lowest CaO/Al_2O_3 ratio and may have undergone clinopyroxene fractionation. Olivine and clinopyroxene fractionation is also supported by the inverse correlation between Mg# and both Ni (50–100 ppm) and Cr (50–350 ppm). However, the exact role of clinopyroxene is still unresolved since it is rarely observed as a phenocryst phase.

Incompatible elements (i.e., Zr, Nb, Y, Ti, and P) are well correlated. For instance, Zr and Nb are positively correlated (Fig. 47) with an average Zr/Nb ratio of 11–13. This ratio is significantly lower than that observed in Indian Ocean normal mid-ocean ridge basalts (N-type MORB) (Zr/Nb = 40–56) (Price et al., 1986) but higher than "hot spot" type basalts from Kerguelen (Zr/Nb = 5–8) and Heard islands (Zr/Nb = 5–7) (Storey et al., 1988). Basalts from Hole 747C have similar Zr/Nb ratios to some of the older basalts from Kerguelen Island (Zr/Nb = 11–12) (Storey et al., 1988) and oceanic flood basalts such as

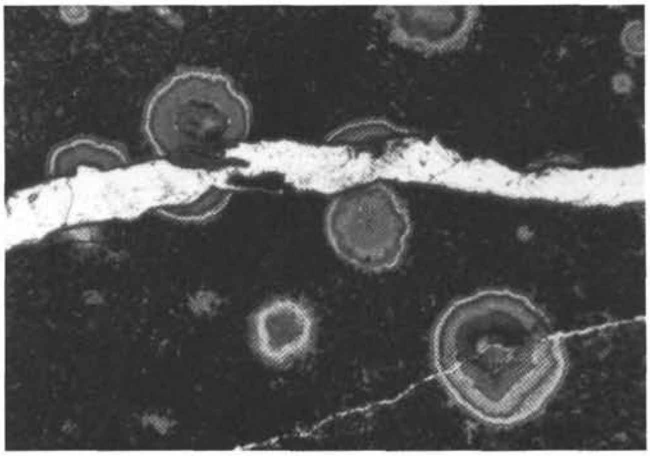

Figure 42. Photomicrograph of veinlets filled with calcite crosscutting zeolite and clay-filled amygdules. Width of field of view = 2.5 mm. Sample 120-747C-11R-1, 26–28 cm, plane polarized light.

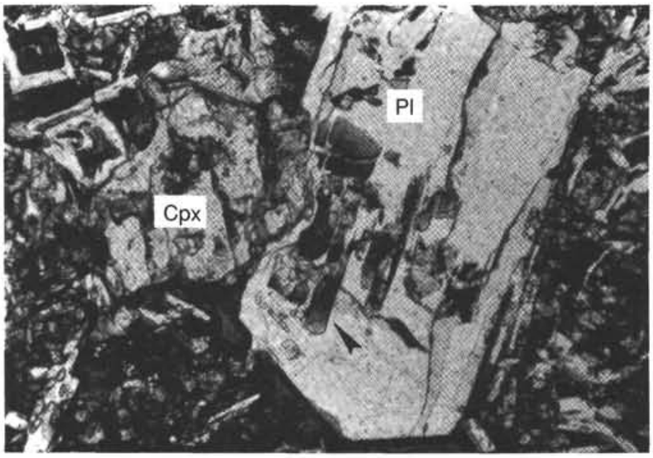

Figure 43. Photomicrograph of a zoned euhedral plagioclase lath (Pl) in contact with a subhedral clinopyroxene crystal (Cpx). Plagioclase contains brown smectite (arrow), which may represent devitrified melt inclusions. Width of field of view = 1.0 mm. Sample 120-747C-12R-4, 41–44 cm, plane polarized light.

Figure 44. Photomicrograph of zeolite-lined and clay-filled vesicles. Width of field of view = 2.5 mm. Sample 120-747C-11R-1, 26–28 cm, crossed nichols.

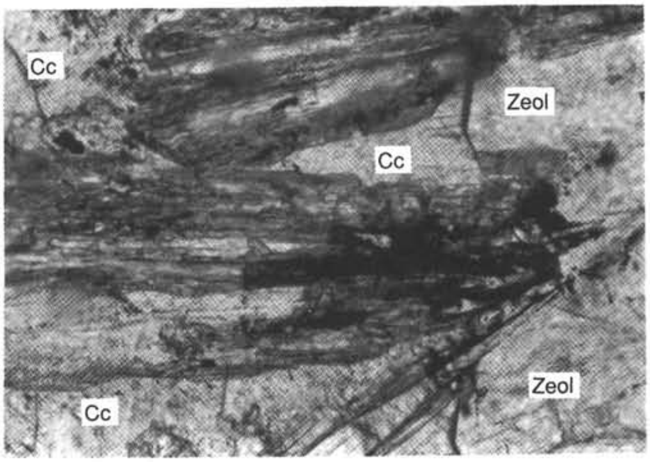

Figure 45. Photomicrograph of radiating prehnite crystals(?) in a zeolite-lined (Zeol) and calcite-filled (Cc) vein. Width of field of view = 1.0 mm. Sample 120-747C-11R-1, 18–20 cm, plane polarized light.

the Nauru Basin (Zr/Nb = 10–18) (Saunders, 1985). Basalts from Hole 747C are transitional between N-MORB and normal ocean-island basalts (OIB).

Summary

The cored basement at Hole 747C consists of up to 12 lava flows separated by brecciated basalt. The volcanics were probably erupted under subaerial conditions and were emplaced on a near-horizontal surface. They range from aphyric to sparsely olivine, plagioclase, and minor clinopyroxene phyric basalts. They are mainly hypersthene normative and, relative to N-MORB, are enriched in incompatible trace elements. In terms of the Zr/Nb ratios and other incompatible trace elements, they are transitional between N-MORB and most ocean-island basalts. They exhibit different degrees of evolution by low-pressure fractional crystallization of mainly olivine and plagioclase. Extensive hydrothermal alteration(s) produced a secondary mineral assemblage consisting of zeolites, smectites, goethite, prehnite(?), and calcite. This assemblage suggests an oxidizing environment and indicates alteration temperatures between 50°C and 100°C.

LOGGING

The initial logging program called for the three standard Schlumberger logging tool strings plus a VSP to be run at Site 747. Only one logging run, the DITE/SDT/NGT/CAL was successfully completed. Further logging runs were cancelled because of deteriorating weather conditions. Prior to logging, the hole was conditioned and displaced to 8.7 lb/gal gelled seawater mud. The bit was mechanically released and the pipe pulled to leave 100 m of BHA/drill pipe below the seafloor.

Schlumberger commenced rigging up at 1100 hr (L), 11 March 1988. The first tool string to be run contained the following tools: AMS (auxiliary measurement sonde), TCCB (telemetry cartridge), GPIT (directional/magnetic sonde), NGT (natural gamma ray tool), MCD (caliper), SDT (multichannel sonic), DITE (phaser induction/resistivity), and VSTP (Lamont-Doherty temperature tool). A more detailed explanation of these and other logging tools used on Leg 120 can be found in the "Explanatory Notes" chapter (this volume).

All tools worked successfully while running in hole. On attempting to log up, it was found that the Schlumberger software was unable to handle the large data output from this particular tool string. No log was recorded. The tool string was pulled to the surface and the GPIT and AMS tools removed. Schlumberger ran in the hole with the revised tool string at 1540 hr (L).

Table 16. Major element analyses and normative mineral proportions of basalts from Hole 747C.

Core, section, interval (cm)	11R-3 32–33	12R-1 56–57	12R-3 75–77	12R-4 45–46	13R-1 45–47	13R-2 15–16	13R-3 104–106	14R-1 20–22	14R-1 113–115	14R-2 28–31	15R-1 35–37	15R-2 91–93	15R-3 110–113	16R-2 85–87	16R-4 26–29
SiO_2	43.15	51.59	48.59	49.46	48.51	47.37	48.41	48.70	48.43	49.86	47.93	48.84	48.53	49.83	48.11
TiO_2	1.49	2.20	1.70	1.62	1.60	2.33	2.47	1.63	1.93	1.96	1.30	1.36	1.55	1.28	1.26
Al_2O_3	13.51	19.85	15.27	14.70	14.62	15.95	17.11	15.88	15.98	16.76	16.22	17.55	18.81	16.19	16.42
Fe_2O_3	14.54	11.20	11.95	12.15	11.40	14.29	13.70	11.76	11.42	11.54	10.84	10.67	9.53	10.93	9.83
MnO	0.25	0.13	0.14	0.19	0.19	0.12	0.14	0.14	0.18	0.11	0.15	0.14	0.13	0.21	0.19
MgO	3.66	4.25	7.67	7.30	7.62	6.44	5.91	8.00	8.22	7.14	8.68	10.74	9.57	8.51	9.75
CaO	18.98	5.47	10.65	11.47	11.67	8.13	7.55	10.45	9.35	8.10	9.50	7.78	9.00	9.64	10.10
Na_2O	1.79	3.26	2.98	2.58	2.61	3.10	3.14	3.67	3.65	3.27	2.55	2.40	2.52	2.31	2.55
K_2O	1.73	1.77	0.40	0.30	0.24	0.74	1.17	0.49	0.62	1.02	1.13	0.94	0.59	1.90	0.90
P_2O_5	0.15	0.24	0.19	0.18	0.18	0.29	0.29	0.20	0.21	0.21	0.18	0.17	0.17	0.16	0.17
Total	99.24	99.95	99.55	99.94	98.65	98.75	99.79	100.93	99.98	99.96	100.59	98.49	100.40	100.95	99.28
LOI	16.65	4.04	1.80	0.61	1.32	3.15	4.12	1.11	4.82	10.20	5.15	6.40	6.25	2.23	6.87
Mg#	NC	NC	53.04	51.27	53.90	44.34	43.20	54.48	55.76	52.20	58.43	63.88	63.81	57.58	63.36
Qz	0	3.31	0	0	0	0	0	0	0	0	0	0	0	0	0
Ne	8.21	0	0	0	0	0	0	3.07	1.70	0	0	0	0	0	0
Lc	8.02	0	0	0	0	0	0	0	0	0	0	0	0	0	0
Or	0	10.46	2.40	1.79	1.45	4.49	7.01	2.90	3.70	6.10	6.85	5.58	3.50	2.40	5.41
Ab	0	27.59	25.56	22.05	22.59	26.86	26.88	25.38	28.02	27.92	22.09	20.35	21.39	25.56	22.89
An	23.72	25.57	27.48	27.91	28.09	28.07	29.47	25.40	25.61	28.29	30.17	34.40	38.38	27.48	31.14
Di	42.63	20.45	23.40	24.58	9.53	5.59	0	20.66	16.27	9.05	13.87	2.70	4.41	20.45	15.15
Hy	0	21.91	5.04	13.87	9.33	10.84	12.74	0	0	12.02	5.16	16.77	14.00	5.04	2.89
Ol	0	0	12.95	5.02	8.12	12.10	10.15	16.72	18.24	10.08	16.71	15.11	13.08	12.95	18.72
Ap	0.35	0.56	0.42	0.40	0.40	0.65	0.64	0.44	0.46	0.46	0.40	0.37	0.37	0.42	0.38
Il	2.83	4.13	3.28	3.11	3.11	4.54	4.75	3.10	3.70	3.76	2.53	2.59	2.96	3.28	2.43
Mt	2.89	2.23	2.41	2.44	2.32	2.91	2.76	2.34	2.29	2.32	2.21	2.13	1.90	2.41	1.99
Cs	5.89	0	0	0	0	0	0	0	0	0	0	0	0	0	0
C	0	3.20	0	0	0	0	0	0	0	0	0	0	0	0	0

Note: LOI = loss on ignition and NC = not calculated.

Table 17. Trace element analyses of basalts from Hole 747C.

Core, section, interval (cm)	Rb	Ba	Nb	Sr	Zr	Y	Zn	Cu	Cr	Ni
120-747C-										
11R-3, 32–33	35	16	8	90	94	44	88	73	190	50
12R-1, 56–57	31	122	12	241	159	26	101	71	304	66
12R-3, 75–77	4	146	10	230	127	25	100	95	229	58
12R-4, 45–46	3	144	11	233	123	25	101	114	202	55
13R-1, 45–47	1	123	10	235	122	25	106	119	228	58
13R-2, 15–16	9	223	15	259	175	33	115	40	52	60
13R-3, 104–106	17	301	15	247	177	30	115	59	57	62
14R-1, 20–22	3	221	12	244	132	24	101	90	71	65
14R-1, 113–115	8	156	12	226	157	36	127	193	188	53
14R-2, 28–31	14	223	13	226	154	36	110	76	98	52
15R-1, 35–37	12	177	9	224	109	21	91	50	325	100
15R-2, 91–93	11	143	9	194	111	23	92	55	317	97
15R-3, 110–113	7	120	10	195	124	24	80	63	345	81
16R-2, 85–87	13	195	9	261	110	20	79	67	313	85
16R-4, 26–29	5	152	9	241	99	21	80	71	309	90

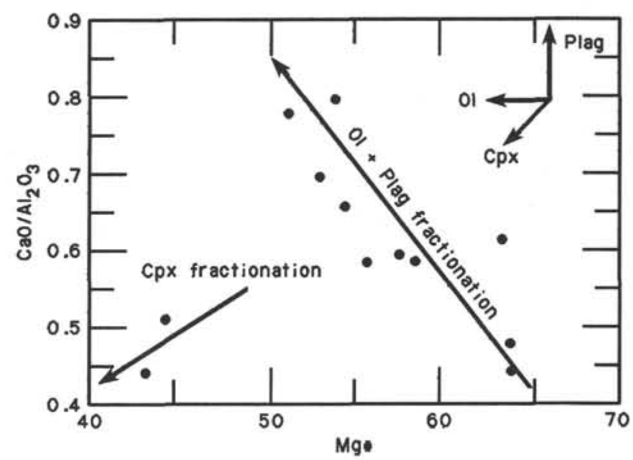

Figure 46. Plot of CaO/Al_2O_3 vs. Mg# showing the effect of olivine (Ol) plus plagioclase (Plag) and clinopyroxene (Cpx) fractionation on magma composition. Samples with no Mg# (120-747C-11R-3, 32–33 cm, and 120-747C-12R-1, 56–57 cm) and with high loss on ignition (120-747C-11R-3, 32–33 cm, and 120-747C-14R-2, 28–31 cm) have been omitted from the figure.

The logging software was successfully tested by up-logging a short section of the drill pipe before continuing downhole.

No problems were encountered while running down to TD through the open hole section; the hole appeared to be in good condition and free of bridges. A downlog was recorded while running down to TD. The TD for this hole was found at 337 mbsf (wireline depth). The hole was up-logged at 850 ft/hr in a single pass from TD back into the drill pipe. Schlumberger was out of the hole at 2000 hr (L).

Log Quality and Interpretation

The raw logs for Hole 747C are presented in Figures 48 and 49. Log quality was markedly affected by the bad weather and ship movement (4-m heave). Several unsuccessful attempts were made to use the wireline heave compensator; however, each time the compensator was activated, it immediately tripped out.

With no heave compensation, the tool string was not being pulled up the hole at a constant rate (see tension curve on Fig. 48). These erratic tool movements affected depth control and general log quality. The sonic log (SDT) was badly affected over the intervals from 193 to 232 mbsf and from 298 to 337 mbsf. Traveltime measurements throughout these intervals are corrupted by cycle skipping.

Preliminary reprocessing of the SDT has improved data quality from the sonic; this is more fully explained in the synthetic seismogram section. Further post-cruise analysis of the sonic waveform logs may result in more useful sonic data being extracted over these intervals. The quality of the resistivity (DITE) and the gamma ray (NGT) measurements suffered to a lesser degree; good quality data was collected from these tools over the entire hole section.

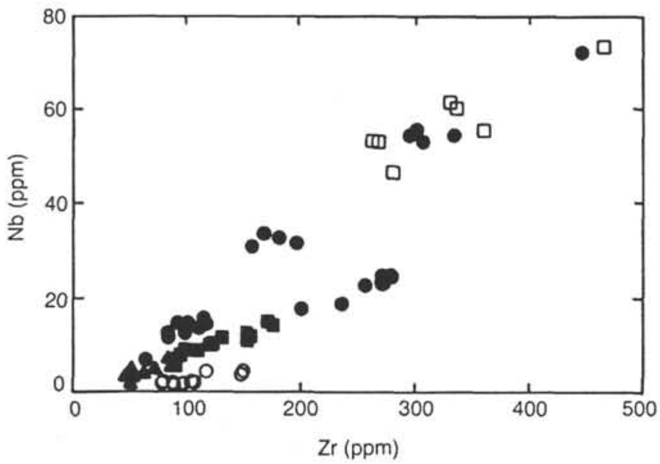

Figure 47. Zr vs Nb plot showing data from basalts from Hole 747C compared with selected basaltic suites from the Indian Ocean. Symbols: Hole 747C = solid squares; open circles = Indian MORB (Price et al., 1986); triangles = Nauru Basin (Saunders, 1985); open squares = Heard Island (Storey et al., 1988); and filled circles = Kerguelen Island (Storey et al., 1988).

Sonic and resistivity porosities have been calculated throughout the hole section. Sonic porosity was calculated from the reprocessed sonic data using a Raymer-Hunt transform, applicable to "soft" formations. Resistivity porosities were calculated assuming a basic Archie relationship. The results show good agreement with porosities derived from physical properties measurements (see "Physical Properties" section, this chapter).

Log-Derived Lithology Horizons

Changes in the character of the log responses have been used to divide the logged interval into four discrete units (log Units 1, 2, 3, and 4). Log Unit 4, the basement unit, has been further subdivided into log Subunits 4A, 4B, 4C, and 4D. These subdivisions are based on the marked resistivity changes seen within log Unit 4.

As changes in log character are generally indicative of changes in lithology, it is to be expected that the log-derived horizons agree with boundaries picked from paleontologic and lithologic analyses of core. The identification of lithology changes from the logs proved particularly useful over the lowermost section of the hole where recovery was poor.

Log Unit 1

Log Unit 1 (115–188 mbsf) is characterized by uniformly low resistivity and low gamma ray readings. Core recovery was still good over this section of the hole, and the log responses are consistent with the core description of a homogeneous deposition of calcareous ooze/chalk. The sonic log is considered valid below 172 mbsf to the base of the unit and indicates a decrease in transit time (and, therefore, porosity) with depth. A sharp decrease in the sonic transit time at 172 mbsf may indicate increased lithification of the calcareous ooze or, alternately, may be due to poor hole conditions.

Log Unit 2

Gamma ray and resistivity curves increase in value over this interval (188–228 mbsf). The log responses are consistent with the presence of volcaniclastic sediments found in cores recovered over this depth interval. At lease three discrete high resistivity peaks can be identified within this unit. These may define distinct horizons within this interval, including the presence of the Cretaceous/Tertiary contact.

A possible discrepancy in sediment thickness is seen between log Unit 2 of Hole 747C and the equivalent lithologic Unit III of Hole 747A (about 20 m to the east). The logs appear to indicate a thicker sediment unit in Hole 747C than was identified in Hole 747A. Throughout this section, the sonic log was badly affected by cycle skipping. The cycle skipping was particularly bad over this section since the tool was attempting to react to subtle changes in lithology while being affected by the heave of the ship.

Log Unit 3

As in log Unit 1, the gamma ray and resistivity tool responses are low in log Unit 3 (228–297 mbsf) and again indicate a massive, fairly homogeneous section of chalk. Lithologic data suggests this particular interval contained chert stringers. These stringers are expected to be on the order of a few centimeters in thickness. The resolution of the tools within this particular logging string was insufficient to detect the presence of any chert stringers. A break in the resistivity and sonic curves is identified at a depth of 244 mbsf; this may indicate a change in mineralogy or lithification within the massive chalk section. Log-derived porosities indicate that this unit exhibits porosities of around 40%, with the porosity slowly decreasing with depth (Fig. 50).

Log Unit 4

Log Unit 4 (297–337 mbsf) is the most complex section of the log. The whole of log Unit 4 shows an increase in gamma ray reading with respect to the overlying chalk section. This can be associated with an increase in the presence of clay and/or volcanic material. The NGT ratio curves presented in Figure 49 indicate the increase in gamma ray can be primarily attributed to an increase in potassium content. A decrease in the measured hole size as we enter log Unit 4 indicates that the hole is not badly washed out and would suggest that the formation is more competent. The sonic log exhibits severe cycle skipping throughout the whole of log Unit 4 and was therefore of little use.

The subdivision of log Unit 4 is prompted by the marked changes in resistivity throughout this unit. Core recovery over this unit was very poor (15%–50%), making core/log correlation difficult. Log data proved very useful in refining the stratigraphy in the basement section of this hole.

Log Subunit 4A

Log Subunit 4A (297–306 mbsf) is characterized by a large, but gradual increase in the deep and medium induction resistivities. The gamma ray and particularly the spherically focused resistivity logging (SFL) curves show marked fluctuations, which suggest internal layering within this subunit. These log responses are thought to correspond with alternating layers of basalt flows and brecciated, highly altered basalt. It has been assumed that the brecciated basalts give rise to the relatively low resistivity readings by virtue of their water-filled fractures and vugs. The SFL suggests that this unit may contain up to seven distinct lava flows, each flow corresponding to a peak in the resistivity.

Log Subunit 4B

Log Subunit 4B (306–313 mbsf) exhibits a relatively low resistivity (3 ohmm). The resistivity is not, however, as low as in the chalk section (log Unit 3). The low resistivity may be due to a massive section of brecciated, clay-altered basalt.

Log Subunit 4C

A sharp increase in the resistivity would suggest that log Subunit 4C (313–320 mbsf) is another basaltic unit. The logs suggest this subunit is not as distinctly layered as log Subunit 4A, although thin stringers of highly altered-lower resistivity basalt

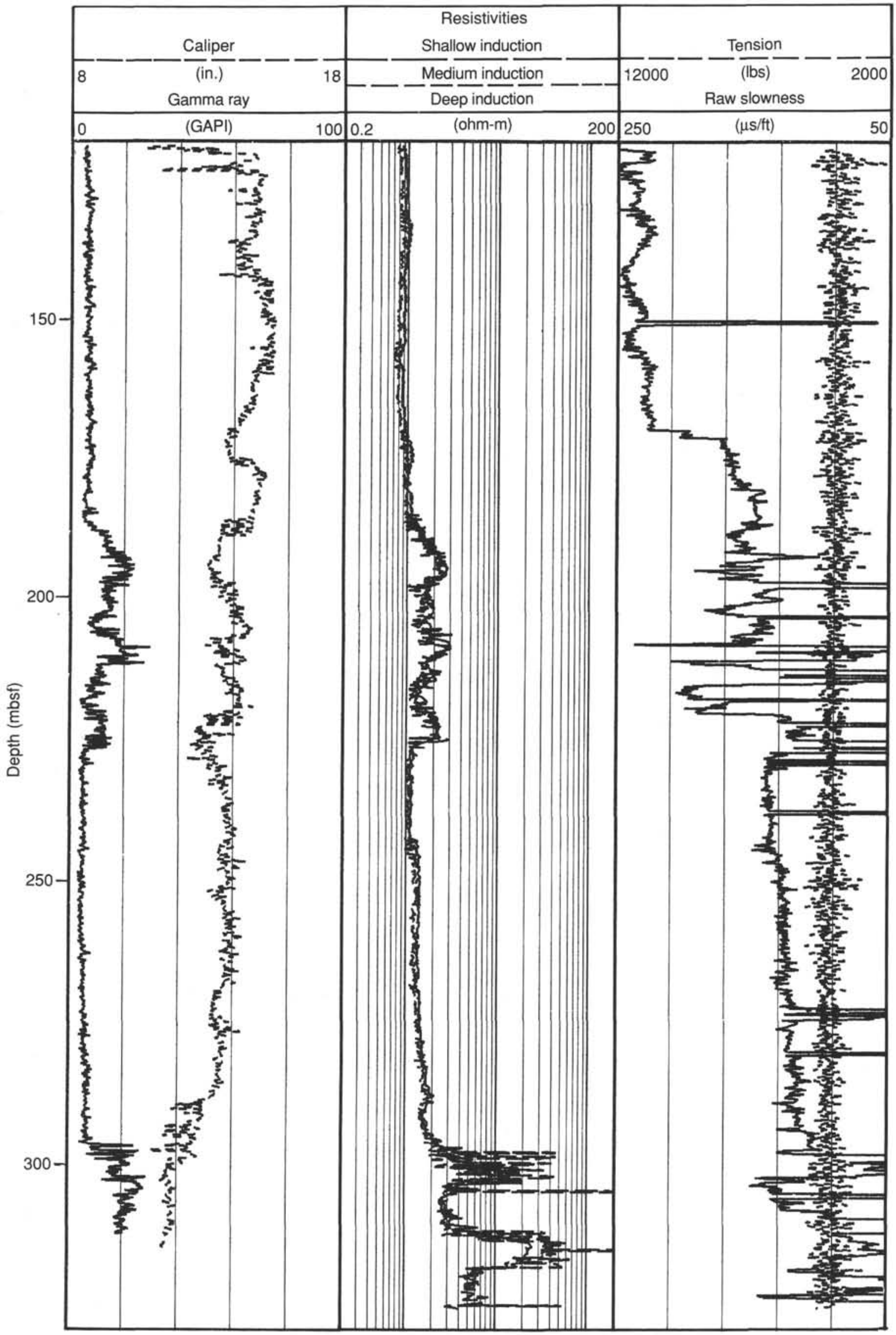

Figure 48. Raw DITE/SDT/NGT/MCD log data for Hole 747C.

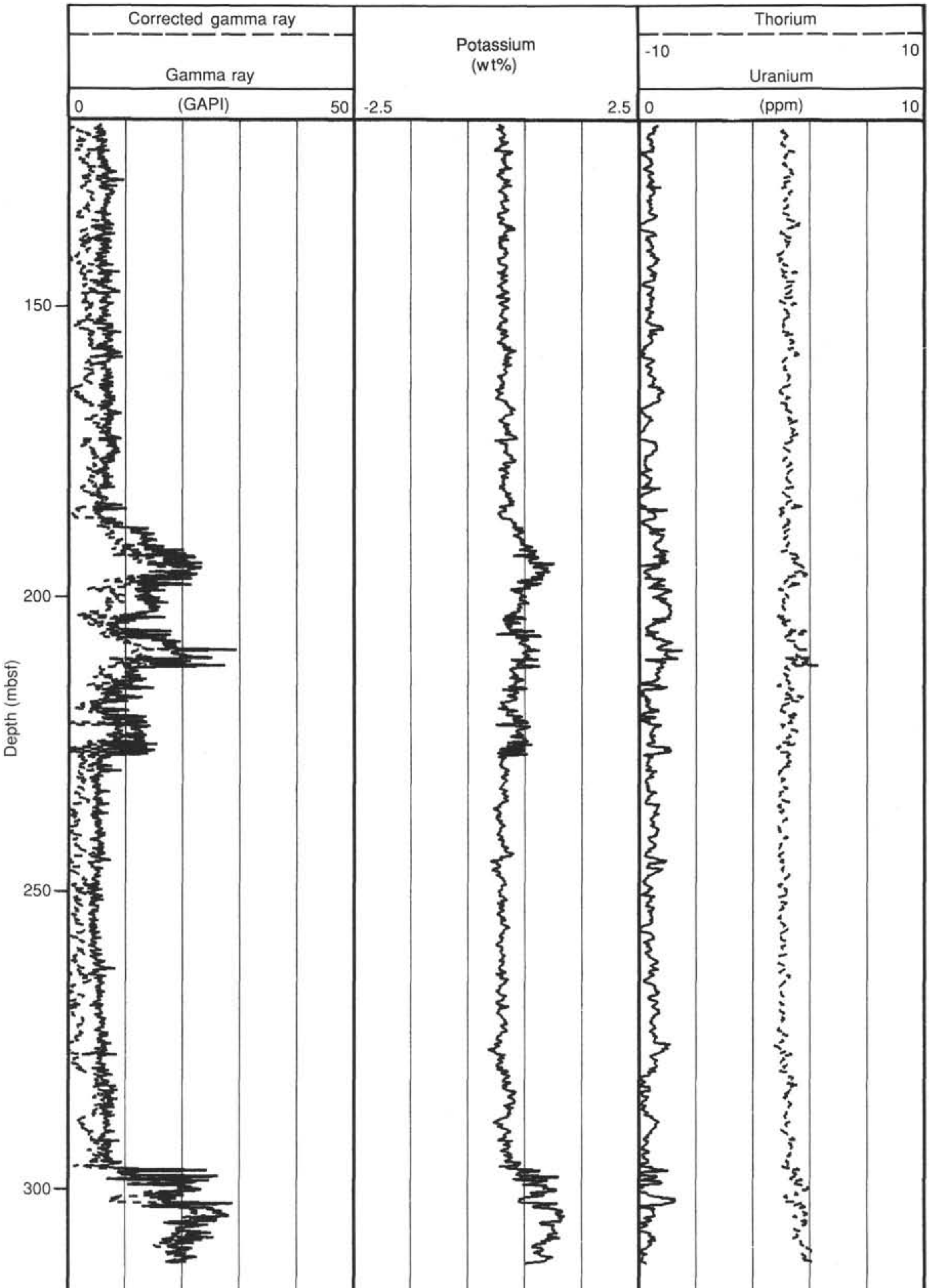

Figure 49. Natural gamma ray curves showing the relative abundance of potassium, thorium, and uranium in Hole 747C.

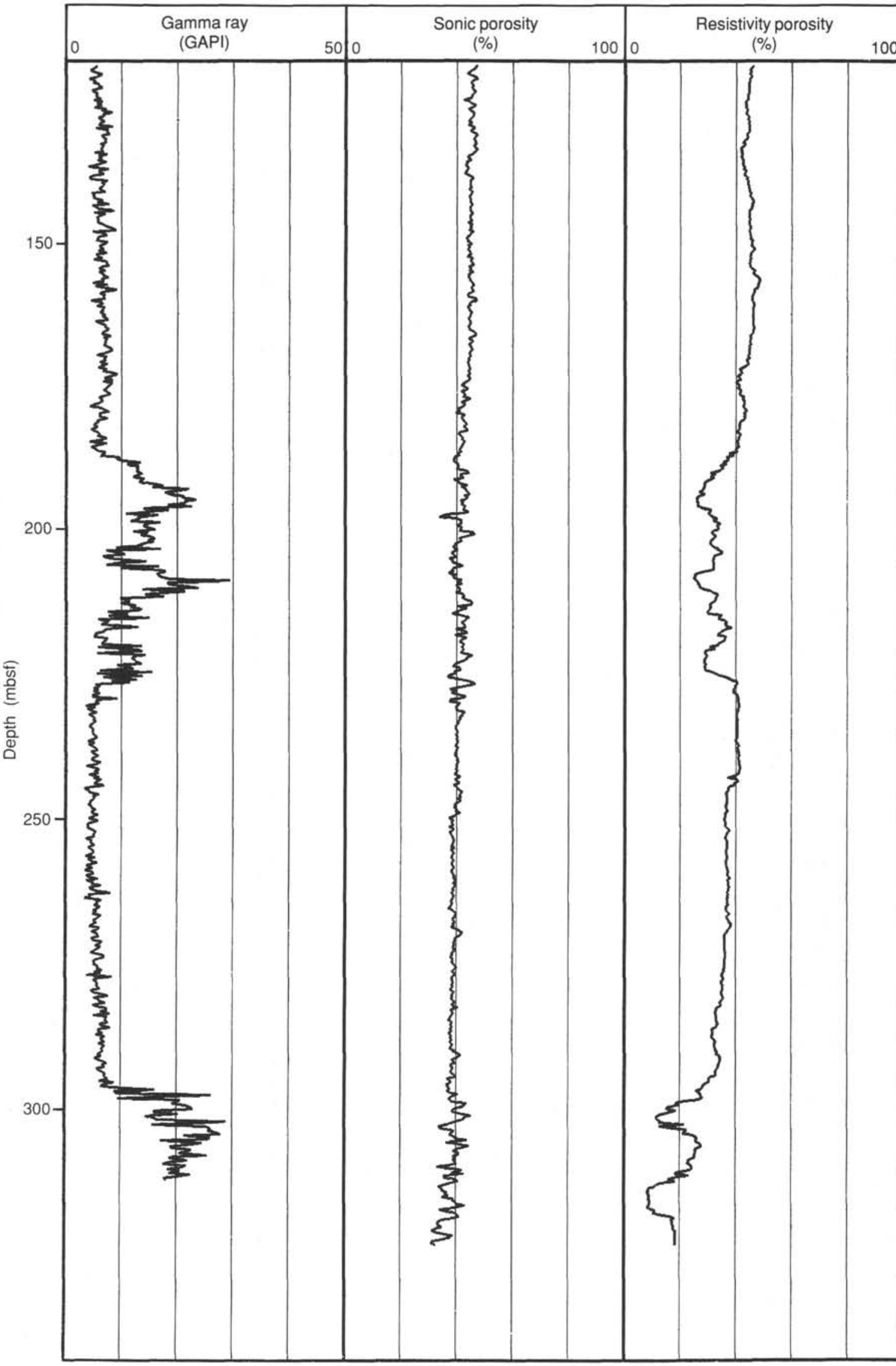

Figure 50. Comparison plot of gamma-ray curves and sonic (Raymer-Hunt) and resistivity (Archie-derived) porosities in Hole 747C.

can again be identified. The SFL resistivity curve suggests that this unit may contain up to five individual lava flows.

Log Subunit 4D

Again, resistivity drops to a moderately low value (5–6 ohmm) in log Subunit 4D (320–337 mbsf), which may indicate the presence of a second brecciated and highly altered basalt unit.

Synthetic Seismogram

A synthetic seismogram, computed for Hole 747C, allowed a more accurate correlation of the lithologies, determined from core and log data, with reflectors on the multichannel seismic section (MD47-03). The synthetic seismogram also proved useful in defining the vertical resolution of the seismic reflectors in terms of measurable bed thickness.

As the original sonic log for this hole was badly affected by cycle skipping, it was necessary to reprocess the raw sonic data before attempting any seismic processing. Initial reprocessing of the sonic data was performed by Schlumberger Well Services. A comparison of the raw and reprocessed log is shown in Figure 51. Although certain sections of the log are still quite noisy (e.g., 193–232 mbsf and 298–337 mbsf), data quality is sufficiently improved for the sonic to be used in creating a synthetic seismogram.

A density log was not recorded at this site; however, bulk density data is available from core measurements (see "Physical Properties" section, this chapter). A stair-step pseudodensity log was constructed using average values over intervals of similar densities. The densities used range from 1.75 to 2.75 g/cm^3 (Fig. 51). The pseudodensity log is a simplified estimate of actual rock properties. Its use does not seriously affect the accuracy of the interpretation; density variations are small compared to the much larger changes in formation sonic velocities.

Sonic velocities were multiplied with density values to obtain an impedance log. The impedance log was then convolved with a 30-Hz, zero-phase Ricker wavelet to obtain a seismic trace. To avoid an erroneous reflector at the top of the logged interval, a constant velocity, chosen to be consistent with the first data point, has been assumed in the overlying sediments.

Comparison of the synthetic seismic trace with the seismic section yields a relatively good character match. A trace reduced to the same scale as the seismic section is presented in Figure 52. Although the exact location of the hole has been approximated on the diagram, the three dominant peaks correlate in amplitude and frequency with the reflectors observed on the seismic section.

Unit boundaries, as interpreted on the logs, can be correlated with the synthetic trace from the depth track. The boundary between log Units 1 and 2 is characterized by a relatively high-amplitude positive reflector. This positive reflector is caused by an increase in velocity and density of the underlying volcaniclastic sediments in relation to the overlying calcareous oozes and chalks. The high amplitude of this reflector may be somewhat exaggerated by the increased noise in the sonic log recorded in the underlying unit.

The boundary between log Units 2 and 3 is less clear; however, it is picked at the inflection point of the next major wavelet. The lower amplitude of this wavelet indicates a smaller change of acoustic impedance. The top of log Unit 4, the basement unit, appears on the synthetic seismic section as a strong, high-amplitude wavelet. A high-amplitude reflector is to be expected at this point, as there is a marked impedance contrast between the basalt and the overlying chalk section. A secondary doublet can be identified in this reflector; this is probably due to underlying layers of altered and unaltered basalt.

Summary

The seismic/stratigraphic tool string run in Hole 747C was successful in identifying the major lithologic changes present in this hole section. Despite adverse weather conditions that impaired tool performance, four major lithologic units were identified. Log responses in log Unit 2 were used to characterize more fully the nature of the sediment boundaries and identify additional lithologic horizons within the unit.

The logging data was most useful, however, in the basement section of the hole, where core recovery was very poor. The logs allowed us to construct a more complete stratigraphic picture of the interbedded basalt lava flows. A preliminary synthetic seismogram generated at the site allowed depth and log unit boundaries to be correlated with the seismic section. The synthetic also provided a valuable check on existing seismic data.

SEISMIC STRATIGRAPHY

The seismic sections at Site 747 (Figs. 2, 3, 7, and 8) show two distinct sedimentary sequences, resting upon a well-defined basement reflector (see "Site Geophysics" section, this chapter). This basic subdivision is obvious from most of the geological and physical observations made at this site. Core description revealed two striking lithologic changes: the first corresponds to the entire Unit III of the sedimentary column, between 181.95 and 189.50 mbsf (Hole 747A) or 180.96 and 206.50 mbsf (Hole 747C), and the second corresponds to the top of Unit V at 296.6 mbsf.

Unit III contains the first occurrence of volcaniclastics, breccia, and cobbles; and the top of Unit V corresponds to the first observed basalt flow (see "Lithostratigraphy and Sedimentology" section, this chapter). The physical properties (mainly index properties, compressional wave velocities, and thermal conductivity) measured on board at Site 747 also indicate clear changes in the lithologic column.

Two major events are observed at 175–190 and 291.5 mbsf, respectively. The first event corresponds to an important decrease of water content and porosity, correlative to an increase of the bulk density, and the second lies just above the basement contact (see "Physical Properties" section, this chapter). Finally, interpretation of the logging data (multichannel sonic log, resistivity, natural gamma ray) also identified two major lithologic events: the first at the base of Log Unit 1 at 188 mbsf, and the second at the top of Log Unit 4 at 297 mbsf. The synthetic seismogram computed for Hole 747 shows good correlation with the seismic section MD47-03, shot point 11400 (see "Logging" section, this chapter).

The upper seismic sequence above the first reflector is 0.22–0.24 s TWT thick (see "Site Geophysics" section, this chapter). From the shipboard velocity measurements (Figs. 31 and 32), we estimate a mean velocity of 1.55 km/s for the upper sedimentary sequences and calculate a thickness of 171 to 186 m for the seismic sequence. This seismic sequence is composed of high-amplitude, continuous reflectors in its upper part and low-amplitude reflectors in its lower part. The sequence thickens toward the west and northwest by toplap, and few onlaps are seen to the west on the seismic section. This upper seismic sequence corresponds to lithologic Units I and II (Fig. 9).

The lower seismic sequence resting upon the acoustic basement is 0.11–0.13 s TWT thick. Assuming for this sequence a mean velocity of 1.80 km/s, derived as before from the shipboard velocity measurements (Fig. 31), the sequence is 99–117 m (0.13–0.11 s TWT) thick. This lower seismic sequence is characterized by low-amplitude, continuous reflectors; its thickness increases toward the west and northwest by onlap. This lower seismic sequence corresponds to lithologic Unit IV.

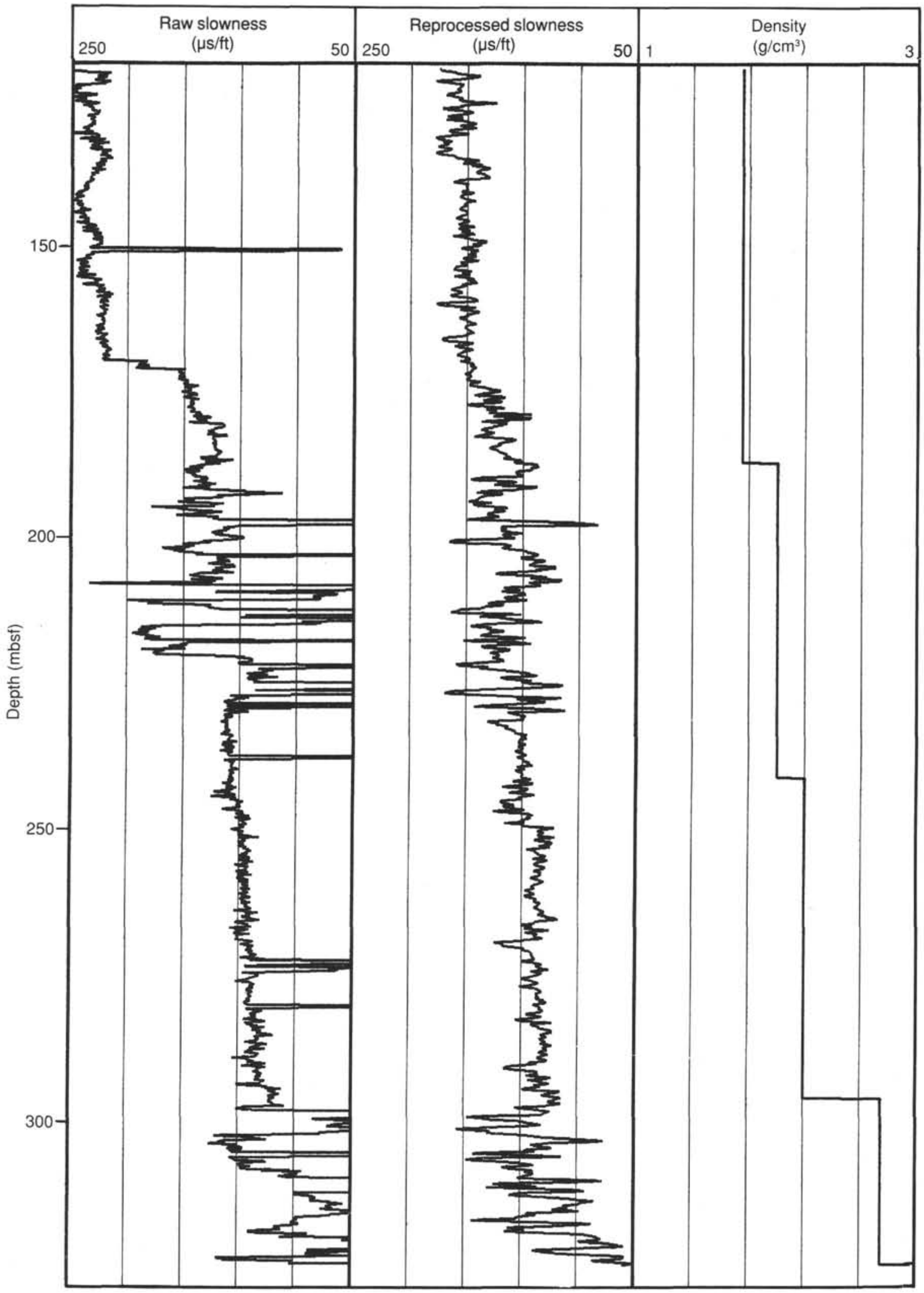

Figure 51. Plot of input logs for synthetic seismic calculations. Raw Schlumberger slowness is compared with the reprocessed log. The density log shows intervals of averaged densities based on physical core measurements.

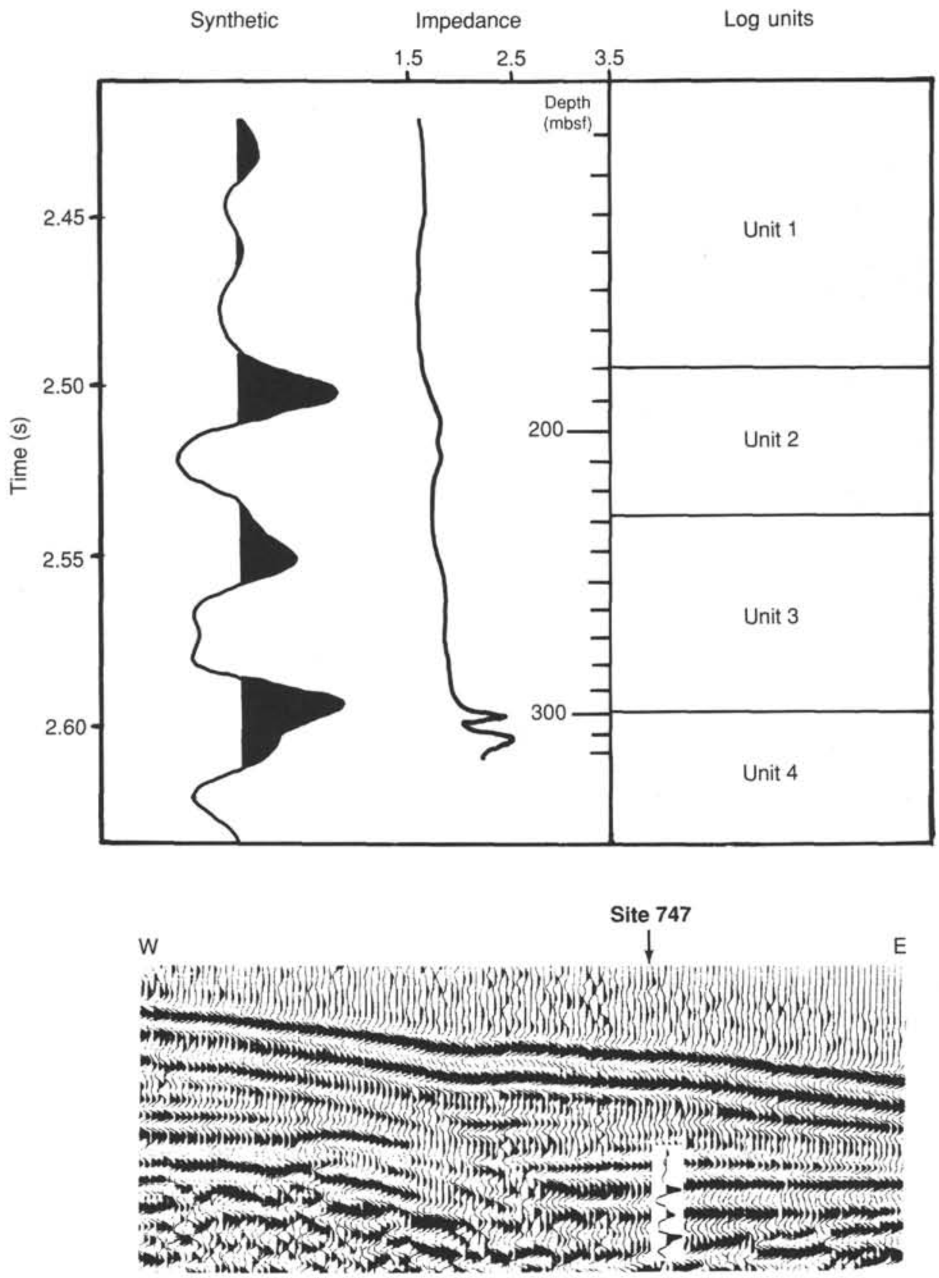

Figure 52. Synthetic seismogram and impedance curve plotted vs. time and depth for Hole 747C. Lower figure is a portion of the seismic section MD47-03 crossing Site 747 with an overlay of the synthetic.

The two sedimentary sequences are separated by a high-amplitude horizon that corresponds to lithologic Unit III. The two sequences represent a sedimentary cover of 288–285 m (first reflector at 0.22 s or 0.24 s TWT). The top of the basement is clearly defined at Site 747 (Fig. 53). Close to the site, to the west and northwest, it is possible to identify dipping reflectors, which could indicate a layered basement structure (Figs. 2 and 3).

Site 747 is located 10 nmi to the west of the northern end of the north-trending 77°E Graben (Fig. 5). At this latitude, the structure corresponds to a clear 500-m deep graben and is about 18 km across. Farther to the south, the graben is offset to the east by about 36 km and is almost trending in the same direction. The graben structure is even more highly accentuated (see "Background and Objectives" and "Site Geophysics" sections, this chapter).

The acoustic basement at Site 747 corresponds to basalt. Twelve lava flows separated by brecciated, veined, and altered basalt were identified. The volcanics were probably erupted under subaerial conditions and were emplaced on near-horizontal surface (see "Igneous Petrology" section, this chapter). These basalt flows extend and thicken considerably northwestward, as can be observed on the Australian seismic section RS02-13 (Fig. 3). The origin of these flows is not known, although the basalts show geochemical similarities with the Kerguelen Island plateau basalt. However, they are clearly different from the recent OIB-type volcanic rocks of the Kerguelen and Heard islands.

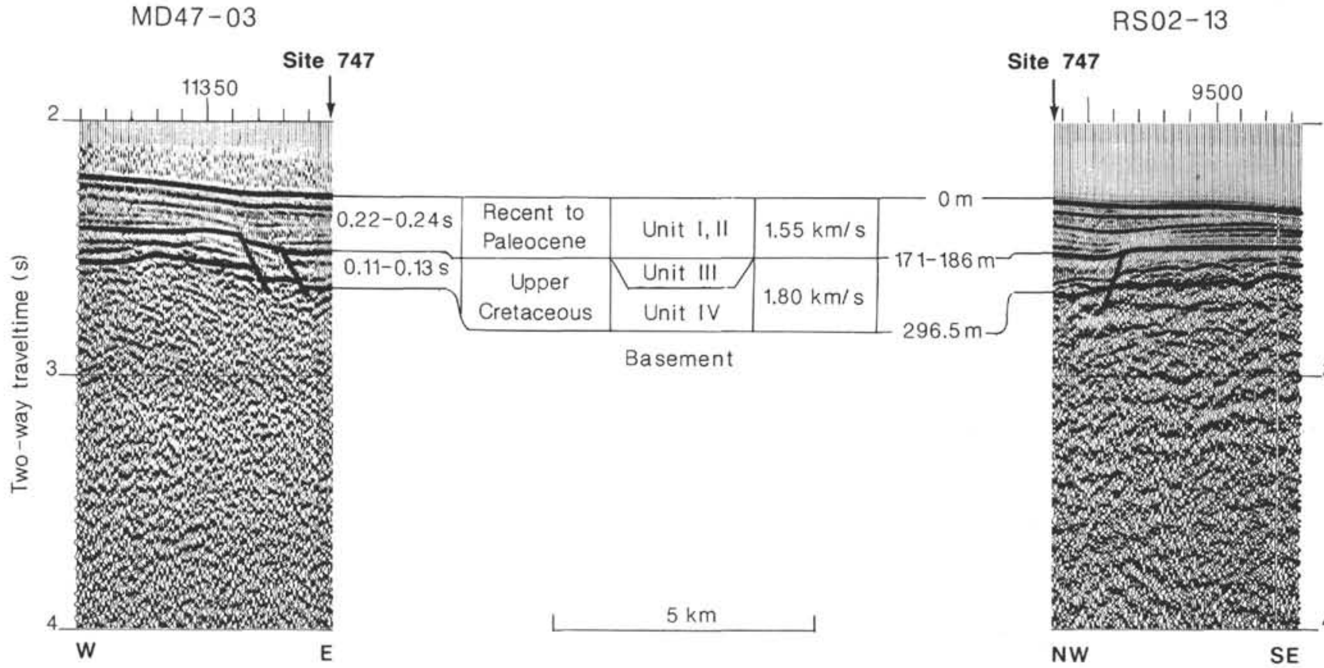

Figure 53. Interpreted seismic sections (MD47-03 and RS02-13) at Site 747. Correlation with lithologic units.

The evolution of the Southern Kerguelen Plateau derived from all these observations (see "Lithostratigraphy and Sedimentology" and "Biostratigraphy" sections, this chapter) and from the seismic stratigraphy can be summarized as follows:

1. The basement slowly subsided and sedimentation began in the early Santonian. The slow subsidence episode extends until the late Maestrichtian (68-69 Ma) at a rate of 15-25 m/m.y. The sedimentation rate for the same period of time is almost constant and equal to 20 m/m.y. (see "Sedimentation Rates" section, this chapter).

2. Three important hiatuses occurred between the late Maestrichtian (about 68.5 Ma) and the late Eocene (37.8 Ma). The first, between 68.5 and 66.2 Ma, corresponds to a major tectonic episode affecting the plateau, whereas Site 747 was subsiding from about 200-500 m to 2000 m at a rate of about 600-800 m/m.y. This extremely high subsidence rate is related to the formation of the 77°E Graben, characterized near Site 747 by listric faults separating tilted blocks, and possibly to the breakup between the Southern Kerguelen Plateau and Broken Ridge-Diamantina Zone. During the Paleocene, between 66.2 and 63.8 Ma, sedimentation occurred at a very low rate (2-5 m/m.y.) and is composed of nannofossil chalks with basaltic cobbles, volcanogenic sand, and pebbles indicating the proximity of an emerged feature. The second hiatus, between 63.8 and 58 Ma, could be related to a slight uplift of the plateau (500 m). In the early Eocene, between 58 and 52.9 Ma, sedimentation is characterized by pelagic nannofossil chalk with a very low sedimentation rate (0.4 m/m.y.). The third and major hiatus, between the early Eocene (52.9 Ma) and late Eocene (37.8 Ma), is accompanied by a subsidence of the Kerguelen Plateau near Site 747 of about 500 m (30 m/m.y.). This event is related to the breakup between the Northern Kerguelen Plateau and Broken Ridge, dated at 43-42 Ma (Munschy and Schlich, 1987).

3. Since the late Eocene (37.8 Ma), the sedimentation—mainly nannofossil chalks and oozes—has been essentially continuous with a sedimentation rate of about 5 m/m.y., and the plateau has remained at the same depth.

SUMMARY AND CONCLUSIONS

Site 747 (proposed Site SKP-1; 54°48.68′S, 76°47.64′E; water depth = 1697.2 m) lies in the transition zone between the northern and southern parts of the Kerguelen Plateau approximately 500 km south of the Polar Front (Antarctic Convergence). As this is the most northern site where basement can easily be reached by drilling on the Kerguelen Plateau, the prime objective was to determine the nature and age of the basement and to compare the results with data from Leg 119 and 120 basement sites on the Southern Kerguelen Plateau. As summarized previously (see "Introduction," this volume), the origin and crustal structure of the Kerguelen Plateau is still a matter of controversy.

A 295.1-m-thick lower Santonian through upper Pleistocene pelagic sedimentary section and 53.9 m of underlying basalt were cored in three holes using various combinations of APC, XCB, and RCB core barrels. Although located beneath the present-day Antarctic water mass, the sediments contain carbonate throughout except for predominantly Maestrichtian volcaniclastic sands, breccias, and cobbles, which denote a major episode of uplift and erosion of the plateau. The primary objective was achieved with the coring through nearly 54 m of basement basalts.

Operations

Hole 747A was cored via the APC and XCB to 256.0 mbsf with 88.7% recovery, whereupon the upper 48.91 m was double APC cored in Hole 747B with 97.2% recovery in order to obtain a more complete upper Miocene to Pleistocene section for detailed paleoclimatic studies. The mud line established at Hole 747B is 2.7 m shallower than at Hole 747A, where the first APC apparently overshot the mud line due to excessive heave of the ship; this factor should be taken into consideration when correlating among the three holes at this site. Hole 747C was rotary cored, beginning with an interval of special interest through the lower Oligocene to Maestrichtian between 159.0 and 206.5 mbsf (Cores 120-747C-1R to -5R). The hole was then washed to 252.0

mbsf and cored continuously through Cretaceous chalks and cherts to 295.1 mbsf with 13.1% recovery. Next the center bit was put into place, and the hole was drilled ahead to clean chert fragments from the hole. Basaltic basement was encountered after only 1.5 m of penetration, however; therefore, the sediment/basement contact was not captured in a core. Basalts were cored to a TD of 350.5 mbsf with 37.8% recovery.

Geophysics

Site 747 is located at the intersection of French MCS line MD47-03 (shot point 11400) and Australian MCS line RS02-13 (shot point 9000). Both multichannel seismic reflection profiles show a clear basement reflector overlain by two distinct sedimentary sequences. To the west and to the northwest the sediment coverage progressively increases, whereas toward the east and northeast it rapidly diminishes to less than 200 m. Site 747 is located on a basement high in a northwest-trending direction and abutting almost at a right angle the northern end of the north-trending 77°E Graben.

At Site 747 the basement reflector lies at about 0.35 s TWT below the seafloor, whereas the reflector separating the two sedimentary sequences can be traced between 0.22 and 0.24 s TWT. The correlation of the two MCS lines with the *JOIDES Resolution* approach site survey line is unambiguous, but the high noise level prevents one from scaling these reflectors precisely on the single channel seismic record.

Lithobiostratigraphy and Igneous Petrology

Lithologic units (Fig. 54; Table 2) recognized at Site 747 are presented as a composite section from the seafloor down as follows:

Unit I: depth, 0–32.7 mbsf; age, Pleistocene to early Pliocene; foraminifer diatom ooze. Minor ice-rafted debris and dropstones are prevalent only in the upper 20 m, whereas occasional vitric ash layers occur throughout. The carbonate content (Fig. 54) increases downward from 20% at the top to 90% toward the base. A hiatus of about 2.5 m.y. duration is inferred between the lower Pliocene and upper Miocene (see "Sedimentation Rates," this chapter).

Unit II: depth, 32.7–181.9 mbsf; age, late Miocene to Paleocene; white nannofossil ooze and chalk divisible into three subunits.

Subunit IIA: depth, 32.7–151.5 mbsf; age, late Miocene to late Oligocene; white to light gray nannofossil ooze with occasional vitric ash layers and possible ice-rafted quartz.

Subunit IIB: depth, 151.5–170.5 mbsf; age, late Oligocene to early Eocene; pale brown nannofossil chalk. A prominent hardground at 169.37 mbsf (Core 120-747C-2R-1, 87 cm; Fig. 14) is marked by manganese crust and represents a disconformity. A lower Oligocene interval is missing that spans at least the last appearance datums of the nannofossils *Isthmolithus recurvus* and *Reticulofenestra umbilica*.

Subunit IIC: depth, 170.5–181.9 mbsf; age, early Eocene to Paleocene; large burrow, white nannofossil chalk (Fig. 15). The burrows are centimeter scale, and there are occasional shallow-water fossils (bivalve fragments, larger benthic foraminifers). The base is gradational into Unit III with an increasing abundance of sand to pebble size, angular to rounded volcanogenic debris sprinkled randomly and unsorted into the chalk.

Two hiatuses, one at the top of Subunit IIC and one within are noted as follows: (1) in Core 120-747C-2R-3, 142 cm (172.92 mbsf), a disconformity at the top of Subunit IIC represents a 15-m.y. hiatus corresponding to the late Eocene–early Eocene nannofossil Zones NP18–NP14; and (2) in Cores 120-747C-2R-4, 133 cm, or 120-747C-2R-5, 10 cm (174.33 or 174.60 mbsf, respectively, the hiatus may span as much as 4–7 m.y. (early Eocene to upper Paleocene, or some portion thereof). Heavy bioturbation through this unit and/or reworking, however, makes this determination difficult.

Unit III: depth, 181.9–189.5 mbsf; age, early Paleocene to late Maestrichtian; multicolored volcaniclastics, polygenetic sands, breccia, and cobbles, probably deposited as debris flows (Fig. 55; see also Figs. 16 and 17).

Angular to rounded clasts are composed of chalks (Campanian to Maestrichtian), cherts, clays, or relatively fresh to devitrified volcanics. Igneous components include hard black, aphyric and aphanitic basalt, ferruginous vesicular basalt, and waxy clay clasts. The latter show original hyaloclastic or variolitic basalt structures, including vesicles and fracture fillings, that indicate a history of devitrification before transport; some clasts may have experienced two cycles of erosion and transport. Electric logs (Fig. 54; see below) indicate the presence of perhaps three thick, separate beds of volcaniclastics down to 205 mbsf in Hole 747C intercalated among chalk layers.

Unit III is thicker in Hole 747C than in 747A where some of the volcaniclastics appear to be represented by thin, one-grain-thick layers (e.g., Core 120-747A-21R-3, 86–93 cm). Much of the upper and middle Maestrichtian appears to be missing, but the exact locations of disconformities within the debris flow sequence are difficult to specify due to spotty core recovery and strong mixing by downslope processes and bioturbation.

Unit IV: depth, 189.5–295.1 mbsf; age, late Maestrichtian to early Santonian) white nannofossil chalk with thin, nodular black chert layers.

Lower Maestrichtian chalks at the top of Unit IV lack chert and are therefore undisturbed by drilling. They exhibit zones with faint to strongly pronounced horizontal laminations with little or no evidence of bioturbation. In Section 120-747A-21X-4, the laminations are especially colorful and progress from dark brown to chrome yellow brown to grayish green to bluish turquoise before reverting to a more common pale blue green (Fig. 21). Thin brown, brittle phosphate seams 5 mm across symmetrically divide the yellow brown laminae. Overall, the laminae seem to fall into cyclic units about 30 cm thick, are largely undisturbed by bioturbation, and apparently represent suboxic conditions.

The majority of Unit IV consists of rather pure, white nannofossil chalk with chert, scattered inoceramid fragments, rare pelagic crinoid columnals, and a rare mollusc fragments. Core 120-747C-10R, however, contained a few pieces of whitish calcarenite with 10% glauconite, a few dark volcaniclastic grains, cross and parallel laminations, and a few large burrows. This core is dated as early Santonian by nannofossils, which implies a hiatus of 10 m.y. between Cores 120-747C-9 and -10.

Unit V: depth, 296.6–350.5 mbsf; basalt flows composed of variably brecciated, veined, and altered aphyric to sparsely phyric basalts.

Based on macroscopic observations, the recovered basement rock consists of up to 12 separate lava flows separated by brecciated basalt. The flows were emplaced on a near-horizontal topography and average about 1 m in thickness (5.4 m maximum); wireline logs indicate that much of the breccias were not recovered. The separate flows appear similar in composition and consist of predominantly aphyric, sparsely plagioclase-pyroxene phyric, and olivine-plagioclase phyric basalts. The apparent lack of glassy rinds, hyaloclastites, and pillow structures, as well as the presence of vesicles and oxidized flow tops, suggest subaerial eruption.

All volcanics exhibit variable degrees of brecciation, veining, and alteration. Crosscutting relationships between amygdules and veins suggest at least two successive hydrothermal events. The alteration minerals consist of zeolites (heulandite-clinoptilolite, chabazite, and stilbite), pore and interlayered smectites, prehnite, goethite, calcite and quartz fillings in veins, vesi-

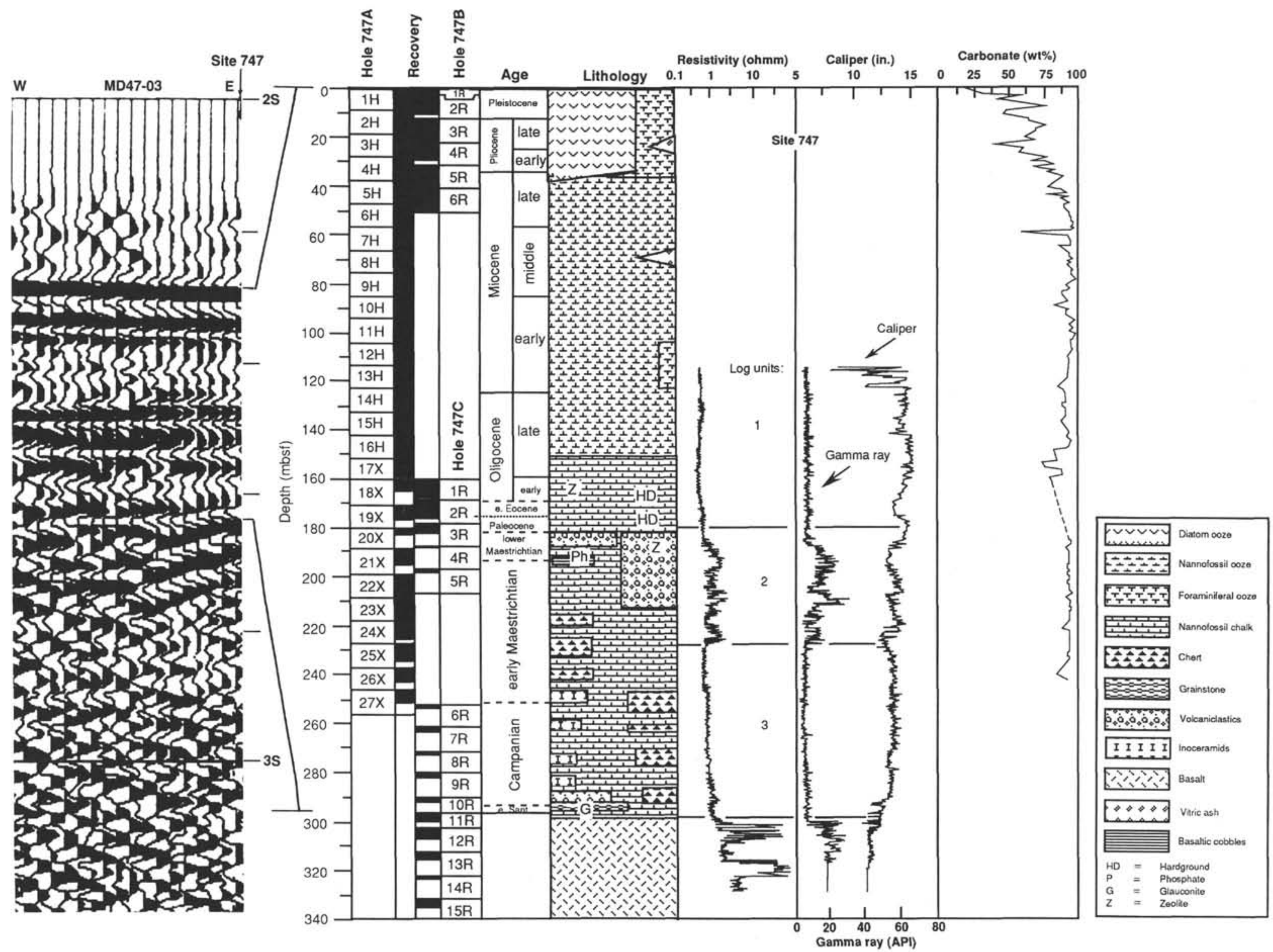

Figure 54. Composite stratigraphic section at Site 747 showing correlation of seismic stratigraphy, lithobiostratigraphy, wireline logs, and carbonate content. By ODP convention, all cores are plotted at the top of the drilled interval although the material may have come from anywhere within that interval. This leads to uncertainty for the placement of core material within partially recovered intervals, such as at 180 m where the wireline logs and seismic stratigraphy suggest that Cores 120-747A-20X and -3R probably came from the base of the drilled intervals. There is also some uncertainty in the placement of the wireline logs due to excessive ship heave experienced during the logging run. Wireline logs were taken in Hole 747C.

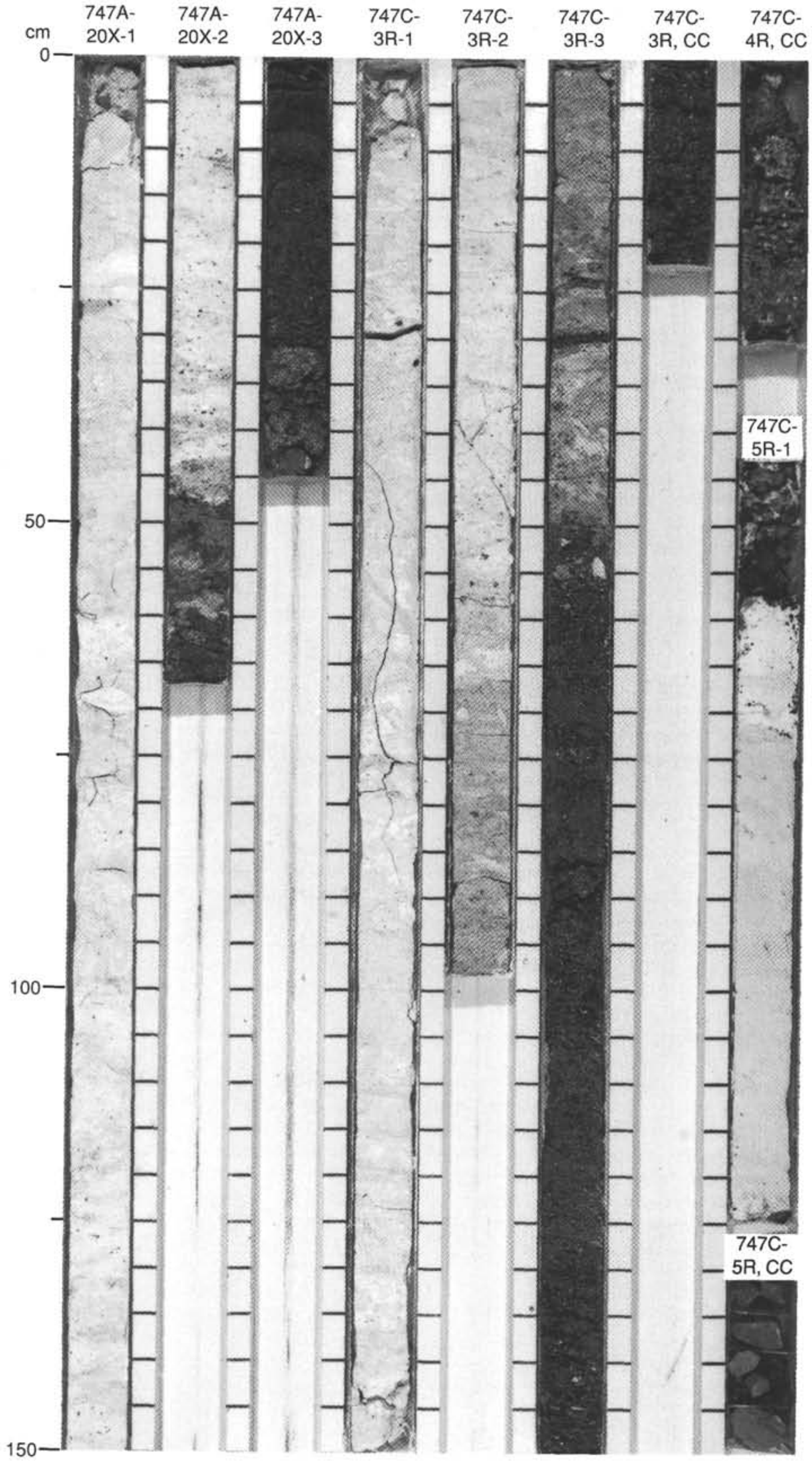

Figure 55. Maestrichtian–lowermost Paleocene basalt breccia debris flows cored in Holes 747A (left, Core 120-747-20X) and 747C (right, Cores 120-747C-3R to -5R).

cles, and amygdules. The coexistence of these alteration minerals suggests metamorphism in an oxidizing environment. The zeolite assemblages correspond to the intermediate temperature zone of the zeolite facies.

Relatively fresh material was recovered from three flows. With the exception of two silica undersaturated rocks (nepheline normative), the flows consist of olivine-hypersthene normative basalts. Relative to mid-ocean ridge basalts (MORB), they are enriched in incompatible trace elements. In terms of their Zr/Nb ratio and other incompatible trace elements, they are transitional between MORB and most ocean island basalts (i.e., compositionally similar to T-MORB).

Physical Properties and Heat Flow

Trends in index physical properties, plus changes in compressional wave velocity, allow the section at Site 747 to be divided tentatively into five geotechnical zones that correspond closely with the lithologic units. These are:

Unit G1 (0–34 mbsf; equivalent to Unit I): wet-bulk density increases, water content and porosity decrease.

Unit G2 (34–151.5 mbsf; equivalent to Subunit IIA): trends as above.

Unit G3 (151.5–190 mbsf; equivalent to Subunits IIB and IIC and a portion of Unit III): above trends reverse.

Unit G4 (190–296.5 mbsf; equivalent to portion of Unit III and all of IV): above trends reverse again).

Unit G5 (below 296.6 mbsf, Unit V): basalt.

Thermal conductivity was measured in cores using a needle probe; only runs which displayed a temperature drift rate of less than 0.04°C/min were analyzed. Three downhole temperatures were measured with the Uyeda temperature probe at 53.0, 94.5, and 123.0 mbsf. The average geothermal gradient and an average thermal conductivity of 1.28 W/m·K were used to calculate a mean value for heat flow equal to 61 mW/m^2.

Logging

The sequence below 90 mbsf in Hole 747C was successfully logged with one tool string before gale force winds forced abandonment of the site. The logged interval is divided into four discrete units (see "Logging" section, this chapter, for unit definitions) that correspond closely to the lithologic units (Fig. 54). The resistivity and natural gamma ray logs (Fig. 54) clearly delimit the major altered and less altered zones in the basement complex (which was cored with only 38% recovery due to high seas). The logs also detected three major basalt breccia debris flows in the Maestrichtian. The debris flows are characterized by peaks in the resistivity and gamma ray logs that oppose those in the caliper log. Only the uppermost debris flow (Fig. 55) was cored in both Holes 747A and 747C, and only a portion of the second flow or perhaps a minor flow was captured in Core 120-747C-5R. The rest of the second debris flow and the third (at 220 mbsf) was not cored in either hole and would not have been detected without the electric logs.

Seismic Stratigraphy, Depositional and Tectonic History

As stated previously, the seismic section at Site 747 shows two distinct sedimentary sequences resting upon a well-defined basement reflector. The reflector at 0.22–0.24 s TWT probably corresponds to Unit III between 181.45 and 197.20 mbsf, and basement matches a major reflector at 0.35 s TWT (Fig. 54). These results agree quite well with the physical properties data (see "Physical Properties" section, this chapter) and the logging curves (see "Logging" section, this chapter). The upper seismic sequence (0.22–0.24 s TWT thick) corresponds to Units I and II; the lower seismic sequence resting upon basement (0.13–0.11 s TWT thick) corresponds to Unit IV. Taking into account the shipboard compressional wave velocity measurements, the two seismic sequences represent a total thickness of about 288–282 m, in good agreement with the drilling results, which located the basement at a depth of 296.5 mbsf (see "Seismic Stratigraphy" section, this chapter). Note, however, that the deepest sediment recovery was 295.1 mbsf.

The sedimentary sequence and basaltic basement at Site 747 document a succession of structural and paleoceanographic events that highlight the geologic and tectonic evolution of this portion of the Kerguelen Plateau. These are discussed in stratigraphic order.

The basement of Site 747 is comprised of a number of vesicular basalt flows that were probably deposited in a subaerial environment. The Zr/Nb ratios (11–13) of Site 747 basalts are significantly lower than those of Indian Ocean MORB (Zr/Nb = 40–56; Price et al., 1986) but higher than ocean-island-basalts from Kerguelen (Zr/Nb = 5–8) and Heard islands (Zr/Nb = 5–7) (Storey et al., 1988; also pers. comm.). Compositionally, Site 747 basalts show similarities with other oceanic flood basalts, such as those from the Nauru Basin (Zr/Nb = 10–18; Saunders, 1985). Thus, they are transitional between typical MORB and normal ocean-island-type basalts.

The common occurrence of plagioclase and olivine phenocrysts suggests low-pressure crystallization (e.g., Bender et al., 1978), but reaction textures exhibited by some plagioclase and clinopyroxene glomerocrysts may suggest two-stage, polybaric crystallization (i.e., high-pressure crystallization followed by low-pressure reaction and/or magma-mixing) (Kuo and Kirkpatrick, 1982; Barton et al., 1982). The secondary mineralogy of the Site 747 basalts is reminiscent of those from regions of high heat flow in the extensive subaerial tholeiitic flood basalts of Iceland (Kristmannsdòttir and Tòmasson, 1978; Pàlmason et al., 1979).

Slow subsidence at a rate of about 15–25 m/m.y. of this portion of the plateau and the accumulation of marine sediments began by early Santonian times, and the oldest sediments recovered are relatively shallow-water glauconitic calcarenites with admixtures of fine volcanic debris eroded from the basement. These are overlain disconformably by somewhat deeper-water mid-Campanian to Maestrichtian chalks with chert stringers and some *Inoceramus* and pelagic crinoid remains.

With one major exception, Cretaceous planktonic foraminifers and calcareous nannofossil assemblages are strongly austral and resemble those described from the Falkland Plateau (cf. Sliter, 1977; Wind, 1979; Wise, 1983). The high-latitude calcareous nannofossil assemblages are characterized by species of *Nephrolitus, Biscutum magnum, Biscutum coronum, Biscutum dissimilis, Monomarginatus quaternarius,* and *Thierstenia ecclesiastica,* whereas the planktonic foraminifers are dominated by hedbergellids rather than by globotruncanids. The lowest Campanian core, however, denotes a more temperate influence, as indicated by *Quadruum gothicum* and *Q. trifidum* among the nannofossils and by a much higher proportion of globotruncanids of the transitional faunal province among the planktonic foraminifer assemblages.

Campanian-Maestrichtian sedimentation rates were a high 20 m/m.y., which denote rather shallow basin depths, little carbonate dissolution, and productive surface waters, as indicated by the numerous chert stringers impeding our coring efforts. The paleodepth of deposition is estimated to have been about 500 m.

Maestrichtian pelagic sedimentation is interrupted by a series of debris flows consisting of clay-, sand-, and cobble-size clastics and breccias (Unit III; Fig. 55) eroded subaerially from volcanic basement during what appears to have been a major tectonic event that apparently affected much of the Southern Kerguelen Plateau as well (see Leclaire et al., 1987; Schlich et al., 1988; Colwell et al., 1988). The debris flows include angular clasts of previously lithified Campanian chalk and chert that indicate substantial faulting of the seafloor. Uppermost Maestrichtian to lowermost Danian sediments are missing, but scattered volcanic debris were shed into the overlying heavily bioturbated Danian chalks. As the Maestrichtian and Danian pelagic sediments are still of a basinal facies, they were probably receiving coarse debris flow sediments from a nearby uplifted or tilted basement block being eroded at or above wave base. The veritable absence of upper Maestrichtian sediments could indicate that the basin itself was briefly subjected to erosion.

The basement rock being eroded during the Maestrichtian could be that which is presently exposed today along the margin of an offshoot of the 77°E Graben system, some 6–7 km east and southeast of our site (Fig. 56; see also Fig. 5). This basement block could have been tilted or thermally domed upward during an early phase of rifting, possibly related to a breakup between the Southern Kerguelen Plateau and the Broken Ridge–Diamantina Zone (see "Seismic Stratigraphy" section, this chapter). Subsequently, the graben margin and the site of deposition could have undergone rapid subsidence (600–800 m/m.y.) as a result of extensional tectonics associated with the final rifting on the dissipation of the thermal anomaly beneath the plateau. Benthic foraminifer assemblages for the overlying Danian sediments suggest a paleodepth of deposition ranging up to as much as 2000 m. Alternatively, the 77°E Graben may represent the plate boundary between the two Kerguelen provinces, in which case it may have behaved as a strike-slip fault with relatively little extension (Royer and Sandwell, in press).

Core recovery plus the wireline logs indicate that the debris flows are more numerous and begin lower in the section at Hole 747C than at Hole 747A, which was drilled only 20 m away. Aside from the upper debris flow cored in Core 120-747A-20X, the only other traces of the debris flows in Hole 747A are the thin, one-grain-thick horizons in the lower Maestrichtian of Core 120-747A-21X. Taking into account the core data and the geophysical logs (which may have suffered some smearing of the signals due to excessive ship heave), an interpretation of the Unit III sequence is given in Figure 57, which shows a series of debris flow lobes separated by intercalated calcareous oozes. This interpretation suggests that the debris flows began during the early Maestrichtian and reached their peak by the middle or late Maestrichtian. Note that only Hole 747C was logged, and that the cores taken in that hole do not cover all of the debris flows shown to be present on the logs. Considering the east-west alignment of the two holes, it appears that the debris flows came from the south or southeast rather than the east.

One consequence of the tectonic event may have been the restriction of circulation over the site of deposition and the development of a suboxic depositional environment, thereby allowing the formation of the colorful laminae seen near the top of Unit IV (Core 120-747A-21X-4; see Fig. 21).

The remaining Paleocene–lower Oligocene section is highly condensed and cut by the three disconformities where most or all of the upper Paleocene, middle to lower upper Eocene, and a small portion of the upper lower Oligocene are missing. These plus the corresponding hardgrounds denote several episodes of erosion or strong current activity, possibly associated with changes in circulation patterns as tectonics continued to affect this region and to change the configuration of the seafloor, plateaus, and ridges. The most conspicuous hiatus in this part of the section at Site 747, which spans much of the Eocene, probably corresponds to "discordance A" of Munschy and Schlich (1987), which is related to the separation by seafloor spreading of the Kerguelen-Heard Plateau and Broken Ridge.

Sedimentation rates for the remainder of the Neogene are remarkably constant at about 5 m/m.y., and sedimentation for this interval appears to have been continuous until the late Pleistocene except for a hiatus across the Miocene/Pliocene boundary (see "Sedimentation Rates" section, this chapter). A disconformity at this juncture is widespread in the Southern Ocean region (Wise et al., 1982) and is generally associated with the effects of late Miocene Antarctic glaciations. The Neogene sedimentation rates, however, are relatively low and denote somewhat diminished surface-water productivities as are commonly found within the interiors of gyral systems rather than along the margins of major water masses, where mixing and upwelling is more likely to occur.

Although the predominance of biosiliceous ooze throughout the Pliocene-Pleistocene denotes the presence of the Antarctic Water Mass over this site, several species of both planktonic foraminifers and calcareous nannoplankton lived in the surface waters. The top of the section is dated at 0.35 Ma.

The essentially continuous calcareous upper Oligocene to upper Pleistocene record at a site this far south of the present-day Polar Front was unexpected, and this section will serve as an important reference section for an integrated high-latitude calcareous and siliceous microfossil biostratigraphy correlated with magnetostratigraphy and lower latitude zonations. A good paleomagnetic polarity record was obtained down to the lower/upper Oligocene contact. Virtually all major events (anomaly correlatives) can be recognized as well as the structure of most of the polarity chrons. Excellent preservation of planktonic and benthic foraminifers should allow a complementary stable isotope record to be established following shore-based analysis. Also noteworthy is the pristine preservation of the Danian calcareous microfossils and the occurrence of a Paleocene larger benthic foraminifer. The incursions of such "larger" neritic foraminifers into Australian basins represent climatic warmings and the influx of tropical faunal elements (McGowran, 1979). At Site 747, such a form represents a shallow-water environment, and it was probably brought to the site by downslope processes.

In summary, the primary tectonic and depositional events recorded at Site 747 (see "Lithostratigraphy and Sedimentology," "Biostratigraphy," and "Sedimentation Rates" sections, this chapter) and derived from seismic stratigraphy analysis (see "Seismic Stratigraphy" section, this chapter) can be outlined as follows.

1. Following the subaerial eruption of the last plateau basalt lavas, subsidence of the site commenced at a slow rate, which only slightly exceeded marine pelagic sedimentation of 20 m/m.y. from Santonian through middle Maestrichtian times.
2. A major, widespread tectonic episode beginning during the early Maestrichtian and extending into the earliest Danian resulted in the uplift and erosion of nearby basaltic basement and the influx of the erosional products as debris flows at our site of deposition. An upper Maestrichtian hiatus in the sequence may indicate erosion of the depositional site as well.
3. Rapid subsidence of the site was underway by early Danian times, possibly as the result of extensional tectonics related to the rifting (e.g., of the nearby 77°E Graben) or the dissipation of a thermal anomaly beneath the plateau. Alternatively, there may have been strike-slip motion along the 77°E Graben (Royer and Sandwell, in press). Any extensional tectonics may have accompanied the breakup between the Southern Kerguelen Plateau and the Broken Ridge–Diamantina Zone.
4. Pelagic sedimentation during the Paleogene was slow, far less than the subsidence rate, and interrupted by three hiatuses. One of these, of 15-m.y. duration, spans much of the early to late Eocene, and may correspond to the breakup between the Kerguelen-Heard Plateau and the Broken Ridge.
5. Sedimentation during the remainder of the Cenozoic was nearly continuous and at a remarkably constant but low rate of about 5 m/m.y., with predominantly pelagic carbonate deposi-

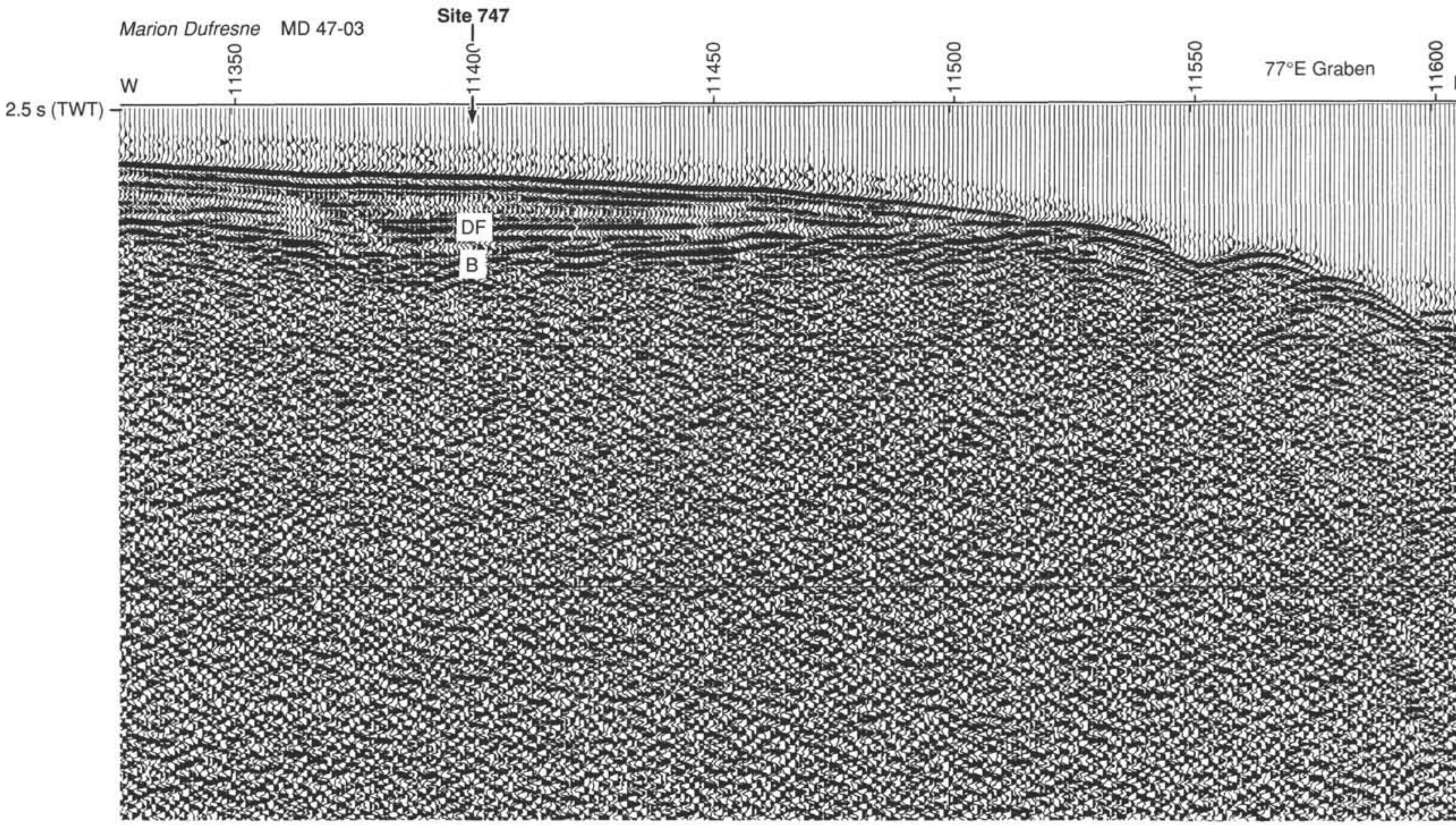

Figure 56. *Marion Dufresne* multichannel seismic reflection profile MD47-03 through Site 747 showing position of the Maestrichtian-lowermost Paleocene volcaniclastic debris flows (DF) that onlap exposed basement (B) to the east along the margin of an extension of the 77°E Graben to the east.

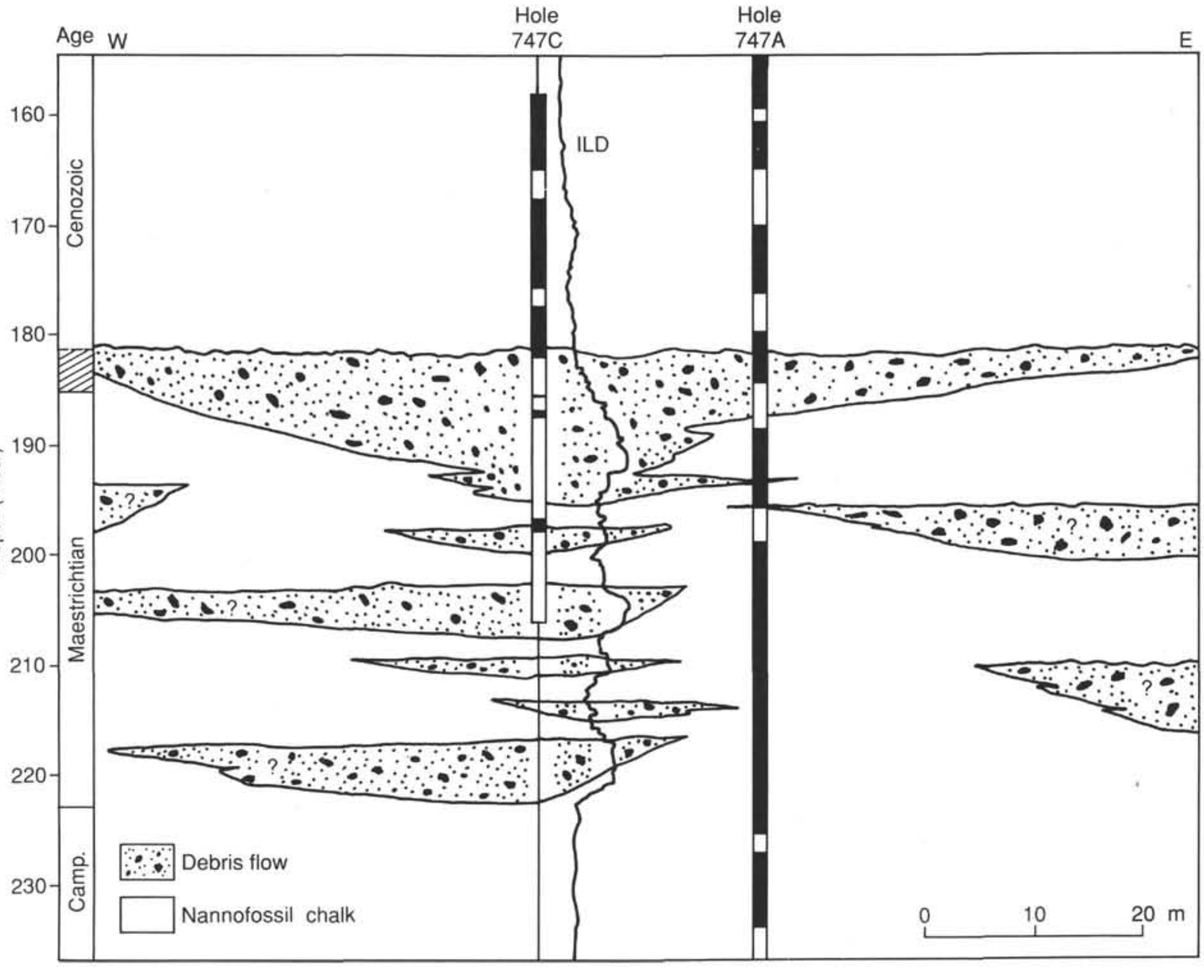

Figure 57. Interpretive reconstruction (to scale) of the Maestrichtian-lowermost Danian basalt breccia debris flow sequence cored or logged at Site 747. The resistivity log (ILD = deep induction log) is from Hole 747C, which was cored only between 159 and 206.5 mbsf but was drilled throughout the entire sequence (see also Fig. 54 above).

tion changing to mainly biosiliceous sedimentation during the Pliocene-Pleistocene in response to the deterioration of late Cenozoic climates.

REFERENCES

Barker, P. F., Kennett, J. P., et al., 1988. *Proc. ODP, Init. Repts.*, 113: College Station, TX (Ocean Drilling Program).

Barton, M., Varekamp, J. C., and van Bergen, M. D., 1982. Complex zoning of clinopyroxenes in the lavas of Vulisini Latinum, Italy: evidence for magma mixing. *J. Volcanol. Geotherm. Res.*, 14:361-388.

Belford, D. J., 1959. The stratigraphy and micropalaeontology of the Upper Cretaceous of Western Australia. *Geol. Rundsch.*, 47:629-647.

———, 1960. Upper Cretaceous foraminifera from the Toolonga Calcilutite and Gingin Chalk, Western Australia. *Bull. Bur. Miner. Resour., Geol. Geophys. Aust.*, 57:1-198.

Bender, J. F., Hodges, F. N., and Bence, A. E., 1978. Petrogenesis of basalts from the Famous area: experimental studies from 0 to 15 kb. *Earth Planet. Sci. Lett.*, 41:277-302.

Berggren, W. A., Aubry, M.-P., and Hamilton, W. N., 1983. Neogene magnetobiostratigraphy of Deep Sea Drilling Project Site 516 (Rio Grande Rise, South Atlantic). *In* Barker, P. F., Carlson, R. L., Johnson, D. A., et al., *Init. Repts. DSDP*, 72: Washington (U.S. Govt. Printing Office), 939-948.

Berggren, W. A., Kent, D. V., and Flynn, J. J., 1985a. Jurassic to Paleogene: Part 2, Paleogene geochronology and chronostratigraphy. *In* Snelling, N. J. (Ed.), *The Chronology of the Geological Record.* Geol. Soc. Mem. (London), 10:141-195.

Berggren, W. A., Kent, D. V., Flynn, J. J., and Van Couvering, J. A., 1985b. Cenozoic geochronology. *Geol. Soc. Am. Bull.*, 96:1407-1418.

Berggren, W. A., Kent, D. V., and Van Couvering, J. A., 1985c. The Neogene: Part 2, Neogene geochronology and chronostratigraphy. *In* Snelling, N. J. (Ed.), *The Chronology of the Geological Record.* Geol. Soc. Mem. (London), 10:211-160.

Berggren, W. A., and Miller, K. G., 1988. Paleogene tropical planktonic foraminiferal biostratigraphy and magnetochronology. *Micropaleontology,* 34:362-380.

Boyce, R. E., 1976. Definitions and laboratory techniques of compressional sound velocity parameters and wet-water content, wet-bulk density, and porosity parameters by gravimetric and gamma ray attenuation techniques. *In* Schlanger, S. O., Jackson, E. D., et al., *Init. Repts. DSDP,* 33: Washington (U.S. Govt. Printing Office), 931-955.

———, 1977. Deep Sea Drilling Project procedures for shear strength measurements of clayey sediment using modified Wykeham Farrance laboratory vane apparatus. *In* Barker, P. F., Dalziel, I.W.D., et al., *Init. Repts. DSDP,* 36: Washington (U.S. Govt. Printing Office), 1059-1068.

Bryant, W. R., Bennett, R. H., and Katherman, C. F., 1981. Shear strength, consolidation, porosity, and permeability of oceanic sediments. *In* Emiliani, C. (Ed.), *The Sea* (Vol. 7): New York (Wiley), 1555-1615.

Bukry, D., 1973. Low-latitude coccolith biostratigraphic zonation. *In* Edgar, N. T., Saunders, J. B., et al., *Init. Repts. DSDP,* 15: Washington (U.S. Govt. Printing Office), 685-703.

Caron, M., 1985. Cretaceous planktic foraminifera. *In* Bolli, H. M., Saunders, J. B., and Perch-Nielsen, K. (Eds.), *Plankton Stratigraphy:* Cambridge (Cambridge Univ. Press), 17-86.

Chen, P. H., 1975. Antarctic radiolaria. *In* Hayes, D. E., Frakes, L. A., et al., *Init. Repts. DSDP,* 28: Washington (U.S. Govt. Printing Office), 437-513.

Ciesielski, P. F., 1983. The Neogene and Quaternary diatom biostratigraphy of subantarctic sediments, Deep Sea Drilling Project 71. *In* Ludwig, W. J., Krasheninnikov, V., et al., *Init. Repts. DSDP,* 71, Pt. 2: Washington (U.S. Govt. Printing Office), 635-665.

Coffin, M. F., Davies, H. L., and Haxby, W. F., 1986. Structure of the Kerguelen Plateau province from SEASAT altimetry and seismic reflection data. *Nature,* 324:134-136.

Colwell, J. B., Coffin, M. F., Pigram, C. J., Davies, H. L., Stagg, H.M.J., and Hill, P. J., 1988. Seismic stratigraphy and evolution of the Raggatt Basin, Southern Kerguelen Plateau. *Mar. Pet. Geol.,* 5: 75-81.

Dosso, L., Vidal, P., Cantagrel, J. M., Lameyre, J., Marot, A., and Zimine, S., 1979. Kerguelen: continental fragment or oceanic island?: petrology and isotopic geochemistry evidence. *Earth Planet. Sci. Lett.,* 43:46-60.

Fröhlich, F., Caulet, J. P., Clement, P., Fellah, N., Giannesini, J. P., Wicquart, E., Averous, P., Blanc, G., Giannoni, A., Martin, L., Phillipot, F., and Prost, S., 1983. Mise en évidence d'une série sédimentaire pélagique du Paléogène et du Crétacé Supérieur sur le plateau de Kerguelen. Résultats préliminaires de la campagne océanographique MD35 D.R.A.K.A.R. (mars 1983) du *N.O. Marion Dufresne. C. R. Acad. Sci., Ser. 2,* 297:153-156.

Gieskes, J. M., 1974. Interstitial water studies, Leg 25. *In* Simpson, E.S.W., Schlich, R., et al., *Init. Repts. DSDP,* 25: Washington (U.S. Govt. Printing Office), 361-394.

Gieskes, J. M., and Peretsman, G., 1986. Water chemistry procedures on SEDCO 471—some comments. *ODP Tech. Note,* No. 5.

Gombos, A. M., Jr, and Ciesielski, P. F., 1983. Late Eocene to early Miocene diatoms from the southwest Atlantic. *In* Ludwig, W. J., Krasheninnikov, V. A., et al., *Init. Repts. DSDP,* 71, Pt. 2: Washington (U.S. Govt. Printing Office), 583-634.

Heezen, B. C., and Tharp, M., 1966. Physiography of the Indian Ocean. *Philos. Trans. R. Soc. London, Ser. A,* 259:137-149.

Herb, R., 1974. Cretaceous planktonic foraminifera from the eastern Indian Ocean. *In* Davies, T. A., Luyendyk, B. P., et al., *Init. Repts. DSDP,* 26: Washington (U.S. Govt. Printing Office), 745-769.

Honnorez, J., 1981. The aging of the oceanic crust at low temperature. *In* Emiliani, C. (Ed.), *The Sea* (Vol. 7): New York (Wiley), 525-587.

Houtz, R. E., Hayes, D. E., and Markl, R. G., 1977. Kerguelen Plateau bathymetry, sediment distribution and crustal structure. *Mar. Geol.,* 5:95-130.

Humphris, S. E., and Thompson, G., 1978. Hydrothermal alteration of oceanic basalts by seawater. *Geochim. Cosmochim. Acta,* 42:107-125.

Jenkins, D. G., 1971. Cenozoic planktonic foraminifera of New Zealand. *Paleontol. Bull., N. Z. Geol. Survey,* 42:1-278.

Jenkins, D. G., and Srinivasan, M. S., 1985. Cenozoic planktonic foraminifers from the equator to the subantarctic of the southwest Pacific. *In* Kennett, J. P., von der Borch, C. C., et al., *Init. Repts. DSDP,* 90: Washington (U.S. Govt. Printing Office), 795-834.

Kennett, J. P., 1978. The development of planktonic biogeography in the Southern Ocean during the Cenozoic. *Mar. Micropaleontol.,* 3: 301-345.

Kennett, J. P., and Srinivasan, M. S., 1983. *Neogene Planktonic Foraminifera: A Phylogenetic Atlas:* Stroudsburg, PA (Hutchinson Ross).

Kent, D. V., and Gradstein, F. M., 1985. A Cretaceous and Jurassic geochronology. *Geol. Soc. Am. Bull.,* 96:1419-1427.

Kristmannsdòttir, H., and Tòmasson, J., 1978. Zeolite zones in geothermal areas in Iceland. *In* Sand, L. B., and Mumpton, F. A. (Eds.), *Natural Zeolites: Occurrences, Properties, and Use:* Oxford (Pergamon), 277-284.

Kuo, L. C., and Kirkpatrick, R. J, 1982. Pre-eruption history of basalts from DSDP Legs 45 and 46: evidence from morphology and zoning patterns in plagioclase. *Contrib. Mineral. Petrol.,* 79:13-27.

Lambe, T. W., and Whitman, R. V., 1969. *Soil Mechanics:* New York (Wiley).

Laughton, A. S., Matthews, D. H., and Fisher, R. L., 1970. The structure of the Indian Ocean. *In* Maxwell, A. E. (Ed.), *The Sea* (Vol. 4), New York (Wiley-Interscience), 543-586.

Leclaire, L., Bassias, Y., Denis-Clocchiatti, M., Davies, H., Gautier, I., Gensous, B., Giannesini, P.-J., Patriat, P., Segoufin, J., Tesson, M., and Wannesson, J., 1987. Lower Cretaceous basalt and sediments from the Kerguelen Plateau. *Geo-Mar. Lett.,* 7:169-176.

Leclaire, L., Denis-Clocchiatti, M., Davies, H., Gautier, I., Gensous, B., Giannesini, P.-J., Morand, F., Patriat, P., Segoufin, J., Tesson, M., and Wannesson, J., 1987. Nature et âge du plateau de Kerguelen-Heard, secteur sud. Résultats préliminaires de la campagne "N.A.S.K.A.-MD48". *C. R. Acad. Sci., Ser. 2,* 304:23-28.

Lee, H. J., 1982. Bulk density and shear strength of several deep-sea calcareous sediments. *In* Demars, K. R., and Chaney, R. C. (Eds.), *Geotechnical Properties, Behavior, and Performance of Calcareous Soils.* ASTM Spec. Tech. Publ., 777: 54-78.

McGowran, B., 1979. The Tertiary of Australia: foraminiferal overview. *Mar. Micropaleontol.,* 4:235-264.

McIver, R., 1975. Hydrocarbon occurrence from JOIDES Deep Sea Drilling Project. *World Pet. Contr.,* 9:269-280.

Mackensen, A., Grobe, H., Hubberten, H. W., Spiess, V., and Fütterer, D. K., in press. Stable isotope stratigraphy from the Antarctic continental margin during the last one million years. *Mar. Geol.*

Manheim, F. T., and Sayles, F. L., 1974. Composition and origin of interstitial waters of marine sediments, based on deep-sea drill cores. *In* Goldberg, E. D. (Ed.), *The Sea* (Vol. 5): New York (Wiley), 527-568.

Martini, E., 1971. Standard Tertiary and Quaternary calcareous nannoplankton zonation. *In* Farinacci, A. (Ed.), *Proceedings of the Second International Conference on Planktonic Microfossils, Roma*: Rome (Ed. Technoscienza), 739-785.

Müller, P. J., and Suess, E., 1979. Productivity, sedimentation rate, and sedimentary organic carbon content in the oceans. 1. Organic carbon preservation. *Deep-Sea Res.,* 26A:1347-1362.

Munschy, M., and Schlich, R., 1987. Structure and evolution of the Kerguelen-Heard Plateau (Indian Ocean) deduced from seismic stratigraphy studies. *Mar. Geol.,* 76:131-152.

Pàlmason, G., Arnòrsson, S., Fridleifsson, I. B., Kristmannsdòttir, H., Saemundsson, K., Stefànsson, V., Steingrìmsson, B., Tòmasson, J., and Kristjànsson, L., 1979. The Iceland crust: evidence from drillhole data on structure and processes. *In* Talwani, M., Harrison, C. G., and Hayes, D. E. (Eds.), *Deep Drilling Results in the Atlantic Ocean: Ocean Crust:* Washington (American Geophysical Union), 43-65.

Price, R. C., Kennedy, A. K., Riggs-Sneeringer, M., and Frey, F. A., 1986. Geochemistry of basalts from the Indian Ocean triple junction: implications for the generation and evolution of Indian Ocean Ridge basalts. *Earth Planet. Sci. Lett.,* 78:379-396.

Robinson, P. T., Von Herzen, R. P., et al., 1989. *Proc. ODP, Init. Repts.,* 118: College Station, TX (Ocean Drilling Program).

Royer, J.-Y., and Sandwell, D. T., in press. Evolution of the eastern Indian Ocean since the Late Cretaceous: constraints from GEOSAT altimetry. *J. Geophys. Res.*

Saunders, A. D., 1985. Geochemistry of basalts from the Nauru Basin, Deep Sea Drilling Project Legs 61 and 89: implications for the origin of oceanic flood basalts. *In* Moberly, R., Schlanger, S. O., et al., *Init. Repts. DSDP,* 89: Washington (U.S. Govt. Printing Office), 499-517.

Schlich, R., 1975. Structure et âge de l'océan Indien occidental. *Mem. Hors-Ser. Soc. Geol. Fr.,* 6:1-103.

———, 1982. The Indian Ocean: aseismic ridges, spreading centers, and oceanic basins. *In* Nairn, A.E.M., and Stehli, F. G. (Eds.), *The Ocean Basins and Margins: The Indian Ocean* (Vol. 6): New York (Plenum), 51-147.

Schlich, R., Delteil, J., Moulin, J., Patriat, P., and Guillaume, R., 1971. Mise en évidence d'une sédimentation de marge continentale sur le plateau de Kerguelen-Heard. *C. R. Acad. Sci., Ser. 2,* 272: 2060-2063.

Schlich, R., Coffin, M. F., Munschy, M., Stagg, H.M.J., Li, Z. G., and Revill, K., 1987. *Bathymetric Chart of the Kerguelen Plateau.* [Jointly edited by Bureau of Mineral Resources, Geology and Geophysics, Canberra; Institut de Physique du Globe; France; and Territoire des Terres Australes et Antarctiques Françaises, Paris.]

Schlich, R., Munschy, M., Boulanger, D., Cantin, B., Coffin, M. F., Durand, J., Humler, E., Li, Z. G., Savary, J., Schaming, M., and Tissot, J. D., 1988. Résultats préliminaires de la campagne océanographique de sismique reflexion multitraces MD47 dans le domaine sud du plateau de Kerguelen. *C. R. Acad. Sci., Ser. 2,* 305:635-642.

Shipboard Scientific Party, 1988a. Site 689. *In* Barker, P. F., Kennett, J. P., et al., *Proc. ODP, Init. Repts.,* 113: College Station, TX (Ocean Drilling Program).

Shipboard Scientific Party, 1988b. Site 690. *In* Barker, P. F., Kennett, J. P., et al., *Proc. ODP, Init. Repts.,* 113: College Station, TX (Ocean Drilling Program).

Sliter, W. V., 1972. Cretaceous foraminifers—depth habitats and their origin. *Nature,* 239:514-515.

________, 1976. Cretaceous foraminifers from the southwestern Atlantic Ocean, Leg 36, Deep Sea Drilling Project. *In* Barker, P. F., Dalziel, I.W.D., et al., *Init. Repts. DSDP,* 36: Washington (U.S. Govt. Printing Office), 519-573.

Stainforth, R. M., Lamb, J. C., Luterbacher, H.-P., Beard, J. H., and Jeffords, J. M., 1975. Cenozoic planktonic foraminiferal zonation and characteristics of index forms. *Univ. Kans. Paleontol. Contrib. Pap.,* 62.

Storey, M., Saunders, A. D., Tarney, J., Leat, P., Thirlwall, M. F., Thompson, R. N., Menzies, M. A., and Marriner, G. F., 1988. Geochemical evidence for plume-mantle interactions beneath Kerguelen and Heard Islands, Indian Ocean. *Nature,* 336:371-374.

Taylor, E., 1984. Oceanic sedimentation and geotechnical stratigraphy: hemipelagic carbonates and red clays [Ph.D. dissert.]. Texas A&M Univ., College Station.

Tjalsma, R. C., 1977. Cenozoic foraminifera from the South Atlantic, DSDP Leg 36. *In* Barker, P. F., Dalziel, I.W.D., et al., *Init. Repts. DSDP,* 36: Washington (U.S. Govt. Printing Office), 493-517.

Tjalsma, R. C., and Lohmann, G. P., 1983. Paleocene-Eocene bathyal and abyssal benthic foraminifera from the Atlantic Ocean. *Micropaleontology, Spec. Publ.,* 4:1-90.

Vacquier, V., 1985. The measurement of thermal conductivity of solids with a transient linear heat source on the plane surface of a poorly conducting body. *Earth Planet. Sci. Lett.,* 74:275-279.

Von Herzen, R. P., and Maxwell, A. E., 1959. The measurement of thermal conductivity of deep-sea sediments by a needle probe method. *J. Geophys. Res.,* 65:1557-1563.

Watkins, N. D., Gunn, B. M., Nougier, J., and Baksi, A. K., 1974. Kerguelen: continental fragment or oceanic island? *Geol. Soc. Am. Bull.,* 85:201-212.

Weaver, F. M., and Gombos, A. M., Jr., 1981. Southern high-latitude diatom biostratigraphy. *In* Warme, J. E., Douglas, R. C., and Winterer, E. L. (Eds.), *The Deep Sea Drilling Project: A Decade of Progress.* Spec. Publ., Soc. Econ. Paleontol. Mineral., 32:445-470.

Wicquart, E., and Frohlich, F., 1986. La sédimentation sur le plateau de Kerguelen-Heard: relations avec l'évolution de l'océan Indien au Cenozoique. *Bull. Soc. Geol. Fr.,* 8:569-57 .

Wind, F. H., 1979. Maestrichtian-Campanian nannofloral provinces of the southern Atlantic and Indian Oceans. *In* Talwani, M., Hay, W., and Ryan, W.B.F. (Eds.), *Deep Drilling Results in the Atlantic Ocean: Continental Margins and Paleoenvironment:* Washington (American Geophysical Union), 123-137.

Wise, S. W., Jr., 1983. Mesozoic and Cenozoic calcareous nannofossils recovered by Deep Sea Drilling Project Leg 71 in the Falkland Plateau Region, southwest Atlantic Ocean. *In* Ludwig, W. J., Krasheninnikov, V. A., et al., *Init. Repts. DSDP,* 71, Pt. 2: Washington (U.S. Govt. Printing Office), 481-550.

Wise, S. W., Ciesielski, P. F., MacKenzie, D. T., Wind, F. H., Busen, K. E., Gombos, A. M., Haq, B. U., Lohmann, G. P., Tjalsma, R. C., Harris, W. K., Hedlund, R. W., Beju, D. N., Jones, D. L., Plafker, G., and Sliter, W. V., 1982. Paleontologic and paleoenvironmental synthesis for the southwest Atlantic Ocean basin based on Jurassic to Holocene faunas and floras from the Falkland Plateau. *In* Craddock, C. (Ed.), *Antarctic Geoscience:* Madison (Univ. of Wisconsin Press), 155-163.

MS 120A-109

NOTE: All core description forms ("barrel sheets") and core photographs have been printed on coated paper and bound as Section 3, near the back of the book, beginning on page 377.

Summary Log for Hole 747A